Advances in Isotope Geochemistry

Paul B. Tomascak
Tomáš Magna
Ralf Dohmen

Advances in Lithium Isotope Geochemistry

Springer

Advances in Isotope Geochemistry

Series editor

Jochen Hoefs, Göttingen, Germany

More information about this series at http://www.springer.com/series/8152

Paul B. Tomascak · Tomáš Magna
Ralf Dohmen

Advances in Lithium Isotope Geochemistry

Springer

Paul B. Tomascak
State University of New York at Oswego
Oswego, NY
USA

Tomáš Magna
Czech Geological Survey
Prague
Czech Republic

Ralf Dohmen
Institute of Geology, Mineralogy
and Geophysics
Ruhr-University Bochum
Bochum, Nordrhein-Westfalen
Germany

ISSN 2364-5105 ISSN 2364-5113 (electronic)
Advances in Isotope Geochemistry
ISBN 978-3-319-01429-6 ISBN 978-3-319-01430-2 (eBook)
DOI 10.1007/978-3-319-01430-2

Library of Congress Control Number: 2015953806

Springer Cham Heidelberg New York Dordrecht London

Printed on acid-free paper

Springer International Publishing AG Switzerland is part of Springer Science+Business Media (www.springer.com)

Preface

In this book we decided to attach the permil sign (‰) to all Li isotopic quantities. One way of viewing stable isotopes denoted by δ is that the arithmetic sets the results as being part-per-thousand quantities, so to place the ‰ on a value is redundant. However, this implies a certain familiarity from the reader. Our decision regarding the ‰ in this volume was guided by the potential that the audience may include those not so steeped in the thinking of stable isotopes. This calls to mind a historical note regarding Li isotopes. Readers of the early literature on the subject (beginning with Chan in 1987) will find papers that use δ^6Li. Prior to 2000, using the now-accepted δ^7Li notation was viewed as an unwanted usurpation by at least one prominent geochemist. Nevertheless, being clear is important, and although δ^7Li was not the first notation employed, it follows stable isotope convention. We find that students have a hard enough time understanding isotope geochemistry, so to oppose the notation used in virtually all systems (positive values are isotopically heavier than negative values) invites confusion. Hence, our use of the ‰ is a further step to make this compilation clear for all.

Acknowledgements

Once upon a time Jochen Hoefs approached one of us (P.T.) about putting together a book for this Springer Advances series. Thus began an unexpectedly long sojourn, during which the use of Li isotopes has come of age. Jochen had faith enough in us to persevere (keeping in mind the invitation to write this came in 2008!). For this opportunity and for his overall encouragement we are extremely thankful.

Two other names that need to be mentioned prominently are those of Lui-Heung Chan and Jan Košler, who passed away in 2007 and 2014, respectively. Anyone who works with Li isotopes owes Lui a debt of gratitude. Her passing saddened all with whom she had come in contact and was a great loss for the geochemical community as a whole. Jan was the M.Sc. supervisor for T.M., who brought him the idea of developing Li analytical chemistry for mantle rocks and who, with time, became a close friend. Jan's scientific contributions, especially to the ICP-MS community, are diverse and lasting. His presence as a colleague and friend will be badly missed.

Throughout the construction of this work we have asked for input of various kinds from a number of individuals, who have graciously helped. To this end, we would like to thank Natalie Caciagli-Warman, Rick Carlson, Alain Coc, Brian Fields, C. Eric Hellquist, Nick Prantzos, John Rakovan, Gary Steigman, Elisabeth Vangioni, Aurelie Verney-Carron and Nathalie Vigier for their assistance.

We have received a high level of support and almost unreasonable positivity from the editorial staff at Springer. How they had the patience to put up with our constant delays speaks of their desire to see the project through to completion. In particular we thank Janet Sterritt and Annett Buettner.

R.D.: I would like to thank Joana Polednia for help with compiling the experimental data.

T.M.: I wish to acknowledge my family in the first place, as their support is the most prominent and most important everlasting key for my human being. Numerous colleagues with whom I have had multiple disputations and discussions over the years deserve thanks for their inspiration. While not possible to list all of these, here are some of the prominent ones: Lukáš Ackerman, James Day, Alex Deutsch, Vojtěch Erban, Tim Grove, Nikolaus Gussone, Alex Halliday, Darrell Harrison, Vojtěch Janoušek, Timm John, Klaus Mezger, Fred Moynier, Clive Neal, Felix Oberli, Andreas Pack, Franck Poitrasson, Vladislav Rapprich, Erik Scherer, Michael Seitz, Zach

Sharp, Tony Simonetti, Andreas Stracke, Larry Taylor, Dewashish Upadhyay, Uwe Wiechert, Rainer Wieler and Karel Žák. I am grateful to the Czech Science Foundation for partial support through projects P210/12/1990, 13-22351S and 15-08583S.

P.T.: I thank my university for supporting my ability to continue to conduct research and to the many students with whom I have had the pleasure to interact over the years. The goal of bringing geochemistry from the hazy and somewhat scary distance to clear focus continues to be a beloved challenge, which is made worthwhile by passionate students.

Contents

Introduction 1

Lithium (Li) was discovered by J. August Arfvedson in 1817 (Berzelius 1817). The newly isolated alkaline compound in the Swedish petalite sample was given the Greek name for stone: λίθος (lithos); the metal was dubbed lithium. In the following year Sir Humphry Davy described the isolation of metallic Li using electrolysis (Anonymous 1818), although this development is commonly considered contemporaneous with the work of Brande (Weeks 1956). Using a more modern electrolytic process, Bunsen and Matthiessen succeeded in isolating multi-gram quantities of Li metal (Bunsen 1855). Commercial production of Li started only after World War I. A more massive production commenced after World War II with the findings of potential Li utility in the nuclear industry.

Lithium as an element has a number of peculiar properties. For example, it is the lightest of all solids of the periodic table of elements with a density of just 0.543 g cm^{-3}, meaning that it floats on the water. It also has the highest specific heat capacity of all solids (5.38 kJ kg^{-1} K^{-1}). Its melting and boiling temperatures (180.5 and 1342 °C, respectively) are the highest of alkali metals of group 1A of the periodic table and, similarly, its first ionization energy (5.39 eV) is also higher compared with other elements of this group.

Because of some of these properties, the utility of Li has found its peak applications in the ceramic industry, electronics and electrical industry, metallurgy, medicine, the optical industry, organic and polymer chemistry, the nuclear industry, as well as in the production of grease and lubricants, and as a desiccant (halogens, hydroxide, peroxide, perchlorate) in air cleaning devices for submarines, spacecraft, etc. Lithium ion batteries constitute a major and growing industrial channel for the element, with the proliferation of mobile electronic devices and the diversification of electric-powered vehicles. These demands for Li are reflected in a dramatic increase in Li production during the last two decades (Fig. 1.1). Earlier commercial exploitation of Li came from primary magmatic sources, such as large pegmatite bodies with Li-bearing minerals (amblygonite, eucryptite, lepidolite, petalite, spodumene), and less commonly from evaporites. More recently exploitation of brine pools (salars) have become by far the dominant source of the element, with principal resources currently in Australia, China, and South America. Brine resources appear to be the stable producers of Li also in the near future (Ebensperger et al. 2005; Kesler et al. 2012) although alternative sources of Li as a side product of other economic activities are also being explored (Qin et al. 2015). Future demands appear likely to continue to grow, and the recycling of the element may become an integral part of the Li business (Mohr et al. 2012).

Just over a decade has passed since the publication of a broadly inclusive summary of Li isotopic research in the world (Tomascak 2004). Despite the short time, the use of this isotopic

P.B. Tomascak et al., *Advances in Lithium Isotope Geochemistry*,
Advances in Isotope Geochemistry, DOI: 10.1007/978-3-319-01430-2_1

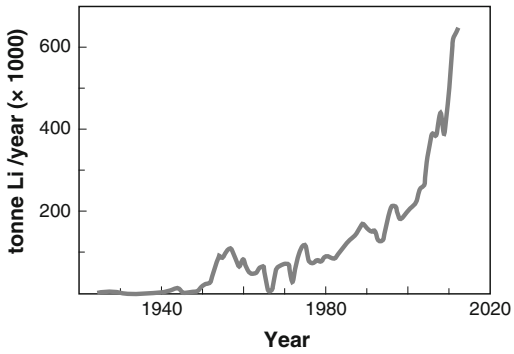

Fig. 1.1 Worldwide production of lithium. A dramatic increase after World War II was caused by the demand for Li in the nuclear industry, whereas more recent increase reflects rapid diversification of commercial applications. Data from Jaskula (2015)

system in the investigation of geo- and cosmochemical questions has truly exploded, hinging in part on the arrival of analytical technology at the close of the millennium (Fig. 1.2). Prior to 2004, approximately 50 publications with Li isotope data existed in the accessible peer-reviewed literature, of which almost 30 % were purely analytical studies (i.e., not specifically addressing research questions, but rather reporting laboratory methods). Articles with dates of 2004 and later currently number over 220. Technically-based studies have not disappeared in the era of advanced analytical capabilities (about 6 % of the post-2003 studies are principally technique articles), but clearly many of the earlier analytical issues have been overcome, facilitating the current research boom.

In response to this explosion, we have endeavored to accumulate the trove of new findings into an updated summary of the state of Li isotopic science. Although this engenders a degree of repetition of results and findings from existing summary works (e.g., Burton and Vigier 2011; Chan 2004; Elliott et al. 2004; Tang et al. 2007; Tomascak 2004), the focus of this compilation is to distill the more modern studies and to highlight major developments to date. Given that the history of the development of Li isotopic geochemistry is covered in detail in other works, our goal here is to concentrate on modern research and the directions it currently takes.

The title of this work accurately defines our focus, which is primarily the compilation and interpretation of the isotopic results in geo- and cosmochemical studies. Lithium as an element has its own important role in studies of these kinds. Although we touch on this role in places (necessarily in the discussion of laboratory experiments, Chap. 4), the reader is referred to the literature for additional detail on Li—the element—as used in the Earth sciences. Additionally, Li is of great importance in many other fields, ranging from ecology, biomedicine, and pharmacology, to materials, energy, and nuclear science and engineering. The reader is again directed to the primary literature of these areas for information.

This volume is broken down along conventional lines. We have endeavored to the greatest extent to repeat as little as possible from previous compilations, attempting to integrate and highlight newer findings. We begin in Chap. 2 with a summary of the analytical techniques used, past and present, to isolate and measure Li isotopic ratios. Unlike many other fields in analytical geochemistry, the community has not converged on a single "standard operating procedure" when it comes to either the chemical separation and purification of the element or to the quantification of its isotopes. There remains a variety of methods still in wide use.

The summary of Li isotope cosmochemistry in Chap. 3 sets the stage for the deeper focus of Li in our planet. A general outlay of Li in the cosmos is established, giving the major background necessary to appreciate Li in the terrestrial neighborhood. This chapter attempts to cast the ultimate origins of the isotopes of Li in terms that are understandable for a non-astrophysicist audience.

Chapter 4 takes as its focus the synthetic studies that are designed to help understand Li behavior in natural settings. In order to use Li isotopes in a quantitative way in natural systems, constraints must exist from experiments, and as we probe deeper into natural samples the demand for accurate and meaningful laboratory constraints intensifies. The diversification of experimental approaches to understanding Li isotopes

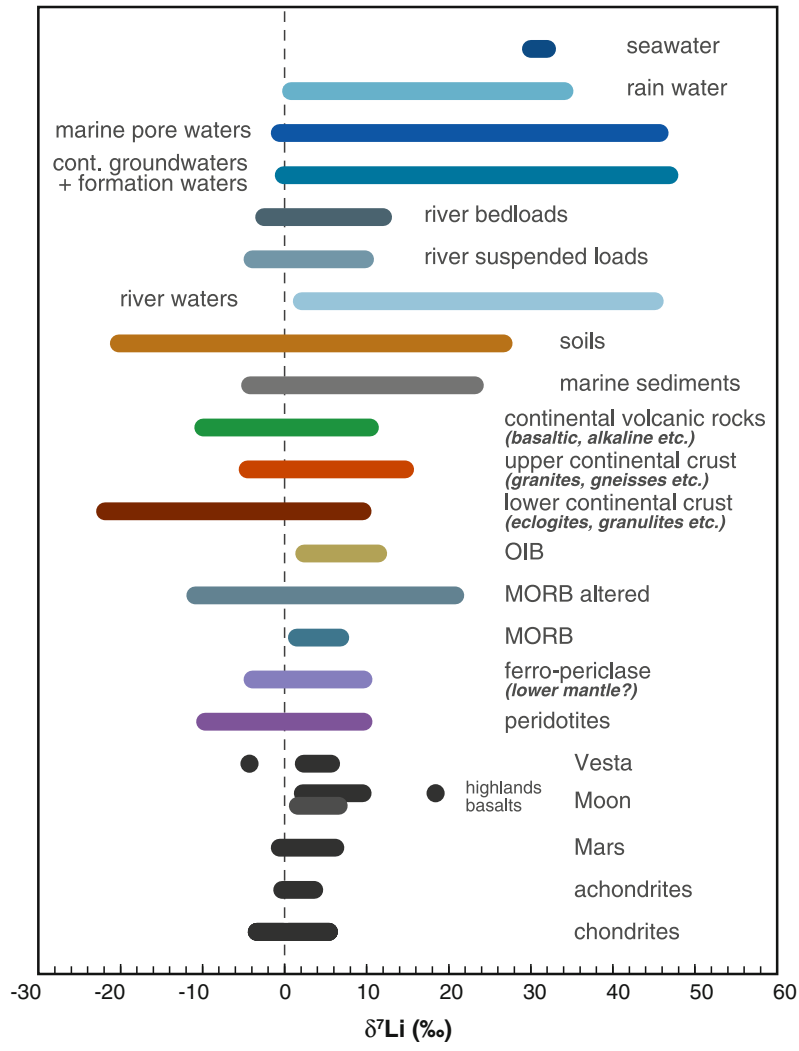

Fig. 1.2 Lithium isotopic composition of various extra-terrestrial and terrestrial reservoirs. The details of individual reservoirs and δ^7Li variations are discussed throughout the volume. For marine sediments, samples with obvious metamorphic effects are excluded (see Chap. 6). Soil samples include loess and similar detritus. For river waters and continental groundwaters and formation waters, only samples without discernible anthropogenic influence were included. Also, for river waters, those affected by hydrothermal input were ommitted (see Chap. 6)

has been great in recent years, particularly with the acceptance that diffusion produces, in many settings, effects that must be considered. This chapter summarizes existing results and draws attention to where conclusions drawn from laboratory and theoretical studies appear to most significantly affect the interpretation of data from natural systems. The fast pace of change in the field as a whole dictated by experimental studies is highlighted.

The solid Earth is the target of Chap. 5, with emphasis on the interpretation of data from mantle and crustal igneous and metamorphic rocks. As the mantle is the primary reservoir of Li in the Earth, it is critical to understand its bulk Li isotopic composition in order to guide solar system-scale interpretations. The bulk composition of the mantle and the transit of Li between mantle and crustal reservoirs are major topics addressed in this chapter.

In Chap. 6 we consider the many studies that deal with the domain in which the bulk of Li isotope fractionation takes place on Earth: near-surface processes. Since stable isotopic fractionation predominates in conditions of low temperature, the bulk of the Li isotopic "action"

in the Earth system can be said to exist within the narrow fringe where rock, water, and atmosphere closely coexist. Applications of Li isotopes in this realm are manifold and extend to studies of the Earth's evolving climate system, as well as the potential for use as a tracer of environmental contaminants.

The volume concludes in Chap. 7 with a distillation of major findings with indications of fertile areas for continued discovery. This section partly reprises an earlier set of recommendations for future study (Tomascak 2004), in an attempt to gauge what the geochemical community has learned from this stable isotopic system.

References

Anonymous (1818) An account of the new alkali lately discovered in Sweden. Q J Sci Arts 5:337–340

Berzelius JJ (1817) Ein neues mineralisches Alkali und ein neues Metall. J Chem Phys 21:44–48

Bunsen R (1855) Darstellung des Lithiums. Justus Liebig Annalen der Chemie 94:107–111

Burton KW, Vigier N (2011) Lithium isotopes as tracers in marine and terrestrial environments. In: Baskaran M (ed) Handbook of environmental isotope geochemistry; Adv Isotope Geochem 4:41–59

Chan LH (2004) Mass spectrometric techniques for the determination of lithium isotopic composition in geological material. In: de Groot PA (ed) Handbook of stable analytical techniques, vol 1, issue 6, pp 122–141

Ebensperger A, Maxwell P, Moscoso C (2005) The lithium industry: its recent evolution and future prospects. Resource Policy 30:218–231

Elliott T, Jeffcoate A, Bouman C (2004) The terrestrial Li isotope cycle: light-weight constraints on mantle convection. Earth Planet Sci Lett 220:231–245

Jaskula BW (2015) Lithium. USGS Minerals Yearbook, 2013, pp 11

Kesler SE, Gruber PW, Medina PA, Keoleian GA, Everson MP, Wallington TJ (2012) Global lithium resources: relative importance of pegmatite, brine and other deposits. Ore Geol Rev 48:55–69

Mohr SH, Mudd GM, Giurco D (2012) Lithium resources and production: critical assessment and global projections. Minerals 2:45–64

Qin S, Zhao C, Li Y, Zhang Y (2015) Review of coal as a promising source of lithium. Int J Oil Gas Coal Technol 9:215–229

Tang YJ, Zhang HF, Ying JF (2007) Review of the lithium isotope system as a geochemical tracer. Int Geol Rev 49:374–388

Tomascak PB (2004) Developments in the understanding and application of lithium isotopes in the Earth and planetary sciences. In: Johnson CM, Beard BL, Albarède F (eds) Geochemistry of non-traditional stable isotopes. Rev Mineral Geochem 55:153–195

Weeks ME (1956) Discovery of the elements. Easton, Pennsylvania. J Chem Educ 1956, pp 910

Methodology of Lithium Analytical Chemistry and Isotopic Measurements

2

2.1 Historical Perspective

Lithium was discovered as an elemental species in 1817 by J.A. Arfvedson and isolated as a metal one year later by Sir H. Davy. The existence of two naturally occurring isotopes of lithium, ^{6}Li and ^{7}Li, was unambiguously proven by A.J. Dempster (1921) and the atomic weight of Li and the individual isotope masses were first determined with reasonable accuracy and precision by F.W. Aston (1932) (few available data are referenced therein) at 6.928 ± 0.008, 6.012, and 7.012 atomic mass units, respectively (atomic mass unit, *amu*, is defined as $1.660538921 \pm 73 \times 10^{-27}$ kg and corresponds to 1/12 of mass of unbound neutral ^{12}C in nuclear and electronic ground state; modern physics uses the term "unified atomic mass" abbreviated as 'u' or dalton). In the decades that followed this, however, only a few attempts to refine the absolute atomic weight as well as its uncertainty (see summary in Svec and Anderson 1965) were implemented. The actual atomic weights of ^{6}Li and ^{7}Li are 6.0151223 ± 5 and 7.0160040 ± 5 *u*, respectively. The actual atomic weight of Li, currently accepted by IUPAC, is 6.941 ± 0.002 (Wieser 2006) and it may well be that this level of precision will not improve significantly in the near future due to natural variations in ^{7}Li/^{6}Li exceeding ~80 ‰ (Tomascak 2004, this volume).

The natural variations of ^{7}Li/^{6}Li were not measured extensively or with clearly established reproducibility until late 1980s (Chan 1987). This article reported a method for chemical separation and precise isotopic measurements with ~2.5 ‰ external uncertainty. Although earlier measurements which used mass spectrometry were performed on a range of terrestrial and extraterrestrial samples (e.g., Balsiger et al. 1968; Brown et al. 1977; Eugster and Bernas 1971; Krankowsky and Müller 1967; Michiels and De Bièvre 1983), data reported in these studies were usually expressed in absolute ^{7}Li/^{6}Li ratios with errors exceeding several per mil. This severely hampered data comparison and the overall utility of Li isotopes in geochemistry.

A major problem of early reports on Li isotopic compositions was the lack of a widely distributed reference material that would allow for reliable inter-laboratory comparison of measured isotopic ratios. In 1973, Flesch and co-workers isolated Li from "virgin" spodumene-rich ores from the granitic pegmatite at Kings Mountain, North Carolina, USA, and determined its isotopic composition at ^{7}Li/^{6}Li = 12.0192 ± 0.0002 (Flesch et al. 1973). The isolated Li was made available by the National Bureau of Standards (now NIST) as L-SVEC (since reassigned as SRM 8545). The availability of an external standard permitted calibration of measured ^{7}Li/^{6}Li and presentation of data relative to L-SVEC in permil deviations. Chan (1987) and several papers that followed employed the normalized ^{6}Li/^{7}Li (δ^{6}Li). Since that time, though, the use of the δ^{7}Li value has prevailed, as it is consistent with the other major

P.B. Tomascak et al., *Advances in Lithium Isotope Geochemistry*,
Advances in Isotope Geochemistry, DOI: 10.1007/978-3-319-01430-2_2

stable isotopic systems (i.e., positive values reflect enrichment in the heavy isotope). This nominal $\delta^7Li = 0$ ‰ mimics the Li isotopic composition of global magmatic continental crust (Bryant et al. 2004; Magna et al. 2010; Teng et al. 2004, 2008, 2009). Considering that the δ^7Li values in mineral phases from worldwide granitic pegmatites vary greatly (e.g., Magna et al. 2013), the choice of this particular spodumene by Flesch et al. was quite serendipitous.

The L-SVEC reference standard has proven, perhaps fortuitously, robust, with proven Li isotopic homogeneity within better than ±0.1 ‰ (2σ) for aliquots allocated to different laboratories (Magna et al. 2004). This is noteworthy in the view of homogeneity problems encountered for reference materials used in several other stable isotopic systems (e.g., NIST SRM 980 for Mg; Galy et al. 2003), Si isotopic discrepancies for IRMM-018 versus NBS-28 (see Reynolds et al. 2006 and discussion therein), or different values in newly marketed reference materials compared to older, exhausted resources, such as for Ca (note differences in $\delta^{44/40}Ca$ between SRM 915a and 915b; Heuser and Eisenhauer 2008). Recently, however, the L-SVEC reference material has run out and was replaced by the new IRMM-016 artificial material with $\delta^7Li_{L\text{-}SVEC} = -0.2$ to +0.3 ‰ (Aulbach and Rudnick 2009; Aulbach et al. 2008; Caciagli et al. 2011; Huang et al. 2010; Jeffcoate et al. 2004; Kasemann et al. 2005; Millot et al. 2004; Penniston-Dorland et al. 2010; Qi et al. 1997b; Simons et al. 2010; Teng et al. 2006; Zack et al. 2003). This can thus be considered identical within external analytical uncertainty of Li isotopic measurements and no further recalculation is required. Care should be exercised, however, to juxtapose L-SVEC and IRMM-016 when significantly different δ^7Li values emerge (e.g.,<–0.5 ‰; Liu et al. 2010; Marks et al. 2007) that are slightly beyond the level of current analytical uncertainties.

Yet another problem for Li isotopic analyses is represented by laboratory-induced contamination that may seriously compromise the intrinsic $^7Li/^6Li$ in natural samples as these ratios often show large variations in commercially available Li materials (Qi et al. 1997a) and even minimal exposure to such reagents may result in erratic $^7Li/^6Li$ (Košler and Magna 2014). Vigilance in areas of sample preparation is just as critical as in the chemistry laboratory (as discussed below) for the production of verifiable Li isotopic data. For example, in many rock processing facilities the preparation of samples for XRF or other flux-fusion methods has taken place. Traces of residual dust from Li-borate flux, even years later, threaten samples being processed for mineral separates or rock powders in such spaces.

2.2 Lithium Isolation by Cation Exchange Chromatography

Separation of Li from other elements in natural materials is challenging owing to M/Li ratios commonly in excess of 10^4 (e.g., Na/Li in seawater), as well as the similarity of the ion exchange partitioning of Li to some major cations. Pioneering work on partitioning of Li and other elements between ion exchangers and various types of elution media stressed the efficacy of mineral acids such as HCl and HNO_3 in separating Li (Strelow et al. 1974; Šulcek et al. 1965; Šulcek and Rubeška 1969), in particular when mixed with organic solvents (e.g., methanol and ethanol, although other organic elution media may be used for specific purposes; Kim 2001). All major subsequent analytical developments adopted this approach with different combinations of these mineral acids and simple alcohols.

A major consideration when ion exchange is applied to Li isolation is the large isotopic fractionation introduced during chromatographic separation as a consequence of greater affinity of ^6Li to stationary phase (Taylor and Urey 1938). As a result of incomplete Li recovery, unintended isotopic fractionation can be caused. For example, Moriguti and Nakamura (1998) and Košler et al. (2001) have shown that Li isotopic fractionation may reach several tens of percent with ^7Li eluting first and ^6Li tailing (Fig. 2.1) as a result of equilibrium fractionation of Li between the solid phase and solvent (Schauble 2004); thus, ~100 % yields are indeed essential. This differs from elements with more than two isotopes where

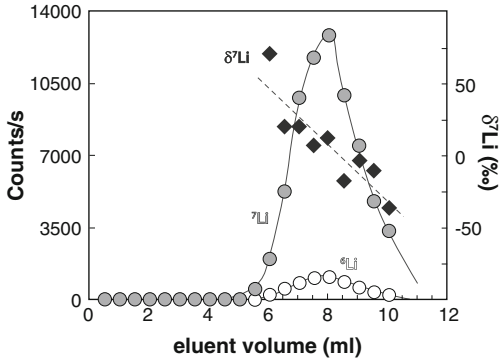

Fig. 2.1 Example of Li isotopic fractionation during ion exchange chromatography (after Košler et al. 2001). A progressive shift from isotopically heavy to light fractions during ongoing chromatographic isolation of Li, with a δ^7Li range of ~100 ‰ during elution. A failure to complete recovery of Li would result in the collection of a sample with an erroneous isotopic composition

internal corrections for incomplete recovery may be applied. Unfortunately for the laboratory geochemist, achieving quantitative recovery is not simply a matter of calibrating ion exchange columns. Position of the elution peak for Li from exchange columns is affected by the bulk chemical composition of the sample and the ion load to the column. Thus, separate elution recipes may be necessary for different sample types (Fig. 2.2). The reality of this issue was driven home by Chan et al. (1999), where biased δ^7Li results resulted in the publication of a correction (Chan et al. 2002). Analyses of rocks yielding distinct (and geologically reasonable) isotopic compositions were shown, after chemical separation issues were solved, to be isotopically homogeneous and with no anomalous samples.

The sensitivity of different instrumental methods to analyte solutions that lack complete purification is variable, but, for plasma-based methods, it is clear that significant amounts of contaminant elements may compromise the accuracy and precision of Li isotopic determinations. Hence, the quality of ion exchange separation is an important issue in sample preparation. The effects of imperfect separation of Li from other elements have been demonstrated by many studies (e.g., Huang et al. 2010; Jeffcoate et al. 2004; Magna et al. 2004; Moriguti and Nakamura 1998; Nishio and Nakai 2002; Rosner et al. 2007; Tomascak et al. 1999). In particular, the removal of Na, as the nearest major element to be eluted after Li, has received attention; avoiding or eliminating Na tailing in the Li fraction during chromatographic separation is the goal here. The extent to which contaminant elements may compromise successful isotopic analysis depends largely on the measurement technique. Whereas there is some degree of freedom in matrix concentrations for plasma-based techniques (Huang et al. 2010; Jeffcoate et al. 2004; Košler et al. 2001; Magna et al. 2004; Rosner et al. 2007; Tomascak et al. 1999), little tolerance is apparent with thermal ionization methods (Hoefs and Sywall 1997; James and Palmer 2000; Moriguti and Nakamura 1998; Xiao and Beary 1989).

Early attempts to measure Li isotopic compositions in natural samples required several hundreds of nanograms Li (e.g., Chan 1987; Chan and Edmond 1988; You and Chan 1996) but these requirements were alleviated with technical improvements; high-sensitivity ICP-based mass spectrometers now allow accurate analyses with less than 5 ng Li. The need to prepare such large samples, especially for relatively low-Li materials like mantle rocks, required large-volume columns packed with ion-exchange resins and large amounts of collection media (sometimes several hundred milliliters). This made early techniques rather time consuming and prone to elevated procedural blanks. With diminishing sample size came the capacity to analyze materials with very low Li abundance and/or samples of very small size, critical for high spatial resolution as well as when limited amounts of sample were available.

Exchange media with Li-specific characteristics are not available, unlike for certain elements or elemental groups (e.g., Dow AMBERLITE™ for B, Sr. Spec for Sr and Pb, and Eichrom TRU Resin for actinides). The use of cation exchange resins such as AG50W-X8 appears to provide high efficiency in separating Li from other elements, but optimization of the geometry of chromatographic columns also plays a role in quality of element separation, blank suppression, and time cost.

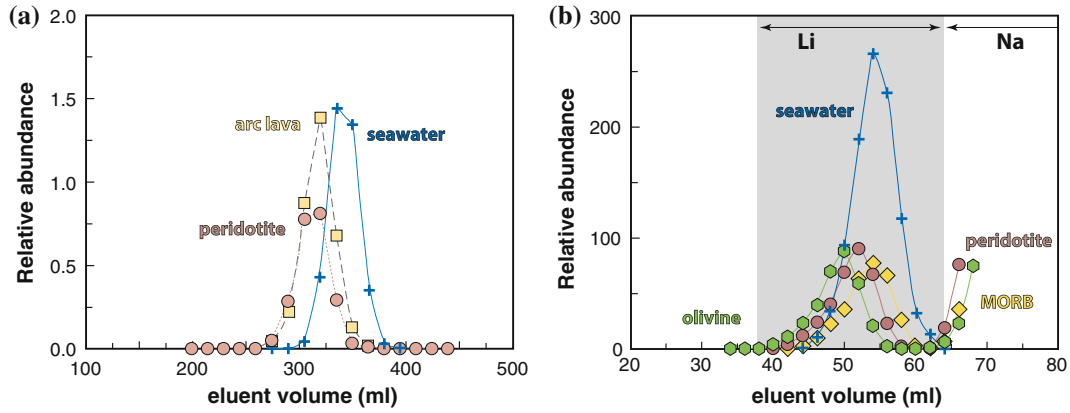

Fig. 2.2 Examples of the difference in cation exchange elution peaks for Li resulting from various matrices (e.g., peridotites and other silicate rocks, seawater). Improper column calibration may lead to incomplete collection of the Li fraction (Chan et al. 1999, 2002)

Mixtures of mineral acids with methanol or ethanol provide better separation of Li from other elements than strictly inorganic eluants. The increasing concentration of alcohols at a given molarity of the respective mineral acid increases the separation factor between Li and Na (as the next element to elute), such that 80 % by volume methanol solution roughly triples the separation over 60 % methanol solution. This is counter-balanced by decreasing separation factor when the molarity of the respective acid increases. Therefore, a near-ideal formula entails low-molarity acid mixed in high percentage organic solvent. There is apparently little difference between HCl and HNO_3, the former providing slightly larger separation factor between Li and Na and the latter quantitatively eliminating some elements such as Fe, Zn and Cd, which may appear in HCl-based elution schemes (Strelow et al. 1974). One practical downside of the acid–organic mixture is the formation of small bubbles in the resin. This phenomenon restricts both choice of the internal diameter of a column (which cannot be too narrow) and the column material (e.g., non-wetting material like PFA Teflon versus quartz glass).

A glut of methods have been successfully employed in geochemistry and cosmochemistry: pure HCl (Chan 1987; James and Palmer 2000; Misra and Froehlich 2009; Moriguti and Nakamura 1998; Oi et al. 1997; Sahoo and Masuda 1995a, 1998), HCl–ethanol (Jeffcoate et al. 2004 in second step), pure HNO_3 (Hoefs and Sywall 1997 and Magna et al. 2006 in second step) and HNO_3–methanol (Huang et al. 2010; Choi et al. 2010; Košler et al. 2001; Magna et al. 2004; Nishio and Nakai 2002; Seitz et al. 2004; Tomascak et al. 1999). These studies encompass a wide variety in resin mesh size (100–200 vs. 200–400), cross-linkage (X8 vs. X12; see Schönbächler and Fehr 2014 for a more detailed review of issues related to ion exchange chromatography), and column size/volume, but they all seem to provide a reasonable means of Li separation. Inasmuch as no single method presents a clear best-case separation (i.e., one that minimizes reagents and time whilst maximizing ease of use and flexibility of sample type), there appears to be room for further analytical improvements. Perhaps in the near future a selective complexing agent or the use of other solvents (e.g., acetone) will further improve the process of Li separation for isotopic measurement.

2.3 Methodology of Li Isotopic Measurements

At present, a plethora of technical possibilities exists for measurements of Li isotopic compositions, but superior performance with respect to the accuracy and precision of isotopic data

collection is represented by plasma-based techniques (Q-ICPMS, SF-ICPMS, MC-ICPMS), thermal ionization (TIMS), and secondary ionization (SIMS). Although this instrumentation and its technical aspects are rather complex and expensive, these methods provide the data output required for geochemistry and cosmochemistry. Nevertheless, other methods have also been developed for specific purposes and we discuss them here briefly. Also, it is important to note the prevalence of the δ^6Li notation, where negative values represent isotopically heavier values, in most of the earlier publications. Following the Goldschmidt 2002 geochemical conference a more logical δ^7Li notation has uniformly been accepted (Coplen et al. 2002). The conversion can simply be performed with the following equation:

$$\delta^7\mathrm{Li} = -\frac{\delta^6\mathrm{Li}}{\left(1+\left(\frac{\delta^6\mathrm{Li}}{1000}\right)\right)}$$

This conversion must be performed for δ^6Li values outside the range ~–10 to ~+10 ‰. Within this range the sign-changed difference between δ^6Li and δ^7Li values results in shifts <0.1 ‰ whereas for δ^6Li values in the range of seawater (–31.0 ‰; Millot et al. 2004) the difference is ~1 ‰. It increases to ~+10 ‰ at δ^7Li > 100 ‰ and to ~40 ‰ at δ^7Li > 200 ‰, found for anthropogenically fractionated samples (Millot et al. 2010; Négrel et al. 2010).

2.3.1 Mass Spectrometry-Based Methods of Widest Use

2.3.1.1 TIMS

Prior to the diversification of ICP and SIMS instruments, thermal ionization was the primary method of choice in yielding high-precision Li isotopic compositions for several decades. Indeed, the first absolute Li isotopic compositions were obtained by TIMS (Balsiger et al. 1968; Svec and Anderson 1965, 1966) or its modifications (Brown et al. 1977) and this remains the only reliable method for determination of absolute Li isotopic abundances, as the plasma-based instruments always return mass-biased results and the instrumental fractionation is too great and variable to effectively correct back to absolute ratios. As such TIMS has represented a cornerstone for resolving even small differences in δ^7Li considering ±1 ‰ errors that were routinely obtained (Chan 1987). It is unfortunate that, despite the generation of the L-SVEC standard in the early 1970s, TIMS studies throughout the 1970s and 1980s failed to measure this material, making it impossible to recalculate data to modern systematics.

Several strategies have been developed that employed polyatomic species, such as $Li_2BO_2^+$ (Bickle et al. 2000; Datta et al. 1992; Chan 1987; Sahoo and Masuda 1995b), $LiNaBO_2^+$ (Chan et al. 1992), Li_2F^+ (Green et al. 1988), or metal Li^+ ion (Ahmed et al. 2002; Jabeen et al. 2003; James and Palmer 2000; Michiels and De Bièvre 1983; Moriguti and Nakamura 1998; Sahoo and Masuda 1995a, 1998; Xiao and Beary 1989; You and Chan 1996). These approaches combined different loading procedures, utilizing $Li_2B_4O_7$, Li_3PO_4, LiCl + H_3BO_3, LiOH, LiI, LiF, LiCl (but other possibilities were also explored, see Xiao and Beary 1989), with various filament configurations: single Re, Ta–Re or double Re, or triple Re filament assembly.

The developments by Chan et al. in measurement by TIMS, making use of the L-SVEC standard, broke the logjam and ushered in a new era of Li isotopic geochemistry. Studies using this technique introduced several first-order observations on the geochemical cycle of Li, making the first steps into this *terra incognita* (e.g., Chan et al. 1992, 1993, 1994; You et al. 1995). However, with the advent and rapid development of MC-ICPMS instrumentation (e.g., Halliday et al. 1995, 1998), TIMS techniques quickly became a somewhat obsolete approach for determination of Li isotopic compositions in natural samples considering the more time consuming mass spectrometry and lesser opportunity to monitor shifts in instrumental mass bias. Despite these drawbacks, TIMS

remains the only method capable of directly measuring the absolute Li isotopic abundances and as such, it will continue to have importance for precise validation of Li isotopic abundances in reference materials.

2.3.1.2 ICPMS

Despite the explosion in the use of plasma-based technologies in early 1980s, these methods did not find broad application to Li isotopic measurements until much later. The early generation of single-collector quadrupole ICP instruments was not well suited for isotopic determinations in geological samples but the few attempts returned data that were fully in the context of contemporaneous investigations (Grégoire et al. 1996; Vanhoe et al. 1991). Despite larger inaccuracy of Li isotopic measurements by this technique, it was applied to, for example, serious social–medical questions (Sun et al. 1987).

Košler et al. (2001) presented an improved quadrupole ICPMS protocol for determining Li isotopic compositions in natural samples (foraminiferal species) with external reproducibility approaching the ±2 ‰ (2σ) barrier which would be adequate for many geological applications. Further optimization has improved these statistical parameters (Carignan et al. 2007; Misra and Froehlich 2009). The higher sensitivity sector-field (single-collecting) ICPMS does not appear to represent significant improvement in accuracy and long-term precision of Li isotopic measurements compared to quadrupole instruments (Janoušek et al. 2010; Magna et al. 2010). Nonetheless, Li isotopic measurement by Q-ICPMS is not a "routine" practice, and as such the diversification of MC-ICPMS instruments leaves ICPMS a less used alternative today. However, for studies for which precision of ±1.0 ‰ is sufficient, it is a viable method that is certain to continue to be applied.

2.3.1.3 MC-ICPMS

With the advent of MC-ICPMS instrumentation and subsequent rapid developments in accurate, high-precision stable isotopic measurements (Halliday et al. 1995, 1998), it was only a matter of time before the tool was brought to bear on Li isotopes (Tomascak et al. 1999). The possibility of monitoring the varying instrumental bias by alternating samples and reference materials (L-SVEC; Fig. 2.3) on short time scales (plus the capability of monitoring abrupt changes in instrumental bias) promoted a massive increase in number of available data for Li isotopic compositions in all manner of geological settings, as well as some of the first credible data on non-terrestrial materials (*cf.* Tomascak 2004 and later development discussed in several sections of this volume). The major advantages of this technique lie in rapid throughput of solute samples, possibility to monitor instrumental bias during the analytical session, and low consumption of material that may, under suitable circumstances (sample/noise ratio), utilize less than one nanogram of Li with sub-permil external reproducibility. Furthermore, MC-ICPMS appears less susceptible to undesired shifts in measured $^{7}Li/^{6}Li$ ratios resulting from the presence of matrix elements due to imperfect chemical separation of Li (e.g., Bryant et al. 2003; Jeffcoate et al. 2004; Magna et al. 2004; Nishio and Nakai 2002; Rosner et al. 2007; Tomascak et al. 1999). Despite the strong fractionation of Li isotopic ratios with MC-ICPMS compared to TIMS, the method of measuring samples bracketed by standards has effectively circumnavigated this problem.

The issue of accuracy and inter-laboratory comparison is only secured by the availability of reference rock materials. At present, several of these are utilized worldwide (e.g., the basalts BHVO-2, JB-2, BCR-2, and IRMM BCR-403 or IAPSO seawater) and many others have been characterized for their $\delta^{7}Li$ through multiple independent measurements. Considering this wide range of materials of distinctive chemical compositions, it may be a prerequisite to "matrix-match" complete analytical procedures with corresponding reference materials instead of relying solely on one reference material.

Technical approaches to the measurement by MC-ICPMS are diverse. Overall, solutes are aspired into the plasma via low-flow nebulizers, nominally 30–100 μL min^{-1}, where the plasma may be "hot" (~1200–1400 W) or "cool"

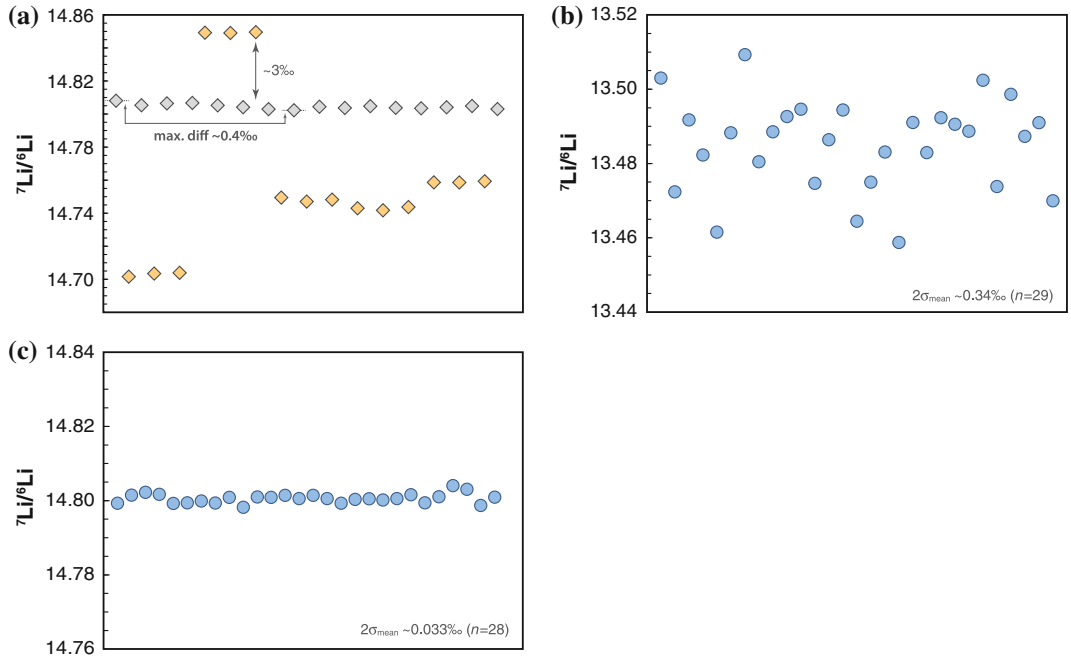

Fig. 2.3 Example of analytical sequences with standard–sample bracketing, as commonly used with MC-ICP-MS measurement (**a**). Calculation of the final δ^7Li may be performed in two ways: (i) relative to the average ^{7}Li/^{6}Li of two bracketing reference solution measurements irrespective of the actual measured ^{7}Li/^{6}Li (~14.80 for the depicted analytical sequence), or (ii) recalculating the measured values to the natural ^{7}Li/^{6}Li of ~12.1. Both alternatives should yield identical results. Stability of the instrumental bias is among the key factors for accurate determination of Li isotopic composition, here exemplified by a maximum ^{7}Li/^{6}Li variability of ~0.4 ‰ over >5 h. In **b** and **c**, example of noisy and stable measurement is apparent by a ~10-fold difference in internal errors of the measurement of the same solution over two different analytical sessions, performed within 1 week

(~700–800 W; Bryant et al. 2003; Choi et al. 2013); aspiration is often aided by desolvation, resulting in more homogeneous droplet size just prior to dispersion in plasma. During an analytical session, a solution is introduced after the background signal level is reached that may require significant washout time, but alternative switch between sample and standard solution without rinsing was also explored (Rosner et al. 2007). This latter approach requires a complete signal intensity match to better than ±5 % in order to avoid instrumental bias introduced by improperly balanced signals of bracketing standard and unknown sample (Huang et al. 2010; Magna et al. 2004; Rosner et al. 2007). The isobaric interferences from $^{12}C^{++}$, $^{14}N^{++}$ and $^6LiH^+$ appear to pose a minor problem and were indeed not detected at mass resolution of ~1400 (Magna et al. 2004) despite lower mass resolving power required to delimit these individual peaks. When Tomascak et al. (1999) introduced MC-ICPMS measurement protocols for Li isotopic measurements with the first generation instruments, a reproducibility of ±1.1 ‰ (2σ), basically equivalent to TIMS analysis, was achieved. Currently, the long-term reproducibility of MC-ICPMS measurements using more modern instruments appears to be at the ±~0.3–0.4 ‰ (2σ) level (Jeffcoate et al. 2004; Magna et al. 2004; Millot et al. 2004). Although short-term reproducibility may surpass this level, it is not apparent in the current literature that any group is able to do demonstrably better for true, long-term conditions.

At present the literature on Li isotopes is dominated by data generated with solution

MC-ICPMS. Recently, le Roux (2010) presented a laser ablation (LA) MC-ICPMS method. In this study, they performed in situ measurements of Li isotopic composition in reference glasses whose Li isotopes had been characterized by means of solution MC-ICPMS. It appears that combination of LA with MC-ICPMS may result in rapid determination of Li isotopic compositions on the sub-0.1 mm scale if followed by technical improvements in detection limits and sensitivity. For example, minerals with 10–20 ppm Li generated ~0.1 V signals on mass ^{7}Li against 6–8 V for 10 ppb Li solutions routinely obtained with solution MC-ICPMS. Also, diligent matrix matching appears to be essential for laser sampling, which demands a suite of homogeneous and well characterized glass reference standards. The recent report of Xu et al. (2013) showed the spatial capabilities coupled with high sample throughput weighed against still rather high analytical errors (mostly >1.8 ‰, 2σ) and poor reproducibility for a large selection of reference glass standards. It shows that this methodology yet awaits further detailed analytical efforts before it may become a fast and lower-cost analytical alternative.

2.3.1.4 SIMS

Although it may seem that implementation of laser ablation into MC-ICPMS could represent a new and straightforward in situ means of Li isotopic determination, SIMS technology is far ahead in terms of spatial resolution, sensitivity, and overall technical abilities in investigations of Li isotopic compositions. The first real attempts to measure Li isotopic compositions with a secondary or sputtering ion source were performed on meteorites (Gradsztajn et al. 1967; Poschenrieder et al. 1965) and lunar rocks (Eugster and Bernas 1971), although the precision and accuracy were apparently too low for any valuable scientific statements apart from the ^{7}Li/^{6}Li ratios identical to those found for terrestrial rocks within large uncertainties. Nevertheless, further measurements of Li isotopic compositions in geological samples were mostly obtained by TIMS and later MC-ICPMS; only relatively recently have studies utilizing SIMS measurement of Li isotopes emerged (e.g., Barrat et al. 2005; Beck et al. 2004; Decitre et al. 2002; Chaussidon and Robert 1999; Kobayashi et al. 2004; Richter et al. 2003).

Whereas SIMS requires precise matrix matching for any elemental and/or isotopic determinations, little effort has been exerted for characterization of suitable geological reference materials in terms of Li isotopic compositions (Jochum et al. 2006; Kasemann et al. 2005). This appears a persistent problem and may require further experimental work. Such inferences are stressed by apparent matrix-induced fractionation of Li isotopes (Bell et al. 2009) which may indeed impart an additional uncertainty to in situ measurements unless these matrix effects are not disentangled correctly. It would follow that an instrumental mass fractionation factor may be estimated from false data and that not only must a mineral phase be matched, but also its major element composition should be more or less identical with unknown samples. These matrix effects may partly be responsible for a larger uncertainty linked to SIMS, that in most applications is limited to ~±2 ‰ (2σ). It is expected that this can be significantly reduced in carefully controlled experiments (Marks et al. 2008).

Marks et al. (2008) provided a detailed investigation and SIMS–MC-ICPMS cross-calibration of pegmatitic Na-rich arfvedsonite and aegirine in order to determine the matrix effects caused by SIMS. These authors found a significant difference in resulting δ^{7}Li of the two methods at the level of 4–5 ‰ (see also Kasemann et al. 2005), and differences on the order of nearly 10 ‰ for NIST 610, 612 and 614 glasses. Similarly, Bell et al. (2009) applied a differential matrix correction factor deduced from experimentally verified fractionation of Li isotopes in response to major chemical composition of olivines (Mg#). Recently, Su et al. (2015) have provided a detailed SIMS, ICPMS and MC-ICPMS comparison of multiple grains of olivine, clinopyroxene and orthopyroxene from ultramafic rocks collected in China, with the aim of establishing well-characterized mineral reference materials for in situ techniques. While laborious by nature, these analyses showed that

(i) SIMS results for olivine may strongly depend on Mg# [molar MgO/(MgO + FeO_t) × 100] which would demand careful daily calibration over a range of Mg# values, and (ii) significant δ^7Li variations of several ‰ persisted between different laboratories and even between different sessions conducted in a single laboratory. This may, in part, be linked with different instrumental optimization parameters because the reported Li contents in mineral phases were shown to be reproducible.

The homogeneity in Li contents is also an important factor to consider, as has been underscored by inter-laboratory consistency of Li abundances in a natural quartz specimen (Audétat et al. 2015). Therefore, combined analytical tools may become a truly essential strategy for further SIMS studies of, for example, meteoritic constituents such as chondrules and calcium–aluminum-rich inclusions, considering both their small sizes and the important message they may carry since their formation in the earliest era of the Solar system. In fact, Li partitioning within single crystals of a mineral species may depend on major element composition, such as shown for plagioclase (Coogan 2011).

2.3.2 "Other" Analytical Methods

2.3.2.1 Atomic Absorption Spectrometry (AAS)

This technique has been successfully applied to rapid determination of Li isotopic compositions in the nuclear industry. Lithium-6 has large cross section for thermal neutrons (~942 barns) and the knowledge of ^{6}Li level is important for its burnup rate and for estimation of the production rate of tritium through the ^{6}Li(n,α)^{3}H reaction. The possible usage of AAS for determining Li isotopic ratios was first explored by Wheat (1971) who employed a mono-isotope hollow cathode lamp. For AAS, it is essential to precisely know the Li content in unknown samples; Li isotopic ratios are calculated from measured absorbance of ^{6}Li (Meier 1982) but the linearity of these absorbance determinations, which is prerequisite for exact data acquisition, appears to be disputed (Kushita 1986). Chapman and Dale (1976) reported on an AAS methodology for fast determination of ^{7}Li/^{6}Li in a range of samples which Chapman et al. (1980) suggested to approach analytical precision obtained by classical TIMS techniques. However, the data of Kushita (1986) show that this expectation was largely over-estimated.

In later progress, many problems were overcome (Wizemann and Niemax 2000), but the precision of Li isotopic determinations reached with AAS remains an issue. Moreover, results obtained for many natural samples (Meier 1982) that are likely to have non-extreme isotopic compositions (e.g., natural waters) show extremely light compositions. Therefore, the reliability of AAS (and also atomic emission spectrometry; ur Rehman et al. 2009) or laser-induced breakdown/atomic fluorescence (Smith et al. 1998) may be adequate for nuclear research, but geochemical applications require much more precise data, largely beyond capabilities of these techniques.

2.3.2.2 Nuclear- and Charged-Particle-Based Techniques

The general use of neutron activation analysis (NAA) in ^{7}Li/^{6}Li determination has been explored, with primary application to the nuclear industry. In principle, the abundance of one of the Li isotopes is determined precisely and total Li abundance is then measured by an independent method; the final ^{7}Li/^{6}Li can then be calculated (Wiernik and Amiel 1970). Wölfle and Neubert (1977) introduced an activation analysis method for simultaneous determination of ^{6}Li and ^{7}Li, and applied it to aqueous solutions, but the approach is less effective for natural samples. On the other hand, Rajan et al. (1980) applied nuclear techniques to ^{7}Li/^{6}Li determination of several stony meteorites, showing largely homogeneous Li isotopic compositions within ±10 ‰ of terrestrial value (given by analysis of spodumene) which is broadly compatible with recent high-precision MC-ICPMS investigations (e.g., Seitz et al. 2007; see Chap. 3) but any inter-sample relations cannot be accounted for by this method. It may be that NAA techniques

(Chao and Tseng 1995; Itoh et al. 1993) and other more or less related methods, such as proton induced gamma-ray emission (Trompetter et al. 1999) or nuclear track detection (Kjellman et al. 1985), remain permissible methods for fast determination of Li contents in geological and other samples (see Räisänen 1992 for review), but they are less useful in determining Li isotopic compositions and their subtle variations at precisions of less than several permil, seriously limit their utility in the examination of a large range of geochemical processes.

2.3.2.3 Resonance Ionization and Other Techniques

Of the less-commonly applied methods to measure Li isotopes, resonance ionization mass spectrometry (RIMS), could offer an alternative to destructive methods (Suryanarayana et al. 1998) due to its extremely low detection limits (on the order of several tens femtograms of Li). The possible application of this technique to cosmochemical studies (Knight et al. 2007; Levine et al. 2009) could provide answers to some fundamental questions of the origin of the Solar system, presuming continued technical advancement. Laser spectroscopy was developed for studies of nuclear properties of different Li isotopes (Hergenröder et al. 1993; Nörtershäuser et al. 2011) but seems to be less applicable to geochemistry.

References

Ahmed S, Jabeen N, ur Rehman E (2002) Determination of lithium isotopic composition by thermal ionization mass spectrometry. Anal Chem 74:4133–4135

Aston FW (1932) The isotopic constitution and atomic weights of caesium, strontium, lithium, rubidium, barium, scandium and thallium. Proc R Soc Lond A 134:571–578

Audétat A, Garbe-Schönberg D, Kronz A, Pettke T, Rusk B, Donovan JJ, Lowers HA (2015) Characterisation of a natural quartz crystal as a reference material for microanalytical determination of Ti, Al, Li, Fe, Mn, Ga and Ge. Geostand Geoanal Res 39:171–184

Aulbach S, Rudnick RL (2009) Origins of non-equilibrium lithium isotopic fractionation in xenolithic peridotite minerals: examples from Tanzania. Chem Geol 258:17–27

Aulbach S, Rudnick RL, McDonough WF (2008) Li-Sr-Nd isotope signature of the plume and cratonic lithospheric mantle beneath the margin of the rifted Tanzanian craton (Labait). Contrib Mineral Petrol 155:79–92

Balsiger H, Geiss J, Groegler N, Wyttenbach A (1968) Distribution and isotopic abundance of lithium in stone meteorites. Earth Planet Sci Lett 5:17–22

Barrat JA, Chaussidon M, Bohn M, Gillet P, Göpel C, Lesourd M (2005) Lithium behavior during cooling of a dry basalt: an ion-microprobe study of the lunar meteorite Northwest Africa 479 (NWA 479). Geochim Cosmochim Acta 69:5597–5609

Beck P, Barrat JA, Chaussidon M, Gillet P, Bohn M (2004) Li isotopic variations in single pyroxenes from the Northwest Africa 480 shergottite (NWA 480): a record of degassing of Martian magmas? Geochim Cosmochim Acta 68:2925–2933

Bell DR, Hervig RL, Buseck PR, Aulbach S (2009) Lithium isotope analysis of olivine by SIMS: calibration of a matrix and application to magmatic phenocrysts. Chem Geol 258:5–16

Bickle MJ, Chapman HJ, You C-F (2000) Measurement of lithium isotopic ratios as lithium tetraborate ions. Int J Mass Spectrom 202:273–282

Brown HL, Biltz C, Anbar M (1977) A precision isotope ratio mass spectrometer for the analysis of ^{6}Li/^{7}Li. Int J Mass Spectrom Ion Phys 25:167–181

Bryant CJ, McCulloch MT, Bennett VC (2003) Impact of matrix effects on the accurate measurement of Li isotope ratios by inductively coupled plasma mass spectrometry (MC-ICP-MS) under "cold" plasma conditions. J Anal Atom Spectrom 18:734–737

Bryant CJ, Chappell BW, Bennett VC, McCulloch MT (2004) Lithium isotopic compositions of the New England Batholith: correlations with inferred source rock compositions. Trans R Soc Edinburgh—Earth Sci 95:199–214

Caciagli N, Brenan JM, McDonough WF, Phinney D (2011) Mineral-fluid partitioning of lithium and implications for slab-mantle interaction. Chem Geol 280:384–398

Carignan J, Vigier N, Millot R (2007) Three secondary reference materials for lithium isotope measurements: Li7-N, Li6-N and LiCl-N solutions. Geostandards Geoanal Res 31:7–12

Chan LH (1987) Lithium isotope analysis by thermal ionization mass spectrometry of lithium tetraborate. Anal Chem 59:2662–2665

Chan LH, Edmond JM (1988) Variation of lithium isotope composition in the marine environment: a preliminary report. Geochim Cosmochim Acta 52:1711–1717

Chan LH, Edmond JM, Thompson G, Gillis K (1992) Lithium isotopic composition of submarine basalts: implication for the lithium cycle in the oceans. Earth Planet Sci Lett 108:151–160

Chan LH, Edmond JM, Thompson G (1993) A lithium isotope study of hot springs and metabasalts from

mid-ocean ridge hydrothermal systems. J Geophys Res 98:9653–9659
Chan LH, Gieskes JM, You C-F, Edmond JM (1994) Lithium isotope geochemistry of sediments and hydrothermal fluids of the Guaymas Basin, Gulf of California. Geochim Cosmochim Acta 58:4443–4454
Chan LH, Leeman WP, You C-F (1999) Lithium isotopic composition of Central American Volcanic Arc lavas: implications for modification of subarc mantle by slab-derived fluids. Chem Geol 160:255–280
Chan LH, Leeman WP, You C-F (2002) Lithium isotopic composition of Central American Volcanic Arc lavas: implications for modification of subarc mantle by slab-derived fluids: correction. Chem Geol 182:293–300
Chao J-H, Tseng C-L (1995) Determination of low-level lithium in environmental water samples by neutron activation. Appl Radiat Isot 46:211–215
Chapman JF, Dale LS (1976) The determination of lithium isotope abundances with a dual-beam atomic absorption spectrometer. Anal Chim Acta 87:91–95
Chapman JF, Dale LS, Fraser HJ (1980) The atomic absorption spectrometric determination of lithium isotope abundances by direct measurement of the absorbance ratio. Anal Chim Acta 116:427–431
Chaussidon M, Robert F (1999) Lithium nucleosynthesis in the Sun inferred from the solar-wind $^{7}Li/^{6}Li$ ratio. Nature 402:270–273
Choi MS, Shin HS, Kil YW (2010) Precise determination of lithium isotopes in seawater using MC-ICP-MS. Microchem J 95:274–278
Choi MS, Ryu J-S, Park HY, Lee K-S, Kil Y, Shin HS (2013) Precise determination of the lithium isotope ratio in geological samples using MC-ICP-MS with cool plasma. J Anal Atom Spectrom 28:505–509
Coogan LA (2011) Preliminary experimental determination of the partitioning of lithium between plagioclase crystals of different anorthite contents. Lithos 125:711–715
Coplen TB, Böhlke JK, De Bièvre P, Ding T, Holden NE, Hopple JA, Krouse HR, Lamberty A, Peiser HS, Révész K, Rieder SE, Rosman KJR, Roth E, Taylor PDP, Vocke RD Jr, Xiao YK (2002) Isotope-abundance variations of selected elements. Pure Appl Chem 74:1987–2017
Datta BP, Khodade PS, Parab AR, Goyal AH, Chitambar SA, Jain HC (1992) Thermal ionisation mass spectrometry of $Li_2BO_2^+$ ions: determination of the isotopic abundance ratio of lithium. Int J Mass Spectrom Ion Proc 116:87–114
Decitre S, Deloule E, Reisberg L, James RH, Agrinier P, Mével C (2002) Behavior of Li and its isotopes during serpentinization of oceanic peridotites. Geochem Geophys Geosys 3, paper number. doi:10.1029/2001GC000178
Dempster AJ (1921) Positive ray analysis of lithium and magnesium. Phys Rev 18:415–422
Eugster O, Bernas R (1971) Li, B, Mg and Ti isotopic abundances and search for trapped solar wind Li in Apollo 11 and Apollo 12 material. Proc Lunar Sci Conf 2:1461–1469
Flesch GD, Anderson AR, Svec HJ (1973) A secondary isotopic standard for $^{6}Li/^{7}Li$ determinations. Int J Mass Spectrom Ion Phys 12:265–272
Galy A, Yoffe O, Janney PE, Williams RW, Cloquet C, Alard O, Halicz L, Wadhwa M, Hutcheon ID, Ramon E, Carignan J (2003) Magnesium isotope heterogeneity of the isotopic standard SRM980 and new reference materials for magnesium-isotope-ratio measurements. J Anal At Spectrom 18:1352–1356
Gradsztajn E, Salome M, Yaniv A, Bernas R (1967) Isotopic analysis of lithium in the Holbrook meteorite and in terrestrial samples with a sputtering ion source mass spectrometer. Earth Planet Sci Lett 3:387–393
Green LW, Leppinen JJ, Elliot NL (1988) Isotopic analysis of lithium as thermal dilithium fluoride ions. Anal Chem 60:34–37
Grégoire DC, Acheson BM, Taylor RP (1996) Measurement of lithium isotope ratios by inductively coupled plasma mass spectrometry: application to geological materials. J Anal Atom Spectrom 11:765–772
Halliday AN, Lee D-C, Christensen JN, Walder AJ, Freedman PA, Jones CE, Hall CM, Yi W, Teagle D (1995) Recent developments in inductively coupled plasma magnetic sector multiple collector mass spectrometry. Int J Mass Spectrom Ion Proc 146/147:21–33
Halliday AN, Lee D-C, Christensen JN, Rehkämper M, Yi W, Luo X, Hall CM, Ballentine CJ, Pettke T, Stirling CH (1998) Applications of multiple collector-ICPMS to cosmochemistry, geochemistry and paleoceanography. Geochim Cosmochim Acta 62:919–940
Hergenröder R, Veza D, Niemax K (1993) Detection limit and selectivity for lithium isotopes in continuous wave field ionization laser spectroscopy. Spectrochim Acta (B) 48:589–569
Heuser A, Eisenhauer A (2008) The calcium isotope composition ($\delta^{44/40}Ca$) of NIST SRM 915b and NIST SRM 1486. Geostand Geoanal Res 32:311–315
Hoefs J, Sywall M (1997) Lithium isotope composition of Quaternary and Tertiary biogene carbonates and a global lithium isotope balance. Geochim Cosmochim Acta 61:2679–2690
Huang K-F, You C-F, Liu Y-H, Wang R-M, Lin P-Y, Chung C-H (2010) Low-memory, small sample size, accurate and high-precision determinations of lithium isotopic ratios in natural materials by MC-ICP-MS. J Anal Atom Spectrom 25:1019–1024
Itoh M, Yamada Y, Kiriyama N, Komura K, Ueno K, Sakanoue M (1993) Neutron activation analysis of low level lithium in water samples. J Radioanal Nucl Chem 172:289–298
Jabeen N, ur Rehman E, Ahmed S (2003) Determination of lithium isotopic composition by thermal ionization mass spectrometry in seawater. J Radioanal Nucl Chem 258:427–430
James RH, Palmer MR (2000) The lithium isotope composition of international rock standards. Chem Geol 166:319–326
Janoušek V, Erban V, Holub FV, Magna T, Bellon H, Mlčoch B, Wiechert U, Rapprich V (2010)

Geochemistry and genesis of behind-arc basaltic lavas from eastern Nicaragua. J Volcanol Geotherm Res 192:232–256

Jeffcoate AB, Elliott T, Thomas A, Bouman C (2004) Precise, small sample size determinations of lithium isotopic compositions of geological reference materials and modern seawater by MC-ICP-MS. Geostand Geoanal Res 28:161–172

Jochum KP, Stoll B, Herwig K, Willbold M, Hofmann AW, Amini M, Aarburg S, Abouchami W, Hellebrand E, Mocek B, Raczek I, Stracke A, Alard O, Bouman C, Becker S, Dücking M, Brätz H, Klemd R, de Bruin D, Canil D, Cornell D, de Hoog CJ, Dalpé C, Danyushevsky L, Eisenhauer A, Gao Y, Snow JE, Groschopf N, Günther D, Latkoczy C, Guillong M, Hauri EH, Höfer HE, Lahaye Y, Horz K, Jacob DE, Kasemann SA, Kent AJR, Ludwig T, Zack T, Mason PRD, Meixner A, Rosner M, Misawa K, Nash BP, Pfänder J, Premo WR, Sun WD, Tiepolo M, Vannucci R, Vennemann T, Wayne D, Woodhead JD (2006) MPI-DING reference glasses for in situ microanalysis: new reference values for element concentrations and isotope ratios. Geochem Geophys Geosys 7, paper number Q02008. doi:10.01029/02005GC001060

Kasemann SA, Jeffcoate AB, Elliott T (2005) Lithium isotope composition of basalt glass reference material. Anal Chem 77:5251–5257

Kim DW (2001) Chromatographic enrichment of lithium isotopes by hydrous manganese(IV) oxide. Bull Korean Chem Soc 22:503–506

Kjellman N, Kristiansson K, Malmqvist L (1985) Selective determination of lithium and boron in minerals by means of an SSNTD-technique. Nucl Instr Methods Phys Res A 235:193–197

Knight KB, Savina MR, Davis AM, Pellin MJ, Levine J, Grossman L, Simon S (2007) Application of RIMS to the study of beryllium chronology in early Solar System condensates. Workshop on the chronology of meteorites and the early Solar System, #4088

Kobayashi K, Tanaka R, Moriguti T, Shimizu K, Nakamura E (2004) Lithium, boron and lead isotope systematics of glass inclusions in olivines from Hawaiian lavas: evidence for recycled components in the Hawaiian plume. Chem Geol 212:143–161

Košler J, Magna T (2014) Developments in clean lab practices. In: McDonough WF (ed) Treatise on geochemistry, vol 15, 2nd edn. Elsevier Ltd., Oxford, pp 111–122

Košler J, Kučera M, Sylvester P (2001) Precise measurement of Li isotopes in planktonic foraminiferal tests by quadrupole ICPMS. Chem Geol 181:169–179

Krankowsky D, Müller O (1967) Isotopic composition and abundance of lithium in meteoritic matter. Geochim Cosmochim Acta 31:1833–1842

Kushita K (1986) Atomic absorption spectrometric determination of the isotopic composition of lithium by an ultimate absorbance-ratio technique. Anal Chim Acta 183:225–230

le Roux PJ (2010) Lithium isotope analysis of natural and synthetic glass by laser ablation MC-ICP-MS. J Anal Atom Spectrom 25:1033–1038

Levine J, Savina MR, Stephan T, Dauphas N, Davis AM, Knight KB, Pellin MJ (2009) Resonance ionization mass spectrometry for precise measurements of isotope ratios. Int J Mass Spectrom 288:36–43

Liu X-M, Rudnick RL, Hier-Majumder S, Sirbescu M-LC (2010) Processes controlling lithium isotopic distribution in contact aureoles: a case study of the Florence County pegmatites, Wisconsin. Geochem Geophys Geosys 11, paper number Q08014. doi:10.01029/02010GC003063

Magna T, Wiechert UH, Halliday AN (2004) Low-blank separation and isotope ratio measurement of small samples of lithium using multiple-collector ICPMS. Int J Mass Spectrom 239:67–76

Magna T, Wiechert U, Halliday AN (2006) New constraints on the lithium isotope compositions of the Moon and terrestrial planets. Earth Planet Sci Lett 243:336–353

Magna T, Janoušek V, Kohút M, Oberli F, Wiechert U (2010) Fingerprinting sources of orogenic plutonic rocks from Variscan belt with lithium isotopes and possible link to the subduction-related origin of some A-type granites. Chem Geol 274:94–107

Magna T, Novák M, Janoušek V (2013) Lithium isotopes in giant pegmatite bodies—implications for their sources and evolution. In: Geological Association of Canada and Mineralogical Association of Canada annual meeting, Winnipeg, Canada. Abstract volume, p 135

Marks MAW, Rudnick RL, McCammon C, Vennemann T, Markl G (2007) Arrested kinetic Li isotope fractionation at the margin of the Ilímaussaq complex, South Greenland: evidence for open-system processes during final cooling of peralkaline igneous rocks. Chem Geol 246:207–230

Marks MAW, Rudnick RL, Ludwig T, Marschall H, Zack T, Halama R, McDonough WF, Rost D, Wenzel T, Vicenzi EP, Savov IP, Altherr R, Markl G (2008) Sodic pyroxene and sodic amphibole as potential reference materials for *in situ* lithium isotope determinations by SIMS. Geostand Geoanal Res 32:295–310

Meier AL (1982) Determination of lithium isotopes at natural abundance levels by atomic absorption spectrometry. Anal Chem 54:2158–2162

Michiels E, De Bièvre P (1983) Absolute isotopic composition and the atomic weight of a natural sample of lithium. Int J Mass Spectrom Ion Phys 49:265–274

Millot R, Guerrot C, Vigier N (2004) Accurate and high-precision measurement of lithium isotopes in two reference materials by MC-ICP-MS. Geostand Geoanal Res 28:153–159

Millot R, Petelet-Giraud E, Guerrot C, Négrel P (2010) Multi-isotopic composition (δ^7Li–δ^{11}B–δ D–δ^{18}O) of

rainwaters in France: Origin and spatio-temporal characterization. Appl Geochem 25:1510–1524

Misra S, Froehlich PN (2009) Measurement of lithium isotope ratios by quadrupole-ICP-MS: application to seawater and natural carbonates. J Anal Atom Spectrom 24:1524–1533

Moriguti T, Nakamura E (1998) High-yield lithium separation and the precise isotopic analysis for natural rock and aqueous samples. Chem Geol 145:91–104

Nishio Y, Nakai S (2002) Accurate and precise lithium isotopic determinations of igneous rock samples using multi-collector inductively coupled plasma mass spectormetry. Anal Chim Acta 456:271–281

Négrel P, Millot R, Brenot A, Bertin C (2010) Lithium isotopes as tracers of groundwater circulation in a peat land. Chem Geol 276:119–127

Nörtershäuser W, Sánchez R, Ewald G, Dax A, Behr J, Bricault P, Bushaw BA, Dilling J, Dombsky M, Drake WF, Götte S, Kluge H-J, Kühl T, Lassen J, Levy CDP, Pachucki K, Pearson M, Puchalski M, Wojtaszek A, Yan Z-C, Zimmermann C (2011) Isotope-shift measurements of stable and short-lived lithium isotopes for nuclear-charge-radii determination. Phys Rev A 83, paper number 012516

Oi T, Odagiri T, Nomura M (1997) Extraction of lithium from GSJ rock reference samples and determination of their isotopic compositions. Anal Chim Acta 340:221–225

Penniston-Dorland SC, Sorensen SS, Ash RD, Khadke SV (2010) Lithium isotopes as a tracer of fluids in a subduction zone mélange: Franciscan Complex, CA. Earth Planet Sci Lett 292:181–190

Poschenrieder WP, Herzog RF, Barrington AE (1965) The relative abundance of the lithium isotopes in the Holbrook meteorite. Geochim Cosmochim Acta 29:1193–1195

Qi HP, Coplen TB, Wang QZ, Wang YH (1997a) Unnatural isotopic composition of lithium reagents. Anal Chem 69:4076–4078

Qi HP, Taylor PDP, Berglund M, De Bièvre P (1997b) Calibrated measurements of the isotopic composition and atomic weight of the natural Li isotopic reference material IRMM-016. Int J Mass Spectrom Ion Proc 171:263–268

Räisänen J (1992) Analysis of lithium by ion beam methods. Nucl Instr Methods Phys Res B 66:107–117

Rajan RS, Brown L, Tera F, Whitford DJ (1980) Lithium isotopic composition in some stone meteorites. Earth Planet Sci Lett 51:41–44

Reynolds BC, Georg RB, Oberli F, Wiechert U, Halliday AN (2006) Re-assessment of silicon isotope reference materials using high-resolution multi-collector ICP-MS. J Anal At Spectrom 21:266–269

Richter FM, Davis AM, DePaolo DJ, Watson EB (2003) Isotope fractionation by chemical diffusion between molten basalt and rhyolite. Geochim Cosmochim Acta 67:3905–3923

Rosner M, Ball L, Peucker-Ehrenbrink B, Bluzstajn J, Bach W, Erzinger J (2007) A simplified, accurate and fast method for lithium isotope analysis of rocks and fluids, and δ^7Li values of seawater and rock reference materials. Geostandards Geoanal Res 31:77–88

Sahoo SK, Masuda A (1995a) High precision isotopic measurement of lithium by thermal ionization mass spectrometry. Int J Mass Spectrom Ion Proc 151:189–196

Sahoo SK, Masuda A (1995b) Simultaneous measurement of lithium and boron isotopes as lithium tetraborate ion by thermal ionization mass spectrometry. Analyst 120:335–339

Sahoo SK, Masuda A (1998) Precise determination of lithium isotopic composition by thermal ionization mass spectrometry in natural samples such as seawater. Anal Chim Acta 370:215–220

Seitz H-M, Brey GP, Lahaye Y, Durali S, Weyer S (2004) Lithium isotopic signatures of peridotite xenoliths and isotopic fractionation at high temperature between olivine and pyroxenes. Chem Geol 212:163–177

Seitz H-M, Brey GP, Zipfel J, Ott U, Weyer S, Durali S, Weinbruch S (2007) Lithium isotope composition of ordinary and carbonaceous chondrites, and differentiated planetary bodies: bulk solar system and solar reservoirs. Earth Planet Sci Lett 260:582–596

Schauble EA (2004) Applying stable isotope fractionation theory to new systems. In: Johnson CM, Beard BL, Albarède F (eds) Geochemistry of non-traditional stable isotopes. Rev Mineral Geochem 55:65–111

Schönbächler M, Fehr MA (2014) Basics of ion exchange chromatography for selected geological applications. In: McDonough WF (ed vol 15) Treatise on geochemistry, 2nd edn. Elsevier Ltd., Oxford, pp 123–146

Simons KK, Harlow GE, Brueckner HK, Goldstein SL, Sorensen SS, Hemming NG, Langmuir CH (2010) Lithium isotopes in Guatemalan and Franciscan HP–LT rocks: insights into the role of sediment-derived fluids during subduction. Geochim Cosmochim Acta 74:3621–3641

Smith BW, Gornuskhin IB, King LA, Winefordner JD (1998) A laser ablation-atomic fluorescence technique for isotopically selective determination of lithium in solids. Spectrochim Acta (B) 53:1131–1138

Strelow FWE, Weinert CHSW, van der Walt TN (1974) Separation of lithium from sodium, beryllium and other elements by cation-exchange chromatography in nitric acid-methanol. Anal Chim Acta 71:123–132

Sun XF, Ting BTG, Zeisel SH, Janghorbani M (1987) Accurate measurement of stable isotopes of lithium by inductively coupled plasma mass spectrometry. Analyst 112:1223–1228

Suryanarayana MV, Sankari M, Gangadharan S (1998) Determination of ^{6}Li/^{7}Li isotope ratio using two photon resonance three photon resonance ionization mass spectrometry. Int J Mass Spectrom Ion Proc 173:177–189

Svec HJ, Anderson AR (1965) The absolute abundance of the lithium isotopes in natural sources. Geochim Cosmochim Acta 29:633–641

Svec HJ, Anderson AR (1966) A mass spectrometer for the precise assay of the lithium isotopes. J Sci Instrum 43:134–137

Su B-X, Gu X-Y, Deloule E, Zhang H-F, Li Q-L, Li X-H, Vigier N, Tang Y-J, Tang G-Q, Liu Y, Pang K-N, Brewer A, Mao Q, Ma Y-G (2015) Potential orthopyroxene, clinopyroxene and olivine reference materials for in situ lithium isotope determination. Geostand Geoanal Res 39:357–369

Šulcek Z, Rubeška J (1969) Bestimmung des Lithiumspurengehaltes in Gesteinen. Collect Czechoslovak Chem Commun 34:2048–2056

Šulcek Z, Povondra P, Štangl R (1965) Chromatographische Trennung der Lithium- und Natriumionen. Collect Czechoslovak Chem Commun 30:380–387

Taylor TI, Urey HC (1938) Fractionation of the lithium and potassium isotopes by chemical exchange with zeolithes. J Chem Phys 6:429–438

Teng F-Z, McDonough WF, Rudnick RL, Dalpé C, Tomascak PB, Chappell BW, Gao S (2004) Lithium isotopic composition and concentration of the upper continental crust. Geochim Cosmochim Acta 68:4167–4178

Teng F-Z, McDonough WF, Rudnick RL, Walker RJ (2006) Diffusion-driven extreme lithium isotopic fractionation in country rocks of the Tin Mountain pegmatite. Earth Planet Sci Lett 243:701–710

Teng F-Z, Rudnick RL, McDonough WF, Gao S, Tomascak PB, Liu Y (2008) Lithium isotopic composition and concentration of the deep continental crust. Chem Geol 255:47–59

Teng F-Z, Rudnick RL, McDonough WF, Wu F-Y (2009) Lithium isotopic systematics of A-type granites and their mafic enclaves: further constraints on the Li isotopic composition of the continental crust. Chem Geol 262:370–379

Tomascak PB (2004) Developments in the understanding and application of lithium isotopes in the Earth and planetary sciences. In: Johnson CM, Beard BL, Albarède F (eds) Geochemistry of non-traditional stable isotopes. Rev Mineral Geochem 55:153–195

Tomascak PB, Carlson RW, Shirey SB (1999) Accurate and precise determination of Li isotopic compositions by multi-collector sector ICP-MS. Chem Geol 158:145–154

Trompetter WJ, Reyes AG, Vickridge IC, Markwitz A (1999) Lithium and boron distributions in geological samples. Nucl Instr Methods Phys Res B 158:568–574

ur Rehman E, ur Rehman S, Ahmed S (2009) ^{6}Li atom percentage determination by atomic absorption-emission spectrometry using a natural lithium hollow cathode lamp. Appl Spectrosc 63:971–973

Vanhoe H, Vandecasteele C, Versieck J, Dams R (1991) Determination of lithium in biological samples by inductively coupled plasma mass spectrometry. Anal Chim Acta 244:259–267

Wheat JA (1971) Iosotpic analysis of lithium by atomic absorption spectrophotometry. Appl Spectrosc 25:328–330

Wiernik M, Amiel S (1970) Determination of lithium and its isotopic composition by activation analysis and measurement of ^{8}Li and ^{17}N. J Radioanal Chem 5:123–131

Wieser ME (2006) Atomic weights of the elements 2005 (IUPAC technical report). Pure Appl Chem 78:2051–2066

Wizemann HD, Niemax K (2000) Measurement of ^{7}Li/^{6}Li isotope ratios by resonant Doppler-free two-photon diode laser atomic absorption spectroscopy in a low-pressure graphite furnace. Spectrochim Acta (B) 55:637–650

Wölfle R, Neubert A (1977) Determination of isotopic composition of lithium by neutron activation analysis; comparison with mass spectrometry. J Radioanal Chem 39:375–384

Xu R, Liu Y, Tong X, Hu Z, Zong K, Gao S (2013) In-situ trace elements and Li and Sr isotopes in peridotite xenoliths from Kuandian, North China Craton: Insights into Pacific slab subduction-related mantle modification. Chem Geol 354:107–123

Xiao YK, Beary ES (1989) High-precision isotopic measurement of lithium by thermal ionization mass spectrometry. Int J Mass Spectrom Ion Proc 94:101–114

You C-F, Chan LH (1996) Precise determination of lithium isotopic composition in low concentration natural samples. Geochim Cosmochim Acta 60:909–915

You C-F, Chan LH, Spivack AJ, Gieskes JM (1995) Lithium, boron and their isotopes in sediments and pore waters of Ocean Drilling Program Site 808, Nankai trough: implications for fluid expulsion in accretionary prisms. Geology 23:37–40

Zack T, Tomascak PB, Rudnick RL, Dalpé C, McDonough WF (2003) Extremely light Li in orogenic eclogites: the role of isotope fractionation during dehydration in subducted oceanic crust. Earth Planet Sci Lett 208:279–290

Cosmochemistry of Lithium

3

3.1 Cosmology of Lithium: Big Bang Nucleosynthesis, Evolution of the Universe, and Stellar Processes

The purpose of this chapter is to inform the reader in a simplified way about the importance of Li in astrophysics and stellar physics and its impact (i) on extreme processes and events taking place during Big Bang Nucleosynthesis (hereafter referred to as BBN) and shortly after the BBN ceased, and (ii) after more regular processes of forming new matter of the Universe were launched. For a more interested reader the literature is rich in studies dealing with the history of light nuclei during the evolution of our Galaxy (e.g., Prantzos 2012) as well as the perspective on evolution of Li during cosmic history (see reviews by Reeves 1994; Iocco et al. 2009, for example, or recent proceedings edited by Charbonnel et al. 2009).

3.1.1 The Earliest History and Further Evolution of Lithium

With the advent of and further improvements in astronomical and astrophysical observations, it became clear that Li belongs to the few key elements that may provide critical information on the earliest history of cosmic matter as well as place stringent constraints on stellar evolution. This stems from the fact that Li, more precisely ^{7}Li, is among the very few stable species synthesized during the Big Bang Nucleosynthesis (BBN), the others being ^{2}H (≡D; deuterium), ^{3}He, ^{4}He, and a few radioactive nuclei like ^{3}H (≡T; tritium, decaying to ^{3}He). A number of other very short-lived nuclei (e.g., ^{11}C) that either decayed or participated in subsequent fusion reactions (Fig. 3.1) and perhaps paltry amounts of stable ^{9}Be (^{9}Be/H $\sim 10^{-18}$) were also produced by the end of the BBN process.

Lithium-7 is an important child of BBN and can be produced by two chains of reactions: (i) T $(\alpha,\gamma)^{7}$Li, and (ii) ^{3}He$(\alpha,\gamma)^{7}$Be$(n,p)^{7}$Li. The ^{7}Be → ^{7}Li decay via electron capture appears to be responsible for c. 90 % of the ^{7}Li formed during BBN; the remaining ∼10 % was synthesized directly as primordial ^{7}Li. The ^{7}Be half-life of c. 53.1 days was measured by Jaeger et al. (1996) while the half-life of 53.22 days is given by Audi et al. (2003). Despite its consumption much ^{7}Be remained alive until BBN ceased (Fig. 3.2).

Conversely, ^{7}Li is mostly destroyed by the reaction ^{7}Li$(p,\alpha)^{4}$He. Overall, the T → ^{7}Li reaction is the most important, but at high baryonic densities (roughly speaking a ratio of protons and neutrons to photons) the ^{7}Li → ^{4}He reaction appears to reach approximately similar leverage, balancing the contribution from T → ^{7}Li reaction, and under such conditions Li is mainly produced by the decay of ^{7}Be.

The BBN contribution to cosmic Li abundances can be observed from a so called "Spite plateau" (Fig. 3.3) in the Li/H versus [Fe/H] plot of old halo stars. The ratio [Fe/H] is called metallicity, the abundance of all elements in stars

P.B. Tomascak et al., *Advances in Lithium Isotope Geochemistry*,
Advances in Isotope Geochemistry, DOI: 10.1007/978-3-319-01430-2_3

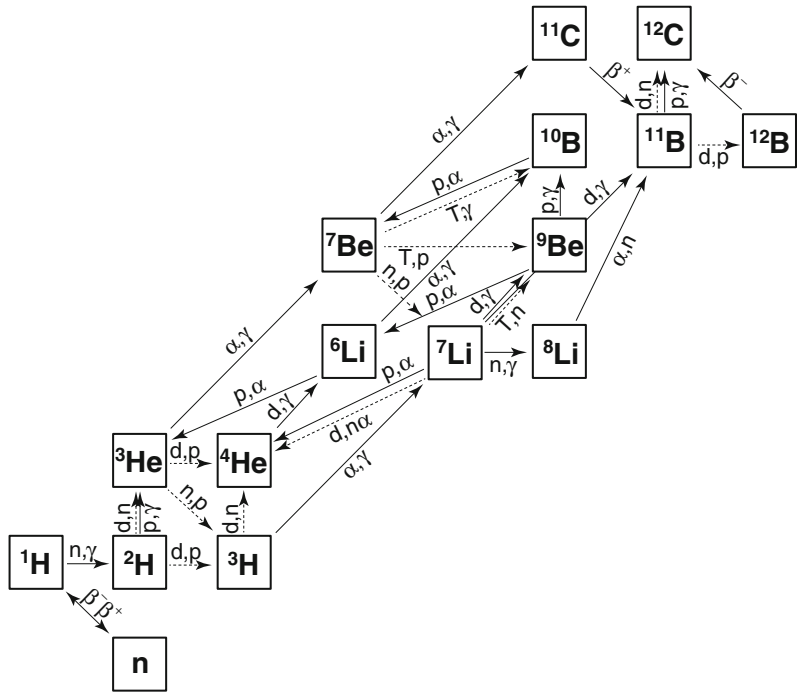

Fig. 3.1 Big Bang Nucleosynthesis (BBN) nuclear reactions up to CNO (modified from Coc et al. 2012). Deuterium formation represents a key event for the subsequent chain of nuclear reactions

heavier than H and He. It is defined as follows: $[Fe/H] = \log_{10} (N_{Fe}/N_H)_{star} - \log_{10}(N_{Fe}/N_H)_{Sun}$ (N = number of atoms per unit of volume; Fe is taken as an element that is easy to measure in the visible spectrum and, more importantly, an element fully synthesized in stars and not during BBN). Ancient metal-poor halo stars have constant ^{7}Li abundances for a large range of metallicities whereas abundances of those nuclei that are produced during the galactic epoch (such as Be and B) increase almost constantly (Spite and Spite 1982). Earlier calculations implied that for the standard BBN theory, primordial ^{7}Li/H abundance is between 5×10^{-10} and 2×10^{-9} and that over the history of the Universe ^{7}Li abundance has steadily grown and decreased (Delbourgo-Salvador et al. 1985; Steigman 1993). Predictive theoretical models for the primordial BBN ^{7}Li abundance suggest a very narrow range between $8 \times 10^{-11} < {}^7\text{Li/H} < 2 \times 10^{-10}$ (Steigman and Walker 1992). This range is consistent with the estimates of Audouze et al. (1983) and Reeves (1994) at ^{7}Li/H between 1 and 3×10^{-10}, with more elaborate calculations of Ryan et al. (2000) at $\sim 1.2 \times 10^{-10}$, and with empirical observations for warm ($T \geq \sim 5500$ K) metal-poor ([Fe/H] ≤ –1.3) Population II stars (Spite and Spite 1982). The revised calculations, underscored by advancements both in the experimentally determined cross-section of the ^{3}He(α, γ)^{7}Be reaction (important for production of ^{7}Li) and tighter constraints placed on the cosmic baryon density using Wilkinson Microwave Anisotropy Probe (WMAP) measurements, have delimited the primordial ^{7}Li/H at $\sim 5.2 \times 10^{-10}$ (Cyburt et al. 2008).

Yet, a so-called "cosmic lithium problem" still exists: the predicted Li abundance is a factor of 2–4 higher than the observed (Asplund et al. 2006; Coc 2013; Fields 2011). This appears to impart unsolved problems to the existing models of particle physics. Fields (2011) offers several solutions to this "cosmic lithium problem" with respect to astrophysical observations, cosmological models of BBN predictions and more complex solutions beyond standard models of particle physics. The recent observations of up to several-times larger ^{7}Li depletions (lower than would be predicted solely by BBN) in very old Population II dwarfs with [Fe/H] <–4 (e.g., Caffau et al. 2011; Sbordone et al. 2010) combined with a significant scatter of the Spite plateau at

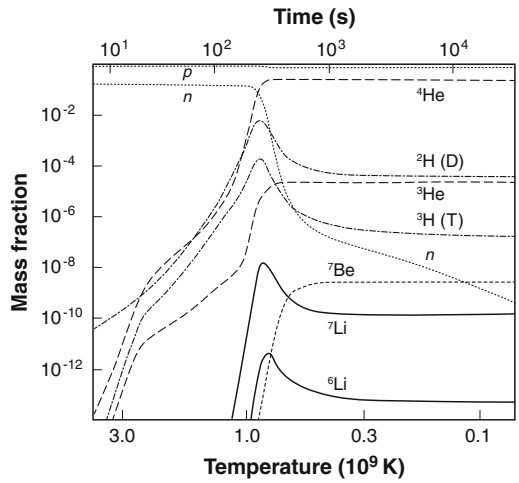

Fig. 3.2 Production of light nuclei during BBN (modified from Coc et al. 2012). The abundance of other stable nuclei (e.g., ^{9}Be, CNO) was several orders of magnitude lower

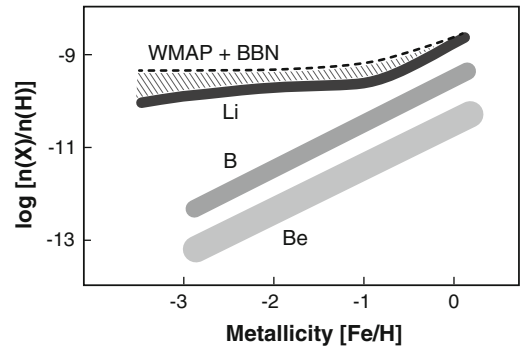

Fig. 3.3 Schematic plot of abundance of light elements (Li, Be, B) as a function of stellar metallicity. The so-called Spite plateau is apparent for Li whereas abundance of Be and B grows constantly over a range of metallicities. The difference between modern predictions (*dashed line*) and long-term observations of Li abundance in stars (*dark grey solid line*) is depicted by a stippled area

such low and even lower metallicities (so-called "meltdown") may imply not-yet completely understood astrophysical processes causing the dispersion of Li abundance in these otherwise very similar, metal-deficient old stars rather than invoking new cosmological theories. These latter observations may also imply high temperatures ($>2 \times 10^6$ K) in the prior history of stellar material with extreme Li depletions on the order of up to 10^5 or, alternatively, distinct stellar processes that could once have led to efficient depletion in Li.

Whereas recent findings of Howk et al. (2012) are in broad agreement with combined WMAP + BBN predictions, their observations also tell us very little about primordial lithium. The reason is that Howk et al. (2012) observed lithium in a gas cloud system whose metallicity is intermediate between primordial (i.e., very low metallicity of the Spite plateau stars) and Solar. It has been known that in its post-BBN evolution, the lithium abundance increased from a low primordial value to the value inferred from the Solar System or from the interstellar medium of the Galaxy. The results of Howk et al. (2012) are expectedly intermediate between the Spite plateau and the Solar abundance but they lack a model for evolution of the primordial abundance of Li.

During the subsequent evolution of the Universe, primordial ^{7}Li decreased due to astration, the destruction of ^{7}Li in stars (in particular important at high metallicities), but was constantly replaced by production from other sources. For low-metallicity stars, ^{7}Li started to be continuously produced during stellar nucleosynthesis and through spallation reactions on C, N, and O nuclei as well as α + α fusion reactions of Galactic Cosmic Rays (GCR) interacting with the interstellar medium (ISM). In this respect, it is noteworthy that stellar Li–Be–B depletion is not paralleled by lowered GCR Li–Be–B abundances (Fig. 3.4). This clearly supports GCR as an important input of these light nuclei. It is also speculated that a less significant proportion of ^{7}Li may perhaps be formed in core-collapse Type II supernovae by neutrino interactions with predominantly ^{4}He and ^{12}C (Woosley et al. 1990) in AGB stars (e.g., Romano et al. 2001) and by $^{7}\text{Be} \rightarrow {}^{7}\text{Li}$ reaction in novae, the latter type of stars being among significant Li suppliers (Romano et al. 2001; Tajitsu et al. 2015).

Contrary to the clear variability in ^{7}Li production owing to three different mechanisms (BBN, GCR, stellar nucleosynthesis), ^{6}Li is nearly solely produced by spallative interactions of GCR with ISM. A very subordinate proportion of ^{6}Li was probably synthesized during BBN. The BBN production of ^{6}Li is dominated by the $D(\alpha,\gamma)^{6}Li$ reaction, which is largely ineffective,

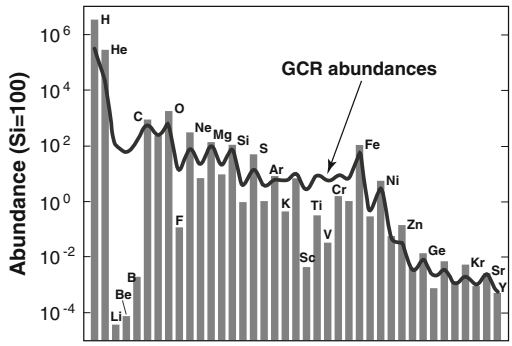

Fig. 3.4 Solar abundance of elements (in order of increasing Z, up to 39) normalized to Si, relative to Galactic Cosmic Ray abundance (*dark grey line*). Notably, light nuclei (Li, Be, B) are depleted in the Sun, attesting to significant production of these nuclei in GCR reactions and consumption in the Sun

producing only vanishingly small amounts of ^{6}Li (Fig. 3.1). Thus, the primordial ^{6}Li/H was variously estimated at $\sim 10^{-14}$ levels (i.e., ^{7}Li/^{6}Li $\sim 10^{4}$; Hammache et al. 2010; Nollett et al. 1997; Vangioni-Flam et al. 2000, 1999). Most ^{6}Li is produced by much more efficient spallation-induced energetic collisions of GCR through *p*, α + He and CNO → ^{6}Li, ^{7}Li, and fast nuclei (α, C, O) fragmenting on H and He in the ISM (Vangioni-Flam et al. 1999). We refer to a detailed review by Prantzos (2012) for the history and physical processes of Li evolution.

It is generally accepted that the combined reactions of energetic cosmic ray C–N–O nuclei, and cosmic ray H–He interacting with ambient interstellar C, N and O species produce low-energy Li, Be and B nuclei. Indeed, it has been suggested by some that the latter process, which is an important part of the galactic chemical evolution, may dominate the overall production of modern Li in the Galaxy. This is depicted in Fig. 3.4 where the six orders difference between Solar abundances and those determined for GCR manifests an important contribution by GCR reactions to the total Li budget (and also budgets of Be and B). We stress here that the ISM abundance of Li is largely unknown or, at least, less well constrained due to technical difficulties, such as extreme proximity of spectroscopic resonance lines accessible for Li abundance measurements (Steigman 1993). Moreover, it may be plausible that a large fraction of Li is bound in molecules like LiH, or is depleted from the gas into microscopic dust particles known to commonly exist in ISM. The extent of this depletion is largely unknown, however, but may play important role.

Also interesting are the production rates of individual Li isotopes for GCR processes. Audouze et al. (1983) calculated that the maximum production ^{7}Li/^{6}Li$_{GCR}$ cannot exceed 6–7 and ^{7}Li/^{6}Li$_{GCR}$ production ratios as low as ~ 1 were also reported (e.g., Garcia-Munoz et al. 1975; Meneguzzi et al. 1971; Webber et al. 2002). This would mean that either an additional source of ^{7}Li, or a mechanism to efficiently destroy ^{6}Li, or a combination of both, are needed, during Galactic evolution. In fact, lifetime in the stellar environment is $\sim 100 \times$ shorter for ^{6}Li compared to ^{7}Li given the greater fragility of the former nuclide at high temperatures, and it appears that in massive stars initial ^{7}Li was not destroyed (Audouze et al. 1983). Alternatively, it was destroyed but was subsequently compensated for by synthesis of ^{7}Li in the neutrino process. Several measurements of Li abundance in ISM regions yielded Li/H of ~ 0.6 to 4×10^{-10} (Knauth et al. 2003) although Li abundance may vary between distinct ISM regions. The measurements of ISM appear to find Li isotopic ratios that are somewhat lower than meteoritic ^{7}Li/^{6}Li (e.g., Ferlet and Dennefeld 1984). Meyer et al. (1993) reported ^{7}Li/^{6}Li values for two ISM regions between 5.5 and 6.8 whereas Lemoine et al. (1993) found ISM ratios which were very close to meteoritic (~ 12).

These variations were further underscored by later data from Knauth et al. (2000), who reported on observations of ^{6}Li and ^{7}Li abundance in several interstellar clouds, with ^{7}Li/^{6}Li ratios varying between 1.7 and 10.6 (i.e., broadly meteoritic vs. highly non-Solar). The decreased ^{7}Li/^{6}Li is suggested to derive from recent massive interactions with energetic particles that may result in ^{7}Li/^{6}Li ratios as low as ~ 1 through cosmic ray spallation (see above). Knauth et al. (2000) also estimated the interstellar Li/H abundance at $\sim 1 \times 10^{-9}$ and speculated that low ^{7}Li/^{6}Li ~ 2 may be intrinsic to the interstellar gas and that contamination with

high-^{7}Li/^{6}Li material would be warranted. The weighted mean ^{7}Li/^{6}Li of 7.6 ± 2.3 (1σ) in several ISM regions was more recently given by Kawanomoto et al. (2009). Such Li isotopic variability of the ISM was corroborated by Knauth et al. (2003) who investigated ^{7}Li/^{6}Li ratios of ISM in the vicinity of active star-forming regions. These authors confirmed low ^{7}Li/^{6}Li ratios in several ISM regions but they also provided additional support for ^{7}Li/^{6}Li ratios that are approximately chondritic (c. 12.5).

3.1.2 The Vicinity of the Solar System

The ^{7}Li/^{6}Li ratios of the local ISM appear to be generally in the Solar range, based on observations of other elements (Be, C, O) whose abundances are consistent with an input from environment where some Li is also synthesized, such as asymptotic giant branch stars, Type II supernovae or GCR. Webber et al. (2002) have used data collected with the *Voyager* 1 and 2 spacecraft and included periods where levels of the Solar modulation of energy spectra of various nuclei (^{6}Li, ^{7}Li, ^{7}Be, ^{9}Be, ^{10}B and ^{11}B) were at minima (1986–1988, 1996–2000). From these measurements, interstellar production of ^{7}Li/^{6}Li was estimated to be about 1.4–1.5, consistent with most models of spallogenic ^{7}Li/^{6}Li (see Vangioni-Flam et al. 1999, for a discussion). Consistently, for population I stars such as the Sun, a spallogenic ^{7}Li/^{6}Li of 1.38 was calculated (Steigman and Walker 1992). An additional free parameter requiring consideration is the possible galactocentric variation in ^{7}Li/^{6}Li. Kawanomoto et al. (2009) suggested that such variation appears to be nonexistent for Li isotopes whereas it has been clearly demonstrated for D/H and T/H. On the other hand, advanced modelling of Prantzos (2012) shows that there may be a gradient in our Galaxy both in Li abundance and ^{7}Li/^{6}Li which would be consistent with an increased metallicity toward the inner disc of the Milky Way (Fig. 3.5). These theoretical predictions remain to be yet evaluated.

Reproduction of the depletion in the Solar Li abundance relative to meteoritic Li contents is an important aspect in stellar evolution models and cosmology. Ahrens et al. (1992) discussed that Li depletion of the Sun may have been completed during its pre-main sequence evolution, but this depends on the abundances of He and other metals, on the mixing length, and the thickness of an extra mixing layer. Some ∼200,000 km for the convective zone in the Sun, responsible for Li depletion, was calculated. However, if Li depletion by a factor of ∼150× is considered (roughly the extent of depletion found in the Sun relative to meteoritic matter; Anders and Grevesse 1989), then parallel problems arise with too little Be depletion compared to the observations. Here, we stress that beside Li, only a few other elements show depletion in the Sun relative to chondritic meteorites by the factor of ∼100 (Te, I, Cs and Hg; see a recent compilation in Palme et al. 2014). This is important to note because Solar elemental abundances in fact are similar to those in the meteorites; from the group of light elements Li–Be–B, Li is the most depleted in the Sun (Asplund et al. 2009).

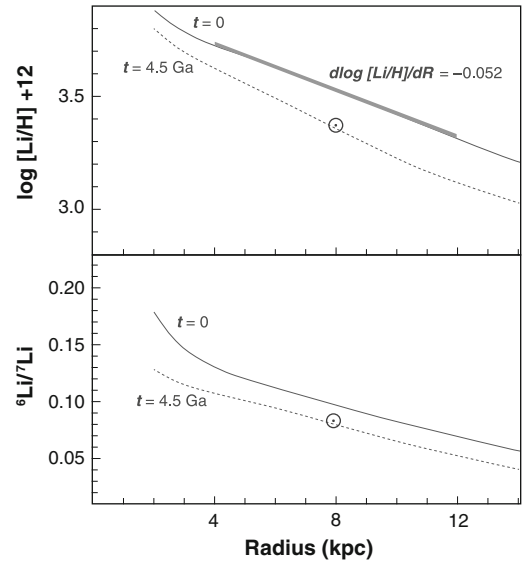

Fig. 3.5 Model calculations of Li abundance (**a**) and ^{6}Li/^{7}Li ratio (**b**) as functions of radial distance from the center of the Milky Way disc (after Prantzos 2012). *Dashed curve* = 4.5 Ga, *solid curve* = present. Thick segments were used to calculate the slope in **a**. More exact evaluation of Li isotopic ratios is hindered by uncertainties in ^{7}Li yields of low-mass sources, ^{6}Li/^{7}Li ratios of ISM, and possible reactions between ISM and GCR (Prantzos 2012)

The major outcome of the calculations of Ahrens et al. (1992) is that any generalization for stars other than Sun should be avoided, or, at least, carefully examined. Indeed, some stars of a Sun-like mass still maintain Li abundances more or less in the range of the original starting values. It follows that the problem lies in reducing or avoiding Li burning in the pre-main sequence evolution rather than proposing mechanisms of Li burning in the main sequence. As a consequence, the Sun may not be the proper choice for calibrating the extent of Li depletion in stellar regions because in this range of solar masses the dependence of Li depletion on the depth of mixing is scaled up. This was also noted by Steigman (1993) who summarized that stellar production of ^{7}Li was very subordinate during ~4.6 Gyr existence of the Solar System. They suggested that, perhaps, the Sun is not representative of the local ISM at ~4.6 Ga so that Li–Be–B abundances may in fact be overabundant. Moreover, there is a difference between the primordial Li abundance of the Galaxy and the Solar System; Audouze et al. (1983) estimated the primordial Galactic Li abundance at Li/H of $11.8 \pm 3.2 \times 10^{-11}$ whereas the Solar System Li/H starting value was estimated to be as high as $\sim 2 \times 10^{-9}$, requiring enrichments in Li during the Galactic history.

In contrast to general Li depletion in the Sun, some other classes of stars may carry far higher Li loads. Values up to 400× higher than primordial ^{7}Li (Scalo 1976) are quite often observed in giants of various classes (e.g., Brown et al. 1989; Carlberg et al. 2010; Koch et al. 2011; Monaco et al. 2011; Smith et al. 1995; Wallerstein and Sneden 1982), although the nature of these enrichments is not yet completely clear. The ^{7}Li/^{6}Li ratios in these massive stars do not differ from Li-poor regular stellar bodies (Andersen et al. 1984). It may be that ^{3}He circulating from stellar atmospheres into deeper zones transforms into ^{7}Be which decays to ^{7}Li through (α,γ) reaction (Monaco et al. 2011). An important factor in this reaction (see also Sect. 3.1.1) is the need for a hot stellar environment (>10^{7} K) to produce ^{7}Be and its fast transport to cooler subsurface layers (<3×10^{6} K) where the freshly synthesized ^{7}Li is not consumed in nuclear reactions; it is called the Cameron–Fowler transport mechanism (Cameron and Fowler 1971). Capture of a sub-stellar body would enhance abundances of other refractory elements or would have other consequences, none of which, however, are observed (Koch et al. 2011; Kumar et al. 2011).

The photosphere of the Sun (and by inference the Sun as a whole) is depleted in Li by two orders of magnitude compared with meteoritic abundance (~150×; Anders and Grevesse 1989; Asplund et al. 2009), yet it carries distinctively high ^{7}Li/^{6}Li > 33 as measured in sunspots (Ritzenhoff et al. 1997). Technically, sunspots are cooler surface regions and their Li spectra should thus be better resolved; indeed, evidence is provided for small but resolvable amounts of ^{6}Li (Ritzenhoff et al. 1997). The high ^{7}Li/^{6}Li ratios in the Sun probably are the result of differential destruction rates of ^{6}Li and ^{7}Li at 2×10^{6} and $\sim 2.5 \times 10^{6}$ K, respectively (Delbourgo-Salvador et al. 1985). The isotopically heavy values found for sunspots were also obtained in physical samples of implanted solar wind particles in lunar soils. Chaussidon and Robert (1999) provided an estimate for ^{7}Li/^{6}Li > 31 in the solar wind through ion microprobe shallow-depth in situ profiling of exposed lunar soil grains, resulting in a reasonable match between astrophysical predictions and cosmochemical approaches. The analyses also showed that both the solar wind and spallogenic Li penetrate the very surface of lunar materials no deeper than a few tenths of a micrometer. The observation of heavy Li in the outer shells of lunar soil particles was confirmed later by Magna et al. (2006) although not yielding such high ^{7}Li/^{6}Li ratios given the different methodology used to investigate lunar samples.

It is critical to note that, through time, stellar ^{7}Li/^{6}Li ratios might have undergone significant modifications due to stellar processes, as discussed above, while meteoritic Li isotopic ratios appear to be more or less constant over the lifetime of our Solar System. However, the ^{7}Li/^{6}Li at the Solar System start is unknown and alternative ^{7}Li/^{6}Li evolution of the Sun can be sketched

(Fig. 3.6). We cannot therefore postulate unambiguously that the Sun represents the interstellar gas composition at the time of formation at ~4.6 Ga. This may imply a process-oriented dichotomy in Li isotopic evolution of gaseous and solid materials of the Solar System. Of course, for the latter we do have physical samples in the form of primitive and evolved meteorites such as chondrites and meteorites from Mars and asteroidal bodies such as Vesta, as well as samples from the Moon, collectively spanning time from the beginning of the Solar System until present. In general, although the Li isotopic compositions of Solar System solids and the Sun differ significantly today, it may well be that the bulk Solar System started with a more uniform and perhaps chondritic $^{7}Li/^{6}Li$ ~12, or perhaps even a lower value reflecting low $^{7}Li/^{6}Li$ ratios typical of ISM, and evolved to the Sun's present-day $^{7}Li/^{6}Li$ ~33 (see above) as a consequence of stellar processes. Over the same time the composition would have remained essentially constant for solid residua of the Solar proto-nebula from which planets accreted because the accretion process, including multiple impacts, runaway collisions and oligarchic growth of planets, did not impose conditions necessary for major changes in the ratio of Li isotopes.

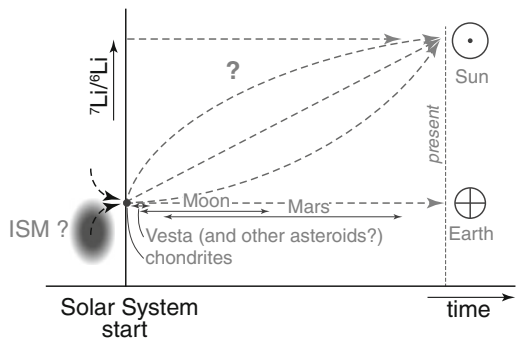

Fig. 3.6 Schematic evolution of $^{7}Li/^{6}Li$ in our Solar System. Solid materials (Earth, Mars, Moon, asteroids, meteorites) all have a constant Li isotopic ratio at ~12 whereas Solar $^{7}Li/^{6}Li$ ratio has apparently evolved toward higher values as a consequence of preferential destruction of ^{6}Li over ^{7}Li. It is unclear, however, what $^{7}Li/^{6}Li$ ratio our Sun started with. Also, local ISM prior to formation of Solar System might have had a range of $^{7}Li/^{6}Li$ ratios and the present-day $^{7}Li/^{6}Li$ value may not necessarily reflect that of a new-born Solar nebula

The uncertainty in deconvolving the history and evolution of $^{7}Li/^{6}Li$ of the Sun may, to some extent, be linked with variations in $^{7}Li/^{6}Li$ ratios of other stars. It is generally difficult to obtain $^{7}Li/^{6}Li$ ratios for stars (Piau 2008) due to technical complexities in resolving the spectra of ^{6}Li and ^{7}Li. As a consequence, the measured $^{7}Li/^{6}Li$ ratios are usually very high and burdened by large analytical errors. In fact, lower $^{7}Li/^{6}Li$ limits at ~20 are typical (e.g., García Pérez et al. 2009; Hobbs and Thorburn 1994; Hobbs et al. 1999; Maurice et al. 1984; Nissen et al. 1999). In this respect, both the low-mass halo stars and metal-poor stars apparently play the determining role in models of evolution of Li and its isotopes because their lifetimes are comparable to those of the Galaxy itself and because precise measurements of individual Li abundances in such stars may be critical in constraining the Galactic history and evolution. Lind et al. (2013) found very high $^{7}Li/^{6}Li$ ratios in several metal-poor stars, showing that these were indeed devoid of ^{6}Li, attesting to standard models of BBN evolution. High $^{7}Li/^{6}Li$ ratios, practically at the edge of current instrumental analytical capabilities, appear to be the common feature of stars. For example, Ghezzi et al. (2009) measured $^{7}Li/^{6}Li$ ratios in several stars and despite many technical barriers and the need for many corrections, they found very high $^{7}Li/^{6}Li$ ratios (≥125) within analytical errors for all studied cases.

3.1.3 Searching for Exoplanets with Lithium

The stellar Li abundance could eventually be useful in searching for the existence of stellar systems with orbiting planets, as spectral measurements of Li abundance are, in some cases, relatively easy. Theoretically, the existence of an orbiting planetary system may affect the stellar angular momentum as well as surface convective mixing because rotational forces produced by the movement of large satellites could impart significant additional energy to mixing of stellar layers. By inference, this would affect the availability of Li for burning. However, alternative explanations may seek Li depletion to be

inherited from the pre-main sequence stage of stellar evolution.

In order to establish Li as a practical proxy for stellar planet-harboring systems, Israelian et al. (2009) reported on a pronounced Li depletion in stars with proven orbiting planets. These authors suggested that stars more massive than the Sun do not suffer from comparable Li depletion due to convective layers that are too shallow to transport Li into greater depths where Li-burning is triggered. It may appear that Li depletion is peculiar to Sun-like stars within a very restricted temperature range (±80 K) and wherein neither age nor metallicity are the major determining parameters of Li depletion (Israelian et al. 2009).

The results of Israelian et al. (2009) were later critically reviewed by Baumann et al. (2010) who concluded that planet-harboring stars do not differ in their Li abundances from stars without anchored planetary systems and that these features may be coupled with different rotation profiles of stars (Charbonnel and Talon 2005). Lithium depletion may be pronounced in stars with thicker convective zones and in stars with a higher degree of differential rotation between the core and envelope so that Li is entrained in deeper, hotter regions. More generally, Baumann et al. (2010) provided evidence against stellar planet-hosts possessing surface Li abundance different to those which would be intrinsic to solitary stars. Also, Ramírez et al. (2012) were not able to statistically distinguish between planet-hosting and planet-free stellar systems despite multiple constraints on surface temperature, mass and metallicity. They concluded that some of the foreseen differences in Li abundance may stem from subtle disparity in these key stellar parameters between the two compared groups.

Recently, Figueira et al. (2014) employed more stringent statistical tools for larger data set and found that differences in stellar surface Li abundance exist at statistically significant levels (>3σ) for planet-devoid and planet-harboring stars whereas a difference in Li abundances at ~7σ level was found for a selected population of stars analyzed by Delgado Mena et al. (2015) and ascribed by the authors to the presence of massive hot Jupiter-size planets migrating closer toward the star. However, one must keep in mind that (i) some of the former stellar systems may host planets not yet detected by our analytical tools and, (ii) depletion in Li of stars may be related to massive Jupiters which may impart more gravitational influence on stellar mixing. Collectively, some limitations resulting from both the model parameters and data evaluation call for further analyses and a better understanding of stellar environments.

3.2 Cosmochemistry of Lithium in Meteorites

Lithium is rendered an important element for stellar nucleosynthesis (see previous section), and holds promise as a petrogenetically meaningful parameter of planetary magmatic differentiation, crustal evolution and alteration/metasomatism. These assumptions partly follow from its moderately volatile behavior with a 50 % condensation temperature from Solar System gas of 1142 K (Lodders 2003) and its incorporation into forsterite and enstatite where it substitutes for Mg. Despite its broad use in understanding magmatic and post-magmatic processes, only a handful of detailed studies of elemental and isotopic distribution of Li in meteorites, considered the building blocks of terrestrial planets, has emerged.

In 1960s and early 1970s, it became clear that (i) chondritic meteorites of diverse classes (carbonaceous, enstatite, ordinary) are uniformly low in Li abundance, generally in the range between 1 and 3 ppm (e.g., Balsiger et al. 1968; Dews 1966; Krankowsky and Müller 1964, 1967; Nichiporuk and Moore 1970, 1974; Tera et al. 1970), (ii) Li resides primarily in the silicate portion of meteorites, (iii) chondrules are generally depleted in Li relative to the bulk sample (Krankowsky and Müller 1967; Shima and Honda 1966), and (iv) some achondrites may carry significant quantities of Li (up to 15 ppm), for example shergottites and nakhlites coming from Mars (see Sect. 3.3.2) and eucrites coming from asteroid 4-Vesta (see Sect. 3.3.3). Most of these preliminary conclusions were later

confirmed by analyses of a larger number of specimens, but the advent and wide application of modern state-of the-art analytical instruments made it clear that Li is distributed heterogeneously on a small scale and that it behaves in a complex fashion (e.g., Hanon et al. 1999; Chaussidon et al. 2006; Maruyama et al. 2009; McDonough et al. 2006; Murty et al. 1983; Seitz et al. 2007, 2012; Sephton et al. 2013).

3.2.1 Lithium in Bulk Chondritic Meteorites

A few early studies of meteorites produced a significant load of Li isotopic data (Balsiger et al. 1968; Dews 1966; Gradsztajn et al. 1967; Krankowsky and Müller 1964, 1967; Poschenrieder et al. 1965; Rajan et al. 1980; Shima and Honda 1966; Yanagita and Gensho 1977) but given the contemporary precision of ~±10 ‰ and considering the lack of a recognized international reference material, the only significant conclusion reached from those investigations was that the Li isotopic signature in meteorites overlaps, within a broad uncertainty; hence it was inferred that the chondritic (and by extension the bulk Earth) $^{7}Li/^{6}Li$ ratio was ~12 (Anders and Grevesse 1989). These early results also placed a benchmark for the astrophysical observations that some interstellar regions of the Universe have $^{7}Li/^{6}Li$ ratios far below the chondritic value, some as low as ~2 (e.g., Knauth et al. 2003, 2000).

Further support for varying $^{7}Li/^{6}Li$ ratios across the Galaxy, or at least across the Solar System, has since come from in situ analyses of presolar SiC grains thought to represent the oldest and chemically and physically extremely resistant material of the Solar System available (Gyngard et al. 2009; Lyon et al. 2007). These studies have shown that some sub-chondritic $^{7}Li/^{6}Li$ ratios (down to ~9) may be related to contribution from GCR spallation reactions, yielding ^{6}Li excess. Chaussidon et al. (2006), though, presented potential evidence of the former existence of live ^{7}Be during the formation of chondrules in the Allende meteorite. These latter results were disputed by Desch and Ouellette (2006) who postulated that corrections for cosmogenic contribution performed by Chaussidon et al. (2006) were overestimated and that there is no real isochron through the data set that would imply the presence of former live ^{7}Be through a correlation between $^{7}Li/^{6}Li$ and $^{9}Be/^{6}Li$. Careful re-examination of the data of Chaussidon et al. (2006) by Leya (2011) partly re-assessed the validity of such an isochron although care must be exercised in proper handling of cosmogenic effects as well as statistical evaluation, combined with cautious petrography.

The non-trivial task of obtaining information from presolar grains has been evaluated by Fujiya et al. (2011) who, using the NanoSIMS technique, investigated Li (and B) isotopic compositions in 12 SiC X grains, thought to originate in Type II supernovae. However, all of the grains analyzed by Fujiya et al. (2011) carried Solar System $^{7}Li/^{6}Li \sim 12$ within analytical errors which the authors ascribed to meteoritic or laboratory contamination. Considering considerably higher Li concentrations in SiC grains of Fujiya et al. (2011) compared with those measured by Gyngard et al. (2009), any contribution by GCR spallation-produced Li has been constrained to < 4 % but will probably be at significantly lower levels.

Only in 2003, McDonough et al. (2003) presented the first quasi-systematic investigation of Li isotopic compositions in several chondritic meteorites of different petrologic types. These results implied a shift in $\delta^{7}Li$ depending on the degree of alteration and/or thermal metamorphism such that aqueous alteration introduced higher $\delta^{7}Li$ whereas low $\delta^{7}Li$ values were associated with higher degrees of thermal metamorphism. Moreover, the preliminary data of McDonough et al. (2003) invoked $\delta^{7}Li \sim 0$ ‰ for the Solar System with profound implications for the inner Solar System planets. However, more recent studies (McDonough et al. 2006; Seitz et al. 2007) did not lend support to these preliminary conclusions and have inferred a Solar System $\delta^{7}Li$ of ~+3–4 ‰, consistent with a large body of other evidence from terrestrial, lunar, martian and asteroidal rocks (see the following sections in this chapter).

One of major obstacles in analyzing meteorites is their petrologic diversity, record of post-solidification processes that could have disturbed the original Li distribution, and intra-sample variability. The latter has clearly been identified in somewhat contrasting results for dark inclusions in the Allende chondritic meteorite (Seitz et al. 2012; Sephton et al. 2006). Furthermore, the remobilization of Li isotopes during thermal metamorphism or aqueous processes could potentially mask the original Li isotopic signature of meteorites. However, in such cases it may provide important information on time scales and temperatures of these secondary events.

The fact that Li isotopic compositions of different meteorite classes do not simply reflect their individual and Li-specific post-crystallization histories, often involving thermal processing, reheating and/or fluid percolation, is mirrored in roughly consistent results for several classes of chondritic meteorites (Pogge von Strandmann et al. 2011; Seitz et al. 2007). In fact, all classes of chondrites, (i.e., carbonaceous, ordinary and enstatite) show a similar extent of δ^7Li variation, paralleled by only slightly different mean values (Fig. 3.7). The carbonaceous chondrites include Allende, Murchison, Orgueil, Karoonda, Ornans, Efremovka, Vigarano, Tagish Lake and several other specimens and have δ^7Li = +3.2 ± 1.7 ‰ (2σ, n = 35); among ordinary chondrites, Bruderheim, Bjurböle, Semarkona, Tuxtuac, Parnallee, Chainpur, Saint-Séverin Forest Vale and Kernouvé were also analyzed, the mean δ^7Li = +2.4 ± 1.6 ‰ (2σ, n = 34); Quingzhen, Indarch, Abee, Hvittis or Neuschwanstein are among the analyzed enstitate chondrites and the group's δ^7Li = +1.9 ± 1.5 ‰ (2σ, n = 10).

A comparison of larger data sets collected for individual samples seems to indicate a sample-scale heterogeneity. For example, available data for carbonaceous chondrite Orgueil yield a mean δ^7Li = +3.6 ± 1.4 ‰ (2σ, n = 5) and a similar extent of variability has been found for the ordinary chondrite Parnallee (δ^7Li = +2.9 ± 1.7 ‰, 2σ; n = 3). Slightly less heterogeneous results were found for other carbonaceous chondrites, Allende (δ^7Li = 2.6 ± 1.0 ‰, 2SD; n = 5) and Murchison (δ^7Li = 3.9 ± 0.8 ‰, 2SD; n = 5). Collectively, most chondritic meteorites span δ^7Li range largely between +1 and +5 ‰, and only carbonaceous chondrites of the Renazzo (CR) type (Fehr et al. 2009), some enstatite chondrites, and a single aubrite (enstatite achondrite) show consistently light Li isotopic signatures (Pogge von Strandmann et al. 2011) that may provide further insights into the distribution of chondrite parent bodies within the early Solar System. From the Li perspective it is difficult to assign enstatite chondrites a major role as building material for the Earth and other large planetary bodies in the Solar System (see also Magna et al. 2015) because their major element composition is in stark contrast with that of the Earth (see discussion in Palme and O'Neill 2014). On the contrary, many other geochemical aspects (in particular isotopic compositions of many refractory elements such as Ti, Cr, Ni, Ba, etc.) are not at odds with a view of enstatite chondrites as major building blocks of terrestrial planets (see also opposing views of Fitoussi and Bourdon 2012 vs. Javoy et al. 2010, and discussion therein). Although it seems that the Earth and Mars were formed from a complex mixture of primitive materials (e.g., Warren 2011), a significant effort should be made toward a better understanding of planetary-forming processes; if the behavior of Li is better understood it could aid in this effort.

Lithium data for other meteorite classes are scant. Olivine from the Admire pallasite showed a rather Li-poor nature (0.8 ppm) and a δ^7Li value (+3.4 ‰) fully in the range of chondritic meteorites (Seitz et al. 2007). Further analyses, conducted using SIMS instrumentation, have confirmed this value although with some scatter and with a few pallasites showing lighter Li isotopic compositions (δ^7Li < + 0.6 ‰; Bell et al. 2008). Preliminary data for olivine and pigeonite extracted from ureilites show somewhat higher (and similar) δ^7Li values for both co-existing minerals (+6.3 and +6.7 ‰, respectively), although pigeonite displayed significantly larger scatter of the Li isotopic compositions (Singletary et al. 2008). Whether or not these signatures reflect kinetic processes on the respective parent bodies remains to be tested. However, only a

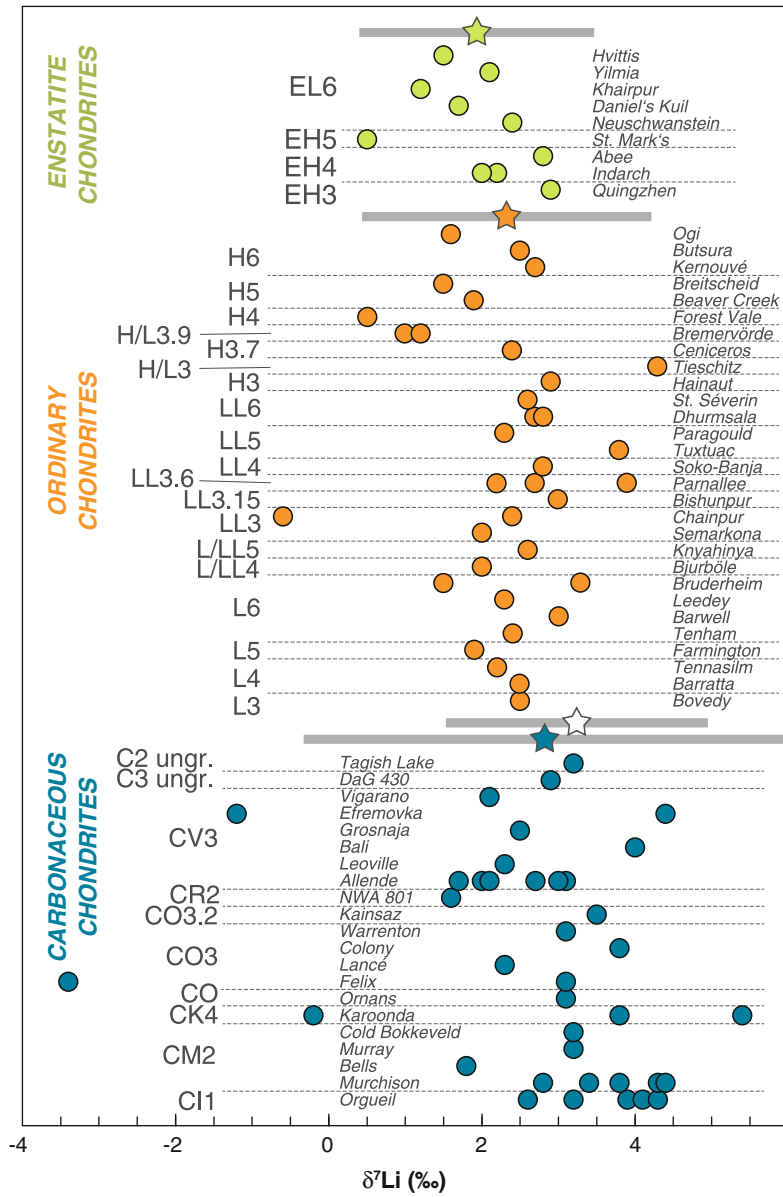

Fig. 3.7 Lithium isotopic composition of different groups of chondritic meteorites. Several features are apparent. First, within rather large uncertainty, all major chondrite groups (carbonaceous, ordinary, enstatite) have broadly similar mean δ^7Li, although the latter group has on average slightly lighter lower mean δ^7Li. Second, some samples show particular variation in δ^7Li (e.g., Orgueil, Murchison, Karoonda, Allende, Parnallee) whereas published data for some others are nearly identical (e.g., Ornans, Dhurmsala, Bremervörde, Indarch). This indicates sample-scale heterogeneity; consequently, care should be exercised when analyzing chondritic materials. It also appears that the data of McDonough et al. (2003) may suffer from yet unaccounted analytical artifacts because other analyses of Karoonda, Felix, Efremovka, and Chainpur are consistent with the chondrite group means. Data sources: James and Palmer 2000; Seitz et al. 2007, 2012; Pogge von Strandmann et al. 2011; Magna et al. 2006; Sephton et al. 2004, 2006, 2013; McDonough et al. 2003

more detailed survey of a larger population of chondrites (and primitive achondrites, such as aubrites, angrites, brachinites, and ureilites), paralleled by considerations of intra-sample heterogeneities, could provide further clues to the history of Li in the early Solar System.

3.2.2 Lithium Distribution and Isotopic Systematics in Constituents of Chondritic Meteorites

The early work of Dews (1966) showed that chondrules are depleted in Li (< 0.27 ppm) relative to bulk chondrites and that there are some variations in Li abundance in chondrules from individual samples. These findings were later reproduced for other meteorites, though with less pronounced Li depletion in chondrules relative to matrix (Nichiporuk and Moore 1970). On the contrary, Krankowsky and Müller (1967), Balsiger et al. (1968) and Murty et al. (1983) reported analyses of chondrules and bulk specimens with somewhat contrasting results, even with up to two-fold Li enrichments in chondrules relative to bulk specimens. More recently, Hanon et al. (1999) used SIMS to determine Li (and Be–B) elemental distribution in several meteorites, including Allende and Semarkona. Their results indicated a rather narrow range of Li concentrations in chondrites (~0.2–2.6 ppm), paralleled by a lesser elemental variability of Li within individual chondrules compared with B. In contrast to preferential incorporation of Be and B into mesostasis, Li partitioning into crystals versus mesostasis between different chondrites is not uniform. The coupled Li–Be–B elemental systematics also indicated immobile character of Li and Be during metamorphism of the parent body of ordinary chondrites (Hanon et al. 1999). The Li–Be–B systematics in Semarkona chondrules were independently also investigated by Chaussidon and Robert (1998) who found much larger variations in Be–B contents relative to Li (from ~0.5 to ~3.7 ppm Li vs. two and three orders of magnitude variations for Be and B, respectively). Moreover, no uniform partitioning between mesostasis and pyroxene was observed (similar to findings of Hanon et al. 1999), implying the lack of magmatic equilibrium due to rapid cooling of chondrules.

Chaussidon and Robert (1998) also reported δ^7Li values for multiple measurements of three chondrules from Semarkona with a mean value for the majority of data points at +10 ± 10 ‰. They suggested that this variation reflected mixing of three different nucleosynthetic sources (BBN, ISM, and dense molecular clouds); at least two different sources (high-energy spallation reactions and a common silicate reservoir) were also invoked for chondrules from the Mokoia meteorite with δ^7Li values as low as −54 ‰ (Robert and Chaussidon 2003). Different distribution of Li and δ^7Li was reported for Allende by Bell et al. (2008) who found generally low Li concentrations (< 1 ppm) for Mg-rich olivine (with forsterite contents > 90 mol%) and between ~0.5 and ~4.5 ppm Li was found in olivine with a larger fayalite component (>10 mol%). The Li isotopic variability in forsteritic olivine (~0 to ~30 ‰) is contrasted by rather uniform δ^7Li = +3 ± 2 ‰ in Fe-rich olivine. Bell et al. (2008) discussed these findings as reflecting preferential loss of ^{6}Li by evaporation at high temperatures.

In situ measurements of Li abundance and isotopic composition in several chondrules from the Allende meteorite by Maruyama et al. (2009) revealed Li-poor character of olivine in three chondrules (generally below 0.3 ppm) whereas olivine in three other chondrules had mean Li abundance from 0.6 to 0.8 ppm. Elevated Li contents were found in low-Ca pyroxene of two chondrules (>3.6 ppm), matrix (~2 ppm), and in Na-rich mesostasis (>1 ppm). Parallel measurements of δ^7Li in selected olivines revealed a significant variation between −32 and +21 ‰ without any clear systematics. Because most mesostasis in Allende is rather low in Li, Maruyama et al. (2009) invoked leaching of Li by aqueous fluids. The Na-rich phases located at chondrule rims appear to have captured some Li although the process of Li mobilization and re-incorporation may have operated at different times. Recently, Seitz et al. (2012) investigated Li elemental and isotopic systematics in ~90 chondrules by means of MC-ICPMS technique. Again, three observations are apparent: (i) no systematic relationship of Li contents and petrogenetic parameters (e.g., magnesium number [Mg#], defined as (molar MgO/(molar MgO + molar FeO^{tot})), (ii) overall low Li contents in chondrules relative to bulk chondrites,

and (iii) a large range in δ^7Li values among the chondrules without any peculiar systematics and relation to the degree of alteration/metamorphism, degree of melting or major element chemistry. From these observations, Seitz et al. (2012) implied compositional heterogeneities in chondrule forming regions in the Solar nebula. Collectively, the data for individual components of chondrites show a large scatter in both Li contents and isotopic compositions, indicating non-uniform behavior of Li during chondrule formation and subsequent processes after the chondrules were embedded into bulk chondritic matter. There is, somewhat surprisingly, limited evidence for post-magmatic re-distribution of Li in chondrites through aqueous alteration or thermal metamorphism whereby the former process could be efficiently tracked with Li (see Chap. 6). This can be linked to the assumption of Seitz et al. (2012) and Sephton et al. (2013) that the whole-rock Li systematics appear to be a mixture of several distinct components with largely different Li characteristics.

Important information on post-magmatic histories of chondrites may also be gathered by applying sequential leaching procedures which seek to selectively dissolve individual components. For example, acetic acid usually removes a non-silicate fraction out of the bulk material. By this technique, Sephton et al. (2004) isolated carbonates, and Fe oxides and oxyhydroxides from the Murchison meteorite. They found substantial δ^7Li variations between the individual components, i.e., carbonate-rich, phyllosilicate-rich matrix and chondrules that simply constitute the bulk mass of the meteorite. Carbonates in their study carried a heavy Li isotopic signature (>+12.6 ‰), which is largely consistent with terrestrial systematics of Li in low-temperature carbonates. A supplementary study by Sephton et al. (2013) found that Fe mineralogy (i.e., the type of the Fe oxide or oxyhydroxide) exerts the major control on abundance of Li in non-silicate (i.e., acetic acid-leachable) phases. Also, acetic acid-leachable phases carried high δ^7Li, similar to the findings of Sephton et al. (2004). These observations may have implications for post-magmatic processes, such as aqueous alteration acting on the meteorite parent bodies at different, albeit low, temperatures (Sephton et al. 2013).

3.2.3 Lithium in Other Meteorites

Beside chondrites and achondrites, a well-populated clan of other meteorite types, pallasites, mesosiderites and iron meteorites, exists (Krot et al. 2014). A significant proportion of these meteorites is formed by Fe–Ni metal in which Li will likely be highly incompatible. This was proven by comparing Li contents in silicate and troilite from Odessa IA iron meteorite with ~1–2 ppm Li in silicate fraction versus ~40 ppb in the metal fraction (Krankowsky and Müller 1967). Murty et al. (1982) investigated iron meteorites from several classes and found that Li is distributed heterogeneously in these meteorites. Moreover, most Li appeared to be concentrated in a non-magnetic fraction whereas the magnetic fraction retains a subordinate proportion of Li. Despite very low Li contents (low tens of ppb Li, as determined from the measured ^{6}Li contents by neutron activation analysis), a resolved difference in Li contents between IA (e.g., Canyon Diablo, Odessa, Toluca) and IIAB (e.g., Coahuila, Sikhote Alin) versus IIIA (e.g., Cape York, Henbury) iron meteorites was found (>~20 ppb in IA–IIAB vs. ~5 ppb in IIIA). However, no further investigations were made that considered these meteorite classes. Given the low abundances of Li in metal, consistent with its lithophile character, the possible implications for histories of the respective parent bodies of iron meteorites may be rather limited.

3.3 Cosmochemistry of Lithium in Planetary Bodies

Comparatively little has so far been done in order to improve our understanding of the behavior of Li and its isotopes in non-terrestrial materials despite at least three decades of successful measurements of Li isotopic compositions and despite the importance of Li in stellar processes. Only with more recent developments and

advancements in analytical techniques and instrumentation (see Chap. 2), several studies have presented precise and accurate measurements of Li isotopic compositions in lunar rocks as well as in martian, Vestan (howardite–eucrite–diogenite [HED] clan) and other meteorites, with some implications for the histories and evolution of their respective parent bodies. Whereas numerous samples of these bodies exist for direct laboratory investigations, recent efforts have also been made to detect Li abundance in Mercury, the innermost planet of the Solar System, for which no physical samples are at present available.

The preliminary report by Irving et al. (2013) on a recent find of North West Africa (NWA) 7325 requires further investigations but Li-depleted character of this meteorite (0.53 ppm) is unique in the context of its provenance from a differentiated planet. Whereas there may be little direct link between the surface Li and atmospheric Li abundance, Sprague et al. (1996) were not able to detect Li in the atmosphere of Mercury. This would be consistent with the extremely depleted nature of NWA 7325, but further investigations are required to answer ticklish questions concerning this meteorite.

3.3.1 Lithium in Earth's Moon

Since the return of Apollo samples, a number of contributions to the annual Lunar and Planetary Science Conference contained Li concentrations for many lunar samples. Some significant observations arise from these studies. For example, Dreibus et al. (1976) estimated 1.6 ppm Li for bulk Moon and implied from Li–Zr elemental correlations that the Moon inherited ~40 % of its mass from high-temperature condensates and the rest of its matter came from Mg-silicates. However, there were some discrepancies between Li/Zr, which scattered significantly, and Li/Be (considered constant at ~4.6 for the Moon, as evidenced from maria basalts and KREEP-rich and KREEP-poor samples; KREEP = potassium–rare earth elements–phosphorus-enriched), which may point to dissimilar behavior of these elements despite their refractory behavior.

Early lunar Li isotopic research was focused on the detection in regolith of a solar wind component (Eugster and Bernas 1971) although measurements were compromised by large analytical errors. Solar wind was theoretically modeled with high $^{7}Li/^{6}Li$ ratios resulting from preferential destruction of ^{6}Li at the bottom of the convective zone in the Sun (Bernas et al. 1967). This overall depletion of Li as well as high $^{7}Li/^{6}Li$ in the Sun was later confirmed theoretically (Delbourgo-Salvador et al. 1985), by direct astrophysical observations (e.g., Ritzenhoff et al. 1997). The early measurements of Eugster and Bernas (1971), however, were unsuccessful in determining ^{7}Li excess in two lunar breccias (10046 and 10074) and a coarse-grained soil (10084), potentially due to long exposure of surface. Empirical support for heavy Li enrichment in solar wind arrived more recently, through high-resolution spatial analysis of individual lunar soil particles (Chaussidon and Robert 1999). Estimates from the analysis by Chaussidon and Robert (1999) of Apollo soils 10060, 79035, 79221 and 79261 suggested that solar wind had very high $^{7}Li/^{6}Li$ of ~31, whereas the bulk Earth value is ~12.

The data of Eugster and Bernas (1971) showed $^{7}Li/^{6}Li$ ratios similar to those found previously for terrestrial materials. Also, Garner et al. (1975) measured $^{7}Li/^{6}Li$ ratios in several lunar soils and rocks; these data too were indistinguishable from the terrestrial reference material. These first measurements, despite the lack of internationally recognized and accepted standardization material, and being far from the current levels of precision and accuracy, provided the first glimpse at the Li isotopic composition of the Moon. The lack of distinction between Li isotopes in lunar and terrestrial materials was only reinforced three decades later by Magna et al. (2006) who analyzed a suite of lunar rocks and soils with different solar wind exposure ages. The results for soils did not deviate drastically from values reported for the bulk silicate Moon and, by inference, from the Earth. The contribution of the solar wind to bulk Li in lunar soils was detected for different size fractions of the lunar soil 67601, with slight ^{7}Li

excess in the finest fractions (<42 μm), most likely formed by degradation of surface shells of regolith particles through long-term solar wind abrasion. Nevertheless, translated into bulk lunar geology, there is no detectable shift in δ^7Li for magmatic rocks (Magna et al. 2006; Seitz et al. 2006), making them suitable candidates in which to study processes of extreme magmatic differentiation in the lunar magma ocean (Snyder et al. 1992) under nominally dry conditions, although the genuine water content of the Moon is contested (e.g., Hauri et al. 2011; Saal et al. 2008; Sharp et al. 2010). This may be important by considering a possible role of chemistry of mineral phases that build Li into their structures and that may thus reflect changes in conditions during magmatic fractionation and/or thermal metamorphism (Chaklader et al. 2006).

Steele et al. (1980) measured Li contents in plagioclase from a wide spectrum of lunar rocks, including anorthosites, troctolites, norites, breccias, and mare basalts. They found surprisingly large variation between 1.2 and 21 ppm Li, with an extraordinary plagioclase measurement from a KREEP (K–REE–P-rich) basalt clast from sample 15344 having 54 ppm Li. The latter concentration reinforces the incompatible element-enriched nature of KREEP (Warren and Wasson 1979). Steele et al. (1980) also found a positive correlation between Li and Na, although mafic mineral phases host significant amounts of Li and plagioclase is the principal carrier for Na. This may mean that buoyant anorthositic lunar crust was derived from a roughly common reservoir whereas high but variable Li contents in plagioclase from Mg-rich lithologies either reflect several isolated and localized sources, or were actively communicating with those regions of residual lunar magma ocean that were not yet solidified.

Very low Li contents (Magna and Neal 2011; Magna et al., 2006) in very ancient anorthosites (>4.3 Ga; e.g., Borg et al. 2011; Carlson and Lugmair 1988; Norman and Taylor 1992) appear to be an intrinsic feature of anorthositic portion of the lunar crust. Terrestrial upper continental crust carries high Li abundance (mean ~35 ppm) and a diagnostic δ^7Li (0 to +2 ‰), and appears to reflect long-term secular evolution of the crust–mantle system. For the Moon, chemically evolved lithologies are quite rare in the Apollo collection, and their origin through silicate liquid immiscibility (e.g., Neal and Taylor 1989) is likely to be dissimilar to the formation of igneous rocks of the terrestrial continental crust (Taylor and McLennan 2009). Whereas many parameters suggest a complementary relationship of mare basalts and anorthosites (Taylor and Jakeš 1974), low Li abundance in lunar highland rocks does not find its equivalent on Earth. Instead, low Li contents in pristine ferroan anorthosites, paralleled by elevated δ^7Li (up to +9 ‰; Magna and Neal 2011; Magna et al. 2006), may imply kinetic effects in a plagioclase-rich layer, although rapid preferential diffusion of ^{6}Li into newly formed plagioclase (Coogan 2011; Coogan et al. 2005) would likely drive ^{7}Li/^{6}Li instead towards low values. Therefore, the heavy Li isotopic signature of the lunar ferroan crust remains somewhat enigmatic and needs to be cautiously modeled.

Shearer et al. (1994) measured the Li, Be and B contents in picritic lunar volcanic glasses and found that Li and other light lithophile element contents vary greatly among different sampling sites (Apollo 11, 12, 14, 15 and 17, respectively). These authors suggested that effusive volcanic glasses cooled quickly under near-vacuum conditions and that they are genetically unrelated to mare basalts; volcanic glasses appear to more closely reflect the intrinsic Li content of the Moon, estimated at ~0.8 ppm (Taylor 1982), although other estimates have been made (see above). The somewhat heterogeneous nature of these glasses, however, is underscored by significant differences in Li abundance and isotopic compositions yielded for different aliquots of green glass 15426 and orange glass 74220 (Magna et al., 2006; Seitz et al. 2006). The nature of this discrepancy remains unresolved at present, although these materials may represent a closer window into the deep lunar mantle (Longhi 1992).

Only rather recently, Magna et al. (2006) and Seitz et al. (2006) published the first high-precision Li isotopic data for bulk lunar samples (Fig. 3.8). Both studies showed

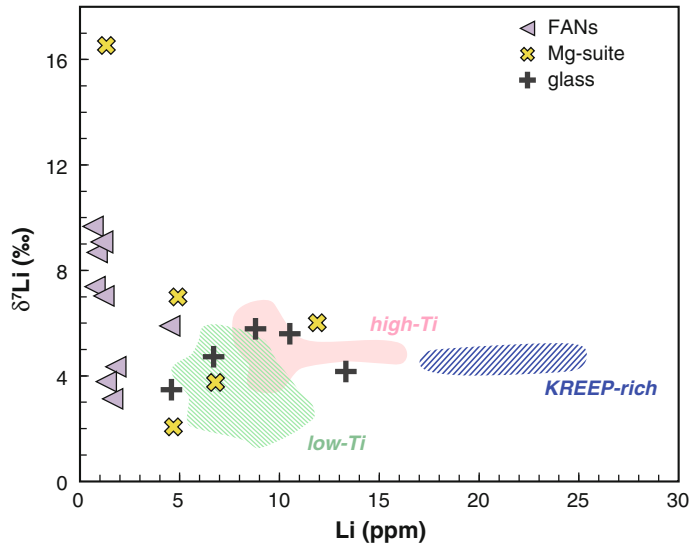

Fig. 3.8 Lithium content versus δ^7Li in lunar samples (Day et al. 2008; Magna and Neal 2011; Magna et al. 2006; 2009; Seitz et al. 2006). An apparent difference between low-Ti and high-Ti basalts, as well as a more detailed assessment of Li systematics in volcanic glasses (Shearer et al. 1994), appear to rule out a single source for these major reservoirs. Notable depletion in Li has been found for ferroan anorthosites (FANs), representative of a significant portion of the lunar highlands. A rather limited variability has been observed for plutonic Mg-suite rocks (dunites, norites, troctolites). A trend toward Li-enriched character of the KREEP reservoir is obvious and is consistent with modelled Li abundance of 56 ppm (Warren and Wasson 1979)

independently that Li isotopic composition of the silicate lunar mantle is nearly identical to that of the Earth, with consequences for the Earth–Moon formation in a giant impact (Canup 2004) and subsequent turbulent exchange of hot ionized gas after the collision (Pahlevan and Stevenson 2007). Importantly, both studies have also shown that lunar rocks may be quite heterogeneous on a specimen scale as is obvious from several samples that were measured independently (such as KREEPy impact melt 14310, orange glass 74220, green glass 15426, quartz-normative mare basalt 15475, and olivine-normative mare basalt 15555) and that, therefore, the δ^7Li of the bulk silicate Moon must be interpreted with caution. This is further stressed by the fact that there are no direct mantle rocks in the Apollo collection and that the chemical and isotopic fingerprints of the deep lunar mantle may thus only be inferred indirectly. Indeed, Magna et al. (2006) and Day et al. (2008) have shown that there are statistical differences between the Li isotopic compositions of low-Ti and high-Ti mare basalts, such that the former are in general isotopically lighter than the latter, and that low-Ti mare basalts may better reflect the silicate mantle of the Moon. This was also invoked from Hf isotopic compositions (Beard et al. 1998) and the distinctly greater proportion of low-Ti mare basalts at the lunar surface (Giguere et al. 2000). A note should be made that the bimodality of lunar mare basalt chemistry based on Ti contents is somewhat ad hoc. More recent remote sensing data reveal a rather continuous range in TiO_2 contents, suggesting that the bimodality is a sampling bias from the locations of sample return sites (Giguere et al. 2000). The Li isotopic dichotomy related to the differences in mantle sources was later confirmed with oxygen, iron and magnesium isotopic differences between these distinctive Ti varieties (Liu et al. 2010; Sedaghatpour et al. 2013; Spicuzza et al. 2007). However, anti-correlated Li and O isotopic compositions may reflect different processes and/or crystallographic control that individual mineral phases may exert on the respective bulk isotopic signatures. For example, a heavy Fe isotopic signature in high-Ti mare basalts (Liu

et al. 2010; Poitrasson et al. 2004) appears to reflect a control by ilmenite (Craddock et al. 2010). Although ilmenite segregation would not affect Li due to incompatibility, it could imply a generic feature of lunar magmas to become a useful proxy for studying crystal fractionation processes in settings where water can be ignored (unlike in most terrestrial igneous systems).

A more comprehensive study of Li isotopes in basalts from different Apollo sites was performed by Magna et al. (2009), who reinforced the Li isotopic dichotomy between isotopically light low-Ti and heavy high-Ti mare basalts (Fig. 3.8) resulting from distinct periods of crystallization of their respective cumulate sources from the residual lunar magma ocean, modeled earlier (Day et al. 2008). Magna et al. (2009) also confirmed variability of Li isotopic compositions within the respective low-Ti and high-Ti mare basalt groups, in many cases on the order of ~3 ‰. An important observation of the modern lunar Li data set is that KREEP-rich rocks such as 15386, 14310, and high-potassium Apollo 11 mare basalts with a (K)REEP signature (10017, 10057, 10069) (Jerde et al. 1994) appear to carry a uniform Li isotopic signature paralleled by elevated Li abundance relative to other Apollo 11 basalts. The high Li abundance in KREEP is a direct consequence of its formation during the last stages of the lunar magma solidification (>99 %; Snyder et al. 1992; Warren and Wasson 1979) combined with the moderately incompatible character of Li in magmatic process. The key aspect of this observation is that the mean δ^7Li of KREEP is slightly lower than that of high-Ti mare basalts although their relative chronology is basically the opposite. The δ^7Li homogeneity observed for KREEP-rich lithologies is important in the view of differences in magmatic ages for Apollo 11 and Apollo 14 and 15 rocks, respectively (Shearer et al. 2006, and references therein), suggesting a relatively uniform process of formation of chemical signatures of this spatially and temporally distinctive reservoir. By considering a Rayleigh process for residual lunar magma ocean (Day et al. 2008), KREEP should have distinctly higher δ^7Li than high-Ti mare basalts. Yet, a broadly similar (or lighter) Li isotopic signature compared to high-Ti mare basalts may imply (i) a role of water that exsolved only after crystallization of high-Ti mare basalts, or (ii) a change in conditions of KREEP crystallization.

Collectively, the lunar crystalline rocks have a rather restricted range in δ^7Li that appears to reflect differences in crystallization assemblages of the two major sampled groups of mare basalts. In order to estimate δ^7Li of the bulk silicate Moon, we tentatively consider low-Ti mare basalts more reliable because their mantle sources were derived earlier in the sequence than those of high-Ti mare basalts (Snyder et al. 1997, 1992; Taylor and Jakeš 1974) and because they form ~90 % of exposed mare basalts (Giguere et al. 2000). The estimated δ^7Li of the bulk silicate Moon is ~ + 4.0 ‰ which is slightly heavier than that of the Earth's upper mantle but within uncertainty. It thus appears that the exotic δ^7Li ~ +15 ‰ inferred for the source of low-Ti basaltic meteorite NWA 479 (Barrat et al. 2005) is less realistic and strong kinetic modifications seem likely.

3.3.2 Lithium in Mars

Contrary to lunar rocks for which we have spatial control through manned collection by the astronauts of six successful landing missions and three robotic sample return missions, it is not easy to assign a specific location on the surface of Mars for the >150 currently known martian specimens, including pairings. This poses problems in putting the petrologic and geochemical information into a broader context of martian magmatic history. To date in terrestrial collections there are basaltic, olivine-phyric, olivine–orthopyroxene-phyric, lherzolitic, diabasic and gabbroic shergottites, cumulate clinopyroxenites (nakhlites), dunites (chassignites), collectively called Shergotty–Nakhla–Chassigny (SNC) meteorites, orthopyroxenite Allan Hills (ALH) 84001, and polymict breccia Northwest Africa (NWA) 7034; some of the specimens are paired whilst some are unique. Apart from petrographic distinctions, shergottites are also classified into depleted, intermediate and enriched shergottites, respectively, according to

their incompatible trace element patterns. In this respect, it is important to note that Li isotopes are not fractionated during impact events (Magna et al. 2011) which are thought to be the major process by which martian meteorites are excavated from the surface. We stress that martian meteorites did not undergo melting but are heavily shocked whereas terestrial impacts produced large amounts of melts (tektites), which resulted from instantaneous melting of surface materials. The original information during these latter events can thus be lost through homogenization of melted sediments and soils, as reported for Li isotopes (Magna et al. 2014b). Therefore, the situation with martian meteorites is fortuitous for further petrogenetic and geochemical studies despite highly shocked nature of these precious samples.

Since it was recognized that some meteorites very probably come from Mars (Becker and Pepin 1984; Bogard and Johnson 1983), several studies focused on their light lithophile element geochemistry (LLE: Li, Be and B). From detailed in situ analysis of LLE abundances in pyroxene from the Shergotty meteorite fall, McSween et al. (2001) inferred that there was significant water present at the time of crystallization of the mineral core at depth and that degassing operated en route to the surface. Lentz et al. (2001), Beck et al. (2004) and Herd et al. (2005) extended these observations of degassing- and water-control on Li elemental and isotopic systematics in Mars to nakhlite meteorites. This idea was, however, soon abandoned (Beck et al. 2006; Herd et al. 2004) through elaboration of the concept of diffusive kinetic modifications of Li (Coogan et al. 2005; Jeffcoate et al. 2007; Lundstrom et al. 2005; Parkinson et al. 2007).

The bulk behavior of Li during planetary crystallization processes remained less constrained (Herd et al. 2004) and the implications

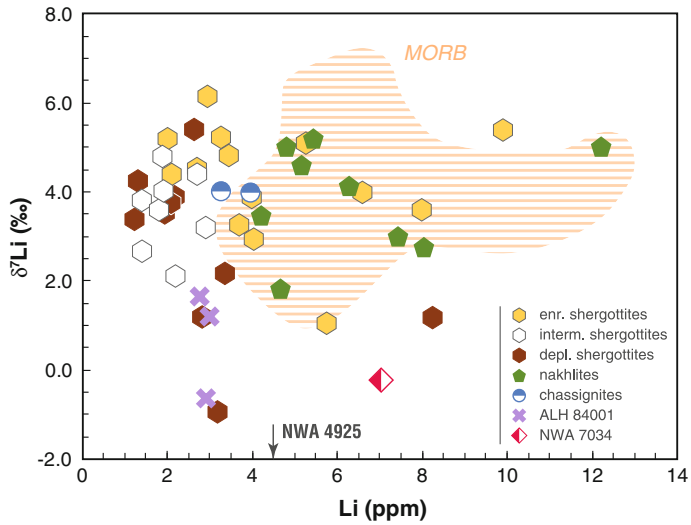

Fig. 3.9 Lithium content versus δ^7Li in Martian meteorites. A rather restricted variation in Li abundance and isotopic composition is observed for intermediate shergotittes compared to the larger range of δ^7Li found for enriched and depleted shergottites. Nakhlites (clinopyroxenites) carry higher Li contents whereas orthopyroxenite ALH 84001 has low Li content and δ^7Li. The polymict breccia NWA 7034 seems to provide first-order constraints on Li systematics of the Martian surface because its major element composition closely resembles some regions of Mars (Agee et al. 2013; McSween et al. 2009). Multiple data obtained for different aliquots of the same samples are not distinguished but they show rather consistent δ^7Li results to within ±1.2 ‰ (2σ), with the exception of Shergotty, Zagami, EETA 79001A and ALH 84001. Some samples appear to have experienced terrestrial weathering (e.g., the low δ^7Li of NWA 4925, discussed in more detail by Magna et al. 2015). Another interesting feature is Li-depleted character of most Martian meteorites when compared to terrestrial MORB (see Sect. 5.2.1). This may imply a distinct magmatic evolution of the Martian mantle because this Li depletion comprises all basaltic rocks (primarily shergottites) and extends over the range of magmatic ages (from about 600 to roughly 150 Ma), recorded for basaltic products of Martian magmatism. Data sources: Magna et al. (2006, 2015), Seitz et al. (2006), Reynolds et al. (2006) and Filiberto et al. (2012)

for Li isotopic compositions were largely unexplored. Magna et al. (2006), Reynolds et al. (2006) and Seitz et al. (2006) published the first Li isotopic data for several martian meteorites (Fig. 3.9) and found that Mars has a similar range in δ^7Li as both the Earth and the Moon, implying that (i) planetary size and timing of bulk planet solidification have little effect on the final Li isotopic composition of the respective silicate mantles, and (ii) all three major planetary bodies appear to have broadly similar Li isotopic composition close to chondritic values with only limited variation (Magna et al. 2015). The δ^7Li of the bulk silicate Mars (BSM) has been estimated to be similar to that of the bulk silicate Earth (Magna et al. 2006; Seitz et al. 2006) from a rather limited number of meteorites analyzed. More recently, Magna et al. (2015) have estimated $\delta^7Li_{BSM} = +4.2 \pm 0.9$ ‰ (2σ) by using a larger meteorite population and considering only (i) falls and cold desert meteorites because these meteorites are less prone to alteration (Fehr et al. 2009) as well as wall-rock contamination, (ii) insignificant fractionation of δ^7Li during magmatic process (Tomascak et al. 1999), and (iii) meteorites with high MgO contents (>15 wt %) because these rocks are thought to most closely approach primitive melt compositions (Nyquist et al. 2009). It is interesting to note that this estimate involves enriched, intermediate as well as depleted shergottites, meaning that whatever process was responsible for the incompatible element patterns in these high-MgO rocks, it apparently did not impose any effect to δ^7Li. Pre-terrestrial as well as terrestrial weathering may become an issue under particular conditions but most martian meteorites appear to be devoid of these effects (Magna et al. 2015).

Contrary to lunar stratigraphy with abundant early crystallized crust (Shearer et al. 2006) and the important role of crustal evolution for global terrestrial geological history (Taylor and McLennan 1985), no clear evidence for a similar major reservoir with vastly different chemistry relative to the mantle has so far been identified on Mars. Orbital remote sensing as well as rover in situ data have shown that surface lithologies of Mars may have basalt-andesitic affinity and that SNC meteorites are less representative of the martian surface (McSween et al. 2009), although petrologically and chemically distinguished lithologies are being increasingly discovered (e.g., Stolper et al. 2013). This may also have profound consequences on bulk planetary Li distribution as the Earth's continental crust carries a significant proportion of Li (Teng et al. 2004) that accumulated during long-term cycles of crustal growth, involving multiple episodes of subduction, re-melting, recycling etc. It is clear that none of the SNC meteorites that were delivered to the Earth via a series of independent impacts on the martian surface between ~0.7 and ~20 Ma (Nyquist et al. 2001) represents a true heritage of the martian crust. This has become evident from Li analyses of a larger number of SNC meteorites (Magna et al. 2015; Seitz et al. 2006) that do not deviate significantly from the Li isotopic range found for chemically similar terrestrial mantle-derived rocks (cf. terrestrial continental crust with different systematics, see Chap. 5).

Although it is not necessary to expect the martian crustal systematics to be similar to those of the Earth (compare, for example, the vastly different and reversed Li systematics of lunar anorthositic crust; see Sect. 3.3.1 and Fig. 3.8), the silicate character of bulk Mars may be indicative of a Li signature broadly similar to that of the Earth. This is underscored by a larger suite of martian meteorites analyzed for Li (Magna et al. 2015). An appealing feature is a low Li content of some of the primitive martian meteorites, often < 2 ppm (Fig. 3.9). These low Li contents are largely missing in pristine mantle-derivative melts on Earth, such as mid-ocean ridge or oceanic island basalts, generally with >3 ppm (see Chap. 5).

More recently, two peculiar martian meteorites were found that may bear some important information on the chemistry of the surface of Mars. The Tissint fall is a depleted shergottite akin to other depleted shergottites in its chemical composition but it contains peculiar black glass enclosed in the main mass that is thought to carry a chemical signature of martian surface and atmosphere (Chennaoui Aoudjehane et al. 2012); we note here the recent disagreement with such a

view (Barrat et al. 2014). The chemical composition of ~4.4 Ga (Nyquist et al. 2013) polymict breccia NWA 7034 fits with in situ and remote sensing data (Agee et al. 2013; Humayun et al. 2013), thus providing evidence for a component of Mars, temporally, chemically and petrologically distinct from the SNC meteorites. In particular, the Li isotopic composition of NWA 7034 (−0.2 ‰; Magna et al. 2015) points toward Li elemental and isotopic distinction between the martian mantle and crust (Fig. 3.9), similar to that observed for the Earth (Teng et al. 2004) despite the smaller magnitude of difference in Li abundance. Here we note moderate Li contents (~10 ppm) in martian surface lithologies, obtained with the *Curiosity* mission (e.g., Ollila et al. 2014).

It is viable that part of the δ^7Li variation recorded in martian meteorites may hint at metasomatic activity during or shortly after the emplacement of lavas at very shallow depths. Such a view is consistent with tight positive correlation between Li and Cl abundances in the martian suite, paralleled by broadly positive correlation of δ^7Li with Li/Cl ratios. Curiously, these observations were also made for geothermal fluids from the Taupo Volcanic Zone, New Zealand, and Yellowstone, USA (Bernal et al. 2014; Millot et al. 2012; Sturchio and Chan 2003), implying a low-tempered origin of Cl-rich fluid percolation in Mars. This suggests that materials relatively enriched in isotopically light Li were available at near-surface levels, such as found for those nakhlites (Magna et al. 2015), which have shallower estimated depths of crystallization (Day et al. 2006). These shallow-seated clinopyroxenites carry a greater proportion of mesostasis with secondary minerals compared to their deeper counterparts having δ^7Li signatures more closely resembling that of bulk Mars. Deeper nakhlites have slightly higher δ^7Li values whereas both known dunites have δ^7Li within the range of mantle olivine from Earth. One potential means of producing this relationship is settling of olivine and clinopyroxene from a magma chamber, perhaps under equilibrium conditions (see Chap. 4 for inter-mineral Li isotopic fractionation). Whether or not clinopyroxenites and cumulate chassignites (dunites) are co-magmatic (McCubbin et al. 2013) remains to be further investigated but available Li data are consistent with that interpretation. Saline brines have also been advocated for ancient ALH 84001 cumulate orthopyroxenite (Lapen et al. 2010), once thought to carry signatures of early pre-terrestrial life (McKay et al. 1996). The light Li isotopic signature in this particular meteorite (Magna et al. 2015; Seitz et al. 2006) is consistent with crustal contamination or the imprint of fluid percolation. Moreover, local brines have also been inferred for NWA 7034 (Agee et al. 2013) and its low δ^7Li may confirm large-scale fluid activity during the earlier, "wetter" history of Mars, considering abundant water dissolved in martian magmas (McCubbin et al. 2012; McSween et al. 2001). A recent theoretical treatment by Fairén et al. (2015) modelled the evolution of Li elemental and isotopic signature during weathering of a basalt on the martian surface because the early atmosphere of Mars was different from the current one and also from the Earth's atmosphere in terms of chemical and physical parameters. The formation of various low-temperature clay minerals could impart distinctive Li systematics to these weathering products in the presence of water. Whether this computational modelling accurately simulates true martian surface conditions remains to be validated with future in situ as well as sample return missions.

3.3.3 Lithium in Vesta

Analyses of howardites–eucrites–diogenites (HED meteorites) that most likely come from asteroid 4-Vesta are less common than those of lunar and martian rocks. With a diameter of ~530 km, Vesta is the second largest asteroid in the Solar System after Ceres. Its ancient age of ~4565 Myr was indicated independently by extant as well as extinct chronometers such as Sm–Nd, Lu–Hf, Hf–W, and Mn–Cr (e.g., Blichert-Toft et al. 2002; Day et al. 2012; Kleine et al. 2004). The HED meteorites differ in chemistry and petrography from other

achondrites and it is apparent that they originated from a moderately small body that experienced igneous processes, formation of a small metallic core, and crust–mantle segregation, followed by thermal metamorphism, the latter likely caused by large impacts. Basaltic eucrites that are thought to originate in the shallow crust of Vesta are significantly enriched in Li (generally >7 ppm and up to 15 ppm; Magna et al. 2014a; Magna et al. 2006; Murty et al. 1983; Pogge von Strandmann et al. 2011; Seitz et al. 2007; Tera et al. 1970), yet their Li isotopic signature is largely invariable with δ^7Li values reported between +2.2 and +4.9 ‰ (Magna et al. 2014a; Magna et al. 2006; Pogge von Strandmann et al. 2011; Seitz et al. 2007), irrespective of major element chemistry.

Several observations can be made for eucrites despite the rather limited Li isotopic range in HED clan meteorites (Fig. 3.10). First, the isotopically heavy eucrite Cachari (Magna et al. 2014a; Magna et al. 2006) appears to have been modified by a currently unidentified process, as also supported by its aberrant oxygen isotopic composition (Wiechert et al. 2004). Whether or not this signature results from low temperature post-magmatic processes is to be further investigated but it could be a hint to secondary processes acting on an asteroidal body. Second, Stannern and Bouvante, representative of possible mixing/contamination of main-trend eucrites with crustal melts enriched in incompatible elements (the so-called Stannern trend), have δ^7Li values that are irresolvable from other eucrites, but appear to carry slightly elevated Li contents (Magna et al. 2014a; Magna et al. 2006; Pogge von Strandmann et al. 2011; Tera et al. 1970). This is contrary to heavy δ^{57}Fe values measured for Stannern-trend eucrites (Wang et al. 2012) which were probably caused by late-stage ilmenite accumulation because these particular eucrites experienced re-melting of a former asteroidal crust with significant amounts of ilmenite (Barrat et al. 2007). Third, the Li isotopic signature of the eucrite Pasamonte (Magna et al. 2006) is similar to other eucrites although its distinctive oxygen isotopic composition (Greenwood et al. 2005; Scott et al. 2009) may indicate its origin from a different parent body than the other eucrites (cf. discussion in Barrat et al. 2011, on this issue). If correct then Li would provide evidence for multiple asteroidal bodies in the early Solar System history that experienced melting and magmatic evolution at asteroidal/planetesimal levels leading to the development of basaltic crusts with largely uniform Li contents and isotopic compositions. Fourth, lower Li abundances found in cumulate eucrites (i.e. those which inherited a large portion of crystals from other sources, such as Serra de Magé and EET 87548) are not reflected in distinctive Li isotopic composition.

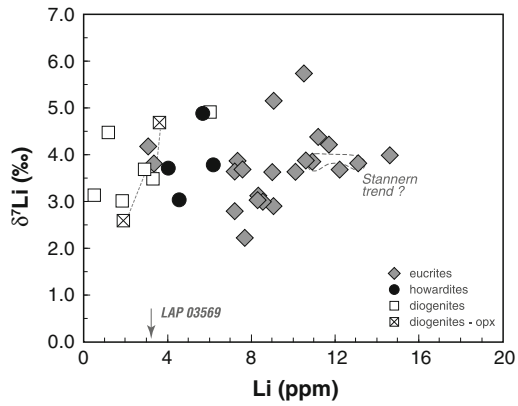

Fig. 3.10 Lithium content versus δ^7Li in meteorites from asteroid Vesta. A range in Li abundance for all major suites (howardites, eucrites, diogenites) is not paralleled by significant variation in δ^7Li. This limited range of δ^7Li values is uncommon to all other major planetary bodies for which multiple data exist (Earth, Moon, Mars) and may hint to short-term magmatism and limited post-magmatic disturbance. The incompatible-element-enriched Stannern trend eucrites do not plot significantly off the major Li trend found for other eucrites. Dashed line connects bulk samples and orthopyroxene from the Johnstown and Bilanga meteorites. La Paz Icefield (LAP) 03569 plots below the depicted range (δ^7Li = −4.25 ‰). Data sources: Magna et al. (2006, 2014a), Seitz et al. (2007) and Pogge von Strandmann et al. (2011)

Diogenites are igneous plutonic orthopyroxene-rich deep-crustal cumulates (Barrat et al. 2010, 2008). Their Li systematics has remained largely unknown with the exception of two values given in Seitz et al. (2007) that showed rather low Li contents (see also Krankowsky and Müller 1964), paralleled by δ^7Li

values similar to the Vesta's mantle. Nevertheless, diogenites with high Li contents also exist, perhaps resulting from the presence of eucritic clasts in diogenitic matrix (e.g., Aioun el-Atrouss). More recent data on diogenites (Magna et al. 2014a) concur with those of Seitz et al. (2007) in that they closely mimic the δ^7Li range found in eucrites (Fig. 3.10). The sole exception to date for the whole HED clan is LAP 03569 diogenite with uniquely low δ^7Li of −4.3 ‰. Such values are known from terrestrial mantle peridotites that experienced kinetic fractionation through diffusive ingress of Li (Chaps. 4 and 5). It is not clear, however, if this could have happened on Vesta too, as this process requires certain conditions such as an active metasomatic environment. Alternatively, such low vaues could hint at contamination during residence on Earth's surface. Howardites are physical mixtures of eucrites and diogenites and the available Li data (Magna et al. 2014a) appear to be consistent with this view. In general, the δ^7Li of the bulk silicate Vesta is well constrained from the available data at +3.7 ± 0.6 ‰ (1σ) which is intermediate between that of the bulk silicate Earth and bulk silicate Mars and Moon, but overlapping within rather broad uncertainties.

Several further observations are clear and it is apparent that Li isotopic variations must be caused by processes other than: (i) core segregation which appears to have had detectable effects on δ^{30}Si values (Pringle et al. 2013), and (ii) volatile loss during large collisions that resulted in stripping off the elements like Zn (Paniello et al. 2012) and Cd (Schönbächler et al. 2008). No such observations of Li modification/loss are currently apparent. Therefore, Li remained largely undepleted in Vesta (Magna et al. 2014a) despite a violent early history comprising a magma ocean stage, thermal metamorphism, cataclysmic bombardments and possible post-magmatic disturbances.

References

Agee CB, Wilson NV, McCubbin FM, Ziegler K, Polyak VJ, Sharp ZD, Asmerom Y, Nunn MH, Shaheen R, Thiemens MH, Steele A, Fogel ML, Bowden R, Glamoclija M, Zhang Z, Elardo SM (2013) Unique meteorite from Early Amazonian Mars: water-rich basaltic breccia Northwest Africa 7034. Science 339:780–785

Ahrens B, Stix M, Thorn M (1992) On the depletion of lithium in the Sun. Astron Astrophys 264:673–678

Anders E, Grevesse N (1989) Abundances of the elements: meteoritic and solar. Geochim Cosmochim Acta 53:197–214

Andersen J, Gustafsson B, Lambert DL (1984) The lithium isotope ratio in F and G stars. Astron Astrophys 136:65–73

Asplund M, Grevesse N, Sauval J, Scott P (2009) The chemical composition of the Sun. Annu Rev Astron Astrophys 47:481–522

Asplund M, Lambert DL, Nissen PE, Primas F, Smith VV (2006) Lithium isotopic abundances in metal-poor halo stars. Astrophys J 644:229–259

Audi G, Bersillon O, Blachot J, Wapstra AH (2003) The NUBASE evaluation of nuclear and decay properties. Nucl Phys A 729:3–128

Audouze J, Boulade O, Malinie G, Poilane Y (1983) Galactic evolution of the lithium isotopes. Astron Astrophys 127:164–168

Balsiger H, Geiss J, Groegler N, Wyttenbach A (1968) Distribution and isotopic abundance of lithium in stone meteorites. Earth Planet Sci Lett 5:17–22

Barrat JA, Chaussidon M, Bohn M, Gillet P, Göpel C, Lesourd M (2005) Lithium behavior during cooling of a dry basalt: an ion-microprobe study of the lunar meteorite Northwest Africa 479 (NWA 479). Geochim Cosmochim Acta 69:5597–5609

Barrat JA, Yamaguchi A, Greenwood RC, Bohn M, Cotten J, Benoit M, Franchi IA (2007) The Stannern trend eucrites: contamination of main group eucritic magmas by crustal partial melts. Geochim Cosmochim Acta 71:4108–4124

Barrat JA, Yamaguchi A, Greenwood RC, Benoit M, Cotten J, Bohn M, Franchi IA (2008) Geochemistry of diogenites: still more diversity in their parental melts. Meteorit Planet Sci 43:1759–1775

Barrat JA, Yamaguchi A, Bunch TE, Bohn M, Bollinger C, Ceuleneer G (2011) Possible fluid–rock interactions on differentiated asteroids recorded in eucritic meteorites. Geochim Cosmochim Acta 75:3839–3852

Barrat JA, Jambon A, Ferrière L, Bollinger C, Langlade JA, Liorzou C, Boudouma O, Fialin M (2014) No Martian soil component in shergottite meteorites. Geochim Cosmochim Acta 125:23–33

Barrat J-A, Yamaguchi A, Zanda B, Bollinger C, Bohn M (2010) Relative chronology of crust formation on asteroid Vesta: Insights from the geochemistry of diogenites. Geochim Cosmochim Acta 74:6218–6231

Baumann P, Ramírez I, Meléndez J, Asplund M, Lind K (2010) Lithium depletion in solar-like stars: no planet connection. Astron Astrophys 519:A87

Beard BL, Taylor LA, Scherer EE, Johnson CM, Snyder GA (1998) The source region and melting mineralogy of high-titanium and low-titanium lunar basalts deduced from Lu-Hf isotope data. Geochim Cosmochim Acta 62:525–544

Beck P, Barrat JA, Chaussidon M, Gillet P, Bohn M (2004) Li isotopic variations in single pyroxenes from the Northwest Africa 480 shergottite (NWA 480): a record of degassing of Martian magmas? Geochim Cosmochim Acta 68:2925–2933

Beck P, Chaussidon M, Barrat JA, Gillet P, Bohn M (2006) Diffusion induced Li isotopic fractionation during the cooling of magmatic rocks: the case of pyroxene phenocrysts form nakhlite meteorites. Geochim Cosmochim Acta 70:4813–4825

Becker RH, Pepin RO (1984) The case for a martian origin of the shergottites: nitrogen and noble gases in EETA 79001. Earth Planet Sci Lett 69:225–242

Bell DR, Buseck PR, Channon M, Hervig RL, Rieck K, Singletary SJ (2008) SIMS analysis of the isotopic composition of lithium in meteorites. Lunar Planet Sci Conf XXXIX, #2276

Bernal NF, Gleeson SA, Dean AS, Liu X-M, Hoskin P (2014) The source of halogens in geothermal fluids from the Taupo Volcanic Zone, North Island. New Zealand Geochim Cosmochi Acta 126:265–283

Bernas R, Gradsztajn E, Reeves H, Schatzman E (1967) On the nucleosynthesis of lithium, beryllium, and boron. Ann Physics 44:426–478

Blichert-Toft J, Boyet M, Télouk P, Albarède F (2002) ^{147}Sm-^{143}Nd and ^{176}Lu-^{176}Hf in eucrites and the differentiation of the HED parent body. Earth Planet Sci Lett 204:167–181

Bogard DD, Johnson P (1983) Martian gases in an Antarctic meteorite? Science 221:651–654

Borg LE, Connelly JN, Boyet M, Carlson RW (2011) Chronological evidence that the Moon is either young or did not have a global magma ocean. Nature 477:70–72

Brown JA, Sneden C, Lambert DL, Dutchover E Jr (1989) A search for lithium-rich giant stars. Astrophys J Suppl 71:293–322

Caffau E, Bonifacio P, François P, Sbordone L, Monaco L, Spite M, Spite F, Ludwig H-G, Cayrel R, Zaggia S, Hammer F, Randich S, Molaro P, Hill V (2011) An extremely primitive star in the Galactic halo. Nature 477:67–69

Cameron AGW, Fowler WA (1971) Lithium and the *s*-process in red-giant stars. Astrophys J 164:111–114

Canup RM (2004) Dynamics of lunar formation. Annu Rev Astron Astrophys 42:441–475

Carlberg JK, Smith VV, Cunha K, Majewski SR, Rood RT (2010) The super lithium-rich red giant rapid rotator G0228 + 73.2600: a case for planet accretion? Astrophys J Lett 723:L103–L107

Carlson RW, Lugmair GW (1988) The age of ferroan anorthosite 60025: oldest crust on a young Moon? Earth Planet. Sci Lett 90:119–130

Coc A, Goriely S, Xu Y, Saimpert M, Vangioni E (2012) Standard Big Bang Nucleosynthesis up to CNO with an improved extended nuclear network. Astrophys J 744, paper number 158, doi: 10.1088/0004-637X/744/2/158

Coc A (2013) Primordial nucleosynthesis. Acta Phys Polonica B 44:521–530

Coogan LA (2011) Preliminary experimental determination of the partitioning of lithium between plagioclase crystals of different anorthite contents. Lithos 125:711–715

Coogan LA, Kasemann SA, Chakraborty S (2005) Rates of hydrothermal cooling of new oceanic upper crust derived from lithium-geospeedometry. Earth Planet Sci Lett 240:415–424

Craddock PR, Dauphas N, Clayton RN (2010) Mineralogical control on iron isotopic fractionation during lunar differentiation and magmatism. 41st Lunar Planet Sci Conf, #1230

Cyburt RH, Fields BD, Olive KA (2008) An update on the big bang nucleosynthesis prediction for ^{7}Li: the problem worsens. J Cosmol Astropart Phys 11, paper number 012, doi:10.1088/1475-7516/2008/1011/1012

Chaklader J, Shearer CK, Borg LE (2006) The behavior of Li and B in lunar mare basalts during crystallization, shock, and thermal metamorphism: Implications for volatile element contents of martian basalts. Am Mineral 91:1553–1564

Charbonnel C, Talon S (2005) Influence of gravity waves on the internal rotation and Li abundance of Solar-type stars. Science 309:2189–2191

Charbonnel C, Tosi M, Primas F, Chiappini C (2009) Light elements in the Universe, IAU Symposium 268. Cambridge Univ. Press, p. 504

Chaussidon M, Robert F (1998) ^{7}Li/^{6}Li and ^{11}B/^{10}B variations in chondrules from Semarkona unequilibrated chondrite. Earth Planet Sci Lett 164:577–589

Chaussidon M, Robert F (1999) Lithium nucleosynthesis in the Sun inferred from the solar-wind ^{7}Li/^{6}Li ratio. Nature 402:270–273

Chaussidon M, Robert F, McKeegan KD (2006) Li and B isotopic variations in an Allende CAI: Evidence for the in situ decay of short-lived ^{10}Be and for the possible presence of the short-lived nuclide ^{7}Be in the early solar system. Geochim Cosmochim Acta 70:224–245

Chennaoui Aoudjehane H, Avice G, Barrat JA, Boudouma O, Chen G, Duke MJM, Franchi IA, Gattacceca J, Grady MM, Greenwood RC, Herd CDK, Hewins R, Jambon A, Marty B, Rochette P, Smith CL, Sautter V, Verchovsky A, Weber P, Zanda B (2012) Tissint martian meteorite: a fresh look at the interior, surface, and atmosphere of Mars. Science 338:785–788

Day JMD, Taylor LA, Floss C, McSween HY (2006) Petrology and chemistry of MIL 03346 and its significance in understanding the petrogenesis of nakhlites on Mars. Meteorit Planet Sci 41:581–606

Day JMD, Rudnick RL, McDonough WF, Walker RJ, Taylor LA (2008) Lithium isotope constraints on magma ocean differentiation and the composition of the terrestrial planets. Lunar Planet Sci Conf XXXIX, #1072

Day JMD, Walker RJ, Qin L, Rumble D (2012) Late accretion as a natural consequence of planetary growth. Nature Geosci 5:614–617

Delbourgo-Salvador P, Gry C, Malinie G, Audouze J (1985) Effects of nuclear uncertainties and chemical evolution on the standard big bang nucleosynthesis. Astron Astrophys 150:53–61

Delgado Mena E, Bertrán de Lis S, Adibekyan VZ, Sousa SG, Figueira P, Mortier A, González Hernández JI, Tsantaki M, Israelian G, Santos NC (2015) Li abundances in F stars: planets, rotation, and Galactic evolution. Astron. Astrophys. 576, paper number A69, doi: 10.1051/0004-6361/201425433

Desch SJ, Ouellette N (2006) Comment on Li and Be isotopic variations in an Allende CAI: Evidence for the in situ decay of short-lived ^{10}Be and for the possible presence of the short-lived nuclide ^{7}Be in the early solar system, by M. Chaussidon, F. Robert, and K.D. McKeegan Geochim Cosmochim Acta 70:5426–5432

Dews JR (1966) The isotopic composition of lithium in chondrules. J Geophys Res 71:4011–4020

Dreibus G, Spettel B, Wänke H (1976) Lithium as a correlated element, its condensation behaviour and its use to estimate the bulk composition of the moon and eucrite parent body. Proc Lunar Sci Conf 7th, 3383–3396

Eugster O, Bernas R (1971) Li, B, Mg and Ti isotopic abundances and search for trapped solar wind Li in Apollo 11 and Apollo 12 material. Proc Lunar Sci Conf 2:1461–1469

Fairén AG, Losa-Adams E, Gil-Lozano C, Gago-Duport L, Uceda ER, Squyres SW, Rodríguez AP, Davila AF, McKay CP (2015) Tracking the weathering of basalts on Mars using lithium isotope fractionation models. Geochem Geophys Geosys 16, doi:10.1002/2015GC005748

Fehr MA, James RH, Sephton MA, Martins Z, Bland PA (2009) Primitive lithium isotope signatures in CR carbonaceous chondrites? Geochim Cosmochim Acta 73:A359

Ferlet R, Dennefeld M (1984) Interstellar lithium and the ^{7}Li/^{6}Li ratio in diffuse clouds. Astron Astrophys 138:303–310

Fields BD (2011) The primordial lithium problem. Annu Rev Nucl Particle Sci 61:47–68

Figueira P, Faria JP, Delgado-Mena E, Adibekyan VZ, Sousa SG, Santos NC, Israelian G (2014) Exoplanet hosts reveal lithium depletion: Results from a homogeneous statistical analysis. Astron Astrophys 570, paper number A21, doi:10.1051/0004-6361/201424218

Filiberto J, Chin E, Day JMD, Franchi IA, Greenwood RC, Gross J, Penniston-Dorland SC, Schwenzer SP, Treiman AH (2012) Geochemistry of intermediate olivine-phyric shergottite Northwest Africa 6234, with similarities to basaltic shergottite Northwest Africa 480 and olivine-phyric shergottite Northwest Africa 2990. Meteorit Planet Sci 47:1256–1273

Fitoussi C, Bourdon B (2012) Silicon isotope evidence against an enstatite chondrite Earth. Science 335:1477–1480

Fujiya W, Hoppe P, Ott U (2011) Hints for neutrino-process boron in presolar silicon carbide grains from supernovae. Astrophys J Lett 730, paper number L7, doi:10.1088/2041-8205/1730/1081/L1087

Garcia-Munoz M, Mason GM, Simpson JA (1975) The isotopic composition of galactic cosmic-ray lithium, beryllium, and boron. Astrophys J 201:L145–L148

García Pérez AE, Aoki W, Inoue S, Ryan SG, Suzuki TK, Chiba M (2009) ^{6}Li/^{7}Li estimates for metal-poor stars. Astron Astrophys 504:213–223

Garner EL, Machlan LA, Barnes IL (1975) The isotopic composition of lithium, potassium, and rubidium in some Apollo 11, 12, 14, 15, and 16 samples. Proc Lunar Sci Conf 6th, 1845–1855

Ghezzi L, Cunha K, Smith VV, Margheim S, Schuler S, de Araújo FX, de la Reza R (2009) Measurements of the isotopic ratio ^{6}Li/^{7}Li in stars with planets. Astrophys J 698:451–460

Giguere TA, Taylor GJ, Hawke BR, Lucey PG (2000) The titanium contents of lunar mare basalts. Meteorit Planet Sci 35:193–200

Gradsztajn E, Salome M, Yaniv A, Bernas R (1967) Isotopic analysis of lithium in the Holbrook meteorite and in terrestrial samples with a sputtering ion source mass spectrometer. Earth Planet Sci Lett 3:387–393

Greenwood RC, Franchi IA, Jambon A, Buchanan PC (2005) Widespread magma oceans on asteroidal bodies in the early Solar System. Nature 435:916–918

Gyngard F, Amari S, Zinner E, Ott U (2009) Interstellar exposure ages of large presolar SiC grains from the Murchison meteorite. Astrophys J 694:359–366

Hammache F, Heil M, Typel S, Galaviz D, Sümmerer K, Coc A, Uhlig F, Attalah F, Caamano M, Cortina D, Geissel H, Hellström M, Iwasa N, Kiener J, Koczon P, Kohlmeyer B, Mohr P, Schwab E, Schwarz K, Schümann F, Senger P, Sorlin O, Tatischeff V, Thibaud JP, Vangioni EAW, Walus W (2010) High-energy breakup of ^{6}Li as a tool to study the Big Bang nucleosynthesis reaction ^{2}H(α, γ)^{6}Li Phys Review C 82, paper number 065803, doi:065810.061103/PhysRevC.065882.065803

Hanon P, Chaussidon M, Robert F (1999) Distribution of lithium, beryllium, and boron in meteoritic chondrules. Meteorit Planet Sci 34:247–258

Hauri EH, Weinreich T, Saal AE, Rutherford MC, Van Orman JA (2011) High pre-eruptive water contents preserved in lunar melt inclusions. Science 333:213–215

Herd CDK, Treiman AH, McKay GA, Shearer CK (2004) The behavior of Li and B during planetary basalt crystallization. Am Mineral 89:832–840

Herd CDK, Treiman AH, McKay GA, Shearer CK (2005) Light lithophile elements in martian basalts: evaluating the evidence for magmatic water degassing. Geochim Cosmochim Acta 69:2431–2440

Hobbs LM, Thorburn JA (1994) Lithium isotope ratios in six halo stars. Astrophys J 428:L25–L28

Hobbs LM, Thorburn JA, Rebull LM (1999) Lithium isotope ratios in halo stars III. Astrophys J 523:797–804

Howk JC, Lehner N, Fields BD, Mathews GJ (2012) Observation of interstellar lithium in the low-metallicity Small Magellanic Cloud. Nature 489:121–123

Humayun M, Nemchin A, Zanda B, Hewins RH, Grange M, Kennedy A, Lorand J-P, Göpel C, Fieni C, Pont S, Deldicque D (2013) Origin and age of the earliest Martian crust from meteorite NWA7533. Nature 503:513–516

Iocco F, Mangano G, Miele G, Pisanti O, Serpico PD (2009) Primordial nucleosynthesis: from precision cosmology to fundamental physics. Phys Reports 472:1–76

Irving AJ, Kuehner SM, Bunch TE, Ziegler K, Chen G, Herd CDK, Conrey RM, Ralew S (2013) Ungrouped mafic achondrite Northwest Africa 7325: a reduced, iron-poor cumulate olivine gabbro from a differentiated planetary parent body. 44th Lunar Planet Sci Conf, #2164

Israelian G, Delgado Mena E, Santos NC, Sousa SG, Mayor M, Udry S, Domínguez Cerdeña C, Rebolo R, Randich S (2009) Enhanced lithium depletion in Sun-like stars with orbiting planets. Nature 462: 189–191

Jaeger M, Wilmes S, Kölle V, Staudt G, Mohr P (1996) Precision measurement of the half-life of ^{7}Be. Phys Rev C 54:423–424

James RH, Palmer MR (2000) The lithium isotope composition of international rock standards. Chem Geol 166:319–326

Javoy M, Kaminski E, Guyot F, Andrault D, Sanloup C, Moreira M, Labrosse S, Jambon A, Agrinier P, Davaille A, Jaupart C (2010) The chemical composition of the Earth: Enstatite chondrite models. Earth Planet Sci Lett 293:259–268

Jeffcoate AB, Elliott T, Kasemann SA, Ionov D, Cooper KM (2007) Li isotope fractionation in peridotites and mafic melts. Geochim Cosmochim Acta 71:202–218

Jerde EA, Snyder GA, Taylor LA, Liu Y-G, Schmitt RA (1994) The origin and evolution of lunar high-Ti basalts: Periodic melting of a single source at Mare Tranquillitatis. Geochim Cosmochim Acta 58:515–527

Kawanomoto S, Kajino T, Aoki W, Bessel M, Suzuki TK, Ando H, Noguchi K, Honda S, Izumiura H, Kambe E, Okita K, Sadakane K, Sato B, Tajitsu A, Takada-Hidai M, Tanaka W, Watanabe E, Yoshida M (2009) The new detections of ^{7}Li/^{6}Li isotopic ratio in the interstellar media. Astrophys J 701:1506–1518

Kleine T, Mezger K, Münker C, Palme H, Bischoff A (2004) ^{182}Hf-^{182}W isotope systematics of chondrites, eucrites, and martian meteorites: Chronology of core formation and early mantle differentiation in Vesta and Mars. Geochim Cosmochim Acta 68:2935–2946

Knauth DC, Federman SR, Lambert DL (2003) An ultra-high-resolution survey of the interstellar ^{7}Li/^{6}Li isotope ratio in the solar neighborhood. Astrophys J 586:268–285

Knauth DC, Federman SR, Lambert DL, Crane P (2000) Newly synthesized lithium in the interstellar medium. Nature 405:656–658

Koch A, Lind K, Rich RM (2011) Discovery of a super-Li-rich turnoff star in the metal-poor globular cluster NGC 6397. Astrophys J Lett 738:L29

Krankowsky D, Müller O (1964) Isotopenhäufigkeit und Konzentration des Lithiums in Steinmeteoriten. Geochim Cosmochim Acta 28:1625–1630

Krankowsky D, Müller O (1967) Isotopic composition and abundance of lithium in meteoritic matter. Geochim Cosmochim Acta 31:1833–1842

Krot AN, Keil K, Scott ERD, Goodrich CA, Weisberg MK (2014) Classification of meteorites and their genetic relationships. In: Davis AM (ed.), Treatise on Geochemistry, Vol 1, 2nd edition. Elsevier Ltd., Oxford pp. 1–63

Kumar YB, Reddy BE, Lambert DL (2011) Origin of lithium enrichment in K giants. Astrophys J Lett 730: L12

Lapen TJ, Righter M, Brandon AD, Debaille V, Beard BL, Shafer JT, Peslier AH (2010) A younger age for ALH84001 and its geochemical link to shergottite sources in Mars. Science 328:347–351

Lemoine M, Ferlet R, Vidal-Madjar A, Emerich C, Bertin P (1993) Interstellar lithum and the ^{7}Li/^{6}Li ratio toward ρ Oph. Astron Astrophys 269:469–476

Lentz RCF, McSween HY, Ryan J, Riciputi LR (2001) Water in martian magmas: clues from light lithophile elements in shergottite and nakhlite pyroxenes. Geochim Cosmochim Acta 65:4551–4565

Leya I (2011) Cosmogenic effects on ^{7}Li/^{6}Li, ^{10}B/^{11}B, and ^{182}W/^{184}W in CAIs from carbonaceous chondrites. Geochim Cosmochim Acta 75:1507–1518

Lind K, Melendez J, Asplund M, Collet R, Magic Z (2013) The lithium isotopic ratio in very metal-poor stars. Astron Astrophys 554, paper number A96, doi:10.1051/0004-6361/201321406

Liu Y, Spicuzza MJ, Craddock PR, Day JMD, Valley JW, Dauphas N, Taylor LA (2010) Oxygen and iron isotope constraints on near-surface fractionation effects and the composition of lunar mare basalt source regions. Geochim Cosmochim Acta 74:6249–6262

Lodders K (2003) Solar system abundances and condensation temperatures of the elements. Astrophys J 591:1220–1247

Longhi J (1992) Origin of picritic green glass magmas by polybaric fractional fusion. Proc Lunar Planet Sci Conf 22:343–353

Lundstrom CC, Chaussidon M, Hsui AT, Kelemen P, Zimmerman M (2005) Observations of Li isotopic variations in the Trinity Ophiolite: Evidence for isotopic fractionation by diffusion during mantle melting. Geochim Cosmochim Acta 69:735–751

Lyon IC, Tizard JM, Henkel T (2007) Evidence for lithium and boron from star-forming regions implanted in presolar SiC grains. Meteorit Planet Sci 42:373–385

Magna T, Neal CR (2011) Lithium isotope composition of lunar crust—rapid crystallization and post-solidification quiescence? Mineral Mag 75: A1385

Magna T, Wiechert U, Halliday AN (2006) New constraints on the lithium isotope compositions of the Moon and terrestrial planets. Earth Planet Sci Lett 243:336–353

Magna T, Šimčíková M, Moynier F (2014a) Lithium systematics in howardite–eucrite–diogenite meteorites: Implications for crust–mantle evolution of planetary embryos. Geochim Cosmochim Acta 125:131–145

Magna T, Žák K, Farkaš J, Trubač J, Rodovská Z, Šimeček M, Skála R, Řanda Z, Mizera J (2014b):

Lithium and magnesium isotopes in sediments of the Ries area: Constraints on the sources of moldavite tektites. Meteorit Planet Sci 49:A254

Magna T, Neal CR, Tomascak PB, Bourdon B, Oberli F, Day JMD (2009) On lithium isotope systematics and abundances in lunar mare basalts. Geochim Cosmochim Acta 73:A816

Magna T, Deutsch A, Mezger K, Skála R, Seitz H-M, Mizera J, Řanda Z, Adolph L (2011) Lithium in tektites and impact glasses: Implications for sources, histories and large impacts. Geochim Cosmochim Acta 75:2137–2158

Magna T, Day JMD, Mezger K, Fehr MA, Dohmen R, Chennaoui Aoudjehane H, Agee C (2015) Lithium isotope constraints on crust-mantle interactions and surface processes on Mars. Geochim Cosmochim Acta 162:46–65

Maruyama S, Watanabe M, Kunihiro T, Nakamura E (2009) Elemental and isotopic abundances of lithium in chondrule constituents in the Allende meteorite. Geochim Cosmochim Acta 73:778–793

Maurice E, Spite F, Spite M (1984) The lithium isotope ratio in metal-deficient stars. Astron Astrophys 132:278–282

McCubbin FM, Elardo SM, Shearer CK, Smirnov A, Hauri EH, Draper DS (2013) A petrogenetic model for the comagmatic origin of chassignites and nakhlites: Inferences from chlorine-rich minerals, petrology, and geochemistry. Meteorit Planet Sci 48:819–853

McCubbin FM, Hauri EH, Elardo SM, Vander Kaaden KE, Wang J, Shearer CK (2012) Hydrous melting of the martian mantle produced both depleted and enriched shergottites. Geology 40:683–686

McDonough WF, Teng F-Z, Rudnick RL, Ash RD (2006) Lithium isotopic analyses of chondrites and chondrules. Lunar Planet Sci XXXVII, #2416

McDonough WF, Teng F-Z, Tomascak PB, Ash RD, Grossman JN, Rudnick RL (2003) Lithium isotopic composition of chondritic meteorites. Lunar Planet Sci XXXIV, #1931

McKay DS, Gibson EK Jr, Thomas-Keprta KL, Vali H, Romanek CS, Clemett SJ, Chillier XDF, Maechling CR, Zare RN (1996) Search for past life on Mars: possible relic biogenic activity in Martian Meteorite ALH84001. Science 273:924–930

McSween HY, Taylor GJ, Wyatt MB (2009) Elemental composition of the Martian crust. Science 324:736–739

McSween HY, Grove TL, Lentz RCF, Dann JC, Holzheid AH, Riciputi LR, Ryan JG (2001) Geochemical evidence for magmatic water within Mars from pyroxenes in the Shergotty meteorite. Nature 409:487–490

Meneguzzi M, Audouze J, Reeves H (1971) The production of the elements Li, Be, B by Galactic Cosmic Rays in space and its relation with stellar observations. Astron Astrophys 15:337–359

Meyer DM, Hawkins I, Wright EL (1993) The interstellar $^{7}Li/^{6}Li$ isotope ratio towards ζ Ophiuchi and ζ Persei. Astrophys J 409:L61–L64

Millot R, Hegan A, Négrel P (2012) Geothermal waters from the Taupo Volcanic Zone, New Zealand: Li, B and Sr isotopes characterization. Appl Geochem 27:677–688

Monaco L, Villanova S, Moni Bidin C, Carraro G, Geisler D, Bonifacio P, Gonzalez OA, Zoccali M, Jilkova L (2011) Lithium-rich giants in the Galactic thick disk. Astron Astrophys 529:A90

Murty SVS, Shukla PN, Goel PS (1982) Non-cosmogenic lithium-6 in iron meteorites. Earth Planet Sci Lett 60:1–7

Murty SVS, Shukla PN, Goel PS (1983) Lithium in stone meteorites and stony irons. Meteoritics 18:123–136

Neal CR, Taylor LA (1989) The nature of barium partitioning between immiscible melts: a comparison of experimental and natural systems with reference to lunar granite petrogenesis. Proc Lunar Planet Sci Conf 19:209–218

Nichiporuk W, Moore CB (1970) Lithium in chondritic meteorites. Earth Planet Sci Lett 9:280–286

Nichiporuk W, Moore CB (1974) Lithium, sodium and potassium abundance in carbonaceous chondrites. Geochim Cosmochim Acta 38:1691–1701

Nissen PE, Lambert DL, Primas F, Smith VV (1999) Isotopic lithium abundances in five metal-poor disk stars. Astron Astrophys 348:211–221

Nollett KM, Lemoine M, Schramm DN (1997) Nuclear reaction rates and primordial ^{6}Li. Phys Rev C 56:1144–1150

Norman MD, Taylor SR (1992) Geochemistry of lunar crustal rocks from breccia 67016 and the composition of the Moon. Geochim Cosmochim Acta 56:1013–1024

Nyquist LE, Bogard DD, Shih C-Y, Greshake A, Stöffler D, Eugster O (2001) Ages and geologic histories of Martian meteorites. Space Sci Rev 96:105–164

Nyquist LE, Bogard DD, Shih C-Y, Park J, Reese YD, Irving AJ (2009) Concordant Rb–Sr, Sm–Nd, and Ar–Ar ages for Northwest Africa 1460: a 346 Ma old basaltic shergottite related to "lherzolitic" shergottites. Geochim Cosmochim Acta 73:4288–4309

Nyquist LE, Shih C-Y, Peng ZX, Agee C (2013) NWA 7034 Martian breccia: disturbed Rb-Sr systematics, preliminary $\sim$4.4 Ga Sm-Nd age. Meteorit Planet Sci 48:A208

Ollila AM, Newsom HE, Clark B, Wiens RC, Cousin A, Blank JG, Mangold N, Sautter V, Maurice S, Clegg SM, Gasnault O, Forni O, Tokar R, Lewin E, Darby Dyar M, Lasue J, Anderson R, McLennan SM, Bridges J, Vaniman D, Lanza N, Fabre C, Melikechi N, Perrett G M, Campbell JL, King PL, Barraclough B, Delapp D, Johnstone S, Meslin P-Y, Rosen-Gooding A, Williams J, MSL Science Team (2014) Trace element geochemistry (Li, Ba, Sr, and Rb) using Curiosity's ChemCam: early results for Gale crater from Bradbury Landing Site to Rocknest. J Geophys Res Planets 119:255–285

Pahlevan K, Stevenson DJ (2007) Equilibration in the aftermath of the lunar-forming giant impact. Earth Planet Sci Lett 262:438–449

Palme H, O'Neill HSC (2014) Cosmochemical estimates of mantle composition. In: Carlson RW (ed) Treatise on Geochemistry, 2nd edn. Elsevier Ltd., Oxford, UK, pp 1–39

Palme C, Lodders K, Jones A (2014) Solar System abundances of the elements. In: Davis AM (ed.), Treatise on Geochemistry, vol 1, 2nd edition. Elsevier Ltd., Oxford, pp. 15–36

Paniello RC, Moynier F, Beck P, Barrat JA, Podosek FA, Pichat S (2012) Zinc isotopes in HEDs: Clues to the formation of 4-Vesta, and the unique composition of Pecora Escarpment 82502. Geochim Cosmochim Acta 86:76–87

Parkinson IJ, Hammond SJ, James RH, Rogers NW (2007) High-temperature lithium isotope fractionation: insights from lithium isotope diffusion in magmatic systems. Earth Planet Sci Lett 257:609–621

Piau L (2008) Lithium isotopes in Population II dwarfs. Astrophys J 689:1279–1288

Pogge von Strandmann PAE, Elliott T, Marschall HR, Coath C, Lai Y-J, Jeffcoate AB, Ionov DA (2011) Variations of Li and Mg isotope ratios in bulk chondrites and mantle xenoliths. Geochim Cosmochim Acta 75:5247–5268

Poitrasson F, Halliday AN, Lee D-C, Levasseur S, Teutsch N (2004) Iron isotope differences between Earth, Moon, Mars and Vesta as possible records of contrasted accretion mechanisms. Earth Planet Sci Lett 223:253–266

Poschenrieder WP, Herzog RF, Barrington AE (1965) The relative abundance of the lithium isotopes in the Holbrook meteorite. Geochim Cosmochim Acta 29:1193–1195

Prantzos N (2012) Production and evolution of Li, Be, and B isotopes in the Galaxy. Astron Astrophys 542, paper number A67, doi:10.1051/0004-6361/201219043

Pringle EA, Savage PS, Badro J, Barrat JA, Moynier F (2013) Redox state during core formation on asteroid 4-Vesta. Earth Planet Sci Lett 373:75–82

Rajan RS, Brown L, Tera F, Whitford DJ (1980) Lithium isotopic composition in some stone meteorites. Earth Planet Sci Lett 51:41–44

Ramírez I, Fish JR, Lambert DL, Allende Prieto C (2012) Lithium abundances in nearby FGK dwarf and subgiant stars: Internal destruction, Galactic chemical evolution, and exoplanets. Astrophys J 756, paper number 46, doi:10.1088/0004-1637X/1756/1081/1046

Reeves H (1994) On the origin of the light elements (Z < 6). Rev Modern Phys 66:193–216

Reynolds VS, McSween Jr HY, McDonough WF, McCoy T (2006) Lithium isotopes in basaltic shergottites: evidence for a hydrated assimilant. Lunar Planet Sci XXXVII, #2206

Ritzenhoff S, Schröter EH, Schmidt W (1997) The lithium abundances in sunspots. Astron Astrophys 328:695–701

Robert F, Chaussidon M (2003) Boron and lithium isotopic composition in chondrules from the Mokoia meteorite. Lunar Planet Sci Conf XXXIV, #1344

Romano D, Matteucci F, Ventura P, D'Antona F (2001) The stellar origin of ^{7}Li. Do AGB stars contribute a substantial fraction of the local Galactic lithium abundance? Astron Astrophys 374:646–655

Ryan SG, Beers TC, Olive KA, Fields BD, Norris JE (2000) Primordial lithium and Big Bang Nucleosynthesis. Astrophys J 530:L57–L60

Saal AE, Hauri EH, Lo Cascio M, Van Orman JA, Rutherford MC, Cooper RF (2008) Volatile content of lunar volcanic glasses and the presence of water in the Moon´s interior. Nature 454:192–196

Sbordone L, Bonifacio P, Caffau E, Ludwig H-G, Behara NT, González Hernández JI, Steffen M, Cayrel R, Freytag B, Van't Veer C, Molaro P, Plez B, Sivarani T, Spite M, Spite F, Beers TC, Christlieb N, François P, Hill V (2010) The metal-poor end of the Spite plateau. I. Stellar parameters, metallicities, and lithium abundances. Astron Astrophys 522, A26, doi: 10.1051/0004-6361/200913282

Scalo JM (1976) Production of Galactic ^{7}Li by slow mass loss. Astrophys J 206:795–799

Scott ERD, Greenwood RC, Franchi IA, Sanders IS (2009) Oxygen isotopic constraints on the origin and parent bodies of eucrites, diogenites, and howardites. Geochim Cosmochim Acta 73:5835–5853

Sedaghatpour F, Teng F-Z, Liu Y, Sears DWG, Taylor LA (2013) Magnesium isotopic composition of the Moon. Geochim Cosmochim Acta 120:1–19

Seitz H-M, Brey GP, Weyer S, Durali S, Ott U, Münker C, Mezger K (2006) Lithium isotope compositions of Martian and lunar reservoirs. Earth Planet Sci Lett 245:6–18

Seitz H-M, Brey GP, Zipfel J, Ott U, Weyer S, Durali S, Weinbruch S (2007) Lithium isotope composition of ordinary and carbonaceous chondrites, and differentiated planetary bodies: Bulk solar system and solar reservoirs. Earth Planet Sci Lett 260:582–596

Seitz H-M, Zipfel J, Brey GP, Ott U (2012) Lithium isotope compositions of chondrules, CAI and a dark inclusion from Allende and ordinary chondrites. Earth Planet Sci Lett 329–330:51–59

Sephton MA, James RH, Bland PA (2004) Lithium isotope analyses of inorganic constituents from the Murchison meteorite. Astrophys J 612:588–591

Sephton MA, James RH, Zolensky ME (2006) The origin of dark inclusions in Allende: new evidence from lithium isotopes. Meteorit Planet Sci 41:1039–1043

Sephton MA, James RH, Fehr MA, Bland PA, Gounelle M (2013) Lithium isotopes as indicators of meteorite parent body alteration. Meteorit Planet Sci 48:872–878

Sharp ZD, Shearer CK, McKeegan KD, Barnes JD, Wang YQ (2010) The chlorine isotope composition of the Moon and implications for an anhydrous mantle. Science 329:1050–1053

Shearer CK, Layne GD, Papike JJ (1994) The systematics of light lithophile elements (Li, Be and B) in lunar picritic glasses: implications for basaltic magmatism on the Moon and the origin of the Moon. Geochim Cosmochim Acta 58:5349–5362

Shearer CK, Hess PC, Wieczorek MA, Pritchard ME, Parmentier EM, Borg LE, Longhi J, Elkins-Tanton LT, Neal CR, Antonenko I, Canup RM, Halliday AN, Grove TL, Hager BH, Lee D-C, Wiechert U (2006)

Thermal and magmatic evolution of the Moon. Rev Mineral Geochem 60:365–518
Shima M, Honda M (1966) Distribution and isotopic composition of lithium in stone meteorites. Geochem J 1:27–34
Schönbächler M, Baker RGA, Williams H, Halliday AN, Rehkämper M (2008) The cadmium isotope composition of chondrites and eucrites. Meteorit Planet Sci 43:A139
Singletary SJ, Bell DR, Buseck PR (2008) SIMS analysis of ureilite lithium isotopic composition. Lunar Planet Sci Conf, XXXIX, #2217
Smith VV, Plez B, Lambert DL, Lubowich DA (1995) A survey of lithium in the red giants of the Magellanic Clouds. Astrophys J 441:735–746
Snyder GA, Neal CR, Taylor RA, Halliday AN (1997) Anatexis of lunar cumulate mantle in time and space: Clues from trace element, strontium and neodymium isotopic chemistry of parental Apollo 12 basalts. Geochim Cosmochim Acta 61:2731–2747
Snyder GA, Taylor LA, Neal CR (1992) A chemical model for generating the sources of mare basalts: combined equilibrium and fractional crystallization of the lunar magmasphere. Geochim Cosmochim Acta 56:3809–3823
Spicuzza MJ, Day JMD, Taylor LA, Valley JW (2007) Oxygen isotope constraints on the origin and differentiation of the Moon. Earth Planet Sci Lett 253:254–265
Spite F, Spite M (1982) Abundance of lithium in unevolved halo stars and old disk stars: interpretation and consequences. Astron Astrophys 115:357–366
Sprague AL, Hunten DM, Grosse FA (1996) Upper limit for lithium in Mercury's atmosphere. Icarus 123:345–349
Steele IM, Hutcheon ID, Smith JV (1980) Ion microprobe analysis and petrogenetic interpretations of Li, Mg, Ti, K, Sr, Ba in lunar plagioclase. Proc Lunar Planet Sci Conf 11:571–590
Steigman G (1993) The significance of the interstellar $^{7}Li/^{6}Li$ ratio. Astrophys J 413:L73–L76
Steigman G, Walker TP (1992) Production of Li, Be, and B in the early Galaxy. Astrophys J 385:L13–L16
Stolper EM, Baker MB, Newcombe ME, Schmidt ME, Treiman AH, Cousin A, Dyar MD, Fisk MR, Gellert R, King PL, Leshin L, Maurice S, McLennan SM, Minitti ME, Perrett G, Rowland S, Sautter V, Wiens RC, MSL Science Team (2013) The petrochemistry of Jake_M: A martian mugearite. Science 341, paper number: 1239463. doi:10.1231126/science.1239463
Sturchio NC, Chan LH (2003) Lithium isotope geochemistry of the Yellowstone hydrothermal system. Soc Econ Geol Spec Publ 10:171–180
Tajitsu A, Sadakane K, Naito H, Arai A, Aoki W (2015) Explosive lithium production in the classical nova V339 Del (Nova Delphini 2013). Nature 518:381–384
Taylor SR (1982) Planetary science: a lunar perspective. Lunar Planet Inst, Houston, USA, pp 502
Taylor SR, Jakeš P (1974) The geochemical evolution of the moon. Proc Lunar Sci Conf 5:1287–1305
Taylor SR, McLennan SM (1985) The continental crust: its composition and evolution. Blackwell, Oxford, UK, pp 312
Taylor SR, McLennan SM (2009) Planetary crusts: their composition, origin, and evolution. Cambridge University Press, Cambridge, UK, pp 378
Teng F-Z, McDonough WF, Rudnick RL, Dalpé C, Tomascak PB, Chappell BW, Gao S (2004) Lithium isotopic composition and concentration of the upper continental crust. Geochim Cosmochim Acta 68:4167–4178
Tera F, Eugster O, Burnett DS, Wasserburg GJ (1970) Comparative study of Li, Na, K, Rb, Cs, Ca, Sr and Ba abundances in achondrites and in Apollo 11 lunar samples. Proc Apollo 11 Lunar Sci Conf, 1637–1657
Tomascak PB, Tera F, Helz RT, Walker RJ (1999) The absence of lithium isotope fractionation during basalt differentiation: new measurements by multicollector sector ICP-MS. Geochim Cosmochim Acta 63:907–910
Vangioni-Flam E, Casse M, Audouze J (2000) Lithium-beryllium-boron: origin and evolution. Phys Reports 333–334:365–387
Vangioni-Flam E, Casse M, Cayrel R, Audouze J, Spite M, Spite F (1999) Lithium-6: evolution from Big Bang to present. New Astron 4:245–254
Wallerstein G, Sneden C (1982) A K giant with unusually high abundance of lithium: HD 112127. Astrophys J 255:577–584
Wang K, Moynier F, Dauphas N, Barrat JA, Craddock P, Sio CK (2012) Iron isotope fractionation in planetary crusts. Geochim Cosmochim Acta 89:31–45
Warren PH (2011) Stable-isotopic anomalies and the accretionary assemblage of the Earth and Mars: A subordinate role for carbonaceous chondrites. Earth Planet Sci Lett 311:93–100
Warren PH, Wasson JT (1979) The origin of KREEP. Rev Geophys Space Phys 17:73–88
Webber WR, Lukasiak A, McDonald FB (2002) *Voyager* measurements of the charge and isotopic composition of cosmic ray Li, Be, and B nuclei and implications for their production in the Galaxy. Astrophys J 568:210–215
Wiechert UH, Halliday AN, Palme H, Rumble D (2004) Oxygen isotope evidence for rapid mixing of the HED meteorite parent body. Earth Planet Sci Lett 221:373–382
Woosley SE, Hartmann DH, Hoffman RD, Haxton WC (1990) The neutrino-process. Astrophys J 356:272–301
Yanagita S, Gensho R (1977) Isotopic composition of lithium in the Allende meteorite. Geochem J 11:41–44

4 Li Partitioning, Diffusion and Associated Isotopic Fractionation: Theoretical and Experimental Insights

4.1 Introduction

Laboratory experiments on the partitioning of elements and isotopes between various phases (minerals, fluids, and melts) at thermodynamic equilibrium are fundamental to the interpretation of geochemical data. In addition to the equilibrium fractionation of stable isotopes, their composition in a mineral depends on the partitioning behavior of the element for simple mass balance reasons. However, the signature of Li concentrations and isotopes stored in minerals also critically depends on the mechanism of the exchange with the given environment (fluids, melts or adjacent minerals). What we measure with our analytical tools is related to the closure of the mineral with respect to exchange of Li with the environment (Dodson 1973), which is strongly sensitive to the active exchange mechanisms.

After a mineral has formed by growth from a fluid, a melt, or a gas, there are three end-member scenarios that can be generally considered to affect Li (or any other element) within the mineral: (i) Recrystallization driven by a chemical gradient—mineral replacement by dissolution re-precipitation processes (e.g., Putnis and John 2010); (ii) Recrystallization driven by interfacial energies or strain—normal grain growth/deformation; (iii) Intra-crystalline diffusion driven by a chemical or isotopic gradient. Mechanism (i) provides element exchange even at low temperatures but requires a fluid or melt that is far from equilibrium with the given mineral, as is typically the case for metasomatic processes or open systems in general. The replacement of minerals and other alteration features can be often identified by petrography and textural observations. The occurrence of mechanism (ii) may also leave textural evidence. However, whether and to what extent the chemistry of the relevant mineral is changed during dynamic recrystallization is a topic that has not yet been studied in great detail. It is commonly assumed that the presence of fluids facilitates re-crystallization, which, as a secondary process, could also affect trace element and isotopic contents of the respective mineral. Mechanism (iii) does not affect the shape of the mineral grain, but can only be identified by in situ measurements of the spatial distribution of elements/isotopes. Zoning of Li preserved within the mineral may be generated by diffusion, but in order to exclude other reasons for intra-grain variations (e.g., growth zoning), in situ measurements and simulations of the isotopic zoning are necessary. The combined information on Li concentration and isotopic abundance is actually a very powerful tool to distinguish between different origins of chemical zoning, as illustrated by the example of Mg and Fe isotopes (Oeser et al. 2015).

Unlike most other elements, Li appears to be a special case since its mobility within mineral

P.B. Tomascak et al., *Advances in Lithium Isotope Geochemistry*,
Advances in Isotope Geochemistry, DOI: 10.1007/978-3-319-01430-2_4

structures is very high, even affecting Li in the core of mm-sized crystals at moderate temperatures (e.g., plagioclase; Giletti and Shanahan 1997). Therefore, solid-state diffusion related to secondary processes has a strong potential to affect the Li chemistry of minerals and bulk rocks, unrelated to their formation. On the other hand, any zoning of Li preserved in minerals also provides a way to determine the time scales of the related geologic process by a diffusion model ("diffusion chronometry"; Chakraborty 2008; John et al. 2012).

For these reasons, we compile and discuss in this chapter the measured partition coefficients of Li and Li isotopes between various phases (mineral–melt, mineral–fluid, and mineral–mineral), and the measured diffusion coefficients of Li in minerals, fluids, and melts. Furthermore, we present and discuss consequences of diffusive fractionation of Li isotopes. Based on the information compiled for partitioning and diffusion behavior of Li, we finally discuss experiments on fluid–rock interaction with special emphasis on the behavior of Li.

Before going into the details of the experimental work dedicated to Li we give a short overview of the general geochemical behavior of Li to provide a framework for the detailed discussions. The alkali element Li is exclusively present as a monovalent cation in minerals (e.g., Wenger and Armbruster 1991) and melts, with chemical bonding dominated by undirected electrostatic interactions (ionic bonding). In aqueous solutions Li forms a hydrated complex, $[Li(H_2O)_n]^+$, and coordinated approximately by 4 oxygens, but the exact coordination changes with the temperature and pressure (Jahn and Wunder 2009; Kowalski and Jahn 2011). Lithium is generally considered a fluid mobile element, especially at hydrothermal conditions (e.g., Chan et al. 1994; Brenan et al. 1998a; Seyfried et al. 1991; see also Chap. 6), but when clay minerals like smectite are formed they can capture Li at lower temperatures (Sect. 4.2.4). The ionic radius of Li^+ for octahedral and tetrahedral coordination within crystals is 0.92 and 0.59 Å, respectively (Shannon 1976), which is very close to the ionic radius of Mg^{2+} at 0.89 and 0.57 Å, respectively. Therefore, Li tends to substitute for Mg in minerals but charge balancing requires a coupled substitution with, for example, a trivalent cation for Mg. For example, in forsterite a coupled substitution with Sc^{3+} was evidenced (Grant and Wood 2010) and in Fe-bearing olivine, Fe^{3+} could be of importance. Alternatively, Li^+ can substitute for Na^+ if the latter is present as a major cation but due to the relatively large difference in the ionic radius (1.18 Å for octahedral coordination; Shannon 1976) this substitution is very limited. Minerals that contain Li as a major element in nature are essentially limited to pegmatite occurrences, like petalite, lepidolite, zinnwaldite (a Li-rich trioctahedral mica), spodumene, amblygonite, lithiophilite, and lithiophosphate. Unlike the stable isotopes of most other elements, in many minerals the light isotope (^{6}Li) partitions preferentially into the solid compared to the fluid (e.g., Wunder et al. 2006; Kowalski and Jahn 2011). This behavior is consistent with natural observations that clearly document a positive flux of δ^7Li into the seawater because of alteration of continental crust, oceanic crust and terrigenous sediments (see Chap. 6).

The diffusion behavior of Li, to the first order, is related to its ionic charge and size. The combination of a low charge (1+) and a relatively small ionic radius compared to other monovalent cations is responsible for the relatively high mobility of Li in solids and melts compared to other cations (see for example Figs. 5, 6, and 7 in Brady and Cherniak 2010). The large mobility of Li in minerals makes the preservation of primary isotopic signatures difficult (as will be discussed below based on the experimental data). However, this may support the potential for Li to be used as a geo-chronometer for low- and medium-temperature processes or for very short-term processes (e.g., Beck et al. 2006; Jeffcoate et al. 2007; John et al. 2012; Charlier et al. 2012). In these studies diffusion of Li in minerals has been identified by associated isotopic fractionation effects producing large anomalies for δ^7Li of around ±10–20 ‰, which will be illustrated in Sect. 4.3.

4.2 Equilibrium Partitioning Behavior of Li

4.2.1 Thermodynamic Background

The Nernst partition coefficient is defined as the ratio of the mass fractions of the element i (or any suitable respective chemical component) in phase α, C_i^α, and phase β, C_i^β:

$$K_{p\,(i)}^{\alpha/\beta} = \frac{C_i^\alpha}{C_i^\beta} \tag{4.2.1}$$

Here we use $K_{p(i)}$ instead of the more commonly used symbol D_i because the latter is also used for the diffusion coefficient. It reminds us of the relation to the equilibrium constant, K, of the corresponding partitioning reaction:

$$i(\beta) = i(\alpha), \tag{4.2.2}$$

which is given, in general, as follows:

$$K(P,T) = \frac{a_i^\alpha}{a_i^\beta} = \frac{C_i^\alpha \gamma_i^\alpha}{C_i^\beta \gamma_i^\beta}, \tag{4.2.3}$$

where a_i^α and a_i^β are the activities of the component i in phase α and phase β, respectively, which depend in general on the chosen reference state (fixed chemical composition of phase α and phase β at any P and T, see for example Ganguly 2008), as do the respective activity coefficients γ_i^α and γ_i^β. For a trace element Henry's law is typically assumed, which means that the latter activity coefficients are constant but only for a fixed major element composition. We can thus conclude from Eq. 4.2.3 that for trace elements the Nernst partition coefficient is independent of their concentrations and in general is a function of P, T and composition of the solvents, X_α and X_β:

$$K_{p\,(i)}^{\alpha/\beta} = K(P,T)\frac{\gamma_i^\beta(X_\beta)}{\gamma_i^\alpha(X_\alpha)}. \tag{4.2.4}$$

However, we will later demonstrate an example where the partition coefficient of Li is also dependent on the concentration of another trace element (Grant and Wood 2010), which is related to a coupled incorporation of two trace elements.

4.2.2 Lattice Strain Model for Element Partitioning

It has been shown by numerous studies that mineral–melt partition coefficients of trace elements strongly correlate with their misfit to the respective lattice site in the mineral (e.g., Blundy and Wood 1991; Beattie 1994). This dependence on the ion size can be illustrated for example by "Onuma" diagrams (Onuma et al. 1968) where the logarithm of $K_{p(i)}$ for an isovalent series of cations is plotted against their ionic radius. This shows a parabolic shape, where the position of the maximum is characteristic of the size of the respective lattice site (Fig. 4.1). This systematic relationship can be quantified by the lattice strain model (Blundy and Wood 1994), which is based on an expression of Brice (1975) for the mechanical energy around a homovalent substitution in an elastically isotropic medium. According to their model, the partition coefficient of a misfit cation entering crystal lattice site M can be approximated by the following expression:

$$K_{p(i^{n+})}^{\alpha/Liq} = K_{p(0)}^{n+} \cdot \exp\left\{\frac{-4\pi E_M^{n+} N_A \left(\frac{r_{0(M)}^{n+}}{2}\left(r_{i^{n+}} - r_{0(M)}^{n+}\right)^2 + \frac{1}{3}\left(r_{i^{n+}} - r_{0(M)}^{n+}\right)^3\right)}{RT}\right\}, \tag{4.2.5}$$

where N_A is Avogadro's number, $K_{p(0)}^{n+}$ is the partition coefficient for an ion with charge n +, $r_{0(M)}^{n+}$ its respective ionic radius, and E_M^{n+} the effective Young's modulus of the site. The fundamental basis of the model is that (i) the ionic radius of the fictive ion *0* is ideal in the sense that it enters site M without inducing any elastic strain and (ii) element i and *0* can be replaced within the melt without any resulting energy change. Although the additional assumption of an elastically isotropic medium is not fulfilled in basically all relevant mineral sites, this model was successfully used to understand the systematics of numerous mineral–melt partition coefficients (e.g., Blundy and Wood 2003a, b). The success of this model may be related to the fact that the anisotropic elastic behavior of the crystal site is

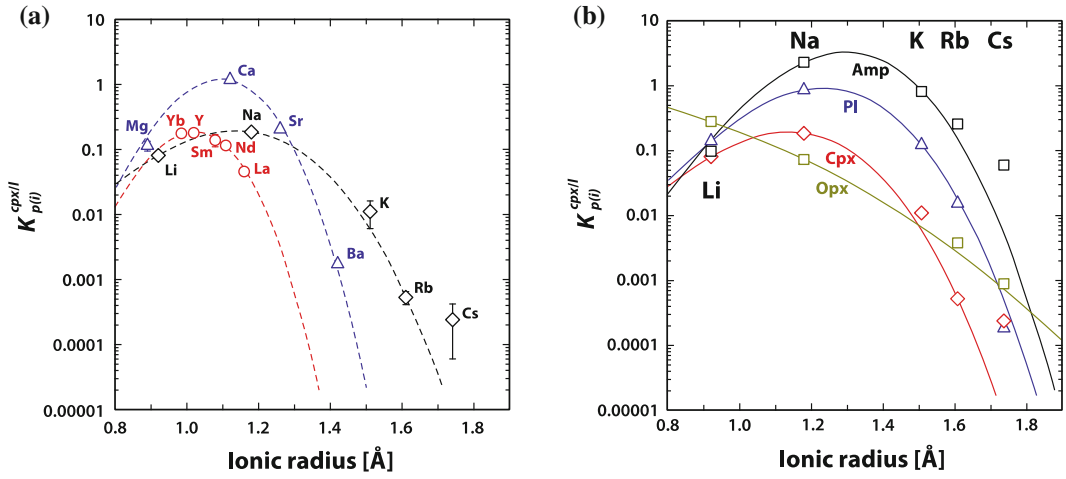

Fig. 4.1 Onuma diagrams of experimentally determined partition coefficients of **a** 1+, 2+, and 3+ cations between clinopyroxene and melt from experiment DC22 of Blundy and Dalton (2000) and **b** 1+ cations between amphibole (run# 1950, Adam and Green 2006), plagioclase (run# 93-8a, Dohmen and Blundy 2014), clinopyroxene (same as in a), orthopyroxene (run# 1949, Adam and Green 2006) and melt, respectively. *Dashed lines* in (**a**) and *solid lines* in (**b**) are regressions of the data for each homovalent series using the lattice strain model (Eq. 4.2.5) and optimization of $K_{p(0)}^{n+}$, E_M^{n+}, and $r_{0(M)}^{n+}$. The effective ionic radii were taken from Shannon (1976) for eightfold coordination. Note the general trend that for monovalent cations the site is more tolerant to misfit ions compared to highly charged cations (2+ and 3+ here), reflected in tighter parabola for the latter and hence larger effective Young's moduli. The ideal cation radius (here the position of the maximum of the parabola) varies for different crystallographic structures and sites

similar for ions of slightly different sizes such that it can be integrated into a unique E_M^{n+}. Note that Eq. 4.2.5 does not imply that partition coefficients of, for example, Li are insensitive to the melt composition (e.g., Blundy et al. 1995; Wood and Blundy 1997). The effect of melt composition is integrated into $K_{p(0)}^{n+}$, but for cations with the same charge, the respective dependence on melt composition is assumed to be the same in Eq. 4.2.5. For limitations of this approximation and corresponding uncertainties see, for example, Schmidt et al. (2006) or Miller et al. (2006).

The lattice strain model was extended to heterovalent substitutions of an ion with charge $m+$ (Wood and Blundy 2001), by considering the electrostatic work required to replace the fictive ideal cation with charge $n+$ by a fictive ideal ion with charge $m+$ in the crystal and the melt. The difference of this electrostatic work was defined as ΔG_{elec} and the partition coefficient for the fictive ideal ion with charge $m+$, $K_{p(0)}^{m+}$ (compare with Eq. 4.2.5), is given by:

$$K_{p(0)}^{m+} = K_{ex}^{m+} \cdot \left\{ \begin{array}{l} X_{m+}^{M} + \left(X_{(m-1)+}^{M} + X_{(m+1)+}^{M}\right)\exp\left(\dfrac{-1^2\Delta G_{elec}}{RT}\right) \\ + \left(X_{(m-2)+}^{M} + X_{(m+2)+}^{M}\right)\exp\left(\dfrac{-2^2\Delta G_{elec}}{RT}\right) + \cdots \end{array} \right\} \quad (4.2.6)$$

where K_{ex}^{m+} is a site- and mineral-specific constant, and X_{j+}^{M} is the fraction of M sites charge-balanced by a $j+$ ion. This fraction therefore considers the contribution to the partition coefficient of an ion j^{m+} by adding the various different combinations of local atomic configurations around the M site to charge-balance 1+, 2+, 3+,… cations. Heterovalent substitutions with atomic configurations of local charge balance are more stable but depending on the magnitude of ΔG_{elec} and the probability of the different configurations (represented here by the magnitude of X_{j+}^{M}), other atomic configurations can become important

(e.g., for REE partitioning between clinopyroxene and melt see Wood and Blundy 2001).

For example, for Li partitioning into clinopyroxene with the structural formula (M2M1) $[T_2O_6]$, the following combinations could be considered: $(LiAl)[Si_2O_6]$, $(LiTi)[AlSiO_6]$, $(CaLi)^{-}[Si_2O_6]$, $(LiAl)^{-}[AlSiO_6]$, where the latter two have an effective negative charge. The probability of these various local configurations is calculated by the assumption of random mixing of the cations on the respective lattice sites, e.g. the molar fraction of $[X^{1+}] = 2X^{M1}_{Al} \cdot \left(X^{T}_{Si}\right)^2 + 2X^{M1}_{Ti} \cdot X^{T}_{Si} \cdot X^{T}_{Al}$ and $[X^{2+}] = (1 - X^{M1}_{Al} - X^{M1}_{Cr} - X^{M1}_{Fe^{3+}}) \cdot \left(X^{T}_{Si}\right)^2 + 2(X^{M1}_{Al} + X^{M1}_{Cr} + X^{M1}_{Fe^{3+}}) \cdot \left(X^{T}_{Si}\right)^2 + X^{M1}_{Ti} \cdot \left(X^{T}_{Al}\right)^2$ (Wood and Blundy 2001). Because Mg occupies the smaller M1 site in clinopyroxene, replacement of Mg by Li would involve the formation of a charged species, $(CaLi)^{-}[Si_2O_6]$, since no trivalent cation present as a minor or major element (Al^{3+} or Cr^{3+}) would occupy the larger M2 site. An alternative candidate would be REE, but unless Li and REE are strongly associated as a defect complex in the structure (e.g., as indicated for garnet in Cahalan et al. 2014), the probability of the species $(REELi)[Si_2O_6]$ would be very small because X^{M2}_{REE} is small. Therefore, although the smaller M1 site should be more suitable for Li, the larger probability of charge balance with Al^{3+} on the M1 site, makes the M2 site more favorable for Li in clinopyroxene. This preference of Li for the M2 site is reflected in Fig. 4.1a where Li fits on the Onuma parabola defined by the larger monovalent cations. The respective size of the ideal cation, $r^{1+}_{0(M)} = 1.139$ Å, is characteristic for the larger M2 site in clinopyroxene.

The lattice strain model was also used to infer from mineral-melt partition coefficients of proxy cations respective mineral-melt partition coefficients of any other cation (e.g., Blundy and Wood 2003a; Gallagher and Elliott 2009; Dohmen and Blundy 2014). For this purpose it is useful to consider homovalent exchange reactions, for example the exchange of Li with Na between mineral α and a liquid (melt or aqueous fluid):

$$\mathrm{Na}\,(\alpha) + \mathrm{Li}\,(\mathrm{Liquid}) = \mathrm{Li}\;\;(\alpha) + \mathrm{Na}\,(\mathrm{Liquid}) \tag{4.2.7}$$

where, from the corresponding mass action law, the ratio of the Li and Na partition coefficient is given by:

$$\frac{K^{\alpha/Liq}_{p(\mathrm{Li})}}{K^{\alpha/Liq}_{p(\mathrm{Na})}} = K_{4.2.7}(P,T)\,\frac{\gamma^{\alpha}_{\mathrm{Na}}(X_{\alpha})}{\gamma^{Liq}_{\mathrm{Na}}(X_{Liq})}\,\frac{\gamma^{Liq}_{\mathrm{Li}}(X_{Liq})}{\gamma^{\alpha}_{\mathrm{Li}}(X_{\alpha})} \tag{4.2.8}$$

According to the lattice strain model and assuming that Li and Na occupy the same crystallographic site, this ratio $K^{\alpha/Liq}_{p(\mathrm{Li})}/K^{\alpha/Liq}_{p(\mathrm{Na})}$ is also given, as follows:

$$\frac{K^{\alpha/Liq}_{p\,(\mathrm{Li})}}{K^{\alpha/Liq}_{p\,(\mathrm{Na})}} = \exp\left\{\frac{-4\pi E^{1+}_{M} N_{\mathrm{A}}\left(\frac{r^{1+}_{0(M)}}{2}\left(r^{2}_{\mathrm{Na}} - r^{2}_{\mathrm{Li}}\right) - \frac{1}{3}\left(r^{3}_{\mathrm{Na}} - r^{3}_{\mathrm{Li}}\right)\right)}{RT}\right\}, \tag{4.2.9}$$

which provides a formula to calculate $K^{\alpha/Liq}_{p\,(\mathrm{Li})}$ if $K^{\alpha/Liq}_{p\,(\mathrm{Na})}$ and the lattice strain parameters for mineral α are known from experiments. The right hand sides of Eqs. 4.2.8 and 4.2.9 should be the same if the lattice strain model is correct. Since the lattice strain model ignores contributions of the melt chemistry on homovalent exchanges, we can immediately conclude that for the validity of this model $\gamma^{Liq}_{\mathrm{Li}}(X_{Liq}) \sim \gamma^{Liq}_{\mathrm{Na}}(X_{Liq})$. Equation 4.2.9 can be also rewritten in the following form:

$$RT\ln\left(\frac{K^{\alpha/Liq}_{p\,(\mathrm{Li})}}{K^{\alpha/Liq}_{p\,(\mathrm{Na})}}\right) = -4\pi E^{1+}_{M} N_{\mathrm{A}}\left(\frac{r^{1+}_{0(M)}}{2}\left(r^{2}_{\mathrm{Na}} - r^{2}_{\mathrm{Li}}\right) - \frac{1}{3}\left(r^{3}_{\mathrm{Na}} - r^{3}_{\mathrm{Li}}\right)\right), \tag{4.2.10}$$

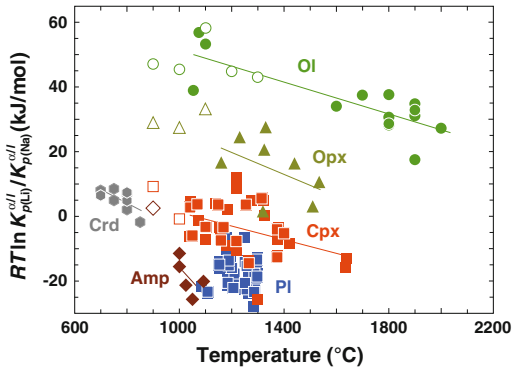

Fig. 4.2 Experimentally observed values of $RT\ln(\frac{K_{p(\mathrm{Li})}}{K_{p(\mathrm{Na})}})$ versus temperature for selected minerals. *Solid symbols* mineral-melt partition coefficients, *open symbols* mineral-fluid partition coefficients. The scatter of data around the general trend for minerals like plagioclase or clinopyroxene could be related to the respective wide variation in mineral chemistry (see also the detailed discussion following for each mineral)

To illustrate the validity of Eq. 4.2.10, we plotted the left hand side for various rock-forming minerals (actually mineral groups, except cordierite), as calculated from experimentally determined partition coefficients between minerals and melts/fluids, against temperature (Fig. 4.2). Although for some mineral groups the mineral composition varies strongly, each mineral group defines a separate range in this plot. Furthermore, apparent trends as a function of temperature can be recognized irrespective of the liquid composition (fluid versus melt). This observation supports the prediction given by the lattice strain model because the strain induced by the exchange in fluid or melt should be very small compared to that induced to the lattice. The numbers for $RT\ln(\frac{K_{p(\mathrm{Li})}}{K_{p(\mathrm{Na})}})$ follow roughly the sequence Ol > Opx > Cpx > Pl > Amp, which can be explained in terms of the lattice strain model by the respective increase in the optimum ionic radius of the respective site for monovalent cations (compare also with Fig. 4.1b). According to Eq. 4.2.10, $RT\ln(\frac{K_{p(\mathrm{Li})}}{K_{p(\mathrm{Na})}})$ should be constant, if both $r^{1+}_{0(M)}$ and E^{1+}_{M} are constant, but both the detailed mineral chemistry and the temperature have their own impact on these quantities. For example, the variability of plagioclase melt partition coefficients with anorthite content and temperature can be explained by the decreasing size of the metal site and the corresponding decrease of $r^{1+}_{0(M)}$ with increasing anorthite component and decreasing temperature (Blundy and Wood 1994; Dohmen and Blundy 2014). An increase of $r^{1+}_{0(M)}$ with temperature could explain negative trends in Fig. 4.2 since increasing the site would make it a better fit for the larger Na^+ ion.

To summarize, in the framework of the lattice strain model, the mineral structure and detailed mineral chemistry have two main impacts for trace element partitioning: (i) the ideal ionic radius and the effective Young's modulus (e.g., Fig. 4.1b), and (ii) depending on the major, minor and even trace element chemistry, different local atomic configurations are possible to allow charge-balanced as well as charged incorporation of a trace element. The melt chemistry also plays a role in trace element partitioning, but under thermodynamic equilibrium, a given mineral chemistry is coupled to the melt/fluid chemistry. Although in the general case the melt/fluid composition is not uniquely defined for a given mineral composition, thermodynamic equilibrium poses additional constraints on the melt/fluid chemistry, in particular the chemical potential of the chemical components. Thus the total degree of freedom for the melt/fluid composition is reduced when a certain mineral composition is stable. For the latter reason, we discuss the experimental partition coefficients mostly in respect to their variation with mineral chemistry.

4.2.3 Mineral-Melt Partitioning

$K^{Min/Melt}_{p(\mathrm{Li})}$ was measured for the following minerals or mineral groups (Table 4.1): amphibole (Amp), apatite (Ap), clinopyroxene (Cpx), cordierite (Crd), garnet (Grt), leucite (Lct), melilite (Mll), olivine (Ol), orthopyroxene (Opx), perovskite (Prv), biotite (Bt), muscovite (Ms), plagioclase (Pl), and spinel (Sp) (mineral abbreviations as recommended by Whitney and

Table 4.1 Published partitioning coefficients of Li between minerals and melts

Reference	Mineral/mineral group	P (MPa)	T (°C)	K_p(Li)
Adam and Green (2006)	Amp	1000	1025	0.09
Adam and Green (2006)	Amp	2000	1050	0.098
Brenan et al. (1998a)	Amp	1500	1000	0.19
Brenan et al. (1998b)	Amp	1500	1000	0.13
LaTourette et al. (1995)	Amp	1500	1092	0.124
Klemme and Dalpe (2003)	Ap	1000	1250	0.039
Klemme and Dalpe (2003)	Ap	1000	1250	0.084
Klemme and Dalpe (2003)	Ap	1000	1250	0.027
Corgne et al. (2005)	$CaSiO_3$ Prv	21,000	20	0.13
Corgne et al. (2005)	$CaSiO_3$ Prv	20,000	2100	0.15
Corgne et al. (2005)	$CaSiO_3$ Prv	25,000	2300	0.05
Taura et al. (2001)	$CaSiO_3$ Prv	25,000	2350	0.17
Corgne et al. (2005)	$CaSiO_3$ Prv	25,000	2300	0.16
Corgne and Wood (2005)	$CaTiO_3$ Prv	0.1	1410	0.05
Corgne and Wood (2005)	$CaTiO_3$ Prv	0.1	1410	0.05
Corgne and Wood (2005)	$CaTiO_3$ Prv	0.1	1410	0.052
Corgne and Wood (2005)	$CaTiO_3$ Prv	3000	1800	–
Corgne and Wood (2005)	$CaTiO_3$ Prv	3000	1800	0.13
Corgne and Wood (2005)	$CaTiO_3$ Prv	0.1	1520	0.057
Corgne and Wood (2005)	$CaTiO_3$ Prv	3000	1750	–
Corgne and Wood (2005)	$CaTiO_3$ Prv	3000	1600	–
Corgne and Wood (2005)	$CaTiO_3$ Prv	3000	1600	0.05
Corgne and Wood (2005)	$CaTiO_3$ Prv	0.1	1600	0.06
Corgne and Wood (2005)	$CaTiO_3$ Prv	0.1	1600	0.11
Corgne and Wood (2005)	$CaTiO_3$ Prv	3000	1620	0.043
Corgne and Wood (2005)	$CaTiO_3$ Prv	3000	1620	0.17
Corgne and Wood (2005)	$CaTiO_3$ Prv	3000	1660	0.025
Corgne and Wood (2005)	$CaTiO_3$ Prv	3000	1660	0.3
Corgne and Wood (2005)	$CaTiO_3$ Prv	0.1	1470	0.05
Corgne and Wood (2005)	$CaTiO_3$ Prv	0.1	1470	0.057
Corgne and Wood (2005)	$CaTiO_3$ Prv	0.1	1400	0.045
Corgne and Wood (2005)	$CaTiO_3$ Prv	0.1	1400	0.069
Corgne and Wood (2005)	$CaTiO_3$ Prv	0.1	1400	0.023
Adam and Green (2006)	Cpx	2500	1160	0.23
Adam and Green (2006)	Cpx	2700	1160	0.26
Adam and Green (2006)	Cpx	2000	1050	0.17
Adam and Green (2006)	Cpx	2500	1180	0.27
Adam and Green (2006)	Cpx	2000	1100	0.16
Adam and Green (2006)	Cpx	2500	1100	0.21
Adam and Green (2006)	Cpx	1000	1075	0.14
Adam and Green (2006)	Cpx	3000	1170	0.35

(continued)

Table 4.1 (continued)

Reference	Mineral/mineral group	P (MPa)	T (°C)	K_p(Li)
Bennett et al. (2004)	Cpx	3000	1330	1.052
Bennett et al. (2004)	Cpx	3000	1298	0.0224
Bennett et al. (2004)	Cpx	3000	1330	1.03
Blundy and Dalton (2000)	Cpx	3000	1375	0.2
Blundy and Dalton (2000)	Cpx	3000	1375	0.095
Blundy and Dalton (2000)	Cpx	3000	1375	0.09
Blundy and Dalton (2000)	Cpx	3000	1635	0.074
Blundy and Dalton (2000)	Cpx	800	1375	0.043
Blundy and Dalton (2000)	Cpx	3000	1640	0.081
Blundy et al. (1998)	Cpx	1500	1255	0.254
Brenan et al. (1998a)	Cpx	1000	1320	0.27
Brenan et al. (1998a, b)	Cpx	0.1	1275	0.14
Brenan et al. (1998a, b)	Cpx	0.1	1275	0.2
Elkins et al. (2008)	Cpx	2500	1420	0.22
Gaetani et al. (2003)	Cpx	1200	1315	0.34
Gaetani et al. (2003)	Cpx	1200	1185	0.26
Hart and Dunn (1993)	Cpx	3000	1380	0.59
Hill et al. (2000)	Cpx	0.1	1218	0.027
Hill et al. (2000)	Cpx	0.1	1218	0.027
Hill et al. (2000)	Cpx	0.1	1218	0.032
Hill et al. (2000)	Cpx	0.1	1218	0.207
Huang et al. (2006)	Cpx	1100	1150	0.25
Huang et al. (2006)	Cpx	1100	1155	0.16
Klemme et al. (2002)	Cpx	3000	1400	0.75
Kuzyura et al. (2010)	Cpx	7000	1265	0.52
Kuzyura et al. (2010)	Cpx	7000	1265	0.43
McDade et al. (2003)	Cpx	1500	1325	0.227
Schmidt et al. (1999)	Cpx	1500	1040	0.173
Wood and Trigila (2001)	Cpx	0.1	1140	0.19
Wood and Trigila (2001)	Cpx	200	1070	0.13
Wood and Trigila (2001)	Cpx	200	1042	0.15
Wood and Trigila (2001)	Cpx	200	1042	0.15
Evensen and London (2003)	Crd	200	850	0.12
Evensen and London (2003)	Crd	200	800	0.13
Evensen and London (2003)	Crd	200	700	0.4
Evensen and London (2003)	Crd	200	750	0.34
Evensen and London (2003)	Crd	200	800	0.21
Evensen and London (2003)	Crd	200	700	0.44
Evensen and London (2003)	Crd	200	800	0.26
Evensen and London (2003)	Crd	200	700	0.33
Evensen and London (2003)	Crd	200	750	0.3

(continued)

Table 4.1 (continued)

Reference	Mineral/mineral group	P (MPa)	T (°C)	K_p(Li)
Evensen and London (2003)	Crd	200	800	0.31
Adam and Green (2006)	Grt	3500	1190	0.0410
Adam and Green (2006)	Grt	2500	180	0.0350
Bennet et al. (2004)	Grt	3000	1330	0.0610
Bennet et al. (2004)	Grt	3000	1402	0.1400
Gaetani et al. (2003)	Grt	1600	1230	0.0200
Klemme et al. (2002)	Grt	3000	1400	0.1200
Kuzyura et al. (2010)	Grt	7000	1265	0.1300
Kuzyura et al. (2010)	Grt	7000	1265	0.0600
Van Westrenen et al. (1999)	Grt	3000	1560	0.0180
Van Westrenen et al. (1999)	Grt	3000	1565	0.0052
Van Westrenen et al. (1999)	Grt	3000	1545	0.4800
Van Westrenen et al. (1999)	Grt	3000	1530	0.0830
Van Westrenen et al. (1999)	Grt	3000	1530	0.3800
Van Westrenen et al. (2000)	Grt	2900	1540	0.0220
Van Westrenen et al. (2000)	Grt	3000	1538	0.0084
Yurimoto and Ohtani (1992)	Grt	20,000	2000	0.5500
Yurimoto and Ohtani (1992)	Grt	16,000	1900	0.6800
Yurimoto and Ohtani (1992)	Grt	16,000	1900	0.3800
Wood and Trigila (2001)	Lct	200	1070	0.032
Lundstrom et al. (2006)	Mll	0.1	1213	0.48
Lundstrom et al. (2006)	Mll	0.1	1200	0.5
Lundstrom et al. (2006)	Mll	0.1	1199	0.62
Corgne et al. (2005)	$MgSiO_3$ Prv	25,000	2300	0.02
Corgne et al. (2005)	$MgSiO_3$ Prv	25,000	2300	0.06
Corgne et al. (2005)	$MgSiO_3$ Prv	25,000	2300	0.17
Corgne et al. (2005)	$MgSiO_3$ Prv	25,000	2300	0.06
Corgne et al. (2005)	$MgSiO_3$ Prv	25,000	2300	0.16
Corgne et al. (2005)	$MgSiO_3$ Prv	25,000	2350	0.07
Liebske et al. (2005)	$MgSiO_3$ Prv	26,000	2300	0.055
Liebske et al. (2005)	$MgSiO_3$ Prv	26,000	2200	0.08
Liebske et al. (2005)	$MgSiO_3$ Prv	26,000	2300	0.04
Taura et al. (2001)	$MgSiO_3$ Prv	25,000	2300	1.2
Adam and Green (2006)	Ol	2000	1100	0.29
Adam and Green (2006)	Ol	1000	1075	0.42
Blundy and Dalton (2000)	Ol	3000	1375	0.127
Blundy and Dalton (2000)	Ol	3000	1375	0.126
Brenan et al. (1998a, b)	Ol	–	–	0.15
Brenan et al. (1998a, b)	Ol	0.1	1349	0.15
Brenan et al. (1998a, b)	Ol	0.1	1349	0.13
Brenan et al. (1998a, b)	Ol	0.1	1349	0.15

(continued)

Table 4.1 (continued)

Reference	Mineral/mineral group	P (MPa)	T (°C)	K_p(Li)
Brenan et al. (1998a, b)	Ol	1000	1320	0.35
Brenan et al. (1998a, b)	Ol	0.1	1349	0.15
Grant and Wood (2010)	Ol	0.1	1390	0.06
Grant and Wood (2010)	Ol	0.1	1390	0.13
Grant and Wood (2010)	Ol	0.1	1390	0.12
Grant and Wood (2010)	Ol	0.1	1390	0.64
Grant and Wood (2010)	Ol	0.1	1390	0.16
Grant and Wood (2010)	Ol	0.1	1390	0.14
Grant and Wood (2010)	Ol	0.1	1390	0.11
Grant and Wood (2010)	Ol	0.1	1390	0.18
Grant and Wood (2010)	Ol	0.1	1390	0.19
Grant and Wood (2010)	Ol	0.1	1390	0.01
Grant and Wood (2010)	Ol	0.1	1390	0.02
Grant and Wood (2010)	Ol	0.1	1390	0.02
Grant and Wood (2010)	Ol	0.1	1390	0.02
Grant and Wood (2010)	Ol	0.1	1390	0.01
Grant and Wood (2010)	Ol	0.1	1390	0.02
Grant and Wood (2010)	Ol	0.1	1390	0.02
Grant and Wood (2010)	Ol	0.1	1390	–
Grant and Wood (2010)	Ol	0.1	1390	–
Grant and Wood (2010)	Ol	0.1	1390	0.13
Grant and Wood (2010)	Ol	0.1	1390	0.18
Grant and Wood (2010)	Ol	0.1	1390	0.13
Grant and Wood (2010)	Ol	0.1	1390	0.01
Grant and Wood (2010)	Ol	0.1	1390	0.02
Grant and Wood (2010)	Ol	0.1	1390	0.17
Grant and Wood (2010)	Ol	0.1	1390	0.53
Grant and Wood (2010)	Ol	0.1	1390	0.39
Grant and Wood (2010)	Ol	0.1	1390	0.68
Grant and Wood (2010)	Ol	0.1	1390	0.78
Grant and Wood (2010)	Ol	0.1	1390	0.03
Grant and Wood (2010)	Ol	0.1	1390	0.1
Grant and Wood (2010)	Ol	0.1	1390	0.25
Grant and Wood (2010)	Ol	0.1	1390	0.67
Grant and Wood (2010)	Ol	0.1	1390	1.04
Grant and Wood (2010)	Ol	0.1	1390	0.02
Grant and Wood (2010)	Ol	0.1	1390	0.02
Grant and Wood (2010)	Ol	0.1	1390	0.05
Grant and Wood (2010)	Ol	0.1	1390	0.13
Grant and Wood (2010)	Ol	0.1	1390	0.2
Grant and Wood (2010)	Ol	0.1	1390	0.25

(continued)

Table 4.1 (continued)

Reference	Mineral/mineral group	P (MPa)	T (°C)	K_p(Li)
Grant and Wood (2010)	Ol	0.1	1390	0.36
Grant and Wood (2010)	Ol	0.1	1390	0.5
Grant and Wood (2010)	Ol	0.1	1390	0.82
Grant and Wood (2010)	Ol	0.1	1390	0.13
Grant and Wood (2010)	Ol	0.1	1390	0.24
Grant and Wood (2010)	Ol	0.1	1390	0.19
Grant and Wood (2010)	Ol	0.1	1390	0.15
Grant and Wood (2010)	Ol	0.1	1390	0.1
Grant and Wood (2010)	Ol	0.1	1390	0.23
Grant and Wood (2010)	Ol	0.1	1390	0.07
Grant and Wood (2010)	Ol	0.1	1390	0.08
Grant and Wood (2010)	Ol	0.1	1390	0.08
Grant and Wood (2010)	Ol	0.1	1390	0.09
Grant and Wood (2010)	Ol	0.1	1390	0.11
Grant and Wood (2010)	Ol	0.1	1390	0.07
Grant and Wood (2010)	Ol	0.1	1390	0.1
McDade et al. 2003	Ol	1500	1325	0.289
Spandler and O'Neill (2010)	Ol	0.1	1300	0.29
Taura et al. (1998)	Ol	7000	1900	0.417
Taura et al. (1998)	Ol	5000	1900	0.4
Taura et al. (1998)	Ol	5000	1800	0.48
Taura et al. (1998)	Ol	5000	1900	0.54
Taura et al. (1998)	Ol	3000	1600	0.33
Taura et al. (1998)	Ol	5000	1700	0.47
Taura et al. (1998)	Ol	7000	1800	0.49
Taura et al. (1998)	Ol	3000	1800	0.21
Taura et al. (1998)	Ol	9700	2000	0.55
Taura et al. (1998)	Ol	9700	1800	0.56
Taura et al. (1998)	Ol	14,400	1900	0.45
Zanetti et al. (2004)	Ol	1400	1055	0.22
Adam and Green (2006)	Opx	2700	1160	0.28
Brenan et al. (1998a, b)	Opx	1000	1320	0.2
Frei et al. (2009)	Opx	1100	1230	0.185
Frei et al. (2009)	Opx	2300	1440	0.2
Frei et al. (2009)	Opx	2700	1510	0.175
Frei et al. (2009)	Opx	3200	1535	0.184
Frei et al. (2009)	Opx	2000	1330	0.2200
McDade et al. 2003	Opx	1500	1325	0.166
van Kan Parker et al. (2010)	Opx	0.1	1390	0.22
van Kan Parker et al. (2010)	Opx	0.1	1350	0.208
van Kan Parker et al. (2010)	Opx	0.1	1326	0.13

(continued)

Table 4.1 (continued)

Reference	Mineral/mineral group	P (MPa)	T (°C)	K_p(Li)
van Kan Parker et al. (2011)	Opx	1100	1430	0.21
van Kan Parker et al. (2011)	Opx	2100	1550	0.22
van Kan Parker et al. (2011)	Opx	2800	1600	0.26
Van Westrenen et al. (2000)	Opx	3000	1538	0.48
Adam and Green (2006)	Phl	2700	1160	0.21
Adam and Green (2006)	Phl	2000	1050	0.19
Adam and Green (2006)	Phl	2500	1100	0.21
LaTourette et al. (1995)	Phl	2000	1109	0.064
Schmidt et al. (1999)	Phl	1500	1140	0.213
Schmidt et al. (1999)	Phl	1500	1040	0.46
Schmidt et al. (1999)	Phl	1500	1140	0.169
Aigner-Torres et al. (2007)	Pl	0.1	1200	0.2944
Aigner-Torres et al. (2007)	Pl	0.1	1180	0.5754
Aigner-Torres et al. (2007)	Pl	0.1	1180	0.6784
Bindeman and Davis (2000)	Pl	0.1	1257	0.2880
Bindeman and Davis (2000)	Pl	0.1	1257	0.2710
Bindeman and Davis (2000)	Pl	0.1	1257	0.3050
Bindeman and Davis (2000)	Pl	0.1	1297	0.2960
Bindeman and Davis (2000)	Pl	0.1	1299	0.2250
Bindeman and Davis (2000)	Pl	0.1	1299	0.2470
Bindeman and Davis (2000)	Pl	0.1	1299	0.2520
Bindeman and Davis (2000)	Pl	0.1	1153	0.2450
Bindeman and Davis (2000)	Pl	0.1	1187	0.3170
Bindeman and Davis (2000)	Pl	0.1	1187	0.2680
Bindeman and Davis (2000)	Pl	0.1	1187	0.2540
Bindeman and Davis (2000)	Pl	0.1	1187	0.2720
Bindeman et al. (1998)	Pl	0.1	1190	0.2530
Bindeman et al. (1998)	Pl	0.1	1190	0.2750
Bindeman et al. (1998)	Pl	0.1	1297	0.2430
Bindeman et al. (1998)	Pl	0.1	1297	0.2570
Bindeman et al. (1998)	Pl	0.1	1250	0.2180
Bindeman et al. (1998)	Pl	0.1	1250	0.2470
Bindeman et al. (1998)	Pl	0.1	1153	0.2100
Bindeman et al. (1998)	Pl	0.1	1153	0.2430
Bindeman et al. (1998)	Pl	0.1	1153	0.2260
Bindeman et al. (1998)	Pl	0.1	1297	0.1600
Bindeman et al. (1998)	Pl	0.1	1297	0.1380
Blundy (1997)	Pl	0.1	1208	0.130
Blundy (1997)	Pl	0.1	1212	0.280
Blundy et al. (1998)	Pl	1500	1255	0.1510
Caciagli et al. (2011)	Pl	1000	1000	0.02

(continued)

Table 4.1 (continued)

Reference	Mineral/mineral group	P (MPa)	T (°C)	K_p(Li)
Caciagli et al. (2011)	Pl	1000	900	0.017
Dohmen and Blundy (2014)	Pl	0.1	1251	0.3614
Dohmen and Blundy (2014)	Pl	0.1	1086	0.1483
Dohmen and Blundy (2014)	Pl	0.1	1251	0.1331
Dohmen and Blundy (2014)	Pl	0.1	1251	0.1427
Dohmen and Blundy (2014)	Pl	0.1	1251	0.0978
Dohmen and Blundy (2014)	Pl	0.1	1251	0.1247
Dohmen and Blundy (2014)	Pl	0.1	1290	0.1422
Dohmen and Blundy (2014)	Pl	0.1	1290	0.1400
Dohmen and Blundy (2014)	Pl	0.1	1290	0.1325
Dohmen and Blundy (2014)	Pl	0.1	1290	0.1404
Dohmen and Blundy (2014)	Pl	0.1	1226	0.1264
Dohmen and Blundy (2014)	Pl	0.1	1184	0.1235
Dohmen and Blundy (2014)	Pl	0.1	1184	0.1541
Dohmen and Blundy (2014)	Pl	0.1	1108	0.1275
Dohmen and Blundy (2014)	Pl	0.1	1108	0.1210
Dohmen and Blundy (2014)	Pl	0.1	1282	0.0892
Dohmen and Blundy (2014)	Pl	0.1	1286	0.1413
Tepley et al. (2010)	Pl	0.1	1264	0.2970
Tepley et al. (2010)	Pl	0.1	1265	0.1810
Elkins et al. (2008)	Spl	2500	1420	0.13
Lundstrom et al. (2006)	Spl	0.1	1213	0.1
Lundstrom et al. (2006)	Spl	0.1	1225	0.184
Icenhower and London (1995)	Bt	200	650	0.8
Icenhower and London (1995)	Bt	200	750	1.01
Icenhower and London (1995)	Bt	200	660	1.67
Icenhower and London (1995)	Bt	200	650	1.64
Icenhower and London (1995)	Ms	200	650	0.82

Evans 2010). $K_{p(\mathrm{Li})}^{Min/Melt}$ was mostly measured for silicate melts and in some cases for carbonate melts (e.g., Blundy and Dalton 2000). For the investigated range of experimental conditions and minerals, $K_{p(\mathrm{Li})}^{Min/Melt}$ cover a range from 0.005 to $\sim$1.7. Therefore, during partial melting Li could behave as an incompatible, moderately incompatible, neutral, or even compatible element depending on the mineral assemblage and detailed mineral chemistry. Even for the same mineral, e.g., clinopyroxene or garnet, depending on their composition, $K_{p(\mathrm{Li})}^{Min/Melt}$ varies over a large range (0.01–1.0) and it is thus not appropriate for geochemical modelling to assign a single typical value of $K_{p(\mathrm{Li})}^{Min/Melt}$ for a given mineral. Simplified statements like 'Li is more compatible in orthopyroxene than in clinopyroxene' appear to be incorrect in the general case. Most values for $K_{p(\mathrm{Li})}^{Min/Melt}$, however, consider only common rock-forming minerals of the crust and the upper mantle with respective typical compositions (excluding synthetic compositions

such as pure forsterite), and are confined to a much smaller range (0.1–0.7).

After a short overview of the experimental methods, we discuss the data for $K_{p(\mathrm{Li})}^{Min/Melt}$ of each mineral individually based on crystal chemistry. Here, we often refer to the lattice strain model to discuss the variability of the experimental data with respect to the mineral chemistry and possible incorporation mechanisms of Li.

Experimental methods. In basically all studies measuring mineral–melt partition coefficients a mineral/rock powder or synthetic glass powder was heated in a chemically inert container (e.g., a noble metal capsule, Au, Pt, etc.) above the solidus or even liquidus temperature at a given pressure for the given bulk composition and then cooled slowly (typically with rates on the order of a few °C/hour) to a final temperature below the liquidus. In some experiments the starting material was directly heated to the final temperature. After the sample reached the final temperature it was immediately quenched or annealed for some time (a couple of hours to days) to completely equilibrate the sample, e.g., by diffusion and recrystallization. The slow cooling rate is largely chosen to ensure the growth of large crystals, at least large enough to allow in situ measurement of the mineral composition. All of the Li partition coefficients reported here were measured using either SIMS or LA-ICP-MS; the major element composition of the respective minerals and the quenched melt was typically measured using electron microprobe (EPMA). It is a fundamental issue of these types of experiments that the temperature of equilibration between the mineral and the melt is not well defined since the mineral grows during cooling and growth zoning of trace and major elements may result. This means that the core composition of the mineral was not necessarily in thermodynamic equilibrium with the melt at the final temperature if the time at this final temperature was not sufficient to re-equilibrate the core with the melt by solid-state diffusion. Rarely, compositional profiles across the minerals and quenched melts were measured in these experimental studies to identify any chemical zoning (e.g., LaTourette et al. 1995), owing mainly to the small crystal sizes obtained. Lithium may be a special case compared to other elements, since it tends to diffuse very quickly within most minerals. At the relatively high temperatures before the final quench, Li should re-equilibrate very quickly if any zoning was formed during the growth (see the characteristic diffusion time scales of Li discussed below), and therefore reflect the equilibrium partitioning at the final temperature.

In most of the papers that are summarized here, the authors focused on the discussion of partition coefficients for other alkali elements (Rb, Cs) or trivalent cations, in particular REE. Studies that also discuss $K_{p(\mathrm{Li})}^{Min/Melt}$ in more detail are those by Brenan et al. (1998a, b), Taura et al. (1998), and Grant and Wood (2010). The data for $K_{p(\mathrm{Li})}^{Min/Melt}$ are discussed separately for the different mineral groups; abbreviations for end members of mineral groups are italicized.

Plagioclase (Pl). $K_{p(\mathrm{Li})}^{Pl/Melt}$ along the albite (*Ab*, $NaAlSi_3O_8$)—anorthite (*An*, $CaAl_2Si_2O_8$) join was measured for *An* contents between 9 and 100 mol% (Blundy 1997; Blundy et al. 1998; Bindeman et al. 1998; Bindeman and Davis 2000; Aigner-Torres et al. 2007; Tepley et al. 2010; Dohmen and Blundy 2014) at atmospheric pressures (except Blundy 1997 at 1.5 GPa) and temperatures between 1090 and 1300 °C. Observed values for $K_{p(\mathrm{Li})}^{Pl/Melt}$ are between 0.09–0.6, which is a relatively small range compared to, for example, garnet, olivine, and clinopyroxene (see below). Based on the work of Blundy and Wood (1991) plagioclase–melt partition coefficients are presented by Bindeman et al. (1998) in the following form:

$$RT\ln K_{p(i^{n+})}^{Pl/Melt} = A_{i^{n+}} + B_{i^{n+}} \cdot X_{An} \qquad (4.2.11)$$

where X_{An} is the molar fraction of anorthite in plagioclase, and $A_{\mathrm{Li}} = -12.1 \pm 1.0$ kJ/mol and $B_{\mathrm{Li}} = -6.9 \pm 1.9$ kJ/mol according to Bindeman et al. (1998). However, the relation in Eq. 4.2.11 does not fully cover the explicit dependence on the *An* content but also reflects that the *An* content is an implicit function of T as discussed in

Bindeman et al. (1998) and Dohmen and Blundy (2014). Dohmen and Blundy (2014) fitted the lattice strain parameters as a function of the *An* content from experiments performed in the pseudo-ternary system diopside–albite–anorthite and obtained a linear dependence of $r^{1+}_{0(M)}$ and E^{1+}_{M} on the anorthite content, X_{An} (see also Blundy and Wood 1994, 2003a, b), as follows:

$$r^{1+}_{0(M)}[\text{Å}] = (1.2370 \pm 0.0020) - (0.0171 \pm 0.0032) \cdot X_{An} \quad (4.2.12a)$$

$$E^{1+}_{M}[\text{GPa}] = (49.5 \pm 0.5) + (17.16 \pm 0.88) \cdot X_{An} \quad (4.2.12b)$$

With Eqs. 4.2.9 and 4.2.12a, b, respectively, $K^{Pl/Melt}_{p(\text{Li})}$ can be predicted for a given *An* content if $K^{Pl/Melt}_{p(\text{Na})}$ is known from other sources (see the possible strategies to calculate $K^{Pl/Melt}_{p(\text{Na})}$ in Dohmen and Blundy 2014). A more general equation than Eq. 4.2.12a, b to calculate $K^{Pl/Melt}_{p(\text{Li})}$ at atmospheric pressures was also given by Dohmen and Blundy (2014) who developed a predictive thermodynamic model for 1+, 2+, and 3+ cations occupying the A site in plagioclase. For the 1+ cations the model is based on the fusion reaction of the *Ab* component combined with the lattice strain model (Eq. 4.2.9), which allows estimation of the effect of T and compositional parameters according to the following equation:

$$RT\ln\left(\Theta \cdot K^{Pl/Melt}_{p(\text{Li})}\right) = 29725 - 1.07928 \cdot T - 0.01499 \cdot T^2 + A_{\text{Li}} + B_{\text{Li}} \cdot X_{An} + C_{\text{Li}} \cdot (X_{An})^2 \quad (4.2.13)$$

where θ is a factor that considers the melt chemistry, which can be assumed to be a constant for a limited compositional range of the melt. The values for A_{Li}, B_{Li}, and C_{Li}, respectively, depend in general on the stable point group related to the Al–Si ordering state, $C\bar{1}$ or $I\bar{1}$, at the given T and X_{An} and the interaction parameters of the anorthite–albite solid solution, W_{An-Ab}. The optimized values for the diopside–albite–anorthite system at 1200 °C are $B_{\text{Li}} = -4.71$ kJ/mol, $A_{\text{Li}} = -18.4$ and –16.56 kJ/mol, $C_{\text{Li}} = 4.0$ and 0.0 kJ/mol for the $C\bar{1}$ and the $I\bar{1}$ stability field, respectively. The parameters B_{Li} and C_{Li} reflect how the chemical potential of the Li-bearing component ($LiAlSi_3O_8$) in plagioclase changes with X_{An}. Recent experiments of Coogan (2011) in which plagioclase with variable X_{An} re-equilibrates Li with each other by solid state diffusion indicate a much stronger dependence of this chemical potential on X_{An}, equivalent to $B_{\text{Li}} \sim -70$ kJ/mol. More experiments are necessary to resolve this discrepancy (see also Sect. 4.2.5). With the set of parameters given by Dohmen and Blundy (2014), the net effect of crystal chemistry for $K^{Pl/Melt}_{p(\text{Li})}$ is relatively small and not drastically different from the empirical relationship of Bindeman et al. (1998).

Olivine (Ol). With the structural formula M1M2[TO_4], where both the M1 and M2 site are sixfold coordinated, olivine usually has low trace element concentrations (in particular REE) compared to pyroxene or garnet. The major element chemistry follows the binary join forsterite (*Fo*, Mg_2SiO_4)—fayalite (*Fa*, Fe_2SiO_4). Even though the mineral chemistry of olivine appears to be simple, a huge variability of $K^{Ol/Melt}_{p(\text{Li})}$ was found, 0.01–1.0, which is similar to clinopyroxene or garnet. $K^{Ol/Melt}_{p(\text{Li})} < 0.13$ was exclusively found in the very detailed study of Grant and Wood (2010) where they explored the effect of trace element chemistry on $K^{Ol/Melt}_{p(\text{Li})}$. All of their experiments were performed with almost pure forsterite at atmospheric pressures and the same temperature of 1390 °C, thus isolating compositional effects of trace elements on $K^{Ol/Melt}_{p(\text{Li})}$ from other factors. Most importantly they found a doping effect and deviation from Henry's law for a system with almost pure forsterite containing

defined doping levels of Sc or Ga (Fig. 2 in Grant and Wood 2010). Mostly, $K_{p(\mathrm{Li})}^{Ol/Melt}$ appears to depend on the concentration of Sc^{3+} in the melt due to the formation of an associated defect containing Sc^{3+} and Li^{+} at concentration levels above ~500 µg/g Sc in the melt (the affinity of Li and Sc in the olivine structure is also reflected by the synthesis of a pure $LiScSiO_4$ endmember; Ito 1977). At lower concentrations it is argued that two Li atoms substitute for one Mg atom where one Li atom goes to an interstitial site. The formation of Li interstitials in olivine is also indicated by diffusion experiments (Dohmen et al. 2010) as discussed in detail below. Similar to Sc, incorporation of Ga into olivine is also coupled to the presence of Li, and association of Li and Ga at relatively high concentrations of around 500 µg/g is suggested (Grant and Wood 2010). This behavior highlights again the importance of a charge balance on mineral–melt partitioning and shows that $K_{p(\mathrm{Li})}^{Ol/Melt}$ tends to increase with the increasing concentration of trivalent cations in the melt that are capable of association with Li within the olivine structure.

In natural olivine Fe^{3+} is potentially important to charge balance Li^{+} in olivine. The concentration of Fe^{3+} in olivine is strongly dependent on the fayalite content, fO_2 and T, with concentrations in the range of ~0.1–10000 µg/g (roughly estimated from point defect calculations in Dohmen and Chakraborty 2007). Other experimental data for $K_{p(\mathrm{Li})}^{Ol/Melt}$ (Brenan et al. 1998a, b; Taura et al. 1998; Blundy and Dalton 2000; McDade et al. 2003; Zanetti et al. 2004; Adam and Green 2006; Spandler and O'Neill 2010) measured over a wide pressure and temperature range (0.1 MPa–14.4 GPa and 1055–1900 °C, respectively) and with *Fo* contents ranging from 78 to 99.9 mol% vary much less than those of Grant and Wood (2010), between 0.13–0.56. This smaller variation of $K_{p(\mathrm{Li})}^{Ol/Melt}$ compared to that of Grant and Wood (2010) seems surprising because of the very different experimental conditions in these other studies. This observation may also indicate that in these experiments enough trivalent elements (e.g., Fe^{3+}, Sc^{3+}, Ga^{3+}) in the melt were available to be incorporated into the M site and charge balance Li^{+} on the same site. Other factors like pressure and temperature as well as fayalite content seem to play a subordinate role for $K_{p(\mathrm{Li})}^{Ol/Melt}$. For example, Taura et al. (1998) specifically investigated the effect of pressure on olivine–melt partition coefficients (experiments at pressures between 3 and 14 GPa) and found on average a small increase of $K_{p(\mathrm{Li})}^{Ol/Melt}$ (factor 2 between 3 and 14 GPa) with increasing pressure.

Clinopyroxene (Cpx). This has the general structural formula (M1, M2) $[T_2O_6]$ where several combinations of occupations of the M sites and T sites are possible. $K_{p(\mathrm{Li})}^{Cpx/Melt}$ was measured at pressures between 0.1 MPa and 7 GPa, temperatures between 1040 and 1640 °C, and a great diversity of Cpx compositions as illustrated in Fig. 4.3a, b. The strong variation of the Cpx chemistry is closely related to the melt chemistry in these experimental studies. For example, the SiO_2 content varies between 4.8 and 26.2 wt% (Blundy and Dalton 2000; Kuzyura et al. 2010) in carbonate melts and between 39 and 64 wt% (Adam and Green 2006; Huang et al. 2006) in silicate melts. In accordance with compositional variability of Cpx, experimentally measured values of $K_{p(\mathrm{Li})}^{Cpx/Melt}$ cover a range from 0.02 to 1.05. For most experiments the compositions of Cpx can be mainly described by the end members *Di+Hd*, *En+Fs*, *Jd*, and *CaTs* (Fig. 4.3) and even for these Cpx with minor contents of the more exotic components *Esk*, *Acm*, *Ca-Acm*, and *CaTi-Ts* (see Fig. 4.3 caption for definition of the components and chemical formulas) the variation of $K_{p(\mathrm{Li})}^{Cpx/Melt}$ is between 0.04 and 1.05. According to the model of Wood and Blundy (2001), $K_{p(\mathrm{Li})}^{Cpx/Melt}$ should be strongly dependent on the availability of sites that allow local charge balance. For example, when the *Jd* component is present in Cpx it would provide a charge-balanced site for other 1+ cations. We can further illustrate this feature of Li partitioning by plotting $K_{p(\mathrm{Li})}^{Cpx/Melt}$ against the *Jd* component. For most experiments we can observe a general trend

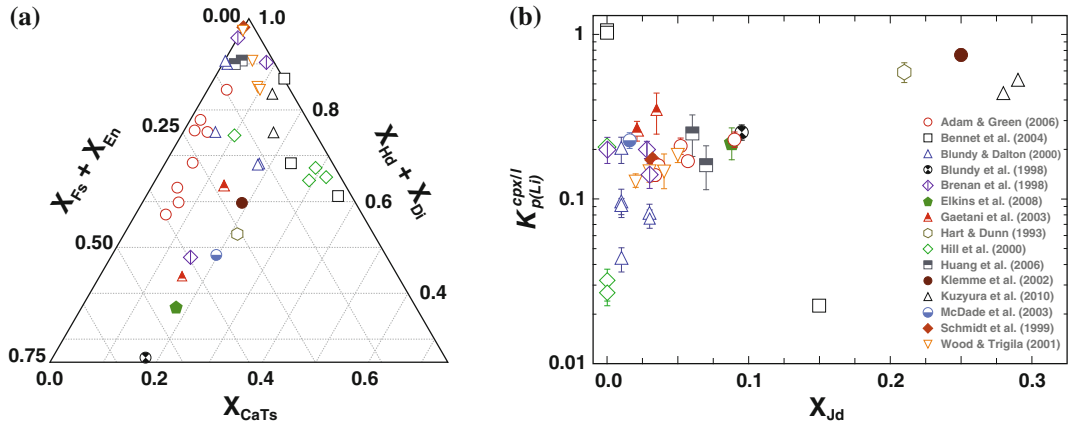

Fig. 4.3 Illustration of the compositional variation of Cpx for which $K_{p(\mathrm{Li})}^{Cpx/Melt}$ was measured and the corresponding variation of $K_{p(\mathrm{Li})}^{Cpx/Melt}$. **a** Ternary plot of the molar fraction of the components jadeite + hedenbergite, enstatite + ferrosilite, and Ca-Tschermak component in Cpx, normalized to 1. **b** Variation of $K_{p(\mathrm{Li})}^{Cpx/Melt}$ with the molar fraction of jadeite in Cpx. The oxide compositions of the respective cpx were recalculated to a normative composition considering the 9 end-members: diopside (*Di*, $CaMgSi_2O_6$), hedenbergite (*Hd*, $CaFeSi_2O_6$), jadeite (*Jd*, $NaAlSi_2O_6$), enstatite (*En*, $Mg_2Si_2O_6$), ferrosilite (*Fs*, $Fe_2Si_2O_6$), Ca-Tschermak (*CaTs*, $CaAl_2SiO_6$), CaTi-Tschermak (*TiTs*, $CaTiAl_2O_6$), Ca-eskolaite (*Esk*, $Ca_{0.5}[\ ]_{0.5}AlSiO$), and acmite (*Acm*, $NaFe^{3+}Si_2O_6$). For the Cpx of Wood and Trigila (2000) instead of *Acm* a $CaFe^{3+}$-Tschermak component ($CaFe^{3+}AlSiO_6$) was needed to reproduce their respective cpx stoichiometry. For the calculation of the normative composition it was assumed that the fraction $Fe^{2+}/(Fe^{2+} + Mg)$ is the same on the M1 and M2 site. The same type of symbols was used in (**a**) as in (**b**) for the data sources, which are given in the respective symbol legend. A rough trend of increasing $K_{p(\mathrm{Li})}^{Cpx/Melt}$ with X_{Jd} can be observed

that $K_{p(\mathrm{Li})}^{Cpx/Melt}$ increases with the *Jd* content. Exceptions are the experiments of Hill et al. (2000) where the Cpx contains the highest amount of *CaTs* (>0.25), one experiment of Bennett et al. (2004) in which Cpx contains the highest amount of the *Esk* (0.37), and experiments of Klemme et al. (2002) and Kuzyura et al. (2010) in which Cpx contains a considerable amount of *Esk*, in the range of 5–31 mol%.

It should be considered that a variable major element composition can also affect the optimum ionic radius for a given site, which may explain the deviation for the general $K_{p(\mathrm{Li})}^{Cpx/Melt}$ versus X_{Jd} trend for Cpx with high contents of components like *Esk* and *CaTs*. In addition to *Jd*, as illustrated here for Li, a number of studies demonstrated that for many elements $K_p^{Cpx/Melt}$ increases with an increasing amount of *CaTs* (or basically the amount of tetrahedrally coordinated Al; e.g., Lundstrom et al. 1998; Blundy and Dalton 2000; Hill et al. 2000), but for $K_{p(\mathrm{Li})}^{Cpx/Melt}$ there is not a similar obvious trend visible (cf. Fig. 4.3 with data of Hill et al. 2000). In addition, deviations from the $K_{p(\mathrm{Li})}^{Cpx/Melt}$ versus X_{Jd} trend seems to be unrelated to the melt composition, since for example data for carbonate melts and silicate melts follow the same trend. Blundy and Dalton (2000) also concluded in their comparative study of $K_p^{Cpx/Melt}$ for silicate and carbonate melts in the diopside–albite and diopside–albite–dolomite system that for alkali elements the difference is small (<3) and similar to the partitioning behavior between immiscible silicate and carbonate melts (e.g., Veksler et al. 1998).

Garnet (Grt). This has the general structural formula $X_3Y_2Z_3O_{12}$ where X, Y, and Z are coordinated by 8, 6, and 4 oxygen atoms, respectively. The major element composition of Grt can be mostly described by the four end-members, pyrope (*Prp*, $Mg_3Al_2Si_3O_{12}$),

almandine (*Alm*, $Fe_3Al_2Si_3O_{12}$), grossular (*Grs*, $Ca_3Al_2Si_3O_{12}$), and spessartine (*Sps*, $Mn_3Al_2Si_3O_{12}$), but at high pressures the majorite component (*Maj*, $Mg_3MgSiSi_3O_{12}$) becomes relevant. $K_{p(\mathrm{Li})}^{Grt/Melt}$ was measured for the following garnet compositions: along the *Prp–Grs* join with *Grs* contents varying from 16 to 90 mol% (van Westrenen et al. 1999; Bennett et al. 2004; Klemme et al. 2002), with some additional *Alm* component varying between 9 and 33 mol% (van Westrenen et al. 2000; Gaetani et al. 2003; Adam and Green 2006; Kuzyura et al. 2010), and experiments at very high pressures between 16 and 20 GPa with garnet containing a significant proportion of *Maj* component with sixfold coordinated Mg and Si on the Y site (Bennett et al. 2004; Kuzyura et al. 2010; Yurimoto and Ohtani 1992). The overall variation of $K_{p(\mathrm{Li})}^{Grt/Melt}$ is between 0.005–0.68. Even for experiments along the *Prp–Grs* join at the same pressure (3 GPa) and a moderate temperature range (1400–1550 °C), $K_{p(\mathrm{Li})}^{Grt/l}$ varies between 0.005 and 0.48, indicating a strong compositional dependence of $K_{p(\mathrm{Li})}^{Grt/Melt}$. The crystal chemistry of garnet dominates the partitioning behaviour of many trace elements. For example, the partition coefficients of trivalent cations can be reproduced by a systematic variation of the lattice strain parameters ($r_{0(X)}^{3+}$, E_X^{3+}, and $K_{p(0)}^{3+}$) with the content of the four end-members, *Prp*, *Alm*, *Grs*, and *Sps* (van Westrenen et al. 1999, 2000). Unfortunately, there are no data available for an isovalent element series of 1+ cations to perform a similar calculation and quantify the effect of composition for $K_{p(\mathrm{Li})}^{Grt/Melt}$. The presence of the *Maj* component could have a twofold effect: (i) a change of the lattice strain parameters (e.g., as calibrated for *Prp*, *Alm*, *Grs*, *Sps*); (ii) due to the presence of Si on the Y site, the number of local atomic configurations to charge balance Li^{1+} on the X-site is increasing by the incorporation of Li as $(Mg_2Li)(AlSi)Si_3O_{12}$. The latter argument seems to be consistent with the high values for $K_{p(\mathrm{Li})}^{Grt/Melt}$ (0.44–0.68) of Yurimoto and Ohtani (1992) for garnets with *Maj* contents of 56–59 mol%. It appears that, in general, Li becomes more compatible in Grt with increasing *Grs* or *Maj* content. The effect of *Maj* on the incorporation of Li into garnet was also studied in Hanrahan et al. (2009) and will be discussed in the Sect. 4.2.5 on inter-mineral partitioning of Li.

Orthopyroxene (Opx). This can be described by the same structural formula as Cpx, (M1, M2) $[T_2O_6]$. $K_{p(\mathrm{Li})}^{Opx/Melt}$ was measured by Adam and Green (2006), Brenan et al. (1998a, b), Frei et al. (2009), McDade et al. (2003), van Kan Parker et al. (2010, 2011), and van Westrenen et al. (2000) at pressures between 0.1 MPa and 3.2 GPa, temperatures between 1160 and 1600 °C, and diverse major element compositions. The Opx stoichiometry can be mainly expressed by the following endmember components: *En*, *Fs*, *Di*, *Hd* and Mg-Tschermak (*MgTs*, $MgAl_2SiO_6$). The compositional variables X_{Di}, X_{MgTs}, and $Mg\# = Mg/(Fe + Mg)$, vary between 0.03–0.23, 0–0.2, and 0.0–0.17, respectively. Despite this variable composition and the very different *P–T* conditions, $K_{p(\mathrm{Li})}^{Opx/Melt}$ is remarkably similar for the 15 published experiments, varying between 0.13 and 0.48 with an average value of 0.22 ± 0.08. There is no clear trend of $K_{p(\mathrm{Li})}^{Opx/Melt}$ with any of the compositional variables, but the highest value of 0.48 was measured by Van Westrenen et al. (2000) for Opx with the highest X_{Di} (0.23) and X_{MgTs} (0.08). Due to the high *MgTs* content in this Opx composition, more charge balanced sites could be provided for Li in the form of $LiAlSi_2O_6$ thereby enhancing the compatibility of Li in Opx.

Perovskite (Prv). This has the structural formula ABO_3 where A and B are 12-fold and sixfold coordinated sites, respectively. $K_{p(\mathrm{Li})}^{Prv/Melt}$ was measured for three different perovskites: $CaSiO_3$ (CaPrv) at *P* between 21–25 GPa and *T* between 2100–2350 °C (Taura et al. 2001; Corgne et al. 2005); $CaTiO_3$ (CaTiPrv) for *P* between 0.1 MPa and 3 GPa, *T* between 1500–1800 °C (Corgne and Wood 2005), and $MgSiO_3$ (MgPrv) for *P* between 25–26 GPa and *T* = 2300–2350 °C

(Taura et al. 2001; Corgne et al. 2005; Liebske et al. 2005). $K_{p(\mathrm{Li})}^{MgPrv/Melt}$ measured by Corgne et al. (2005) and Liebske et al. (2005) are very similar and within the range 0.05–0.08 (6 experiments, where for Corgne et al. 2005 we consider only three values measured by SIMS; in their study $K_{p(\mathrm{Li})}^{Prv/Melt}$ measured by LA-ICP-MS was systematically biased to higher values compared to SIMS data for unknown reasons). Interestingly, the two values of $K_{p(\mathrm{Li})}^{CaPrv/Melt}$ measured by Corgne et al. (2005) are 0.05 and 0.13, very similar to MgPrv. This seems surprising as the Mg site in MgPrv (at the center of a distorted dodecahedron) should be apparently a better fit for Li than the Ca site in CaPrv (at the center of a regular dodecahedron), when inferred from the ionic radii of Mg and Ca (see also Chap. 5). In fact, fitting of the partition coefficients of 1+ cations for MgPrv and CaPrv by the lattice strain model show that the optimum ionic radius for the A site is much smaller in MgPrv compared to CaPrv, c. 1.1 Å versus c. 1.3 Å, respectively (Corgne et al. 2005). The fitted effective Young's modulus, E_A^{1+} is rather similar for the two, but $K_{p(0)}^{1+}$ is significantly larger for CaPrv compared to MgPrv, 0.07 versus 0.9, thus compensating as a net result for $K_{p(\mathrm{Li})}^{Prv/Melt}$ the misfit of Li for CaPrv compared to MgPrv. This higher value of $K_{p(0)}^{1+}$ could be related to the melt chemistry stabilizing CaPrv or the higher availability of sites that charge balance 1+ cations. For example, the presence of Al on the A site could be relevant to form structural units like $Li_{0.5}Al_{0.5}CaO_3$, but in the study of Corgne et al. (2005) the Al content in CaPrv is not generally larger than in MgPrv.

In Taura et al. (2001), a single experiment was published where MgPrv and CaPrv coexisted and $K_{p(\mathrm{Li})}^{MgPrv/Melt} = 1.2$ and $K_{p(\mathrm{Li})}^{CaPrv/Melt} = 0.17$ were measured simultaneously, and thus effects of P, T, and melt chemistry could be excluded to explain this difference. This significantly larger value of $K_{p(\mathrm{Li})}^{MgPrv/Melt}$ compared to those given by Corgne et al. (2005) and Liebske et al. (2005) could be explained by the relatively large Al content of around 1 wt% in the perovskites of Taura et al. (2001), and we can conclude that at identical conditions Li is more compatible in MgPrv compared to CaPrv. $K_{p(\mathrm{Li})}^{CaTiPrv/Melt}$ measured by Corgne and Wood (2005) was found to be very similar to $K_{p(\mathrm{Li})}^{CaPrv/Melt}$ and varies for 20 experiments from 0.025 to 0.3. This variation is not correlated with the strongly different P and T conditions of these experiments (0.1 MPa, c. 1400–1600 °C vs. 3 GPa, 1600–1800 °C). For trivalent and tetravalent cations, Corgne and Wood (2005) demonstrated that for $K_p^{CaTiPrv/Melt}$ the most relevant variable is the CaO content in the melt. This dependence is the result of the substitution of these elements into the A site by a coupled substitution that involves vacancies on the A site. For Li this kind of mechanism is not possible but, as mentioned above, Al on the A site and by inference Al_2O_3 content in the melt could potentially be a more relevant variable.

Mica. These can be generally described by the structural formula $X_2Y_{4-6}[Z_8O_{20}](OH, F)_4$. Mica–melt partition experiments of Li were measured for biotite (Bt) and muscovite (Ms) by Icenhower and London (1995), and for phlogopite (Phl) by LaTourette et al. (1995), Schmidt et al. (1999) and Adam and Green (2006). For Phl, Bt, and Ms the X site is mainly occupied by K and minor amounts of Na. The Y site is occupied mainly by Al in Ms but Fe, Mg, Al, and Ti in Bt and Phl. The main difference between Bt and Phl is the higher degree of the Tschermak substitution of 2 Al^{3+} by Mg^{2+} + Si^{4+} ions in Bt. $K_{p(\mathrm{Li})}^{Phl/Melt}$ was measured at P = 1.5–7 GPa, T = 1040–1150 °C, and varies between 0.06 and 0.46, which is negatively correlated with the Al content of the Z site. This correlation can be explained by considering the coupled substitution of 2 Al^{3+} with Si^{4+} + 2Li^+ ions, similar to derivation of the Li-mineral lepidolite (K_2(Li, Al)$_{5-6}$[$Si_{6-7}Al_{2-1}O_{20}$](OH, F) from pure Ms $K_2Al_4[Si_6Al_2O_{20}](OH, F)$. $K_{p(\mathrm{Li})}^{Bt/Melt}$ was measured at P = 0.2 GPa, T = 650–750 °C, and varies between 0.8 and 1.64; hence Li is generally much more compatible in Bt than in Phl. In Bt

the Al content on the Y site is much higher, thus allowing the potential substitution of $2Mg^{2+}$ ions by coupled Al^{3+} + Li^{+}, all on the Y site. $K_{p(\mathrm{Li})}^{Ms/Melt} = 0.8$ was measured in a single experiment at P = 0.2 GPa, T = 650 °C. Onuma diagrams of $K_{p}^{Phl/Melt}$ for the alkali elements show that $K_{p(\mathrm{Li})}^{Phl/Melt}$ does not fit into the parabola for larger 1+ cations like Na, K, Rb, and Cs (Fig. 6 in Schmidt et al. 1999; Fig. 8 in LaTourette et al. 1995), which occupy the X site. The optimum ionic radius for this site (c. 1.7 Å) is much larger than the ionic radius of Li and hence it is strongly incompatible for the X site. However, as discussed before, Li can be substituted into the much smaller Y site, and therefore, for micas $K_{p(\mathrm{Na})}^{Min/Melt}$ together with Eq. 4.2.10 would be not a good proxy to predict $K_{p(\mathrm{Li})}^{Min/Melt}$.

Cordierite (Crd). It has the structural formula $(Mg, Fe)_2[Si_5Al_4O_{18}]\cdot nH_2O$. Evensen and London (2003) measured $K_{p(\mathrm{Li})}^{Crd/Melt}$ at P = 200 MPa and T = 700–850 °C. Values for $K_{p(\mathrm{Li})}^{Crd/Melt}$ are in the range of 0.13–0.44 where X_{Mg} of the Crd varies between 0.69 and 0.85. Evensen and London (2003) parameterized $K_{p(\mathrm{Li})}^{Crd/Melt}$ as a function of temperature (in °C), as follows, $K_{p(Li)}^{Crd/Melt} = 1.61 - 1.733 \times 10^{-3} \cdot T$.

Several studies suggest that Li enters the cordierite structure by substitution for octahedral cations like Mg and Fe^{2+} (Armbruster and Irouschek 1983; Kirchner et al. 1984; Gordillo et al. 1985). To charge balance Li^{+} the following substitution was suggested by Evensen and London (2003): $Mg^{2+} \rightarrow Li^{+} + Na^{+}$, where Na^{+} occupies non-regular sites within the channels formed by six-membered rings of $(Si, Al)O_4$ tetrahedra in Crd, like other large alkali ions. Therefore, similar to mica, $K_{p(\mathrm{Na})}^{Min/Melt}$ cannot be used as a proxy for $K_{p(\mathrm{Li})}^{Min/Melt}$ together with Eq. 4.2.10 because Na and Li do not enter the same site.

Amphibole (Amp). These have the general structural formula $A_{0-1}B_2C_5[T_8O_{22}](OH, F)_2$, where Na and K occupy the A site, Na, Ca, Mg, Fe^{2+} (as well as Mn and Li) the B site, generally smaller cations than Ca, like Fe^{2+}, Mg^{2+}, Fe^{3+}, and Al^{3+} (as well as Mn and Li) the C site, Si and Al the T site. $K_{p(\mathrm{Li})}^{Amp/Melt}$ was measured mostly for Na–Ca amphiboles at P = 1–2 GPa, T = 1000–1100 °C, and varies a little (0.09–0.19; Adam and Green 2006; Brenan et al. 1998a, b; LaTourette et al. 1995). Naturally occurring compositions of Amp are broadly variable and hence partition coefficients may vary strongly between different amphiboles. The occupation of various cations on the different sites in Amp is well illustrated by Onuma diagrams (e.g., Fig. 7 in Brenan et al. 1998a, b; Fig. 3 in Adam and Green 2006). Similar to micas, alkali elements prefer the large A site in amphiboles, but, apparently, Li tends to substitute into the smaller B site. This may be the reason for the poorer fit of the monovalent series in Fig. 4.1b compared to Cpx or Pl. More details related to the crystal chemistry of Li-bearing amphiboles can be found in Hawthorne et al. (1992, 1993, 1994, 1996a, 1996b), Oberti et al. (2003), and Ottolini et al. (2009).

Apatite (Ap). In three experiments $K_{p(\mathrm{Li})}^{Ap-Melt}$ was in the range of 0.027–0.084 (LA-ICP-MS), measured by Klemme and Dalpe (2003) for carbonatite melts at 1250 °C and 1 GPa.

Leucite (Lct). In a single experiment performed by Wood and Trigila (2001) at 200 MPa and 1070 °C, leucite was formed and $K_{p(\mathrm{Li})}^{Lct-Melt}$ = 0.032 was obtained.

Melilite (Mll) and Spinel (Spl). A handful of mineral–melt partitioning experiments were performed by Lundstrom et al. (2006), motivated by studying the trace element distribution in Ca–Al-rich inclusions (CAIs) in chondrites. They measured melilite–melt and spinel–melt partition coefficients at atmospheric pressures and the final T between 1200 and 1225 °C. Melilite consisted of a solid solution between åkermanite (*Ak*, $Ca_2MgSi_2O_7$) and gehlenite (*Gh*, $Ca_2Al_2SiO_7$) with *Ak* contents of 38–44 mol% and reported $K_{p(\mathrm{Li})}^{Mll/Melt}$ are 0.48–0.62. Two measurements of $K_{p(\mathrm{Li})}^{Spl/Melt}$ for pure $MgAl_2O_4$ spinel were

performed by Lundstrom et al. (2006), 0.1 and 0.184, respectively, and in one experiment of Elkins et al. (2008) for (Fe, Mg)Al_2O_4 spinel $K_{p(\mathrm{Li})}^{Spl/Melt} = 0.1$ at 1420 °C and 2.5 GPa (Table 4.1).

4.2.4 Mineral-Fluid Partitioning and Associated Stable Isotopic Fractionation

Experimental methods. In Table 4.2 the experimental studies where Li partitioning between a mineral and an aqueous fluid, $K_{p(\mathrm{Li})}^{Min/Fluid}$, and $\Delta^7\mathrm{Li}_{Min/Fluid} = \delta^7\mathrm{Li}_{Min} - \delta^7\mathrm{Li}_{Fluid}$ were measured are listed, including details on the experimental conditions as well as the analytical and experimental method used. These experiments can be broadly categorized based on the starting material used: (i) gels or mixtures of solid phases (oxides, hydroxides, etc.) of which the stable phase, the mineral of interest, is supposed to form directly at the given experimental condition; (ii) mineral of interest and a reactive fluid that are supposed to form the stable mineral composition by complete replacement of the initial crystals; (iii) mineral of interest and a less reactive fluid, where trace element equilibrium is supposed to be reached by exchange with the fluid and solid-state diffusion. Ideally, to ensure that thermodynamic equilibrium has been attained reversal experiments are required. In a reversal experiment the equilibrium distribution of the two Li isotopes is achieved from opposite directions in terms of the starting compositions of mineral and fluid. In only a very few of the experimental studies presented below a reversal approach was applied (e.g., a part of the experiments in Caciagli et al. 2011). Attainment of thermodynamic equilibrium becomes usually more problematic at lower temperatures. The type of starting material (i), (ii) or (iii) can be also considered as three end-member mechanisms to reach equilibrium since in any real experiment a combination of these three end-member mechanisms occurs but to different degrees, which not only depends on the starting materials but also (mainly) on the temperature as a fundamental parameter to control the efficiency of the different kinetic processes.

Aside from the problem of reaching equilibrium an additional complication is the analysis of the fluid composition. In several studies the composition of the fluid was not directly measured after annealing but inferred from mass balance using the modal abundance and chemistry of the minerals produced and the initial fluid composition (e.g., Brenan et al. 1998b; Martin et al. 2011; Caciagli et al. 2011; Decarreau et al. 2012). With a large water/mineral ratio, the fluid composition for incompatible elements typically underwent no significant change. Lithium isotopic data were mostly collected from bulk analysis of the product minerals using various chemical procedures (Teng et al. 2004; Wunder et al. 2006, 2007, Vigier et al. 2008). A fundamental issue of experiments with fluids is that some solid material may precipitate from the fluid during the quenching of the sample. The quench products are difficult to identify and separate completely from the mineral of interest, and therefore could affect the measured partition coefficient. Furthermore, the composition of remaining fluid is not representative of the P, T conditions of the experiment. To overcome these issues, a more sophisticated approach was applied by Kessel et al. (2005) to measure the partition coefficients of trace elements between clinopyroxene, garnet, aqueous fluid, hydrous melt and supercritical liquid. They performed the partitioning experiments in a 'rocking' multi-anvil apparatus to homogenize the liquids (Schmidt and Ulmer 2004). To measure the liquid composition after the experiment the capsule and hence the liquid was frozen and directly analyzed in a special setup for LA-ICP-MS (the diamond-trap method; Kessel et al. 2004).

Experimental data for $K_{p(\mathrm{Li})}^{Min/Fluid}$ were measured for amphibole, carbonate, epidote (zoisite), olivine, pyroxene, quartz, serpentine and staurolite. For these minerals, $K_{p(\mathrm{Li})}^{Min/Fluid}$ covers a large range of 0.0004–152. High $K_{p(\mathrm{Li})}^{Min/Fluid} > 1$ were

Table 4.2 Published partitioning coefficients of Li between minerals and fluids including experimental and analytical methods

Reference	Mineral/mineral group	# data points	K_D(Li)	Δ_7Li	P (MPa)	T (°C)	w/r	Exp. setup	Solid			Fluid		Experiment type (see text)
									Starting material	Anal. method	Type of analysis	Starting material	Anal. method	
Brenan et al. (1998a, b)	Cpx	4	0.09–0.25	–	2000	900	50	PC	Natural diospide + silica + albite	SIMS	In-situ	Water or one experiment with 0.5 M NaCl	MB	(ii)
Brenan et al. (1998a, b)	Grt	1	0.0083	–	2000	900		PC	Pyrope almandine garnet	SIMS	In-situ	Pure H_2O	MB	(ii)
Caciagli et al. (2011)	Cpx	7	0.07–0.25	–	1000, 200	800–1100	4–6	PC, CSHV	DD + SiO_2 ± SCO	SIMS	In-situ	H_2O + Li_2CO_3	MB	(ii)
Caciagli et al. (2011)	Cpx	6	–	0 to −3	1000	900–1000	4–6	PC	DD + SiO_2 ± SCO	MC-ICP-MS	Bulk	H_2O + Li_2CO_3	MB	(ii) rev.
Caciagli et al. (2011)	Ol	6	0.17–1.34	–	1000	800–1100	4–6	PC	SCO + SiO_2 ± SCO ± Al_2O_3	SIMS	In-situ	H_2O + Li_2CO_3	MB	(ii)
Caciagli et al. (2011)	Pl	9	0.09–0.3	–	1000	800–1100	4–6	PC	CBB ± SiO_2 ± Al_2O_3 ± Ab	SIMS	In-situ	H_2O + Li_2CO_3	MB	(ii)
Caciagli et al. (2011)	Opx	1	0.02	–	1000	1000	4–6	PC	DD + SCO	SIMS	In-situ	H_2O + Li_2CO_3	MB	(ii)
Decarreau et al. (2012)	Sme	18	0.67–22	–	sat.	75–150	150	TB, C	$Si_4Mg_3O_{11}$; nH_2O (gel) + LiCl	AAS	Bulk	H_2O	AAS	(ii)
Marriott et al. (2004a)	Cal	7	–	−7.6 to −10.1	atm	5–30	40	TP	Cal seed	MC-ICP-MS	Bulk	Syn. Seawater	NA	(i)
Marriott et al. (2004b)	Cal	5	–	−1.9 to −3.1	atm	25	100	TP	Cal seed	MC-ICP-MS	Bulk	Syn. Seawater	NA	(i)
Marriott et al. (2004b)	Arg	5	–	−10.9 to −12	atm	25	100	TP	Cal seed	MC-ICP-MS	Bulk	Syn. Seawater	NA	(i)
Williams and Hervig (2005)	Sme-Ilt	9	0.1	−0.2 to −11.6	100	300	1	CSHV	SWy-1 sme	SIMS	Bulk	DDI + LiOH	MC-ICP-MS	(ii)
Kessel et al. (2005)	Cpx	2	2	–	6	800–1000	0.2	MA	Basalt powder	LA-ICP-MS	In-situ	H_2O	LA-ICP-MS	(ii)
Kessel et al. (2005)	Grt	7	0.13–0.52	–	4,6	700–1200	0.2	MA	Basalt powder	LA-ICP-MS	In-situ	H_2O	LA-ICP-MS	(ii)
Berger et al. (1988)	Chl	12	0.1–2	–	sat.	50–260	2–50	PPV	Silicate glass	Flame spectrometry	Bulk	H_2O	Flame spectrometry	(ii)

(continued)

Table 4.2 (continued)

Reference	Mineral/mineral group	# data points	K_p(Li)	Δ_7Li	P (MPa)	T (°C)	w/r	Exp. setup	Solid			Fluid		Experiment type (see text)
									Starting material	Anal. method	Type of analysis	Starting material	Anal. method	
Berger et al. (1988)	Sme	14	1.6–15	–	sat.	50–260	2–50	PPV	Silicate glass	Flame spectrometry	Bulk	H_2O	Flame spectrometry	(ii)
Berger et al. (1988)	Zeo	8	3–33	–	sat.	50–260	2–50	PPV	Silicate glass	Flame spectrometry	Bulk	H_2O	Flame spectrometry	(ii)
Fabbrizio et al. (2013)	Ol	5	0.07–0.35	–	2000	900–1300	0.2	PC	Peridotite/MSH	LA-ICP-MS	In-situ	H_2O	LA-ICP-MS	(ii)
Fabbrizio et al. (2013)	Opx	3	0.18–0.48	–	2000	900–1100	0.2	PC	Peridotite/MSH	LA-ICP-MS	In-situ	H_2O	LA-ICP-MS	(ii)
Fabbrizio et al. (2013)	Cpx	2	0.25–0.72	–	2000	900–1000	0.2	PC	Peridotite/MSH	LA-ICP-MS	In-situ	H_2O	LA-ICP-MS	(ii)
Fabbrizio et al. (2013)	Amp	1	0.82	–	2000	900	0.2	PC	Peridotite/MSH	LA-ICP-MS	In-situ	H_2O	LA-ICP-MS	(ii)
Lynton et al. (2005)	Qtz	3	–	+8 to +12	50–100	500	0.5	CSHV	Nat. Msc, Qtz, Kfs, Phl	TIMS	Bulk	H_2O + 1MCl	TIMS	(iii)
Lynton et al. (2005)	Msc	3	–	+18 to +20	50–100	500	0.5	CSHV	Nat. Msc, Qtz, Kfs, Phl	TIMS	Bulk	H_2O + 1MCl	TIMS	(iii)
Martin et al. (2011)	Zo	2	0.003, 0.004	–	3000	700–850	0.5	PC	Lws-gel, Qtz	LA-ICP-MS	In-situ	MilliQ	MB	(ii)
Martin et al. (2011)	Lws	2	0.0004, 0.01	–	3000, 3500	650–700	0.5	PC	Lws-gel, Qtz	LA-ICP-MS	In-situ	MilliQ	MB	(ii)
Vigier et al. (2008)	Sme	14	–	−1.6 to −10.9	sat.	25–250	60	TB	$Si_4Mg_3O11;nH_2O$ (gel) + LiCl	AAS, QUAD-ICP-MS, MC-ICPMS	Li separates	Seawater, DDI	AAS, QUAD-ICP-MS, MC-ICPMS	(ii)
Wunder et al. (2010)	Atg	1	65	−1.1	4000	500	0.1	PC	Syn. powder	MC-ICP-MS	Bulk	H_2O	MC-ICP-MS	(ii)
Wunder et al. (2010)	Ctl	2	16, 34	+0.6, +0.9	400	400	0.1	CSHV	Syn. powder	MC-ICP-MS	Bulk	H_2O	MC-ICP-MS	(ii)
Wunder et al. (2010)	Lz	2	83, 152	−2.8, −4.1	200, 400	200–300	0.1	PC	Syn. powder	MC-ICP-MS	Bulk	H_2O	MC-ICP-MS	(ii)
Wunder et al. (2006)	Spd	12	–	−0.7 to −3.8	2000	500–900	0.1–0.2	PC	Syn. powder	MC-ICP-MS	Bulk	H_2O + LiCl, LiOH	MC-ICP-MS	(ii)
Wunder et al. (2007)	St	6	–	+1.1 to +1.6	3500	670–880	0.2	PC	Syn. powder	MC-ICP-MS	Bulk	H_2O + LiCl, LiOH	MC-ICP-MS	(ii)

(continued)

Table 4.2 (continued)

Reference	Mineral/mineral group	# data points	K_p(Li)	Δ_7Li	P (MPa)	T (°C)	w/r	Exp. setup	Solid			Fluid		Experiment type (see text)
									Starting material	Anal. method	Type of analysis	Starting material	Anal. method	
Wunder et al. (2007)	Lpd	16	–	−1.5 to −5.3	2000	350–500	0.1	PC	Syn. powder	MC-ICP-MS	Bulk	H_2O + LiCl, LiOH	MC-ICP-MS	(ii)
Wunder et al. (2011)	Spd	3	–	−1.9 to −3.5	1000–8000	500–625	0.2	PC	Syn. powder	MC-ICP-MS	Bulk	H_2O + LiCl, LiOH	MC-ICP-MS	(ii)
Wunder et al. (2011)	Amp	1	–	−1.7	2000	700	0.2	PC	Syn. powder	MC-ICP-MS	Bulk	H_2O + LiCl, LiOH	MC-ICP-MS	(ii)

CBB Crystal Bay bytownite, *DD* Dekalb diopside, *DDI* Distilled deionized water, *SCO* San Carlos olivine, *C* sealed container, *CSHV* cold seal hydrothermal vessel, *MA* multi-anvil press, *PC* piston cylinder press, *PPV* Prolabo pressure vessel, *TB*teflon bomb, *TP* setup of Tesoriero and Pankow (1996), *sat.* saturated water vapor pressure, *AAS* Atomic absorption spectrometry, *LA-ICP-MS* Laser ablation inductively coupled plasma mass spectrometry, *MB* Mass balance, *NA* Not analyzed, *SIMS* Secondary ion mass spectrometry, *TIMS* Thermal ionization mass spectrometry

measured exclusively for hydrous minerals, like smectite, serpentine and zeolite, which are typical products of aqueous alteration. For pyroxene, amphibole and olivine, $K_{p(\mathrm{Li})}^{Min/Fluid}$ is rather similar to $K_{p(\mathrm{Li})}^{Min/Melt}$ when applied to a similar major element chemistry. Below, the data are discussed in more detail separately for each mineral or mineral group.

Clinopyroxene (Cpx). $K_{p(\mathrm{Li})}^{Cpx/Fluid} = 0.07-2.02$ was measured by Brenan et al. (1998a, b), Kessel et al. (2005), Caciagli et al. (2011), and Fabbrizio et al. (2013) for T = 800–1100 °C and P = 1–6 GPa. Similar to $K_{p(\mathrm{Li})}^{Cpx/Melt}$ the large variability of $K_{p(\mathrm{Li})}^{Cpx/Fluid}$ is most likely related to the variability in major element chemistry as will be discussed below.

Brenan et al. (1998b) measured $K_{p(\mathrm{Li})}^{Cpx/Fluid} = 0.09-0.25$ at P = 2 GPa and T = 900 °C where Cpx consisted mainly of the *Di* component. A slight zoning of Al in Cpx was observed, which was interpreted as growth zoning due to the large compatibility of Al. They found a strong correlation of the Li content with Al, which was associated with a dependence of $K_{p(\mathrm{Li})}^{Cpx/Fluid}$ on the Al content in Cpx. This observation indicates a coupled substitution for Li to form the neutral component $LiAlSi_2O_6$ in Cpx as was also inferred in Sect. 4.2.3 from $K_{p(\mathrm{Li})}^{Cpx/Melt}$. In one experiment 0.5 molal NaCl was added to the fluid, but no effect was apparent for $K_{p(\mathrm{Li})}^{Cpx/Fluid}$.

Caciagli et al. (2011) measured $K_{p(\mathrm{Li})}^{Cpx/Fluid} = 0.07-0.3$ at T = 800–1100 °C and P = 1 GPa, where similar to Brenan et al. (1998a, b) the Cpx consisted of 95–100 % *Di*.

In Kessel et al. (2005) only bulk rock–liquid partition coefficients but no mineral–liquid coefficients were reported. We have calculated $K_{p(\mathrm{Li})}^{Cpx/Liquid}$ (as well as $K_{p(\mathrm{Li})}^{Grt/Liquid}$, see below) from the information given in the electronic appendix of their paper. The experiments were performed at P = 4 and 6 GPa, T = 700–1200 °C, which produced an aqueous fluid, a hydrous silicate melt or a supercritical liquid. A main result of Kessel et al. (2005) was that Li and most trace elements (except heavy REE, Y and Sc) become incompatible in the bulk solid material when a supercritical liquid is stabilized at 6 GPa and $T \geq 800$ °C. For Li this result is partly related to the decreasing modal abundance of Cpx in their experiments at these conditions. The modal abundance of Cpx relative to Grt is of particular importance for Li, since $K_{p(\mathrm{Li})}^{Cpx/Liquid} > 1$ at any of experimental conditions applied by Kessel et al. (2005). In fact, $K_{p(\mathrm{Li})}^{Cpx/Supercritical}$ = 1.98–2.02 at 6 GPa and T = 800 and 1000 °C, respectively, whereas $K_{p(\mathrm{Li})}^{Cpx/Melt}$ = 1.17 at 4 GPa and 1000 °C at conditions where the silicate melt is stable. These high values of $K_{p(\mathrm{Li})}^{Cpx/Liquid}$ at 6 GPa are higher than most of $K_{p(\mathrm{Li})}^{Cpx/Melt}$ measured in the pressure range 3–7 GPa (Sect. 4.2.3). However, as illustrated in Fig. 4.3, $K_{p(\mathrm{Li})}^{Cpx/Melt}$ is strongly correlated to the *Jd* content. The mineral composition of the Cpx and Grt was not given by Kessel et al. (2005), but as the starting composition was an average MORB composition with 3.2 wt% Na_2O, and Grt and Cpx were the only major minerals formed, it is obvious that Cpx contained a significant portion of *Jd*. The corresponding increase of Al on the M site makes the formation of $LiAlSi_2O_6$ more likely.

Fabbrizio et al. (2013) performed experiments with and without the diamond trap method to measure $K_{p(\mathrm{Li})}^{Min/Fluid} = 0.72$ at 2 GPa and T = 900 °C. The starting material consisted of a peridotite or a synthetic $Mg(OH)_2$–SiO_2 mixture both doped with TiO_2, NaCl, and/or CaF_2. The main aim of the study of Fabbrizio et al. (2013) was to investigate the partitioning of halogens into upper mantle minerals; in general, these authors found strong fractionations between Amp, Ol, Cpx, and Opx for trace elements but $K_{p(\mathrm{Li})}^{Min/Fluid}$ was relatively similar for all these phases. For example, in their experiment at 900 °C where all these phases coexisted, $K_{p(\mathrm{Li})}^{Min/Fluid}$ varied only between 0.35 ($K_{p(\mathrm{Li})}^{Ol/Fluid}$) to 0.82 ($K_{p(\mathrm{Li})}^{Amp/Fluid}$) (see also Sect. 4.2.5).

Garnet (Grt). $K_{p(\mathrm{Li})}^{Grt/Fluid} = 0.0083$ was measured by Brenan et al. (1998b) at T = 900 °C and P = 2 GPa and $K_{p(\mathrm{Li})}^{Grt/Fluid} = 0.12-0.52$ by Kessel et al. (2005) at T = 700–900 °C and P = 4 GPa. As discussed before for $K_{p(\mathrm{Li})}^{Grt/Melt}$, the *Maj* component may be of relevance here, which generally increases with increasing P (see also Hanrahan et al. 2009 and discussion below in Sect. 4.2.5). However, Kessel et al. (2005) report no major element data and Grt composition is thus largely unknown.

Olivine (Ol). $K_{p(\mathrm{Li})}^{Ol/Fluid} = 0.14-1.34$ was measured by Caciagli et al. (2011) and Fabbrizio et al. (2013). In both studies very *Fo* rich olivine was produced with Mg# = 97–100 and both data sets show a consistent change of $K_{p(\mathrm{Li})}^{Ol/Fluid}$ with T (at P = 1 and 2 GPa, respectively). Whether this trend relates to the dependence on T related to increasing solute content in the fluid with T (see Fig. 4 in Fabbrizio et al. 2013 and related discussion) or to the detailed olivine chemistry is unclear. Caciagli et al. (2011) parameterized this dependence on T, as follows: $\ln K_{p(\mathrm{Li})}^{Ol/Fluid} = -6.0(\pm 2) + 6.5(\pm 2) \times 1000/T$.

Plagioclase (Pl). $K_{p(\mathrm{Li})}^{Pl/Fluid} = 0.09-0.30$ for *An* rich plagioclase (91–99 % *An*) was measured by Caciagli et al. (2011) at T = 800–1000 °C and P = 1 GPa. A very strong apparent effect of *An* was observed that can be parameterized by the following relationship in kJ/mol (cf. with Eq. 4.2.11):

$$RT\ln K_{p(\mathrm{Li})}^{Ol/Fluid} = 162-188 \cdot X_{An} \qquad (4.2.14)$$

This dependence cannot reflect the explicit effect of *An* according to Dohmen and Blundy (2014). Even when compared to the study of Coogan (2011) this effect is much greater (−188 vs. −70 kJ/mol, see also discussion in Sect. 4.2.5). The variation of the chemical potential of the Li component in plagioclase is controversial and the presence of some amounts of interstitial Li (as indicated for other silicates, Sect. 4.3) may be an explanation.

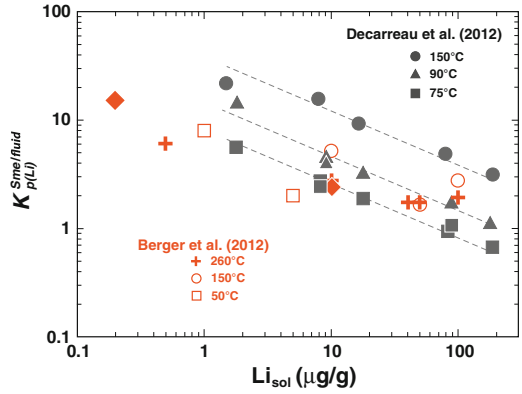

Fig. 4.4 Measured $K_{p(\mathrm{Li})}^{Sme/Fluid}$ plotted against Li in solution for different temperatures as indicated in the figure. The *dashed lines* are linear regressions of data from Decarreau et al. (2012) for each temperature assuming a fixed slope of −1/2. Note that $K_{p(\mathrm{Li})}^{Sme/Fluid}$ of Berger et al. (1988) also depends on the Li content of the solution but follow a different and less systematic trend for each temperature

Smectites (Sme). Decarreau et al. (2012) and Berger et al. (1988) measured $K_{p(\mathrm{Li})}^{Sme/Fluid}$ = 0.67–22 in the temperature range between 50 and 260 °C (Fig. 4.4). In both studies a systematic change of $K_{p(\mathrm{Li})}^{Sme/Fluid}$ with the Li concentration in the solution was observed (Fig. 4.4), but Berger et al. (1988) reported only average values at a given T. Decarreau et al. (2012) measured $K_{p(\mathrm{Li})}^{Sme/Fluid}$ for hectorite, a Mg–Li smectite with the formula $(Mg_{3-x}Li_x)_5[Si_4O_{10}](OH)_2M_x^{exch}$ (M_x^{exch} stands for exchangeable cations on the interlayer site, mainly Na), by synthesis from a gel at 75–150 °C and equilibrium water pressure. The Li concentration in hectorite increased with time until a stable concentration was reached, which was interpreted to represent thermodynamic equilibrium. $K_{p(\mathrm{Li})}^{Sme/Fluid}$ decreased systematically with increasing Li content in the solution, which was explained by the heterovalent exchange of Mg^{2+} with Li^+ charge balanced by Na^+ on the exchangeable interlayer site. Based on the mass action law of this exchange reaction, Decarreau et al. (2012) derived the following relation:

$$\left(C_{\mathrm{Li}}^{Sme}\right)^2 \sim \left(C_{\mathrm{Mg}}^{Sme} C_{\mathrm{Na}}^{Fluid} / C_{\mathrm{Mg}}^{Fluid}\right) \cdot C_{\mathrm{Li}}^{Fluid} \tag{4.2.15}$$

After dividing the above relation by the square of C_{Li}^{Fluid} and using the definition of $K_{p(\mathrm{Li})}^{Sme/Fluid}$ according to Eq. 4.2.1, we obtain a similar relationship for the Li partition coefficient:

$$K_{p(\mathrm{Li})}^{Sme/Fluid} \sim \sqrt{\left(C_{\mathrm{Mg}}^{Sme} C_{\mathrm{Na}}^{Fluid} / C_{\mathrm{Mg}}^{Fluid}\right)} \cdot \frac{1}{\sqrt{C_{\mathrm{Li}}^{Fluid}}} \tag{4.2.16}$$

In the experiments of Decarreau et al. (2012) the factor on the left side of equation was relatively constant, which can thus explain the constant slope of −1/2 in Fig. 4.4.

Berger et al. (1988) reported an average value of 2.4–1.9 between 50 and 260 °C, respectively. Consistent with the study of Decarreau et al. (2012), $K_{p(\mathrm{Li})}^{Sme/Fluid}$ increases with decreasing Li content of the solution (Fig. 4.4). The discrepancy between the data of Decarreau et al. (2012) and Berger et al. (1988) can be explained according to Eq. 4.2.16 by variable major element chemistry of smectite and solution with Li content as given in Table III in Berger et al. (1988).

Based on Fig. 4.4 we can conclude that for typical seawater compositions or hydrothermal vent fluids with Li concentrations in the range of 0.1–1.0 mg/L, $K_{p(\mathrm{Li})}^{Sme/Fluid} \geq 10$; therefore, smectite can represent a major sink for Li during formation by aqueous alteration (see also Sect. 4.4).

Amphibole (Amp). $K_{p(\mathrm{Li})}^{Amp/Fluid} = 0.82$ was measured at $T = 900$ °C and $P = 2$ GPa in a single experiment by Fabbrizio et al. (2013) for a NaCa-amphibole.

Lawsonite (Lws) and Zoisite (Zo). Martin et al. (2011) measured $K_{p(\mathrm{Li})}^{Zo/Fluid} \approx 0.003$ and $K_{p(\mathrm{Li})}^{Lws/Fluid} \approx 0.0004 - 0.01$ with standard deviations that are similar to the measured values and hence these values should be treated with caution. However, it seems obvious that Li is very incompatible in epidotes and structurally similar minerals like lawsonite. The only available site for Li is the large Ca site, which needs charge balance by one 4+ trace cation on the Al site, or one 5+ trace cation on the Si site.

Serpentine (Srp). Wunder et al. (2010) measured mineral fluid partitioning for three different serpentines, chrysotile (Ctl) (at 0.4 GPa, 400 °C), antigorite (Atg) (at 4 GPa, 500 °C) and lizardite (Lz) (at 0.2 GPa, 200–300 °C) and found that Li is generally very compatible in serpentines with

$$K_{p(\mathrm{Li})}^{Ctl/Fluid} = 16-34 < K_{p(\mathrm{Li})}^{Atg/Fluid} = 65 < K_{p(\mathrm{Li})}^{Lz/Fluid} = 83-152$$

Carbonate (Cb). In study of Mariott et al. (2004a, b) calcite and aragonite were precipitated inorganically from continuous influx of carbonate-saturated fluid that was doped with Li at T = 5–30 °C. They determined the exchange partition coefficient (or distribution coefficient) of Li with Ca, $K_{p(\mathrm{Li-Ca})}^{Cb/Fluid} = K_{p(\mathrm{Li})}^{Cal/Fluid} / K_{p(Ca)}^{Cal/Fluid}$ but $K_{p(\mathrm{Li})}^{Cal/Fluid}$ values were not reported separately. Since the Ca content in the solution and in the carbonates were effectively constant in these experiments $K_{p(\mathrm{Li-Ca})}^{Cb/Fluid}$ also gives an indirect inference on the behavior of $K_{p(\mathrm{Li})}^{Cal/Fluid}$. In Marriott et al. (2004a) $K_{p(\mathrm{Li-Ca})}^{Cb/Fluid}$ was shown to depend exponentially on T, decreasing by a factor of about three with T increasing from 5 to 30 °C, and therefore the Li/Ca ratio in carbonate was suggested as a thermometer. However, the Li/Ca ratio is also sensitive to the salinity. Marriot et al. (2004b) revealed that $K_{p(\mathrm{Li-Ca})}^{Cb/Fluid}$ for calcite increases by a factor of four as salinity increases from 10 to 50 ‰. Inorganic aragonite demonstrates no significant change in $K_{p(\mathrm{Li-Ca})}^{Cb/Fluid}$ over the same salinity range (Marriott et al. 2004b). The different behaviour for aragonite and calcite was explained by the different incorporation

mechanism of Li. Substitution of Li^+ in the Ca^{2+} site in aragonite makes the Li/Ca of growth-solution the key variable, while interstitial incorporation of Li^+ in calcite means that the Li concentration of growth-solution is more important. Based on the comparison of the experimental results and Li/Ca ratios of biogenically produced carbonates, Marriott et al. (2004b) argue that there is little biological control during Li incorporation into calcium carbonates.

Zeolite (Zeo) and Chlorite (Chl). Berger et al. (1988) measured $K_{p(\mathrm{Li})}^{Zeo/Fluid} = 3.5-33$ and $K_{p(\mathrm{Li})}^{Chl/Fluid} = 0.35-1.7$ at T = 50–260 °C. For both minerals $K_{p(\mathrm{Li})}^{Min/Fluid}$ show a pronounced increase with decreasing T, which is opposite to the trend observed usually for partition coefficients. Berger et al. (1988) argued that these partition coefficients do not reflect true equilibrium partition coefficients (also $K_{p(\mathrm{Li})}^{Sme/Fluid}$, see above) at these conditions but rather effective partition coefficients that would be relevant for alteration processes at low temperatures.

Theoretical constraints for equilibrium fractionation of Li isotopes. Equilibrium fractionation of stable isotopes is a quantum-mechanical effect and is related to the dependence of the vibrational modes of atoms in a phase on their mass (Urey 1947; Schauble 2004). In general a harmonic oscillator serves as a model to explain this dependence for atoms in crystals, which predicts for most cases that heavy ions concentrate in solids compared to gas/fluids/melts due to the stronger bonding of elements within the crystalline structure. The isotopic fractionation between two phases α and β defined for Li as $\Delta^7Li_{\alpha/\beta} = \delta^7Li_\alpha - \delta^7Li_\beta$ is in general strongly temperature dependent. Based on thermodynamic constraints, Bottinga and Javoy (1973) have shown that for a limited temperature interval the temperature dependence can be expressed as $\Delta^7Li_{\alpha/\beta} = A + B/T^2$, where A and B are material specific constants reflecting the magnitude of isotopic fractionation.

The coordination as well as the bond distance of an element have been used to infer the fractionation of stable isotopes between two phases. For example, the lower coordination of Li in fluid (approximately fourfold) than in many crystal structures (mostly 6–8 fold) is responsible for the preference of light Li in most minerals compared to the fluid (e.g., Wunder et al. 2006). Theoretical calculations of Jahn and Wunder (2009) have also shown that at high fluid densities the fractionation behavior may be reversed and ^6Li preferentially partitions into the fluid compared to minerals where Li is fourfold coordinated (e.g., staurolite). If fluid densities increase above 1.2 g/cm^3, the proportion of fivefold and sixfold coordinated Li is larger than those of threefold and fourfold, and hence the average coordination in the fluid is greater than 4.5. In a subsequent theoretical study Wunder et al. (2011) (e.g., see their Fig. 4.3) have shown that coordination is a good proxy for the magnitude of fractionation but the mean Li–O bond distance is an even better parameter to estimate mineral–fluid fractionation of Li isotopes (and potentially other isotopes). Equilibrium fractionation of Li isotopes was calculated for staurolite, mica, and spodumene by Kowalski and Jahn (2011) using an ab initio approach. The predicted values for $\Delta^7Li_{Min/Fluid}$ agreed with the experimental values to within ±1.0 ‰ where, in general, the theoretical values were higher. The theoretical values were corrected by considering the thermal expansion of the crystals and compression of the fluid, which lowered the theoretical values for $\Delta^7Li_{Min/Fluid}$ and lead to an even better agreement with the experimental data.

Fractionation of Li isotopes due to partitioning between minerals and fluid, $\Delta^7Li_{Min/Fluid}$, was measured for amphibole, carbonate, clinopyroxene, mica, quartz, serpentine, staurolite and clay minerals (illite/smectite); most of these data are shown in Fig. 4.5. In general, each data set follows the theoretically expected linear trend when $\Delta^7Li_{Min/Fluid}$ is plotted against $1/T^2$, and the slopes appear almost parallel. Within the experimental T range each data set could be also fitted assuming a reciprocal T dependence as illustrated in Fig. 4.5 for the data from spodumene by Wunder et al. (2011). Exceptions are the scarce data for T < 100 °C of smectite and

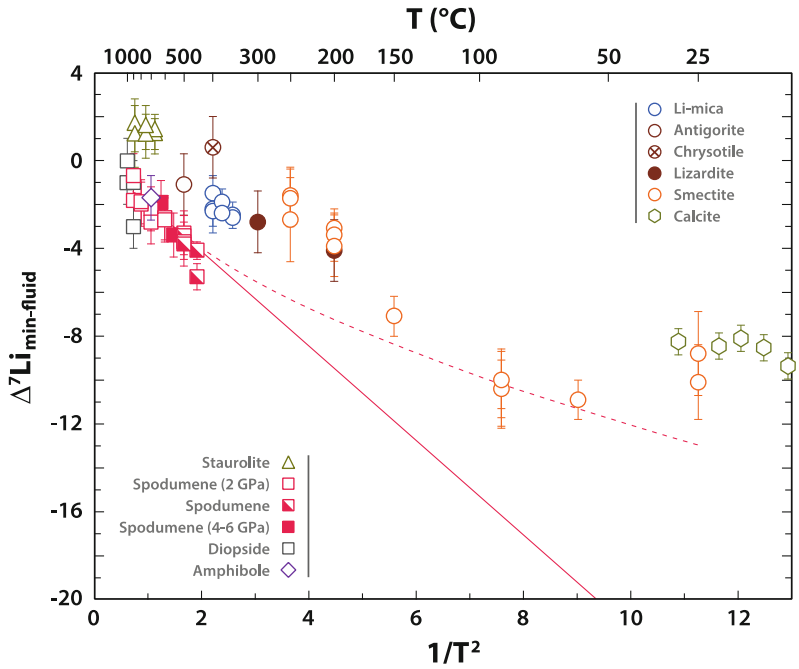

Fig. 4.5 $\Delta^7Li_{Min/Fluid}$ versus $1/T^2$ for various minerals. Note that for T < 100 °C the observed isotope fractionation seems to be relatively constant for smectite and calcite, inconsistent with the strong temperature effects observed at higher temperatures following the theoretically expected relationship. The *solid line* is a linear regression of the data for spodumene, the *dashed line* is a regression assuming $\Delta^7Li_{Min/Fluid}$ is proportional to $1/T$. within the experimental T range both regressions can reproduce the data within the error. References: staurolite + Li-mica, Wunder et al. (2007), spodumene, Wunder et al. (2006, 2011), diopside, Caciagli et al. (2011), amphibole, Wunder et al. (2011), smectite, Vigier et al. (2008), calcite, Marriott et al. (2004a), chrysotile + lizardite + antigorite, Wunder et al. (2010)

calcite, which do not show any significant dependence on T. This feature might indicate disequilibrium in the respective experiments, because of slower reaction rates at these low temperatures. Marriott et al. (2004a) discussed possible kinetic effects on δ^7Li for the precipitation of calcite. Coralline aragonite also does not show a strong effect of T on δ^7Li. If it is related to kinetic effects, the observed δ^7Li in carbonates should be a function of the precipitation rate and hence oversaturation.

In a second set of experiments, Marriott et al. (2004b) precipitated calcite and aragonite at 25 °C with δ^7Li of around −3 and −12 ‰, respectively, showing that ^{6}Li prefers aragonite compared to calcite. The growth rates of calcites in experiments of Marriott et al. (2004a, b) were not directly given but after the similar time (about 5 h) twice as much calcite was grown in the experiments of Marriott et al. (2004b) compared to those of Marriott et al. (2004a). Thus the faster precipitation rate (Marriott et al. 2004b) may be responsible for the smaller fractionation observed. If the growth rate is very fast, trace elements and their isotopic concentrations cannot re-equilibrate with the fluid during growth but are "randomly" incorporated into the mineral structure.

In most minerals ^{6}Li is preferred compared to the fluid. Exceptions are staurolite and chrysotile. The Li–O bond distance, roughly characterized by the coordination of Li, in the respective crystallographic site relative to those in the fluid is the critical parameter which controls the fractionation of the Li isotopes (Wunder et al. 2011). Therefore the preference of ^{7}Li over ^{6}Li in staurolite compared to the fluid was explained by the fourfold coordination in Wunder et al. (2007)

and this behavior was confirmed by theoretical calculations of Kowalski and Jahn (2011). For chrysotile the positive $\Delta^7Li_{Ctl/Fluid}$ was explained by the presence of Li in nano-tubes in their crystallographic structure. For the different types of serpentine Wunder et al. (2010) observed the sequence $\Delta^7Li_{Ctl/Fluid}$ = 0.6–0.9 ‰ > $\Delta^7Li_{Atg/Fluid}$ = −1.1 ‰ > $\Delta^7Li_{Lz/Fluid}$ = −2.8 to −4.1 ‰.

Additional data not shown in Fig. 4.5 are those of Lynton et al. (2005) who observed $\Delta^7Li_{Qtz/Fluid}$ = 8–12 ‰ and $\Delta^7Li_{Ms/Fluid}$ = 18–20 ‰ at 500 °C and 50–100 MPa. The enrichment of ^{7}Li relative to fluid in Qtz and Ms is in contradiction to Wunder et al. (2007) and what would be expected from theoretical constraints based on the Li–O bond distance (Wunder et al. 2011; Kowalski and Jahn 2011). Lynton et al. (2005) used a different experimental strategy: natural minerals were exposed to a Li-rich fluid and did not equilibrate with the fluid by reaction and re-crystallization but by solid-state diffusion of Li into the Qtz and Ms. The ^{6}Li and total Li content in the solid changed, with an overall slight increase of total Li and decrease of δ^7Li after run durations of 15 or 30 days at 500 °C. Whether thermodynamic equilibrium was reached in this study is unclear and Wunder et al. (2007) speculated that diffusive fractionation contributed to the observed fractionation. However, as is illustrated in Sect. 4.3, diffusion of Li into a mineral should produce a negative anomaly for δ^7Li since the ^{6}Li diffuses slightly faster than ^{7}Li. Therefore the origin of the positive values for $\Delta^7Li_{Ms/Fluid}$ remains unclear. For quartz it should also be considered that Li occupies interstitial positions in channels parallel to the c axis, and its presence has been shown to correlate with that of Al, suggesting a coupled substitution of Li + Al^{3+} with Si^{4+} (Dennen 1966; Perny et al. 1992).

One data point measured at 300 °C plots off the general trend for other micas. Wunder et al. (2007) speculated about disequilibrium at these low T conditions and surface energy effects related to the small grain size of the mica. Bulk analytical data are clearly more affected by adsorbed Li if the surface area/volume ratio is large. The contribution of adsorbed Li on mineral surfaces to the bulk δ^7Li was investigated by Williams and Hervig (2005), who measured re-partitioning of Li isotopes during reaction from smectite to illite. It was speculated that the isotopic signature of Li in the exchangeable interlayer site would be similar to the isotopically heavy waters, whereas the octahedrally coordinated Li is light. Partitioning experiments of Decarreau et al. (2012) do not indicate a significant amount of Li present in the interlayer site. In addition, according to Pistiner and Henderson (2003) surface sorption does not induce isotopic fractionation between smectite and fluid. In the study of Williams and Hervig (2005) Li content and δ^7Li increased with decreasing average grain size, which most likely shows the effect of adsorbed Li, since with decreasing grain size the contribution of surficially adsorbed elements to the bulk increases.

4.2.5 Inter-mineral Partitioning

Inter-mineral partitioning of Li may be relevant for closed system processes where intensive parameters like P and T change during cooling and decompression of the rocks. For example, it has been suggested that Li in mantle xenoliths was redistributed between Ol and Cpx during cooling such that Li leaves Ol and enters Cpx, leading to significant diffusive isotopic fractionation (Jeffcoate et al. 2007). The temperature dependence of Li partitioning between minerals and the resulting diffusive exchange during cooling can be used to constrain the respective rate. For example, Coogan et al. (2005) used the re-distribution of Li between Pl and Cpx during cooling to infer the hydrothermal cooling of new upper oceanic crust. So far there are only three studies that examined the partitioning of Li between mineral phases (Coogan et al. 2005; Hanrahan et al. 2009; Yakob et al. 2012). Additional inter-mineral partitioning data for Li can be extracted from multiply saturated mineral–melt or mineral–fluid partitioning experiments assuming bulk thermodynamic equilibrium. Inter-mineral partitioning also provides clues to the relative compatibility of Li in minerals. In Fig. 4.6a an

overview of measured $K_{p(\mathrm{Li})}^{Ol/Cpx}$, $K_{p(\mathrm{Li})}^{Pl/Cpx}$, and $K_{p(\mathrm{Li})}^{Grt/Cpx}$ as a function of T at various pressures is shown. Since Cpx was the most common mineral present in the partitioning experiments, we can use it as a reference mineral here, and these partitioning coefficients provide direct information on the relative compatibility of Li in the most relevant minerals of the upper mantle and the oceanic crust. The disadvantage of using Cpx is that its major element chemistry and hence the compatibility of Li can be quite variable, as discussed before (see Sect. 4.2.3 and Fig. 4.6). Since the present data for $K_{p(\mathrm{Li})}^{Opx/Cpx}$ are close to 1 (Brenan et al. 1998a: 0.74 ± 0.21; Fabbrizio et al. 2013: 0.72 ± 0.55, 0.66 ± 0.27; Adam and Green 2006: 1.08 ± 0.24), Li seems to not partition significantly between two pyroxenes with a typical mantle chemistry. Therefore, at least for the experimental conditions investigated it can be generally concluded that Ol is the most compatible phase for Li among major mantle minerals, which is also consistent with observations in mantle xenoliths (see Chap. 5). Considering the modal abundance of olivine in mantle peridotites it is obvious that the Li budget of the upper mantle is dominated by olivine. For basalts and gabbros, Cpx is more relevant than Pl but the presence of Ol may also contribute to their bulk Li inventory. Lithium appears to become more compatible with pressure in Cpx and Grt, which is related to the respective mineral chemistry (see below). This could have consequences for the compatibility of Li in eclogite.

Next, we discuss the data shown in Fig. 4.6 separately for the three different mineral pairs, with the emphasis on the role of the thermodynamic variables on the inter-mineral partitioning data. It should be noted that in addition to P and T additional thermodynamic variables may be relevant for inter-mineral partitioning depending on the incorporation mechanism of the respective element as shown for Mg partitioning between Pl and Cpx (Faak et al. 2013, where $K_{p(\mathrm{Mg})}^{Pl/Cpx}$ depends on the activity of silica)

Ol-Cpx. Yakob et al. (2012) measured $K_{p(\mathrm{Li})}^{Ol/Cpx}$ at 1.5 GPa between 700–1100 °C using a piston cylinder apparatus and a pressure cell, which was assumed to buffer the fO_2 close to NNO. The starting mix consisted of natural Ol, Cpx, Kfs, Qtz, and a Li-solution. As run product only Cpx and Ol were found together with quench products from the fluid. The final Li concentrations in Ol and Cpx were in the range of 7–30 µg/g and most importantly it was found that $K_{p(\mathrm{Li})}^{Ol/Cpx}$ was effectively constant at 2.0 ± 0.1 and therefore independent of T. Most $K_{p(\mathrm{Li})}^{Ol/Cpx}$ values calculated from multiply saturated mineral–fluid (Caciagli et al. 2011; Fabbrizio et al. 2013) or mineral–melt partitioning experiments (Brenan et al. 1998a; Blundy and Dalton 2000; Ottolini et al. 2009) carried out at different pressures and higher temperatures are in general agreement with this result. $K_{p(\mathrm{Li})}^{Ol/Cpx}$ measured at higher temperatures by Brenan et al. (1998a) and Blundy and Dalton (2000) are slightly lower at about 1.3. The recent data of Fabbrizio et al. (2013) and Caciagli et al. (2011) for $K_{p(\mathrm{Li})}^{Ol/Cpx}$ are significantly different, varying between 0.5 and 10. Considering the discussion above on the large variability of $K_{p(\mathrm{Li})}^{Cpx/Melt}$, this minor variation within a factor of 2–5 can probably be assigned to the variable chemistry of Cpx in the different studies. In addition, for incorporation of Li into olivine, fO_2 or doping with Y_2O_3 seem to be relevant. As discussed before for $K_{p(\mathrm{Li})}^{Ol/Melt}$ and particularly trivalent cations like Fe^{3+} or Sc^{3+} (Grant and Wood 2010) are important in olivine to charge balance Li. Since the variation in the mineral chemistry of the re-crystallized Ol and Cpx in the experiments of Yakob et al. (2012) is relatively small (Cpx with X_{Di} = 0.9–0.99 and small amounts of *En* and *Mg-Ts*) and does not depend systematically on the T of the experiment, their study reflects the intrinsic dependence of the equilibrium constant for $K_{p(\mathrm{Li})}^{Ol/Cpx}$ on T. Therefore, we would not expect re-distribution of Li between Cpx and Ol during cooling and agree with the conclusion by Yakob et al. (2012) that "partitioning of Li between olivine and diopside is not temperature dependent over a

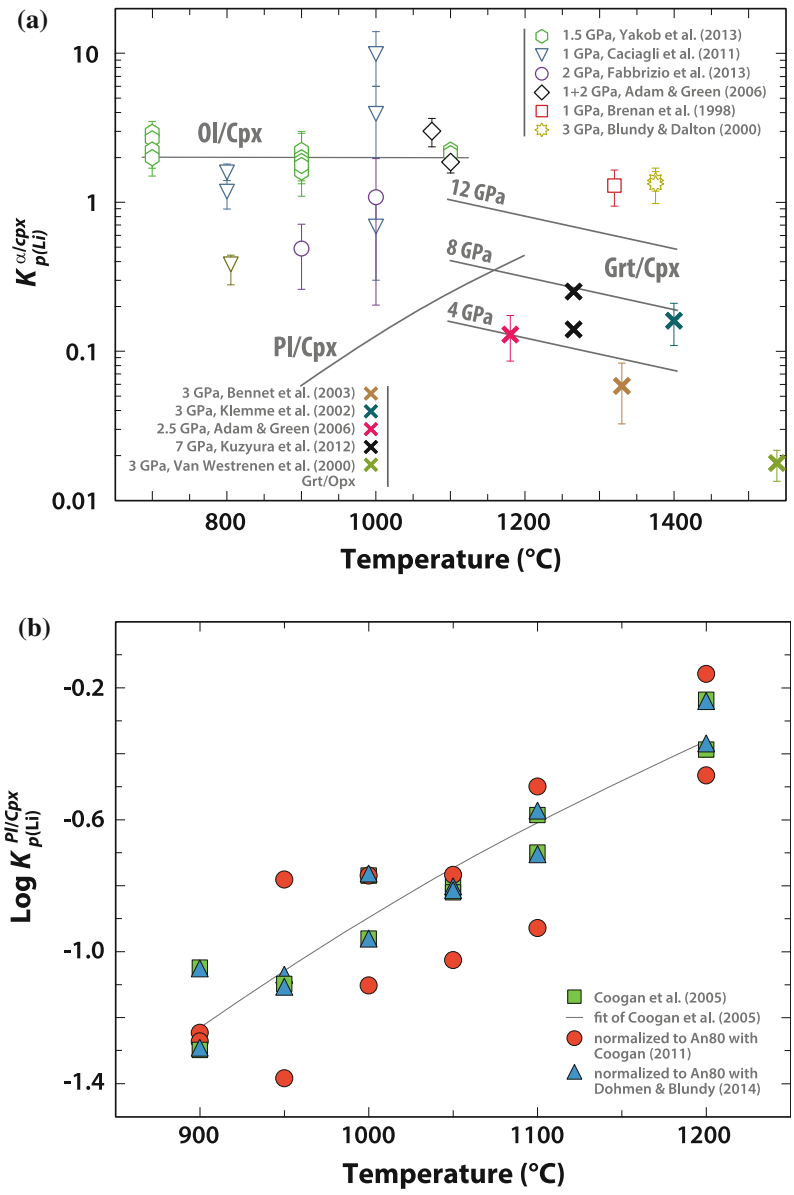

Fig. 4.6 Experimental data for inter-mineral partitioning data of Li between Ol and Cpx, Pl and Cpx, Grt and Cpx as a function of temperature and pressure. **a** *Black solid line* (Yakob et al. 2012) and *open squares* represent $K^{Ol/Cpx}_{p(\mathrm{Li})}$; *Orange solid lines* (parameterization of Hanrahan et al. 2009 for three pressures as given next to the lines) and *open triangles* represent $K^{Grt/Cpx}_{p(\mathrm{Li})}$; *Violet solid line* represents the parameterization of Coogan et al. (2005) for $K^{Pl/Cpx}_{p(\mathrm{Li})}$. The *color of the symbols* indicates the source of the data as given in the legend panel in the figure together with the experimental pressures. **b** Individual data of Coogan et al. (2005) for log $K^{Pl/Cpx}_{p(\mathrm{Li})}$ and their corrected data, considering that $K^{Pl/Cpx}_{p(\mathrm{Li})}$ depends on the anorthite content of Pl (for details of the calculations see text). The solid line is the same as shown in panel (**a**)

range of temperatures relevant to mantle and igneous processes." However, for a significantly different Cpx chemistry this conclusion may not be strictly valid. Furthermore, $K^{Ol/Cpx}_{p(\mathrm{Li})}$ **is** sensitive to detailed mineral chemistry and to infer if Li of Ol and Cpx in mantle samples reflect equilibrium at mantle conditions, this should be taken into account. Consequently, a deviation of the apparent $K^{Ol/Cpx}_{p(\mathrm{Li})}$ from about 2 in mantle samples may not necessarily indicate a re-setting of Li from mantle conditions as argued for example by Seitz and Woodland (2000).

Pl-Cpx. Coogan et al. (2005) measured $K^{Pl/Cpx}_{p(\mathrm{Li})}$ at 0.1 MPa and T = 800–1200 °C and found a significant temperature dependence, which was parameterized as follows (Fig. 4.4b): $\ln K^{Pl/Cpx}_{p(\mathrm{Li})} = 7 + \frac{-11534}{T}$.

The starting material consisted of hand-picked and pulverized Pl and Cpx from mid-ocean ridge gabbro and basalt. The composition of Cpx was

constant, given as $X_{Jd} = 0.03$, $X_{Di} + X_{Hd} = 0.775$, $X_{En} + X_{Fs} = 0.146$, $X_{CaTs} = 0.029$, $X_{TiTs} = 0.016$, and X_{An} of Pl varied between 0.72–0.91. Even for this limited range in *An*, a significant range in measured $K_{p(\mathrm{Li})}^{Pl/Cpx}$ at isothermal conditions can be expected according to Coogan (2011), where partitioning of Li between Pl with different *An* (0.6–0.9) was experimentally investigated. He predicted that $\ln K_{p(\mathrm{Li})}^{Pl/\beta} = f\left(P, T, X_\beta\right) - 6.6 \cdot X_{An}$. If this relation is correct, this dependence needs to be also considered for $\ln K_{p(\mathrm{Li})}^{Pl/Cpx}$ to obtain the explicit dependence of $K_{p(\mathrm{Li})}^{Pl/Cpx}$ on *T*. In Fig. 4.4b, the data of Coogan et al. (2005) are normalized to $X_{An} = 0.8$ using this strong dependence on *An*, but the resulting data are far less systematic compared to the uncorrected data. Alternatively, the thermodynamic model of Dohmen and Blundy (2014) could be used to constrain the effect of *An* on $K_{p(\mathrm{Li})}^{Pl/Cpx}$, which predicts that

$$\ln K_{p(\mathrm{Li})}^{Pl/\beta} = f\left(P, T, X_\beta\right) - 4.71 \frac{\mathrm{kJ}}{\mathrm{mol}} / (RT) \cdot X_{An} + 4.61 \frac{\mathrm{kJ}}{\mathrm{mol}} / (RT) \cdot X_{An}^2$$

and

$$\ln K_{p(\mathrm{Li})}^{Pl/\beta} = f\left(P, T, X_\beta\right) - 4.71 \frac{\mathrm{kJ}}{\mathrm{mol}} / (RT) \cdot X_{An} + 0.61 \frac{\mathrm{kJ}}{\mathrm{mol}} / (RT) \cdot X_{An}^2$$

for the $C\bar{1}$ and the $I\bar{1}$ stability field, respectively. Using this calibration the normalization of $K_{p(\mathrm{Li})}^{Pl/Cpx}$ to $X_{An} = 0.8$ results in a marginal change. We can therefore conclude that the experimental data of Coogan (2011) are inconsistent with the data set for $K_{p(\mathrm{Li})}^{Pl/Cpx}$ of Coogan et al. (2005), which indicates a minor effect of *An* on $K_{p(\mathrm{Li})}^{Pl/Cpx}$, more consistent with the prediction of Dohmen and Blundy (2014).

Grt-Cpx. In study of Hanrahan et al. (2009), $K_{p(\mathrm{Li})}^{Grt/Cpx}$ was measured in the synthetic MASH system. Synthetic glass was used as starting material together with variable doping of Li_3PO_4. Experiments were performed in a multi-anvil device at *P* = 4–13 GPa and *T* = 1100–1400 °C. A strong variation of $K_{p(\mathrm{Li})}^{Grt/Cpx}$ was found with changing *T* and *P*, but in addition the mineral chemistry of both Grt and Cpx changed systematically. The composition of Grt and Cpx can be described here by the following endmembers: *Grs*, *Pyr*, *Maj* and *Di*, *En*, *CaTs*, respectively. Measured $K_{p(\mathrm{Li})}^{Grt/Cpx} < 1$ but with increasing *P* and decreasing *T*, Li becomes increasingly compatible in Grt compared to Cpx in the MASH system (Fig. 4.4a), as given by the parameterization of Hanrahan et al. (2009):

$$\ln K_{p(\mathrm{Li})}^{Grt/Cpx} = 0.2351 \cdot P - 0.00253 \cdot T \tag{4.2.17}$$

Hanrahan et al. (2009) suggested $K_{p(\mathrm{Li})}^{Grt/Cpx}$ could be used as a geobarometer but emphasized that this calibration is only strictly valid for the MASH system and specifically the role of Na needs to be explored in more detail. The increasing compatibility of Li in garnet at high *P* is directly related to X_{Maj} in Grt, which increases in the MASH system continuously from about 0 at 4 GPa to about 0.09 at 13 GPa. Four different substitutions of Li into Grt were suggested by Hanrahan et al. (2009): 1. $(Mg_2Li)Al_2(PSi_2)O_{12}$; 2. $(Mg_3)(LiSi)(PSi_2)O_{12}$; 3. $(Mg_2Li)(AlSi)Si_3O_{12}$; 4. $(Li_2Mg)(Si_2)Si_3O_{12}$, where the substitution 1 could be more relevant at low pressures whereas substitutions 2–4 require the presence of the majorite component to have Si on the Y site in Grt. Correspondingly, in Cpx the *CaTs* component decreases with increasing *P*, which reduces the probability to incorporate Li as $LiAl_2SiO_6$ in Cpx.

The presence of Na could have a strong effect on this relationship since it would stabilize the jadeite component in Cpx, which according to Fig. 4.3b makes Cpx more favorable for Li. Other experimental data shown in Fig. 4.6a for $K_{p(\mathrm{Li})}^{Grt/Cpx}$ are roughly consistent with the predictions by Eq. 4.2.17. With the exception of the results of Bennett et al. (2004), Na was present in

these other experimental studies and Cpx contained a significant portion of *Jd* (Fig. 4.3a). In addition, Grt had in general a much lower *Grs* component (~15 mol% vs. ~30–40 mol% for most experiments in Hanrahan et al. 2009), which could affect the ideal cationic radius for the octahedral site due to the much larger Ca^{2+} (1.12 Å) compared to Mg^{2+} (0.9 Å). So the discrepancy between these data and Hanrahan et al. (2009) are most likely related to the different mineral chemistry.

4.3 Diffusion of Li and Associated Effects on δ^7Li

4.3.1 Theoretical Background

Here we give only a very short introduction into various aspects of diffusion that are relevant to Li diffusion and associated fractionation of Li isotopes in minerals, fluids, and melts. A fundamental introduction into the mathematical treatment of diffusion can be found in Crank (1975). There are also many textbooks about diffusion written mainly by materials scientists and physicists focusing on diffusion in metals, metal alloys and simple oxides (e.g., Manning 1968; Flynn 1972; Philibert 1991; Bokshtein et al. 1985; Glicksman 2000). A recent monograph on diffusion in minerals and melts comprises a basic introduction into the fundamentals of diffusion and a comprehensive data set for diffusion in minerals and melts (Zhang and Cherniak 2010).

4.3.1.1 Diffusion Coefficients

Diffusion of atoms in a phase is a random process related to thermally activated atomic jumps. In crystals at thermodynamic equilibrium certain point defects are present at defined concentrations that allow the movement of atoms within the structure. Vacancies or interstitials are the most common point defects that take an active part in the diffusion of atoms. Diffusion is a process that always occurs, atoms are moving relative to other atoms, but when a concentration gradient of isotopes or elements exists within a phase a net flux is created. In the simplest case of a one-dimensional isotropic diffusion medium, this net flux can be described by Fick's 1st law:

$$J_x^j = -D_j \cdot \frac{\partial C_j}{\partial x} \qquad (4.3.1)$$

which states that the flux of an element j along dimension x, J_x^j (units: mass or amount per unit surface area per unit time), is directly proportional to the concentration gradient along this direction and the proportionality constant is called the diffusion coefficient, D_j. In the general case the diffusion coefficient is a 2nd rank tensor, symmetry of which is constrained by the symmetry of the diffusion medium (for more details, see for example Nye 1957). Hence, fluids, melts, and cubic crystals all represent isotropic diffusion media characterized by a single diffusion coefficient. For other than cubic crystals, in principle the diffusion anisotropy has to be accounted for. However, to date all measurements of diffusion coefficients in minerals show that the anisotropy is often below the accuracy of the diffusion coefficients and almost never larger than a factor of 10 (Brady and Cherniak 2010). A notable exception is rutile (e.g., Sasaki et al. 1985). It should be noted that diffusion anisotropy in a 3D grain can produce chemical and isotopic profiles along certain cross sections that can be grossly misinterpreted (e.g., Costa and Chakraborty 2004).

4.3.1.2 The Isotopic Effect

The diffusion coefficient of an isotope I of Li in a given fluid or solid phase is directly proportional to the jump frequency, Γ_I, which is thermally activated. From dynamic theory it can be derived that the ratio of the jump frequency of any two isotopes of an element is related to the square root of their atomic masses, as follows (e.g., Flynn 1972):

$$\frac{\Gamma_{^7\mathrm{Li}}}{\Gamma_{^6\mathrm{Li}}} = 1 + \Delta K \cdot \left\{ \left(\frac{6}{7} \right)^{0.5} - 1 \right\}, \qquad (4.3.2)$$

where the factor ΔK is necessarily ≤1 and characteristic for the active diffusion mechanism (e.g., Philibert 1991). For example, the factor $\Delta K \approx 1$ for a very light isotope diffusing as an interstitial in a heavy matrix. This case defines

the maximum possible difference between the jump frequency of two isotopes but atomic jumps in any phase are correlated to the movement of other atoms due to geometrical constraints and electrochemical coupling (e.g., Schoen 1958; see also the full formalism for diffusion in melts in Watkins et al. 2014). Consider that Li as a trace element occupies a regular lattice site in a crystal, which is otherwise filled by Mg (such as in forsterite), and that diffusion occurs by the vacancy mechanism. A jump of a Li isotope into an adjacent vacant site would leave a vacancy behind and Li has moved by a distance equal to the distance between the two sites. However, there is also the possibility that an adjacent Mg jumps into this vacant site. In the extreme case if the jump probability of the Mg is negligible, the Li isotope cannot move forward but could jump back and forth between two adjacent sites. Therefore, for a net flux of Li atoms, jumps of Mg atoms are necessary. As a consequence, the diffusion coefficients of the two Li isotopes are related to each other, as follows:

$$\frac{D_{^7\mathrm{Li}}}{D_{^6\mathrm{Li}}} = 1 + f\Delta K\left\{\left(\frac{6}{7}\right)^{0.5} - 1\right\}, \qquad (4.3.3)$$

where f is the correlation factor that depends in general on the relative jump frequencies and the total number of the atoms that are involved in the active diffusion mechanism for the element of interest. As a consequence, f is principally dependent on the crystallographic arrangement of atoms and the diffusion direction and is one factor that contributes to the diffusion anisotropy. For interstitial diffusion of a light element in a heavy matrix f = 1, and hence for this special case the simple isotope effect is obtained:

$$\frac{D_{^7\mathrm{Li}}}{D_{^6\mathrm{Li}}} = \left(\frac{6}{7}\right)^{0.5}. \qquad (4.3.4)$$

The isotopic effect as given by Eq. 4.3.3 has long been recognized in the material science and physics literature and was experimentally verified mainly for diffusion in various metals and semiconductors (e.g., Johnson 1967). The relation given in Eq. 4.3.4 was also experimentally confirmed (e.g., for Li diffusion in Si; Pell 1960). High temperature fractionation of isotopes by diffusion in Earth materials has long been ignored, but experimental studies have documented this effect for diffusion of Li, Mg, Ca, and Fe in aqueous solutions, melts, and silicates (Richter et al. 1999, 2003, 2006, 2008, 2009, 2014; Chopra et al. 2012). In these experimental studies the fractionation of Li isotopes (and in analogous ways isotopes of other elements) is described by a similar equation like Eq. 4.3.4:

$$\frac{D^*_{\mathrm{Li}(7)}}{D^*_{\mathrm{Li}(6)}} = \left(\frac{6}{7}\right)^{\beta}, \qquad (4.3.5)$$

where β is an empirical parameter that is fitted to best describe the observed fractionation effects. Experimentally determined values of β for Li in different diffusion media are reported in Table 4.3. Equation 4.3.5 is not equivalent to Eq. 4.3.3 but it can be numerically shown that the dependence on the mass ratio is roughly the same when we set $\beta = f\Delta K/2$.

4.3.1.3 Diffusive Coupling

Because of the correlation of individual atomic jumps, different diffusion coefficients have been defined depending on the concentration and chemical gradients present, for example, self diffusion, tracer diffusion, chemical diffusion, inter-diffusion, multicomponent diffusion (for definitions of the different types of diffusion coefficients see Flynn 1972; Chakraborty 1995; Ganguly 2002; Costa et al. 2008). As explained above for the case of Li diffusion in an Mg sub-lattice, in principle the net transfer of elements by diffusion in crystals, fluids, and melts, cannot be treated as an isolated process, independent from other elements. Charge balance for ionic diffusion and site balance for crystals are important constraints that lead to the coupling of the diffusive fluxes of various elements within a diffusion medium (e.g., Lasaga 1979). Therefore, in the more general case of a concentration gradient of an element, Eq. 4.3.1 is a simplification, because it treats the diffusive flux of element j as

Table 4.3 Experimentally measured values of β for Li isotopes in different diffusion media

References	Phase	T (°C)	β	D^7Li/D^6Li
Richter et al. (2006)	Water		0.015	0.99772 ± 0.00026
Richter et al. (2003)	Rhyolite/basalt		0.215	0.9674
Richter et al. (2014)	Clinopyroxene	900	0.27	0.9592
Dohmen et al. (2010)	Olivine	800–1000	0.3	0.95 ± 0.05
Johnsons and Kruse (1966)	Rutile	450	0.5	0.93 ± 0.03
Pell (1960)	Si	800	0.5	0.93 ± 0.02

independent of the concentration gradient of other elements. However, in most cases of interest Li can be considered as a trace element, which apparently simplifies how to handle Li diffusion processes in minerals. If for example Li partially substitutes for Na in a Na end-member mineral (e.g., albite), the net diffusive flux of Li in response to a concentration gradient within this mineral is an inter-diffusion process where Na and Li have to exchange on the respective alkali site. Inter-diffusion of ions in a binary system can be described by a single diffusion coefficient, as follows (e.g., Lasaga 1979):

$$D_{\mathrm{Li-Na}} = \frac{D^*_{\mathrm{Li}} \cdot D^*_{\mathrm{Na}}}{X_{\mathrm{Li}} \cdot D^*_{\mathrm{Li}} + X_{\mathrm{Na}} \cdot D^*_{\mathrm{Na}}} \left(1 + \frac{\partial \ln \gamma_{\mathrm{Li}}}{\partial X_{\mathrm{Na}}}\right), \tag{4.3.6}$$

where X_j and D^*_j are the mole fraction of element j on the alkali site and the tracer diffusion coefficient of element j, respectively (note that the term tracer is not related to the term trace element here but to the isotopic tracer). For the limiting case when $X_{\mathrm{Li}} \to 0$ and hence $X_{\mathrm{Na}} \to 1$, Eq. 4.3.6 further simplifies: (i) For low concentrations of Li where Henry's law is valid the activity coefficient of Li is constant in this binary system and hence the thermodynamic factor on the right hand side in Eq. 4.3.6 becomes 1. (ii) Depending on the ratio of $D^*_{\mathrm{Li}}/D^*_{\mathrm{Na}}$ a critical concentration of Li (X_{Li}) exists, where from Eq. 4.3.6 we can show that $D_{\mathrm{Li-Na}} \cong D^*_{\mathrm{Li}}$ (for numerical examples see Costa et al. 2008) and in some analogy to Henry's law, the diffusion coefficient of Li is independent of the concentration. Based on these two approximations, it has been generalized that diffusion of trace elements in an otherwise effectively homogeneous ionic crystal can be described by Fick's 1st law (Eq. 4.3.1) with a constant diffusion coefficient D^*_j, which is basically equivalent to the tracer diffusion coefficient defined in Eq. 4.3.1. However, it should be noted that the critical concentration to justify this simplified treatment might be extremely small depending on the mineral. As such, for the natural concentration range of Li in minerals, coupling of diffusive fluxes with other elements may be relevant, in particular in case of a heterovalent substitution of Li into a mineral (for example when Li substitutes Mg, see Sect. 4.2)

4.3.1.4 Diffusion, Diffusive Fractionation and Time

The concentration distribution with time is governed by the diffusion equation, a partial differential equation (or in the case of diffusion coupling, a set of coupled partial differential equations) that can be derived by applying the mass balance on an infinitesimal volume unit and combining it with the appropriate diffusive flux equation (Crank 1975; Costa et al. 2008). For the flux given in Eq. 4.3.1 for a one-dimensional system we obtain Fick's 2nd law:

$$\frac{\partial C_j}{\partial t} = -\frac{\partial J^j_x}{\partial x} = D_j \cdot \frac{\partial^2 C_j}{\partial x^2}, \tag{4.3.7}$$

where it is assumed that the diffusion coefficient is constant, as is the case for a limiting concentration range of a trace element (see discussion before, Eq. 4.3.6). Solutions of the diffusion equation are given for a number of different geometries, initial and boundary conditions in Crank (1975) or

Carslaw and Jaeger (1959). The latter book presents solutions to thermal conductivity problems which can be transferred easily to diffusion problems as explained in Crank (1975). In general, any observed concentration distribution created by diffusion (for example in a mineral) can be fitted by solving diffusion equations of the type given in Eq. 4.3.7, if appropriate initial and boundary conditions are chosen and the diffusion coefficient is known. The latter quantity is a strong function of temperature and hence additional constraints for the temperature or thermal history are required to obtain information on the time scale of the related geologic process, or, for example, the cooling rate of the system (example shown in Fig. 4.7). Diffusive fractionation of Li isotopes can be modeled by solving Eq. 4.3.7 for both Li isotopes separately (e.g., Richter et al. 2003), assuming any value of $\beta < 0.5$ describing their relative diffusivities according to Eq. 4.3.6. Concentration gradients of Li in plagioclase (Coogan 2011; Charlier et al. 2012), in diopside (Coogan et al. 2005; Beck et al. 2006), and across the bulk rock (Teng et al. 2006; Halama et al. 2009; John et al. 2012; Lai et al. 2015) have been used to infer cooling and ascent rates as well as time scales of fluid release in subduction zones.

4.3.2 Experimental Diffusion Coefficients

Any type of diffusion coefficient as a material constant depends on a number of intrinsic thermodynamic parameters, like T, P, fO_2, and fH_2O, but among these, T is clearly the most relevant variable for minerals and melts of a given major element composition since the atomic jumps are thermally activated (see for example Chakraborty 2008). Experimental diffusion coefficients are usually presented by an Arrhenius law, as follows:

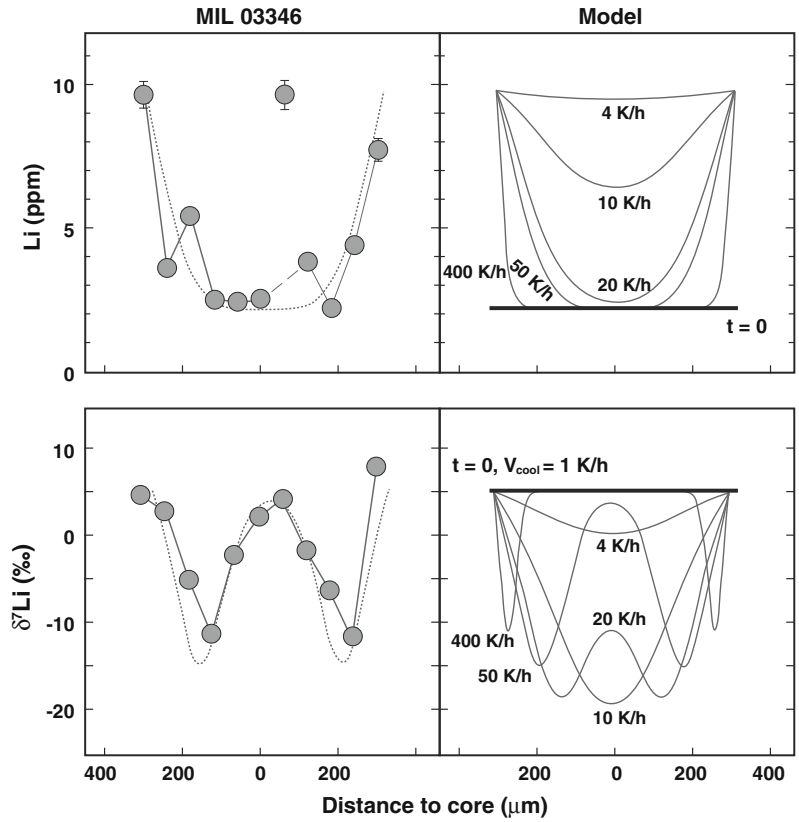

Fig. 4.7 Measured and modeled diffusion profiles of Li and δ^7Li in augite crystals from the Martian meteorite MIL03346 (Beck et al. 2006). On the right side various profiles for different cooling rates are shown. The *dashed lines* on the left are the best fits from which a cooling rate of 50 °C/h from an initial temperature of 1000 °C was derived. Note the strong variation of δ^7Li within 20 ‰ produced by Li diffusion requiring a β of about 0.15. Reprinted with permission from Elsevier

$$D_j = D^{\circ}(fO_2, fH_2O, X_i, \ldots) \cdot \exp\left(-\frac{E + P\Delta V}{RT}\right), \quad (4.3.8)$$

where E is the activation energy at zero pressure (or effectively at atmospheric pressure), ΔV is the activation volume, and D° is the pre-exponent, which may incorporate dependencies in other intrinsic thermodynamic variables like fO_2. The point defect chemistry of a mineral is in general a function of the intrinsic thermodynamic variables and hence are the diffusion coefficients. For example, fO_2 has a control on the concentration of vacancies on the metal site in olivine or spinel (e.g., Dohmen and Chakraborty 2007), whereas fH_2O affects the structure of silicate melts and hence their viscosity and diffusion properties (e.g., Zhang and Ni 2010).

Experimental data for Li diffusion in minerals and melts are illustrated in Fig. 4.8 and details of experimental conditions are given in Table 4.4. In general for a given element, diffusion in fluids is faster than in melts, which is again faster than in minerals, and correspondingly, activation energies increase in the same order (Watson and Baxter 2007; Brady and Cherniak 2010). The same general trend can be also found for Li with a few exceptions (Fig. 4.8). Diffusion of Li parallel to the c-axis in rutile seems to be extremely fast (Johnson 1964), similarly to or even faster than diffusion in aqueous fluids. Diffusion of Li in quartz (Verhoogen 1952) is as fast as in a rhyolite glass (Jambon and Semet 1978). Extrapolation of Li diffusion in plagioclase (Giletti and Shanahan 1997), clinopyroxene (Coogan et al. 2005) and olivine (Li interstitials; Dohmen et al. 2010) to experimental data for basaltic melts around 1200–1300 °C shows that they are comparably fast. Therefore, Li appears to be special in the sense that the difference in its diffusivity between some crystals and melts is much lower compared to other elements. This specific behavior would have consequences for diffusion models considering the Li exchange between melt and crystals since in this case the melt is typically treated as an infinite reservoir, in which diffusion is sufficiently fast that the melt is homogenous. Before taking these experimental observations as fact, it is worth investigating the experimental details and discussing the possible incorporation and diffusion mechanisms of Li in the various minerals.

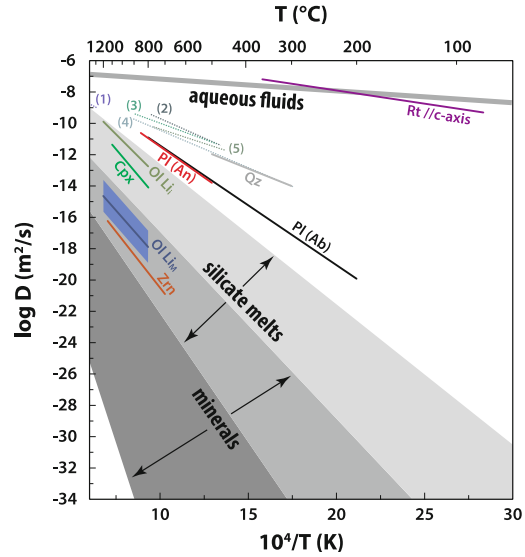

Fig. 4.8 Range of diffusion coefficients for minerals, melts and fluids, as adapted from Watson and Baxter (2007) in comparison to measured Li diffusion coefficients shown in an Arrhenius plot (logarithm of diffusion coefficient vs. reciprocal temperature, compare with Eq. 4.3.8): (*1*)–(*5*) silicate glasses (see Fig. 4.12 for more details; Rt: Johnson 1964; Qz: Verhoogen 1952; Ol: Dohmen et al. 2010; Pl: Giletti and Shanahan 1997; Cpx: Coogan et al. 2005; Zrn: Cherniak and Watson 2010. The *grey areas* indicate the range of diffusion coefficients of other elements in minerals and melts as given in Watson and Baxter (2007). Obviously, D_{Li} for minerals and melts is in general larger than for other elements, except H

Rutile (Rt). Diffusion of Li in rutile was investigated by an unusual experimental setup where rutile was first doped with Li under vacuum at 450 °C for only 10–20 h and then the diffusion annealing was carried out in various baths (distilled water, KNO_3–$NaNO_2$, and KNO_2) to leach Li out of rutile at the surface and maintain approximately a zero concentration at the surface as the boundary condition of the experiment (Johnson 1964). The crucial point here is that the concentration of Li in rutile was not measured directly but inferred indirectly by

optical absorption measurements using monochromatic light. Johnson (1964) assumed that the optical absorption of the rutile crystal is directly proportional to the Li content since Li interstitials acts as a donor for electrons in rutile and should increase the optical absorption. Whether the optical absorption is directly proportional to the Li concentration has not been tested but the solutions have been analyzed after an apparently complete removal of Li from the rutile to calibrate the optical absorption to the apparent Li content. There are two major issues here: (i) It is not clear whether the rutile was completely homogenized with Li in the pre-anneal under vacuum, since it is only the optical absorption which was measured. The optical absorption of rutile changes significantly by just heating in vacuum even without a Li source present. (ii) During the diffusion anneal in the baths the redox conditions are probably different, leading also to changes in the electron structure of rutile that may be completely unrelated to Li. Therefore, the data of Johnson (1964) should be treated with great caution. There are two additional indirect arguments that suggest their data are wrong. If their data were correct it would imply that (i) the diffusion of H in rutile is several orders of magnitude slower than that of Li (see comparison in Van Orman and Crispin 2010); (ii) diffusion of H or Li in water would be smaller than that of Li in rutile. Both implications seem to be very unlikely from all existing empirical evidence. In a follow-up study by Johnson and Krouse (1966), applying a similar experimental setup, the diffusive fractionation of Li isotopes was investigated. They inferred a β value of around 0.5, consistent with theoretical predictions for interstitial diffusion. However, for the same reasons as for the work of Johnson (1964) these data should be treated with caution. New experimental work in which the concentration of Li and Li isotopes are spatially resolved remains to be undertaken.

Quartz (Qz). To measure Li (and Na + K) diffusion in quartz Verhoogen (1952) used another experimental setup in which diffusion of ions is indirectly measured by imposing an electrical gradient across 2–3 mm thick quartz plates that were in contact with LiCl, NaCl, or KCl, on only one side. The diffusion coefficient of positive ions was calculated from the electrical conductivity σ using the relation valid for monovalent ions, $D = \sigma kT/(e^2c)$, where e is the charge of an electron, k is the Boltzmann's constant, and c the concentration of the diffusing ion. The concentration needs to be known to calculate D, but Verhoogen (1952) used a constant concentration, which is only indirectly estimated from conductivity measurements without a Li source, arguing that the concentrations of the ions is equal to some maximum number of point defects in quartz. It is obvious that the derived diffusion coefficients of Li rely on many assumptions there. In addition, it has to be assumed that the charge transport occurs in these experiments through the bulk of the crystal. However, Verhoogen (1952) used natural crystals that may contain a number of linear and planar defects that act as short circuit paths. Yet again, the concentration distributions within the quartz crystals were not directly measured and the author himself states that "These values are not believed to represent more than the order of magnitude of the diffusion coefficients; numerical values may be in error by a factor of 2 or 3". Therefore, we cannot rely on these data as accurate diffusion coefficients.

An independent constraint for Li diffusion in quartz comes from the observation of Charlier et al. (2012) who compared Li concentration profiles in quartz and plagioclase from the same pumice (P1961, Oruanui eruption, New Zealand) and concluded from diffusion modeling that "If the feldspar and quartz crystals in P1961 are assumed to have undergone an identical thermal and decompression history, then the quartz-hosted Li concentration gradients imply a diffusion coefficient that is similar to, or up to about 4 times faster than, that in the feldspar". In another experimental study using a combination of measurements by electrical conductivity and SIMS, two mechanisms of Li diffusion were inferred (Sartbaeva et al. 2005; no diffusion coefficients reported): fast diffusion of Li interstitials along crystallographic channels perpendicular to the c-axis and a slower diffusion

process related to the coupled movement of Li^+ and Al^{3+}.

Plagioclase (Pl). In the experimental study of Giletti and Shanahan (1997), diffusion of ^6Li as an isotopic tracer was measured in natural albite ($Ab_{98.5}Or_{0.8}An_{0.6}$) and anorthite ($An_{95.6}$) crystals. They used films doped with ^6Li as a diffusion source and the diffusion couples were placed in welded Au or Pt capsules and annealed at atmospheric pressures. The concentration distribution of ^6Li after the diffusion anneal was analyzed by SIMS either in depth profiling or step scanning mode, where Giletti and Shanahan (1997) avoided several of the potential pitfalls in profile measurements of Li with SIMS. It is unknown whether in their experiments a concentration gradient for the total Li was imposed and if they fitted the normalized concentration of $^6Li/^7Li$, $^6Li/^{27}Al$, or simply the count rate of ^6Li. This would make a difference since we can consider two scenarios. The first one would be just an isotopic exchange of ^6Li with ^7Li, originally present in the natural crystal. In this case ^6Li could diffuse as an interstitial and exchange with ^7Li on either interstitial sites or alkali sites in plagioclase but the Li concentration stays homogeneous as it should be for an ideal tracer diffusion experiment. The second scenario would be that the diffusion source imposes also a chemical gradient for Li and the total Li concentration increases, which involves the exchange with for example Na atoms on the alkali site (see discussion above related to Eq. 4.3.6) and the diffusion rate could differ from that of the tracer diffusion rate. In any case, Giletti and Shanahan (1997) found very similar Li diffusion rates for albite and anorthite, which are very fast compared to diffusion of other cations in plagioclase, or for Li diffusion in clinopyroxene or olivine (Fig. 4.8). Thus, at temperatures of ~770 °C, according to this data set, Li in plagioclase would record only the final seconds to minutes of a volcanic eruption (Charlier et al. 2012).

Olivine (Ol). Two studies (Dohmen et al. 2010; Spandler and O'Neill 2010) investigated Li diffusion in olivine with various different experimental setups imposing different concentration levels of Li in olivine and corresponding boundary conditions. In Dohmen et al. (2010), the powder source technique was applied (detailed discussion of this technique in Watson and Dohmen 2010). A pre-annealed powder mix of ^6Li-enriched olivine and Li_2SiO_3 acted as the diffusion source for polished, crystallographically oriented San Carlos olivine single crystals (hereafter called as Type I experiment). Diffusion experiments were carried out in gas mixing furnaces at atmospheric pressures under controlled oxygen fugacity, which in all experiments was kept close to the wüstite–magnetite buffer (WM). The resulting diffusion profiles parallel to the c-axis were analyzed with SIMS in the step scanning mode. In addition to the samples from the powder setup, they also measured Li diffusion profiles in olivine crystals that were pre-annealed in a Li contaminated furnace (hereafter referred to as Type II experiment) and in two single crystal diffusion couples consisting of synthetic forsterite and San Carlos olivine from the experimental study of Petry et al. (2004) (hereafter called as Type III experiment).

Overall they observed a diversity in profile shapes (Fig. 4.9) and diffusion rates that can be consistently understood and simulated with a two-species model considering Li_i (Li-interstitials) and Li_{Me} (Li on regular metal sites). Although the model contains more than one fitting parameter it was shown by the profile shape that most of them are independently constrained. For all the different cases observed, a consistent set of diffusion coefficients for Li_i was determined by fitting profiles, and a single Arrhenius relationship can be used to calculate them (Table 4.4, Fig. 4.10a). The diffusion coefficient of Li_{Me} is much lower than that of Li_i (see Fig. 4.10a) and varies strongly depending to first order on the Li concentration at the rim. For different experimental setups (Type I, II, +III) a different rim composition was imposed, varying from hundreds to a few µg/g of Li. For a given setup, and hence roughly constant rim composition, a single Arrhenius relationship was found, indicating a compositional dependence of this diffusion coefficient. Such a compositional dependence can be related to the coupling of the diffusive flux of Li with the diffusivity of other ions (e.g., Fe and Mg), but the origin is yet

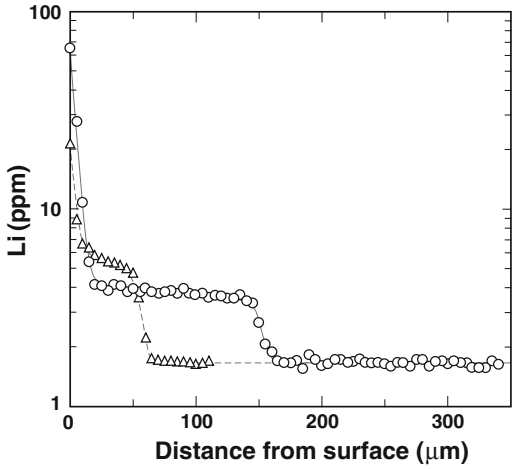

Fig. 4.9 Measured Li profiles in Ol from two experiments of Dohmen et al. (2010) performed at 1000 °C showing an unusual step like profile shape (compare with Fig. 4.7). *Solid lines* are simulated fits with a diffusion model considering two Li species, Li_i and Li_{Me}

unclear. Because of this complexity, Dohmen et al. (2010) recommended a preliminary Arrhenius relationship for the diffusion coefficient of Li_{Me} that applies for typical natural Li concentrations in olivine (Table 4.3, Fig. 4.9) and has an arbitrarily estimated uncertainty of ±1 log unit.

A single data point of D_{Li} for each crystallographic axis was measured by Spandler and O'Neill (2010). A San Carlos olivine single crystal with a drilled hole was filled with a melt that was in chemical equilibrium with the crystal for the major elements at the T = 1300 °C. The melt was doped with various trace elements that diffused into the olivine, but some elements, for example Li, were doped with a low concentration (1.8 μg/g) and diffused out of the olivine. The diffusion anneal was carried out in a gas mixing furnace at an fO_2 equal to FMQ–1 and the main observation of this study was that most of the 19 elements investigated, including REE and Li, diffused at similar rates as Fe and Mg, whose rates were consistent with recent studies on Fe–Mg diffusion in San Carlos olivine (Dohmen and Chakraborty 2007; Petry et al. 2004). A small diffusion anisotropy for Li (log D_{Li} = –15.27 // [010] and –14.82 //[001]) was found, but none for the REE, for example.

Since it was shown by Dohmen et al. (2010) that the net diffusion rate of Li is strongly dependent on the detailed boundary conditions at the rim and decrease with decreasing Li concentrations imposed on the rim by the experimental setup, it could be expected that for diffusion of Li out of olivine and a Li concentration at the rim of around 0.6 μg/g, D_{Li} becomes smaller compared to the simple Arrhenius relation given by Dohmen et al. (2010). In fact, D_{Li} for the M site // c-axis from the Type III experiment at 1200 °C (Fig. 4.8), with a similar concentration range of Li as in Spandler and O'Neill (2010), is consistent with the latter study, considering also the apparent activation energy of Dohmen et al. (2010).

Clinopyroxene (Cpx). Two studies by Coogan et al. (2005) and Richter et al. (2014) were dedicated to the measurement of Li diffusion in clinopyroxene, both using the powder-source technique but that of Coogan et al. (2005) additionally used a ^{6}Li-enriched powder. In the experiments of Coogan et al. (2005), diopside single crystals from Madagascar, with stoichiometry of $(Fe_{0.07}Mg_{0.88}Al_{0.05}Na_{0.016}Mn_{0.002})Ca_{0.99}(Si_{1.94}Al_{0.06})O_6$, were annealed in a gas mixing furnace at controlled and variable fO_2. Concentration profiles of ^{6}Li/^{30}Si were measured by SIMS in the step scanning mode and "normal" diffusion profile shapes were observed. Four experiments, each at a different temperature in the range between 800 and 1100 °C, were performed and two different fO_2 were chosen. The four data points can be reasonably well fitted by one Arrhenius equation (see Table 4.4) and Li diffusion rates are significantly faster compared to Li_{Me} in olivine but slightly slower than Li_i in olivine (Fig. 4.10b).

Since Richter et al. (2014) used a natural isotopic composition they were able to measure also the diffusive fractionation effect (Fig. 4.11) by SIMS. Their diffusion anneals were carried out at a single T (~900 °C) in sealed silica ampules containing a solid-state fO_2 buffer. Two types of single crystals were used, Templeton augite and Dekalb diopside with composition $(Fe_{0.11}Mg_{0.86}Al_{0.01}Na_{0.04})Ca_{0.97}(Si_{1.97}Al_{0.03})O_6$ and $(Fe_{0.02}Mg_{0.97}Al_{0.01}Na_{0.03})Ca_{0.98}(Si_{1.99}Al_{0.01})O_6$, respectively, as recalculated from Table 4.2

Table 4.4 Published diffusion coefficients of Li in minerals (experimental conditions and Arrhenius parameters)

References	Mineral/mineral group	Cryst. orient.	T (°C)	P (MPa)	log fO_2/fO_2 buffer	E (kJ/mol)	log D° (m^2/s)	log D (m^2/s)	Notes
Giletti and Shanahan (1997)	Ab	⊥to (010), (001), (100)	200–800	0.1	Air	146 ± 14	−3.8 ± 1.0	–	–
Giletti and Shanahan (1997)	An	⊥to (010)	500–850	0.1	Air	151 ± 62	−3.6 ± 3.6	–	–
Coogan et al. (2005)	Cpx	II to [010]	800–1100	0.1	−13, −17	258	−1.54	–	–
Richter et al. (2014)	Cpx	–	900	0.1	NNO	–	–	−7.92 to −9.33	Effective diffusion coefficient
Richter et al. (2014)	Cpx	–	900	0.1	WM	–	–	−11.19	Effective diffusion coefficient
Richter et al. (2014)	Cpx	–	900	0.1	IW	–	–	−7.43, −7.48	Effective diffusion coefficient
Verhoogen (1952)	Qtz	II to c	300–500	0.1	Air	86	−6.16	–	–
Johnson (1964)	Rt	II to c	80–360	–	–	31.8 ± 0.3	−4.53 ± 0.04	–	–
Cherniak and Watson (2010)	Zrn	⊥to c	700–1150	0.1	–	275 ± 11	−6.14 ± 0.48	–	–
Dohmen et al. (2010)	Ol	II to [001]	800–1200	0.1	WM	214.2 ± 6.2	−2.32 ± 0.27	–	Li interstitial
Dohmen et al. (2010)	Ol	II to [001]	800–1200	0.1	WM	246	−5.9 ± 1.0	–	Li Me for Ol with Li of 1–10 μg/g
Spandler and O'Neill (2010)	Ol	II to [100]	1300	0.1	−8.3	–	–	−14.99	–
Spandler and O'Neill (2010)	Ol	II to [010]	1300	0.1	−8.3	–	–	−15.27	–
Spandler and O'Neill (2010)	Ol	II to [001]	1300	0.1	−8.3	–	–	−14.82	–

NNO Ni-NiO
WM Wuestite magnetite
IW Iron-wuestite

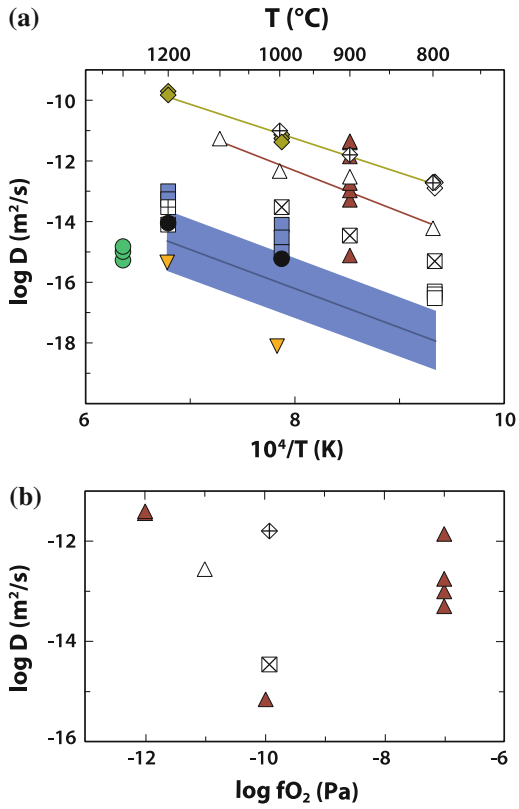

Fig. 4.10 Experimentally measured D_{Li} for Ol and Cpx (diopside) shown as a function of **a** T for various experimental setups and fO_2 and **b** fO_2 at 900 °C: ◇ = D of Li_i //[001] in Ol; □ = D of Li_{Me} //[001] in Ol (Dohmen et al. 2010). Symbol fill denotes the experimental setup: ◇ □ = Type I with San Carlos olivine; ◈ ▣ = Type I with Pakistan Ol; ◈ ⊠ = Type IIb with San Carlos Ol; ⊞ = Type IIa experiment with SC and Pakistan Ol; ◆ ▣ = Type III with forsterite; ▣ = Spandler and O'Neill (2010) with SC olivine parallel to the three main crystallographic axes; triangles = effective D of Li in Cpx: △ = in Madagascar diopside (Coogan et al. 2005); △ = Richter et al. (2014) at different fO_2 with Templeton augite and Dekalb diopside. For the details of Type I, II, and III experimental setups see Dohmen et al. (2010). The *solid lines* are Arrhenius relationships given by Coogan et al. (2005) for Li in diopside and Dohmen et al. (2010) for Li_i and for Li at natural concentration levels. The *blue area* indicates a rough estimate of the uncertainty given by Dohmen et al. (2010) for this relationship, since the exact dependence of Li on its concentration has not been carefully calibrated. Note that the data points of Spandler and O'Neill (2010) would be consistent with this relationship

in Richter et al. (2014). Similar to Dohmen et al. (2010) for olivine, they found various profile shapes (e.g., Fig. 4.11) and effective diffusion rates of Li depending on the type of diffusion reservoir used and the fO_2 of the experiment and the crystal used. Thus, Richter et al. (2014) adopted the two-species model of Dohmen et al. (2010) to quantitatively reproduce their observations, including the different magnitude of δ^7Li anomalies, varying from about 0 to –35 ‰. They obtained this variable behavior by the model assuming different initial vacancy concentrations and different diffusion coefficients of Li_i. As a consequence they determined diffusion coefficients of Li_i which varied over four orders of magnitude depending on the fO_2, defined by Ni–NiO (NNO), wüstite–magnetite (WM), or iron–wüstite (IW) buffer (Fig. 4.10b). The special diffusion behavior of Li in diopside and olivine is discussed in more detail in Sect. 4.3.3.

Zircon (Zrn). In the experimental setup of Cherniak and Watson (2010) the powder-source technique was used with natural spodumene powder (experiments at atmospheric pressure), Li_4SiO_4 mixed with REE-oxides and $ZrSiO_4$ powder (one experiment), or spodumene with quartz (42 wt%) and zircon (17 %) (hydrothermal experiments). For the experiments at atmospheric pressure, the diffusion couples were sealed in silica glass capsules and the hydrothermal experiments were carried out in a piston cylinder apparatus where the fluid was produced by adding oxalic acid to the powder mixture, which should buffer H_2O:CO_2 in the fluid at 1:1. Depth profiles parallel and normal to the c-axis of the oriented and polished single crystals were measured by nuclear reaction resonance analysis (NRA) using the reaction ^{7}Li(p, γ)^{8}Be. The maximum Li concentrations that they obtained after the experiment were in the range of 100–600 µg/g. According to this study Li diffusion in zircon is significantly slower than in all minerals studied so far (Fig. 4.8), and probably defines a lower limit of Li diffusion in minerals. This observation is consistent with the trend for other diffusion data for zircon, which are generally much lower than for other minerals (e.g., for REE and Pb; Cherniak 2010).

Melts. Li tracer diffusion in melts or glasses was determined for the following compositions (Fig. 4.12): albitic glass, orthoclase glass, and

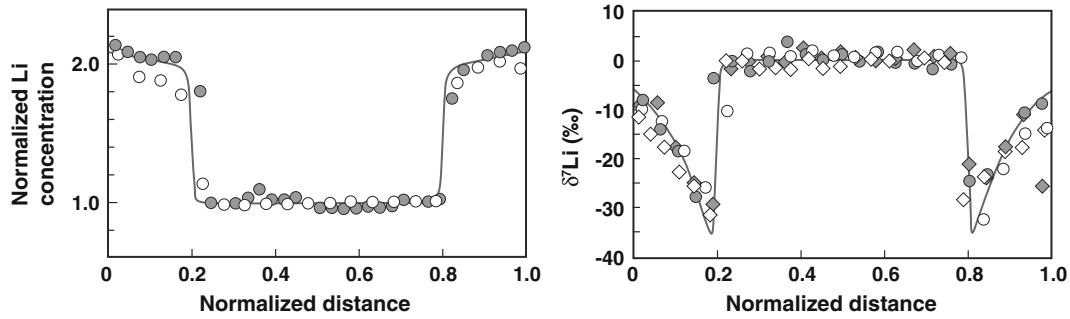

Fig. 4.11 From Richter et al. (2014), showing an unusual step like profile shape: Li profile in Cpx (Templeton augite) at 900 °C on left, δ^7Li profile from the same sample. Reprinted with permission from Elsevier

rhyolitic glass (Jambon and Semet 1978); jadeite glass (Roselieb et al. 1998); andesitic and dacitic melt (Cunningham et al. 1983); basaltic melt (Lowry et al. 1981; Lundstrom 2003). In addition, a number of studies exist where Li self-diffusion was investigated in various Li silicate glasses (e.g., Welsch et al. 2012 and references therein), but here we summarize only data for naturally relevant compositions.

The glasses and melts were mostly completely dry, only the rhyolite contained some water (0.52 wt% H_2O). In most experiments a thin film enriched with Li was used, except for Lundstrom (2003) where a basaltic melt was in contact with a partially molten peridotite. In every study Li profiles were measured using SIMS after the diffusion experiment. As for minerals, Li diffusion in melts is enhanced compared to most other cations due to its low ionic charge and size (see review of Lesher 2010). For example, in Li silicate glasses the ionic conductivity is dominated by Li diffusion (e.g., Welsch et al. 2012). However, at a given temperature the range of published Li diffusion coefficients is very limited when compared to the variability of Li diffusion in minerals. Extrapolated data measured for albitic glass and those measured in basaltic to dacitic melt are very similar (Fig. 4.12). Water is known to affect diffusion in melts up to orders of magnitude (e.g., Behrens and Zhang 2001) because it depolymerizes the melt and lowers the viscosity. Therefore, Li diffusion could be enhanced compared to the experimental studies if a significant amount of water (several wt% H_2O) is dissolved into the melt. Various physical models have been used to predict diffusion coefficients from the viscosity of melts (e.g., Einstein 1905; Eyring 1936). The empirical model of Mungall (2002) relates tracer

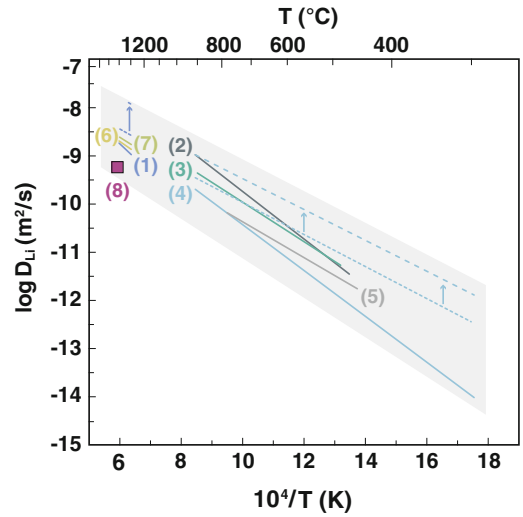

Fig. 4.12 Arrhenius plot of experimentally measured D_{Li} in various melts and glasses: (1) basaltic melt (Lowry et al. 1981); (2) albitic glass (Jambon and Semet 1978); (3) jadeite glass (Roselieb et al. 1998); (4) rhyolitic glass (Jambon and Semet 1978); (5) glass with 39 mol% albite and 61 mol% orthoclase component (Jambon and Semet 1978); (6) andesitic melt (Cunningham et al. 1983); (7) dacitic melt (Cunningham et al. 1983); (8) basaltic melt (Lundstrom 2003). The *dashed lines* are predictions of D_{Li} for the rhyolitic melt and the basaltic melt as calculated from the empirical model of Mungall (2002). The *arrow* points to predictions considering 5 wt% H_2O in the respective melts

diffusivities to temperature, viscosity, melt composition, and cation size. He provides an equation for alkali elements which is not sensitive to viscosity at all, unlike high field strength or intermediate field strength elements, as follows:

$$\log(D_{\mathrm{Li}}) = -3.02 + \left[18.5 \cdot (r_{\mathrm{Li}} - 1.03)^2 + 2.88\right] \cdot M/O - 1/T \cdot \left[538 \cdot \mathrm{Al}/(\mathrm{Na} + \mathrm{K} + \mathrm{H}) + 11910 \cdot (r_{\mathrm{Li}} - 1.03)^2 + 3029\right]$$

The ratios M/O and Al/(Na + K + H) are the molar ratio of non-bridging cations to oxygen anions and molar ratio of the given elements, respectively, and r_{Li} is the ionic radius of Li in the melt. The empirical equation is inferred from a diffusion model for alkalis (A) in melts where pairs of alkalis break a T–O–T bridge into a non-bridging T–O–A A–O–T group (Mungall 2002). Diffusion of alkalis can be therefore seen as coupled diffusion of A_2O. If the alkali concentration is very low the formation of pairs becomes unlikely and the diffusivity of alkalis drops (Mungall 2002). In Fig. 4.12 we have also plotted the predictions from Eq. 4.3.9 for the experimental melt compositions of a rhyolitic and basaltic melt. The predicted D_{Li} is for these two cases about 0.5 log units too high. We also applied Eq. 4.3.9 to estimate the effect of H_2O on D_{Li} and added 5 wt% H_2O to these compositions, which produces a further shift to higher diffusivities by another half order of magnitude.

4.3.3 Characteristic Time Scales of Li Diffusion in Silicates (Ol, Cpx, Pl)

As discussed above, Li diffusion in minerals is very fast compared to other elements with the major geochemical consequence that Li concentrations and δ^7Li can be significantly affected by diffusion at even moderate temperatures within reasonable time scales (e.g., in mantle xenoliths). For δ^7Li we have to consider two effects: (i) the isotopic re-equilibration with a new chemical environment, and (ii) diffusive fractionation. We made attempts to estimate these characteristic time scales applying a simple model geometry. In Fig. 4.13a we illustrate by a normalized concentration distance plot how a spherical grain with diffusion isotropy (cubic crystal) homogenizes with time (initial homogeneous concentration C_0, fixed rim concentration, C_{rim}). The analytical solution of this diffusion problem is given in Crank (1975, p. 91, Eq. 6.18). From Fig. 4.13a we can infer directly that the time

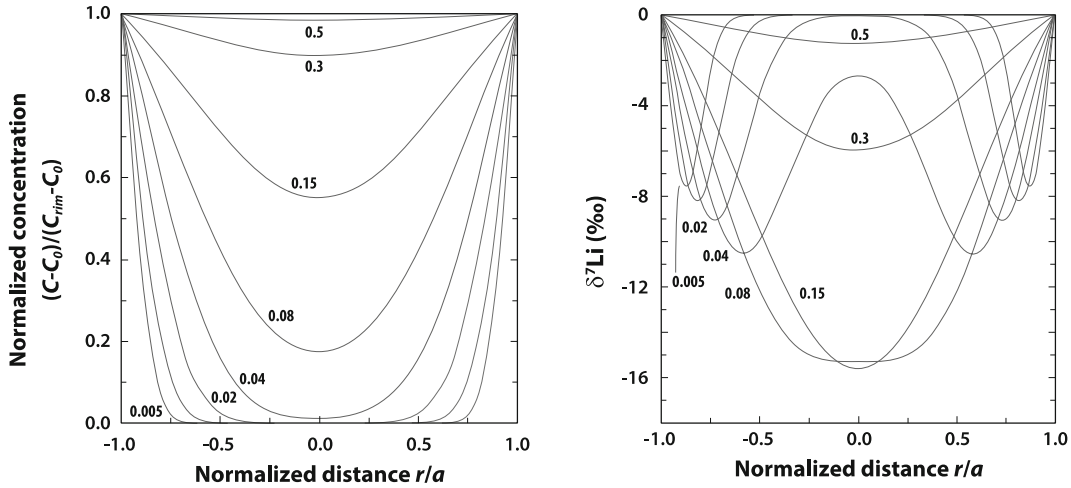

Fig. 4.13 Normalized concentration distance plots for diffusion in a sphere and an infinite plane after various different times: Li flux into a sphere (*left*); δ^7Li corresponding to a ratio of $C_{\mathrm{rim}}/C_0 = 2$ (*right*). All calculations were performed for a value of $\beta = 0.25$. Numbers on the curves denote values of Dt/a^2 for the sphere, where a is the radius

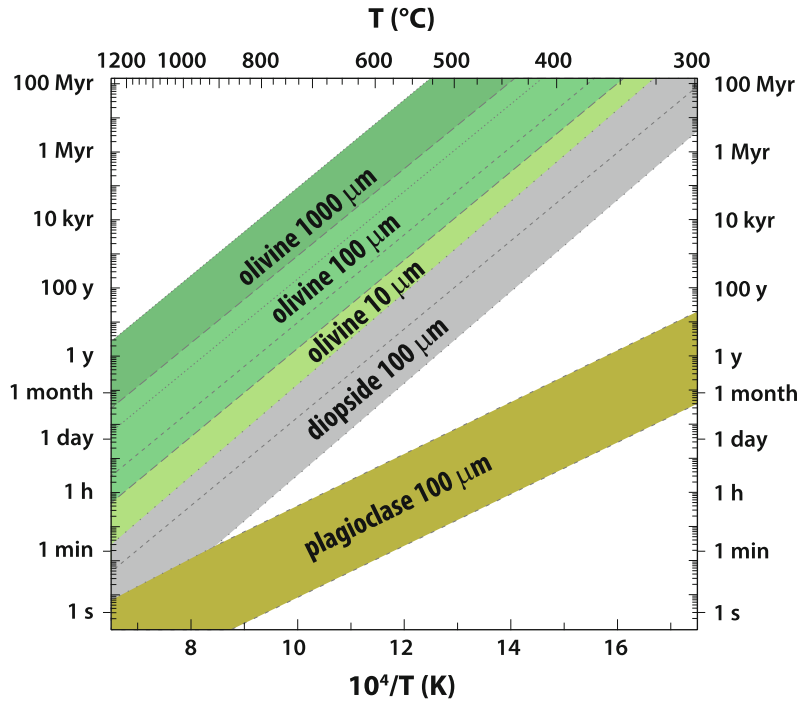

Fig. 4.14 Characteristic time scales of Li diffusion versus temperature for olivine, diopside, and plagioclase. See text for details

required to effectively homogenize the spherical grain is about 0.5 a^2/D and to affect the composition of the region next to the rim (10 % of the radius) a time of about 0.001 a^2/D has to elapse. Hence, assuming a grain size of for example 500 μm, a minimum time of about 2.5 e^{-12} m^2/D is needed to obtain a zoning within the 50 μm next to the rim that could be detected by LA-ICP-MS and SIMS, considering a spatial resolution of about 10–20 μm. These simple relations will be used below to estimate the characteristic time scales of Li diffusion in various minerals as a function of T. We define two characteristic time scales for a given spherical crystal with radius a, at a given temperature: a minimum time scale, $t_{min} = 0.001 \cdot a^2/D(T)$, which would be the time necessary to affect the bulk or average composition of the crystal by diffusion; a maximum time scale, $t_{max} = 0.5\ a^2/D(T)$, which would be the time necessary to effectively homogenize the crystal. Note that the minimum time scale is only a rough estimate since if the bulk composition is affected it depends also on the concentration gradient present (rim composition/initial composition). It is also a rough estimate for the minimum time needed to affect the bulk δ^7Li by diffusive fractionation.

Using these two relationships we illustrate in Fig. 4.14 how the characteristic time scales change with T for olivine, diopside and plagioclase using the published Li diffusion coefficients of Dohmen et al. (2010) for Li_{Me}, Coogan et al. (2005), and Giletti and Shanahan (1997), respectively. The simplified model used here does not consider the complexities of diffusion in diopside and olivine (see below), but still gives a general sense of the relative time scales and their implications. For the calculations we have used a radius of 100 μm and to illustrate the effect of grain size we have used also 1000 and 10 μm for olivine.

In Fig. 4.14 the two characteristic time scales define the upper and lower boundary of a temperature-time window in which the mineral is open to diffusional exchange with the

environment, but does not equilibrate completely. Below this field there is no significant effect of Li diffusion and above this field the mineral is re-equilibrated. A first obvious result of this calculation is that at $T > 1200$ °C, even in larger crystals, Li is re-equilibrated within less than a couple of years. However, at more moderate temperatures (400–700 °C) modification of Li contents in olivine and diopside requires longer time scales. Plagioclase is a rather extreme case since for Li it reacts very quickly to any change in the chemical environment.

In the most simplified form we also simulated diffusive fractionation of Li isotopes by solving Eq. 4.3.7 for ^{6}Li and ^{7}Li separately (e.g., Gallagher and Elliott 2009) assuming any value of $\beta < 0.5$ describing their relative diffusivities according to Eq. 4.3.5. For the same case as above (e.g., initially homogeneous), we plotted the evolution of δ^7Li with time (Fig. 4.13b). Two very general features of isotopic fractionation patterns originated by diffusion can be recognized here: (i) Due to the larger mobility of ^{6}Li compared to ^{7}Li we observe a region within the crystal with a pronounced negative anomaly (or positive anomaly, respectively) for an influx (or flux out) of Li. (ii) The region of this anomaly extends roughly over the region with the chemical zoning where the minimum (or maximum, respectively) of δ^7Li coincides with the point of maximum curvature for the Li profile, $\partial^2 C/\partial x^2$. The magnitude of δ^7Li at this minimum is somehow defined by the ratio of the diffusion coefficients for ^{6}Li and ^{7}Li as well as by the initial concentration gradient (see also Parkinson et al. 2007), given by the difference between C_{rim} and C_0. The time scale over which the diffusive fractionation effect occurs is coupled to the chemical diffusion process and hence the time to homogenize the Li isotopes is roughly equivalent to the time for chemical homogenization, as given here for the spherical model by $t = a^2/D$. Note that in particular for Li this simplified model can be very misleading for the interpretation of naturally occurring δ^7Li profiles, as will be discussed in the next section.

4.3.4 Two Diffusion Mechanisms of Li in Silicates

For three types of silicates, quartz (Sartbaeva et al. 2005), olivine (Dohmen et al. 2010), and clinopyroxene (Richter et al. 2014), experimental evidence was found that Li diffusion occurs via two different mechanisms, as interstitial and as species occupying regular metal sites. The incorporation of Li on interstitial as well as metal sites in forsterite was also confirmed by quantum mechanical methods and significant fractionation of Li isotopes between these two sites was predicted (Zhang and Wright 2012). Such a behavior has not been recognized for any other element, apart from H diffusion in melts (Wasserburg 1988; Zhang et al. 1991) or olivine (Kohlstedt and Mackwell 1998). It seems to be a general phenomenon that ions with small charge and small radius can penetrate into ionic crystals interstitially. The presence of two diffusion mechanisms can produce very unusual profile shapes for Li but also produces isotopic fractionation effects that are less straightforward to interpret compared to the simple case illustrated in Fig. 4.13. This is worth exploring here in more detail. Apparently oxygen fugacity is a critical parameter in that respect. The step-like diffusion profiles for Li in olivine (Fig. 4.9) and orthopyroxene (Fig. 4.11) with a spiky δ^7Li anomaly is characteristic for two diffusion mechanisms.

4.3.4.1 Two Species Diffusion Model

The step profiles were successfully modeled by Dohmen et al. (2010) considering two diffusing Li species in olivine and their model was adapted by Richter et al. (2014) for clinopyroxene (solid lines in Figs. 4.9 and 4.11). Dohmen et al. (2010) assumed two different sites that Li can occupy: Li on the metal site, Li_{Me}, and Li on the interstitial site, Li_i. They further assumed that Li_i is more mobile than Li_{Me} and that Li prefers the metal site, hinging mostly on more favorable energetic stability. Since olivine contains a certain number of vacancies on the metal site, V_{Me} (number of which is relatively well known; Nakamura and

Schmalzried 1983; Dohmen and Chakaraborty 2007), Li_i in a site adjacent to V_{Me} can jump into this vacancy and thereby form a Li_{Me}, as can be described by the following homogeneous reaction between these three point defects:

$$V_{Me} + Li_i = Li_{Me}. \tag{4.3.10}$$

Assuming Henry's law and defining as the reference state for the point defect j one point defect per formula unit of the mineral (M_2SiO_4 or $CaMSi_2O_6$) × 10^6, ppm atomic formula unit (hereafter referred to as ppm afu), the corresponding mass action law to Reaction 4.3.10 is obtained:

$$K(P,T) = \frac{[Li_{Me}]}{[V_{Me}] \cdot [Li_i]}, \tag{4.3.11}$$

where $[j]$ denotes the concentration of species j in ppm afu. Because of this reaction the diffusion equation (Eq. 4.3.4) has to be extended by a reaction term since each of the three relevant species, V_{Me}, Li_i, and Li_{Me}, can be formed or destroyed over time, which is controlled by the equilibrium constant of reaction 4.3.10. Thus, the governing equations for simulating the observed Li diffusion profiles in olivine and clinopyroxene are a coupled set of diffusion equations with j = {V_{Me}, Li_i, and Li_{Me}}:

$$\frac{\partial C_j}{\partial t} = D_j \cdot \frac{\partial^2 C_j}{\partial x^2} + R_j, \tag{4.3.12}$$

where R_j is the rate of production/destruction of diffusing species j. The coupled sets of diffusion equations were solved numerically using the method of finite differences with the assumption that at each grid point, local equilibrium of reaction 4.3.10 was attained within each time step of the calculation (Dohmen et al. 2010; Richter et al. 2014).

4.3.4.2 Modeling Results—Sensitivity to fO_2

Due to the complexity of Li diffusion in various silicates the observed zoning of Li and its isotopes can be strongly variable and depends not only on a single Li diffusion coefficient, but is very sensitive to the initial vacancy and Li concentrations, the equilibrium constant K (Eq. 4.3.11), and the new vacancy and Li concentrations imposed at the rim, as defined by the chemical environment (the initial and boundary conditions of the diffusion problem). To obtain the unique behavior that Li penetrates into the crystal in the form of a front with an almost constant concentration and a sharp drop to the initial concentration behind it, the set of parameters has the following two constraints for the diffusive fluxes and the equilibrium constant: $J_{Li_i} \gg J_{Li_{Me}}$ and $K \gg 1$. The first constraint implies that $D_{Li_i} \gg D_{Li_{Me}}, D_{V_{Me}}$ but also that the boundary conditions (rim compositions) impose certain concentration gradients of the three point defects (Dohmen et al. 2010). Therefore, the overall diffusion behavior of Li in clinopyroxene and olivine can drastically change depending on the chemical environment, in particular the oxygen fugacity and the Li source.

For brevity, we will not explain these features in detail, but the more interested reader can follow the discussions in Dohmen et al. (2010) and Richter et al. (2014). Here, our aim is to illustrate various consequences of these two mechanisms for the rate of diffusive equilibration, diffusive fractionation and for the profile shapes that could be observed in natural crystals. In Fig. 4.15 we show strongly variable profile shapes and fractionation of δ^7Li by varying just the vacancy concentrations at the rim (see also Dohmen et al. 2010 or Richter et al. 2014 for other examples). In all cases we used the following set of parameters, $D_{Li_{Me}} = D_{V_{Me}} = D_{Li_i}/100$ and K = 100, consistent with the experimental observations of Dohmen et al. (2010) and Richter et al. (2014), initially homogenous vacancy concentrations of 50 ppm afu and Li of 21 ppm afu (equivalent to ~1 μg/g in olivine and ~0.7 μg/g in clinopyroxene), and a fixed concentration for Li at the rim of 84 ppm afu (equivalent to ~4 μg/g in olivine and ~2.8 μg/g in clinopyroxene).

Since we fixed the equilibrium constant and the total Li content at the rim, we can change the

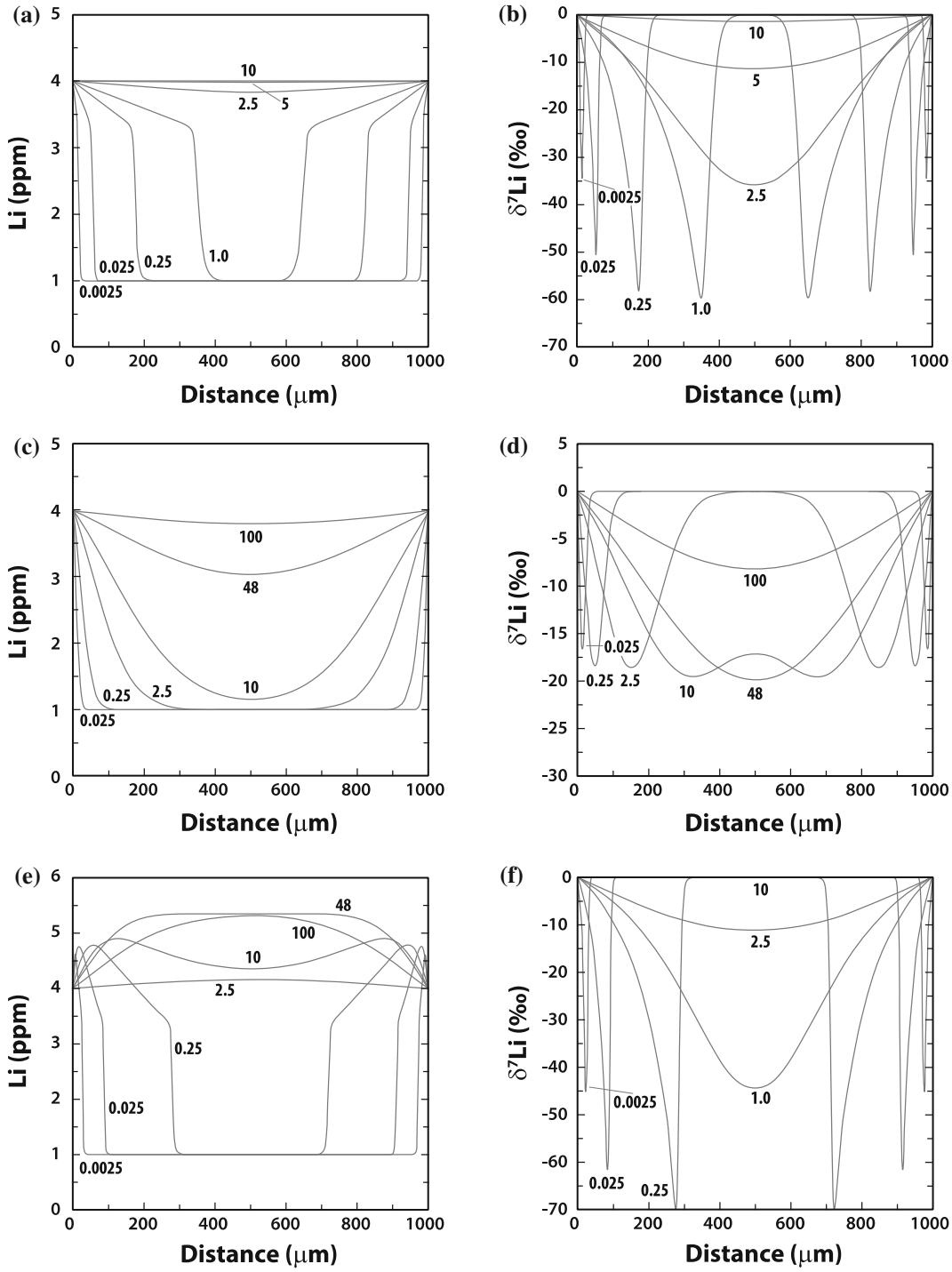

Fig. 4.15 Simulated profiles using the two species diffusion model (Dohmen et al. 2010) for various different vacancy concentrations at the rim, showing that Li diffusion and associated isotopic fractionation strongly depends on the chemical environment as defined by, e.g., the fO_2. **a** and **b**: $[V_{Me}]$ = 0.05 ppm afu; **c** and **d**: $[V_{Me}]$ = 10 ppm afu; **e** and **f**: $[V_{Me}]$ = 0.01 ppm afu. The numbers on the curves denote Dt/l^2 where l is the half diameter of the plane sheet

relative concentrations of Li_i and Li_{Me} by just varying the rim concentration of the vacancies. For example in case (i), for a value of $[V_{Me}]$ = 0.05 ppm afu at the rim, step-like profile shapes are obtained (Fig. 4.15a) and corresponding isotopic fractionation patterns are created (Fig. 4.15b) that are equivalent to those found by Richter et al. (2014). For times where the Li concentration is effectively equilibrated (Dt/l^2 = 2.5 or 5), there is still a significant isotopic anomaly present (down to –30 or –10 ‰, respectively). In case (ii), when we increase $[V_{Me}]$ at the rim to a value of 10 ppm afu, we obtain "normal" profile shapes for both [Li] and δ^7Li (compare Fig. 4.15c–d with Fig. 4.7), and the isotopic anomalies are smaller by a factor of 2–3 than in the former case. However, again, the isotopic anomaly is still present after a critical time where with the common analytical methods a concentration gradient would be not resolvable. The most interesting and counterintuitive case (iii) occurs when we decrease $[V_{Me}]$ to a value of 0.01 (Fig. 4.15e–f). Here, the shape of the Li concentration profile develops in a very complex way, but the δ^7Li profile looks very similar to the case shown in Fig. 4.15b. The concentration of Li decreases towards the rim, but the time evolution of the profile records Li diffusion into the grain. This is also evident from the isotopic fractionation, since the grain becomes lighter within the diffusion zone, showing the case of an uphill diffusion process. Contrary to the previous cases, after a certain time the isotopic ratio is homogeneous whereas there is still a significant concentration gradient present for Li.

The three different cases illustrated above have also been directly observed in experiments with olivine and clinopyroxene: case (i) and (ii) in Dohmen et al. (2010) and Richter et al. (2014), where the different behavior was observed depending on the redox conditions or type of Li reservoir used in the experiments; case (iii) has been observed in an unpublished study on Li diffusion in clinopyroxene (Liu, Marschall, Gaetani, pers. communication to RD, 2014). Most importantly, Richter et al. (2014) were able to reproduce Li and δ^7Li profiles for case (i) and (ii) simultaneously with the same set of parameters (the same β value) but different boundary or initial conditions. The model is relatively simple considering the broad range of different observations it can reproduce.

Based on the simulations with the two species model, Dohmen et al. (2010) concluded that Li_i only becomes relevant if Li concentrations were present in olivine that exceeded typical Li natural concentrations (>10 μg/g). However, the simulations presented in Fig. 4.15 with this model suggest that even for a reasonable range of Li and vacancy concentrations, quite variable net diffusion rates and isotopic fractionations can be expected that are related to the presence of Li_i. A critical thermodynamic parameter appears to be the fO_2, which strongly affects the concentrations of vacancies on the metal site (Nakamura and Schmalzried 1983; Dohmen and Chakraborty 2007). The profile shapes of Li and δ^7Li measured in natural olivine and clinopyroxene do not indicate that the interstitial diffusion mechanism was relevant in these cases. Eventually, more experimental data and detailed spatially-resolved measurements in natural samples are required to resolve this issue. From mantle xenoliths, relative diffusion rates of Li in olivine and clinopyroxene were inferred. According to these data clinopyroxene is faster than olivine by a factor of about 10, which is much smaller than the factor ∼1000 predicted by the relations of Coogan et al. (2005) and Dohmen et al. (2010). This apparent discrepancy could be explained by the two species mechanism and their sensitivity to fO_2 as discussed above.

Because of the complex diffusion behavior of Li one should be very cautious with the interpretation of Li isotopic data. The numerical and experimental examples discussed show that some of the common assumptions for the interpretation of isotopic data have to be abandoned:

(i) Homogeneous Li concentration + negative or positive δ^7Li anomaly does not imply that δ^7Li has been not affected by solid-state diffusion. Note that in this case the δ^7Li gradient can be relatively small and not well resolved with common analytical methods.

(ii) A negative Li concentration gradient towards the rim does not necessarily imply Li loss from the mineral. Here, the δ^7Li profile can help if Li diffused into or out of the mineral.

(iii) Finally, Li is a special case because of the two-species mechanism where both cases may occur: faster equilibration of the isotopes or faster equilibration of the chemical composition.

Independent of these complexities, if the mineral stayed long enough at some critical temperature the memory of the crystal in terms of Li concentration and δ^7Li will be lost and the crystal becomes homogeneous for both quantities. The time to reach this point depends for the two-species model also on the boundary conditions (as indicated by the numbers on the curves in Fig. 4.15) and is significantly different from a simple diffusion problem (Fig. 4.13).

4.3.5 Bulk Diffusion of Li Through Rocks and Characteristic Length Scales

Measurements of Li isotopes across traverses in country rocks indicate that Li diffusion through bulk rocks affects the compositions of rocks on the outcrop scale (e.g., Teng et al. 2006). Diffusion in a multi-phase polycrystalline rock is in principle a complex process, but it can be mathematically shown that after some critical time diffusion through such systems can be characterized by a single bulk diffusion coefficient (e.g., Hashin and Shtrikman 1963; Kaur et al. 1995). Here one speaks of the Type A diffusion regime (e.g., Dohmen and Milke 2010) and this critical time is roughly defined by the time to equilibrate an individual grain by diffusion. For an average grain radius 'a', this time is equivalent to t_{max} as defined above, but using the diffusion coefficient for the mineral with the lowest D. The bulk diffusion coefficient is a weighted average of the diffusion coefficients of the various minerals and those for the grain and interphase boundaries, which are fast diffusion paths. The weighting includes the volume fraction of the diffusion media and the detailed texture (e.g., grain size, crystallographic preferred orientation, etc.; Hashin and Shtrikman 1963; Brady 1983; Dohmen and Milke 2010). However, if the modal composition of a rock is dominated by one mineral (e.g., by plagioclase in basalt and gabbro or olivine in a peridotite xenolith) we can use the respective D and average grain size to calculate a first approximation for the bulk diffusivity, as follows (modified Hart equation from Mortlock 1960):

$$D_{bulk} = D_l \cdot \left[1 + b\frac{s\delta}{2a} \cdot \left(\frac{D_{gb}}{D_l} - 1\right)\right], \quad (4.3.13)$$

where D_l is the diffusion coefficient of the mineral, D_{gb} is the grain boundary diffusion coefficient, s is the segregation coefficient, which is equivalent to the mineral–grain boundary partition coefficient, δ is the width of the grain boundary (typically on the order of nanometers), and b is a geometric factor that considers the detailed texture, which is on the order of 2–3 in most cases. The grain boundary diffusion coefficient is usually several orders of magnitude larger than D_l but, due to the small grain boundary width, the overall contribution of grain boundaries to the bulk diffusivity is very small if there is not a strong tendency of the element to segregate into the grain boundary (e.g., as predicted for strongly incompatible elements; Dohmen and Milke 2010). We use Eq. 4.3.13 to calculate the bulk diffusivity through an olivine and a plagioclase dominated rock, each with an average grain radius of 100 μm, and to estimate the spatial scale on which a bulk rock can be affected by diffusion (Fig. 4.16). This length scale is calculated from the simple relation, $d = 4(D_{bulk}t)^{0.5}$. These simplified calculations show that, for plagioclase-dominated rocks and $T > 800$ °C, Li isotopes could be affected over km scales. At even higher temperatures around 1000 °C Li isotopic compositions of olivine-dominated rocks could be affected by diffusion at outcrop scales.

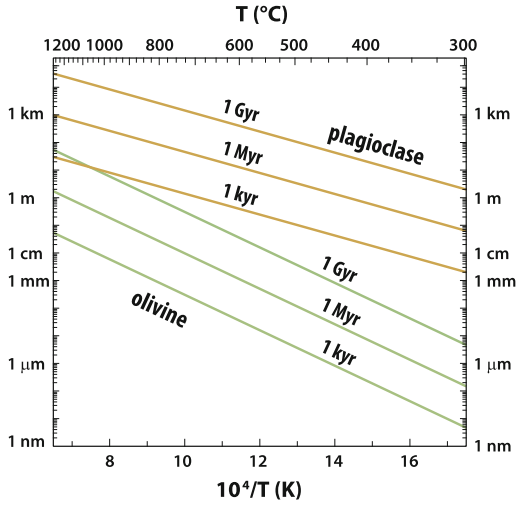

Fig. 4.16 Characteristic length scales of Li diffusion through bulk rocks dominated by either olivine or plagioclase with an average grain size of 100 µm

4.4 Fluid-Rock Interaction

To understand the effects of fluid–rock interaction on Li and its isotopes a number of experiments at low temperatures (25–375 °C) were performed with different starting materials. In most of these studies interaction between basalt and seawater was investigated (e.g., Seyfried et al. 1984; Berger et al. 1987, 1988; Seyfried et al. 1998; James et al. 2003; Millot et al. 2010; Wimpenny et al. 2010; Verney-Carron et al. 2011; Brant et al. 2012) in order to most faithfully reproduce conditions during low-temperature seafloor weathering and alteration by hot vent fluids. In addition, weathering of terrigenous sediments (Chan et al. 1994; You and Gieskes 2001; James et al. 2003), granite (Pistiner and Henderson 2003), and olivine (Berger et al. 1988; Wimpenny et al. 2010) were studied experimentally to investigate associated isotopic fractionation of Li.

The alteration experiments are in some sense not fundamentally different from the experiments to measure equilibrium partitioning between minerals and fluid discussed above, but since they did not reach thermodynamic equilibrium, the measured isotopic composition is strongly dependent on the reaction progress. There are several possible experimental setups but the most typical approach of alteration experiments is to mix the solid material as a powder with water and anneal the sample inside a closed container at the desired temperature and pressure for variable times. The flexible cell hydrothermal solution equipment (Seyfried et al. 1979, 1987) or a modified Prolabo hydrothermal apparatus (Berger et al. 1987) allows periodic sampling of the fluid to monitor the reaction progress without quenching the sample. The fluid is usually filtered before analysis. Containers of the sample material are mostly Teflon bottles, Teflon bombs or Au capsules in a hydrothermal bomb. Critical experimental parameters for the reaction path and reaction progress in addition to the solid starting material, P and T, are the fluid/rock ratio, the solid surface to fluid volume ratio, and the starting composition of the fluid since it controls the stable (or metastable) mineral assemblage as well as the timing of the formation of secondary minerals. For example, in a closed system at relatively low fluid/rock ratio the solution is more quickly saturated with secondary minerals due to dissolution (congruent or incongruent) of the solid material. Alternatively, mixed flow-through reactors are used (Wimpenny et al. 2010) to inhibit saturation of secondary minerals and investigate primarily mineral dissolution processes. Yet another experimental approach was applied by Pistiner and Henderson (2003) to investigate surface sorption of Li on secondary minerals (smectite, gibbsite, ferrihydrite) and associated stable isotopic fractionation: the powder of each mineral was immersed in NIST L-SVEC solution at room temperature for various lengths of time. A complete list of experimental studies with their specific conditions is given in Table 4.5.

The experimental results are summarized in more detail below for the different starting materials and experimental approaches. The solid reaction products are rarely investigated in detail, mostly using X-ray powder diffraction (XRD) or, sometimes, transmission electron microscopy (TEM).

4.4.1 Weathering of Igneous Rocks (Predominantly Basaltic Compositions)

In a series of papers the behavior of Li during weathering of natural and synthetic basalt at temperatures between 25 and 350 °C was investigated (Seyfried et al. 1984, 1998; Berger et al. 1987, 1988; James et al. 2003; Millot et al. 2010; Wimpenny et al. 2010; Verney-Carron et al. 2011; Brant et al. 2012). The modal composition of the basalt, especially the amount of glass, is assumed to have an effect on the reaction products and reaction progress (Brant et al. 2012) because different solid materials react in different ways with water and presumably have different reaction rates and fractionation effects with respect to Li. Most studies used basaltic glass (synthetic or natural) as starting material (see Table 4.5).

Pioneering experimental studies (e.g., Hajash 1975; Seyfried and Bischoff 1979; see also a review by Seyfried 1987) have shown that during weathering of basalt Mg is removed from seawater, and that Ca, Na, and K are leached from basalt, which is related to the formation of palagonite (the amorphous precursor material of smectite), chlorite, and clay minerals (mostly smectite). At temperatures ≤ 70 °C smectite is probably formed but is difficult to detect using XRD because of its small amount and poor crystallinity, as also indicated from TEM investigations (e.g., Millot et al. 2010). The water to rock ratio basically controls the amount of secondary mineral formation. The amount of Mg in the reacting water is also critical for the alteration process. For example, in the absence of dissolved Mg, epidote and plagioclase are the dominant secondary phases instead of smectite or chlorite (Seyfried and Mottl 1982).

With increasing temperature, alteration of basalt becomes more efficient, resulting generally in higher degree of leaching of Li (and Cs, Rb and B) out of the basaltic glass As a consequence, these elements become progressively enriched in the fluid (e.g., James et al. 2003; Millot et al. 2010). The experimental runs are usually quenched when the concentrations in the fluid do not change considerably, which is interpreted as an attainment of a steady state for the reaction system. Berger et al. (1987, 1988) documented the leaching process in glass in more detail by experiments with basaltic glass slabs and powder as starting materials for different extent of compaction. The chemical composition was studied across the sections of the altered samples. The altered rim of the slab had chemical concentration gradients for major elements and also Cs (Li and Rb were not measured) where cations were removed relative to SiO_2. The concentration profiles of major elements and H indicated that reaction progress was controlled by diffusion through the bulk glass (solid state diffusion) in the early stage accompanied later by diffusion of aqueous species in a porous gel layer, which recrystallized continuously. The amorphous silicate gel formed was interpreted to be a precursor for crystalline clays in a later stage. Based on these observations Berger et al. (1987) proposed a four-stage reaction model (see also Fig. 1 of Berger et al. 1994).

It is important to emphasize that the alteration of basalt can be conceptually seen as a combination of two fundamental mechanisms: (i) leaching of the glass (or congruent or incongruent dissolution), and (ii) secondary mineral formation (precipitation). Each of these two mechanisms plays its role in partitioning of Li and its isotopes between the solid and fluid phase. Leaching of the glass produces a flux of Li into the fluid, but during formation of a secondary mineral Li is repartitioned between fluid and solid; this depends on its partition coefficient and the initial Li content in the fluid and the solid. The distribution of Li may not reflect equilibrium partitioning between the bulk fluid and mineral, because it depends on the precipitation rate of the newly formed solids relative to the homogenization rate of the fluid by diffusion and convection. Indeed, relatively slow transport in the fluid could also be responsible for the nucleation of metastable secondary phases (see Ruiz-Agudo et al. 2014 and references therein). In that case an apparently higher partition coefficient for Li between phases needs to be considered.

Table 4.5 List of experimental studies with their specific conditions

Reference	Starting materials					Experimental conditions								Product analysis			Comments	
	Solid	Grain size (μm)	Li (mg/g)	Fluid	Li (ng/g)	S/V (1/cm) surface area/volume of solution	w/r	pH	T (° C)	P (MPa)	Total run duration (h)	Container material	Exp. setup	Solid	Secondary minerals identified	d7Li measured		
Brant et al. (2012)	^{6}Li doped MORB glass powder	63–250	20	IAPSO std seawater	8.90		9.2–9.4	5.7[a]	125	0.23	1986	Ti	Hydrothermal reaction vessel	n.a.		Fluid	Larger depletion of Mg, SO_4	
	^{6}Li doped MORB powder, partly crystallized (200 ° C/min)	63–250	20	IAPSO std seawater	8.90		9.2–9.4	5.6[a]	125	0.23	1986	Ti	Hydrothermal reaction vessel	n.a.		Fluid	Similar texture but smaller plag grains at rapidly cooled MORB	
	^{6}Li doped MORB powder, partly crystallized (30 ° C/min)	63–250	20	IAPSO std seawater	8.90		9.2–9.4	5.5[a]	125	0.23	1986	Ti	Hydrothermal reaction vessel	n.a.		Fluid		
Verney-Carron et al. (2011)	Li enriched synthetic basaltic glass powder	40–100	8950	Pure water	0	0.7[b]	1200	8.3	90	sat.	0.5–96		Savillex(R) PTFE reactor	n.a.		Fluid		
		40–100	8950	Pure water	0	0.7[b]	1200	8.3	50	sat.	6–48		Savillex(R) PTFE reactor	n.a.		Fluid		
		40–100	8950	Pure water	0	7.4, 0.7[b]	120, 1200	8.3	90	sat.	24–1512		Savillex(R) PTFE reactor	n.a.		Fluid		
		40–100	8950	0.001 M HCl	0	0.7[b]	1200	3	90	sat.	2–816		Savillex(R) PTFE reactor	n.a.		Fluid		
		40–100	8950	0.0001 M NaOH	0	0.7[b]	1200	10	90	sat.	2–816		Savillex(R) PTFE reactor	n.a.		Fluid		
Seyfried et al. (1984)	Tholeitic basaltic glass powder	<62	7	Seawater	190		10	5–7	150	50	3564	Au	Dickson hydrothermal apparatus	XRD	Smectite, anhydrite	n.a.		
	Fresh diabase powder	<62	5	Na–K–Ca–Cl-fluid	0		1, 2, 5	n.a.	375	40	1541–2041	Ti	Dickson hydrothermal apparatus	XRD	Smectite, chlorite, actinolite, albite	n.a.		
Seyfried et al. (1998)	Weathered basalt powder (cryst.)	n.a.	8.2	Na–K–Ca–Cl-fluid	0		2	5–5.5	350	50	893	Au	Flexible cell hydrothermal	XRD	Albite, Ca-zeolite, chlorite, smectite	Fluid	Initially ^{7}Li more efficiently leached than ^{6}Li	
Berger et al. (1987)	Tholeitic basaltic glass powder	135–360	8.2	Synthetic seawater (lowered Mg, Ca, and sulfate conc.)	0	4[c]	25	4[a]	200	sat.	23	Pt	Prolab hydrothermal apparatus	XRD, EMPA, STEM	Smectite, chlorite	n.a.	H depth profiles NRA	
		135–360	8.2		0	4[c]	25	3.5[a]	260	sat.	22	Pt	Prolab hydrothermal apparatus	XRD, EMPA, STEM	Smectite	n.a.	H depth profiles NRA	
		135–360	8.2		0	4[c]	25	3–4[a]	320	sat.	20	Pt	Prolab hydrothermal apparatus	XRD, EMPA, STEM	Smectite	n.a.	H depth profiles NRA	

(continued)

Table 4.5 (continued)

Reference	Starting materials					Experimental conditions								Product analysis			Comments	
	Solid	Grain size (μm)	Li (mg/g)	Fluid	Li (ng/g)	S/V (1/cm) surface area/volume of solution	w/r	pH	T (°C)	P (MPa)	Total run duration (h)	Container material	Exp. setup	Solid	Secondary minerals identified	d7Li measured		
Berger et al. (1988)	Li–Sc forsterite (syn.) powder	3–10	3250	Synthetic seawater (lowered Mg and sulfate conc.)	n.a.	5	–	4	260	sat.	17	Pt	Prolab hydrothermal apparatus			n.a.		
Berger et al. (1988)	Basaltic glass slab	–	33,000	10^{-4} M HCl solution	0	1.50E−02	–	4	200	sat.	21	Pt	Prolab hydrothermal apparatus	XRD, EMPA	Hydrated silicate gel	n.a.		
Berger et al. (1988)	Basaltic glass slab	–	33,000	10^{-4} M HCl solution	0	6.00E−04	–	4	300	sat.	3.5	Pt	Prolab hydrothermal apparatus	XRD, EMPA	Hydrated silicate gel	n.a.		
James et al. (2003)	Terrigeneous sediments (fine grained turbidites and hemipelagic muds) multi-phase (quartz, feldspars, lithic fragments (volcanic + mica)	–	40.8	Synthetic seawater (lowered Mg and sulfate conc.)	10	–	4	4.3–7.2	22–350	40	742	Au	Flexible cell hydrothermal	n.a.	–	Fluid	Stepwise heating	
James et al. (2003)	Basaltic powder (hyapilitic texture, plag + cpx, 3 % ol, 3 % glass, 10 % opaque minerals)	–	4.3	Synthetic seawater (lowered Mg and sulfate conc.)	21	–	4	5.3–8.6	22–350	40	737	Au	Flexible cell hydrothermal	n.a.	–	Fluid	Stepwise heating	
Millot et al. (2010)	JB-2 tholeitic basalt powder	–	7.8	Seawater IRMM BCR-403 diluted to 60 % with H_2O	100	–	10	n.a.	25	sat.	245	PFA beaker	Oven	TEM, FTIR, XRD	Unknown	Fluid + solid		
		–	7.8		100	–	10	n.a.	75	sat.	245	PFA beaker	Oven	TEM, FTIR, XRD	Unknown	Fluid + solid		
		–	7.8		100	–	10	n.a.	200	sat.	7	PTFE bomb	Oven	TEM, FTIR, XRD	Smectite	Fluid + solid		
		–	7.8		100	–	10	n.a.	200	sat.	12	Au	Internally heated pressure vessel	TEM, FTIR, XRD	Smectite	Fluid + solid		
		–	7.8		100	–	10	n.a.	250	sat.	7	Au	Internally heated pressure vessel	TEM, FTIR, XRD	Smectite	Fluid + solid		

(continued)

Table 4.5 (continued)

Reference	Starting materials					Experimental conditions								Product analysis			Comments	
	Solid	Grain size (μm)	Li (mg/g)	Fluid	Li (ng/g)	S/V (1/cm) surface area/volume of solution	w/r	pH	T (°C)	P (MPa)	Total run duration (h)	Container material	Exp. setup	Solid	Secondary minerals identified	d7Li measured		
Wimpenny et al. (2010)	Syn. basaltic glass (similar to MORB)	40–100	40–100	Synthetic, HCl, ionic strength 0.01 mol/kg	0	BET 23,000 cm^2/g	Open system 1.5–4 g/min	2–4	25, 55	atm.	70	Ti	Mixed through-flow reactors	ICP-MS, XRD	Unknown	Fluid + solid	Dissolution experiment	No fractionation detected
	San Carlos olivine	40–120	40–120	Synthetic, HCl, ionic strength 0.01 mol/kg	0	BET 800 cm^2/g	Open system 1.5–4 g/min	2–4	25, 55	atm.	80	Ti	Mixed through-flow reactors	ICP-MS, XRD		Fluid + solid	Dissolution experiment	No fractionation detected
	San Carlos olivine	40–120	40–120	Synthetic, HCl, ionic strength 0.01 mol/kg	0	BET 800 cm^2/g	Open system 1.5–4 g/min	10–11	25, 75	atm.	200	Ti	Mixed through-flow reactors	ICP-MS, XRD	Chrysotile	Fluid + solid	Dissolution-precipitation experiment	Fluid ^{7}Li enriched potentially due to preferential enrichment of ^{6}Li into chrysotile
Pistiner and Henderson (2003)	Basalt powder pellet (cryst.): Pl, Ol, Pyx microphenocrysts	–	n.a.	0.8 M $HNCO_3$ solution	0	–	33, 50	n.a.	22, 45	atm	168	–		n.a.		Fluid		
	Basalt powder pellet (cryst.): large Ol phenocrysts, medium grained Pl, Pyx	–	n.a.	0.8 M $HNCO_3$ solution	0	–	33, 50	n.a.	22, 45	atm.	168	–		n.a.		Fluid		
	Granite powder pellet, Qtz, Ap, Pl, oxides, Chl, Ep, Cal	–	n.a.	0.8 M $HNCO_3$ solution	0	–	33, 50	n.a.	22, 45	atm.	168	–		n.a.		Fluid		
Chan et al. (1994)	Shikoku Basin hemipelagic mudstone composed of Qtz, Pl, carbonate, and clay minerals	–	74	Synthetic NaCl–$CaCl_2$ solution, near seawater salinity	0	–	3	n.a.	25–350	80	25.4	Au	Flexible cell hydrothermal	n.a.		Fluid		
		–	74		0	–	3	n.a.	25–350	80	22.5	Au	Flexible cell hydrothermal	n.a.		Fluid	Heating and cooling stage	
You and Gieskes (2001)	Sediment from the decollemnet zone of ODP site 808, Nankai Trough, Japan (Qtz, Pl, carbonate, and clay minerals)	–	74	Synthetic NaCl–$CaCl_2$ solution, near seawater salinity	0	–	3	5–7.3	25–350	80	–	Au	Dickson type rocking autoclave	n.a.		Fluid	6Li doped fluid	Stepwise heating and cooling

[a]pH measured at 25 °C
[b]BET surface area
n.a. not analyzed
[c]Geometric surface area

The effect of rock alteration on δ^7Li of the fluid and the remaining rock is in principle the result of mass balance, equilibrium fractionation and, potentially, kinetic fractionation effects. In the absence of isotopic fractionation and in the case of a mineral–fluid partition coefficient equal to unity, δ^7Li in the fluid can be described by a simple mixing relationship between the fresh rock and the fluid. In the absence of kinetic fractionation effects, the evolution of Li and δ^7Li in the fluid and the alteration product can be modeled from mass balance. During the reaction progress the solid can be separated into reacted and residual unaltered basalt and we obtain the following relationship between the initial and the final Li concentrations from mass balance in a closed system:

$$^6\mathrm{Li}_b^0 \cdot f_b^0 + {}^6\mathrm{Li}_{sol}^0 \cdot f_{sol}^0 = {}^6\mathrm{Li}_b^t \cdot f_b^t + {}^6\mathrm{Li}_{sol}^t \cdot f_{sol}^t + {}^6\mathrm{Li}_{alt}^t \cdot f_{alt}^t \quad (4.4.1)$$

where $^6\mathrm{Li}_b^0$, $^6\mathrm{Li}_{sol}^0$, and f_b^0, f_{sol}^0 are the concentrations of ^{6}Li in the starting basalt and the starting solution and their weight fractions, respectively, and $^6\mathrm{Li}_b^t$, $^6\mathrm{Li}_{sol}^t$, $^6\mathrm{Li}_{alt}^t$, and f_b^t, f_{sol}^t, f_{alt}^t are the concentrations of ^{6}Li in the unreacted part of the basalt, the remaining solution, and the reacted part of the basalt at time t, and their weight fractions, respectively. The weight fractions f_b^0 and f_{sol}^0 can be expressed as a function of the water to rock ratio, w/r: $f_b^0 = \frac{1}{1+w/r}$ and $f_{sol}^0 = \frac{w/r}{1+w/r}$. Assuming that the weight fraction of the fluid stays constant (which is justified for large water/rock ratios in which the mass transfer of H_2O out of the fluid/water into hydrous minerals like smectite or chlorite can be ignored), the concentration of Li in the unreacted part of basalt stays constant, and bulk equilibration between the alteration product and the remaining fluid, described by a partition coefficient, $K_p^6 = \frac{^6\mathrm{Li}_{alt}^t}{^6\mathrm{Li}_{sol}^t}$, we obtain an equation for $^6\mathrm{Li}_{sol}^t$ as a function of the weight fraction of the reacted basalt, f_{alt}^t:

$$^6\mathrm{Li}_{sol}^t = \frac{^6\mathrm{Li}_b^0 \cdot f_{alt}^t + {}^6\mathrm{Li}_{sol}^0 \cdot \left(\frac{w/r}{1+w/r}\right)}{\frac{w/r}{1+w/r} + K_p^6 \cdot f_{alt}^t} \quad (4.4.2)$$

For ^{7}Li we obtain an analogous equation where we introduce in addition the isotopic fractionation factor, $\alpha = \frac{^7\mathrm{Li}_{alt}^t}{^6\mathrm{Li}_{alt}^t} / \frac{^7\mathrm{Li}_{sol}^t}{^6\mathrm{Li}_{sol}^t}$:

$$^7\mathrm{Li}_{sol}^t = \frac{^7\mathrm{Li}_b^0 \cdot f_{alt}^t + {}^7\mathrm{Li}_{sol}^0 \cdot \left(\frac{w/r}{1+w/r}\right)}{\frac{w/r}{1+w/r} + \alpha \cdot K_p^6 \cdot f_{alt}^t} \quad (4.4.3)$$

The amount of reacted basalt, f_{alt}^t, is controlled by the reaction kinetics and, depending on the rate controlling mechanism, is a certain function of time. This simple model ignores the possibility that the altered part of the basalt can be heterogeneous, composed for example of different layers, as observed by Berger et al. (1987). However, even in that case an effective partition coefficient and isotopic fractionation factor can be defined, but it does not reflect thermodynamic equilibrium anymore and these parameters may thus be a function of time. The evolution of f_{alt}^t with t can be described, for example, by a rate law, which is specific for particular operating reaction mechanisms and their rate determining step. Such a rate law containing various relevant parameters (e.g., fluid flux, grain size, temperature) would be necessary to extrapolate the experimental results for different scenarios. From basic kinetic principles it cannot be expected that the results from powder experiments can be applied in a straightforward way to natural rocks (see, for example, Rubie and Thompson 1985).

Using this simple model we can illustrate the effect of various system parameters on the reactive flux of Li and δ^7Li consistent with mass balance and equilibrium partitioning. In Fig. 4.17 we simulate the evolution of [Li] and δ^7Li in the

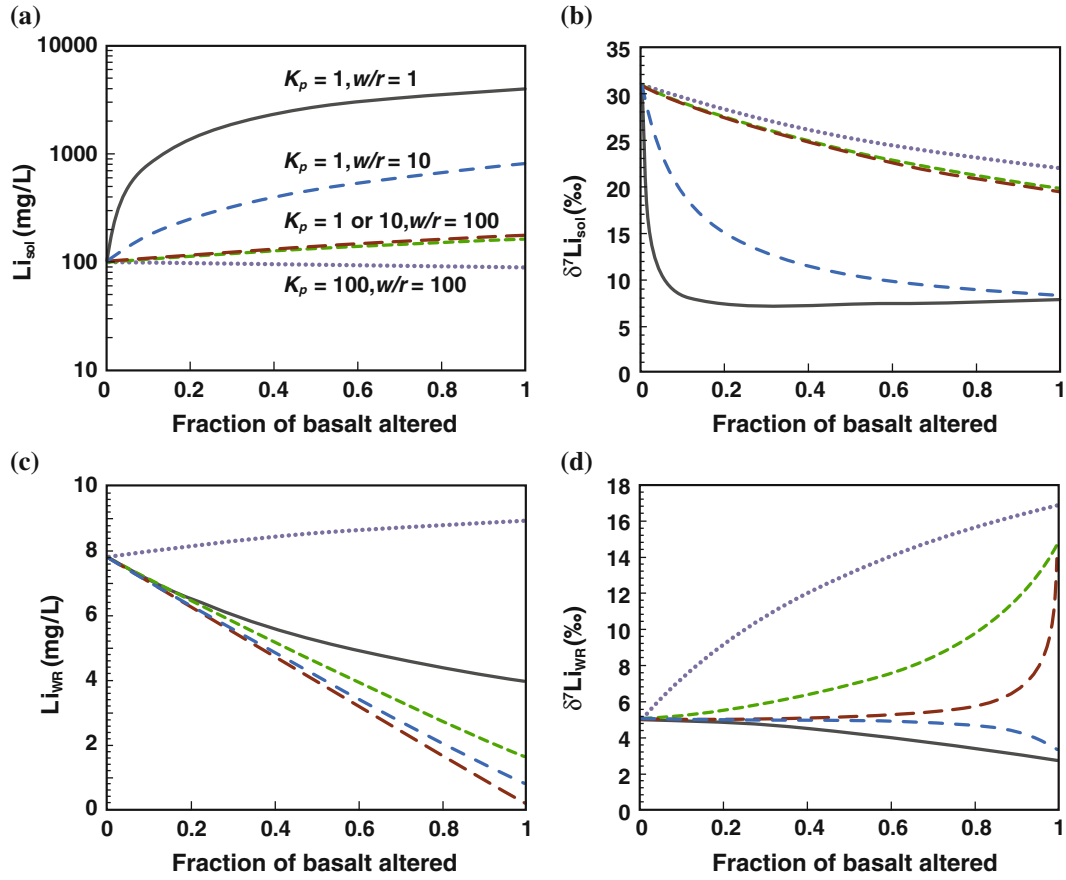

Fig. 4.17 Illustration of the effect of the partition coefficient, K_p, and the water to rock ratio, *w/r*, on the reaction path for Li and δ^7Li in the solution and the bulk rock (altered + fresh basalt) as a function of the fraction of altered rock from the bulk rock. This simulation assumes bulk equilibration between the altered rock and the solution. The values for K_p and w/r are indicated at each line in panel (**a**). The format of corresponding lines in panel (**b**), (**c**), and (**d**) is the same as in panel (**a**). In all cases an isotopic fractionation factor of $\alpha = 0.995$ and the same initial Li and δ^7Li of fluid and basalt were chosen: 100 µg/L and 7.8 µg/g, and δ^7Li = +31 ‰ and δ^7Li = +4.8 ‰

fluid and the bulk rock with reaction progress assuming different values for K_p and *w/r* and constant isotopic fractionation factor $\alpha = 0.995$. This latter value applies to smectite–fluid partitioning at a temperature of ~175 °C (Vigier et al. 2008). According to this simple model four factors control the terminal enrichment of Li in the fluid: the partition coefficient K_p, the reaction progress, characterized here by f^t_{alt}, the initial concentrations of Li in the fluid and the fresh basalt. We can conclude that even though Li is compatible in smectite, the starting fluid in the experiments, similar to seawater, is so dilute with respect to Li that, during reaction and after re-partitioning, Li is still enriched in the fluid.

The pronounced loss of Li into the fluid with increasing temperature observed in experiments could be related to the enhanced reaction progress due to thermally activated kinetic processes (i.e., diffusion). For example, the thickness of the altered rim increases with time and temperature, which could be explained by the strong temperature dependence of the diffusion processes. However, from a general point of view Li is not strongly fluid mobile since the alteration products retain most of the Li as inferred from

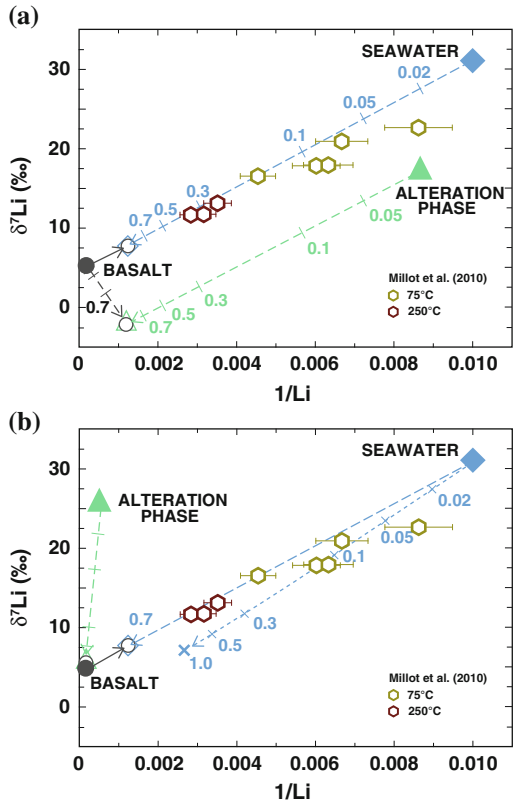

Fig. 4.18 Modeled lithium isotopic compositions of the fluid, alteration phase (smectite), and bulk rock (mixture of altered + fresh basalt) with water to rock ratio of 10 for different stages of the alteration process at **a** 75 °C with $K_p = 1$, α = 0.99, and **b** 250 °C with $K_p = 18$, α = 0.998, according to the experimental partitioning data of Decarreau et al. (2012) and Vigier et al. (2008). *Open diamonds* = fluid; *open circles* = bulk solid; *open triangles* = alteration phase; *dashed lines* = fluid (*blue*) or bulk solid (*black*) composition for a partition coefficient and isotopic fractionation factor α = 1; *open hexagons* = data of Millot et al. (2010) from alteration experiments. Numbers next to the data points indicate the fraction of basalt altered. Note that the reaction path is strongly dependent on the partition coefficient and isotopic fractionation factor, as also illustrated in Fig. 4.17

mineral–fluid partition coefficients of typical alteration products (see Sect. 4.2.4).

The above model assumes bulk equilibration of the alteration product and the fluid, which, especially at low temperature, may be not fulfilled. Alternatively, a Rayleigh fractionation model can be applied assuming successive formation of alteration products (Magenheim et al. 1995). Here the mass balance is applied to each infinitesimal reaction step and after integration one obtains an equation for the concentration of ^{6}Li in solution:

$$^6\mathrm{Li}^t_{sol} = \left(^6\mathrm{Li}^0_{sol} - {}^6\,\mathrm{Li}^0_b/K^6_p\right) \cdot \exp\left(-K^6_p \cdot \left(1 + \frac{r}{w}\right) \cdot f^t_{alt}\right) + {}^6\mathrm{Li}^0_b/K^6_p \quad (4.4.4)$$

For ^{7}Li we obtain an analogous equation:

$$^7\mathrm{Li}^t_{sol} = \left(^7\mathrm{Li}^0_{sol} - {}^7\,\mathrm{Li}^0_b/(\alpha \cdot K^6_p)\right) \cdot \exp\left(-(\alpha \cdot K^6_p) \cdot \left(1 + \frac{r}{w}\right) \cdot f^t_{alt}\right) + {}^7\mathrm{Li}^0_b/(\alpha \cdot K^6_p) \quad (4.4.5)$$

where the same nomenclature as before is used. The same kind of simulations as in Fig. 4.17 using Eqs. 4.4.4 and 4.4.5 show no significant difference between the Rayleigh model and the bulk equilibrium model. Only for high water/rock ratios (>10) marginal differences are observed when the reaction has proceeded to more than 50 %.

The potential effect of temperature was simulated using Eqs. 4.4.4 and 4.4.5 where we have used the experimental calibrations for the equilibrium partition coefficient for smectite–fluid of Decarreau et al. (2012) and the corresponding isotopic fractionation factor of Vigier et al. (2008). The reaction path for δ^7Li of the fluid, alteration phase (smectite), and bulk rock (mixture of altered + fresh basalt) is illustrated in Fig. 4.18. The isotopic fractionation factor and the partition coefficient are important variables driving the evolution of δ^7Li in the fluid and the rock apart from the simple mixing line. In all the simulated cases δ^7Li of the fluid is very sensitive to basalt alteration and decreases with increasing reaction progress. The bulk solid, though, hardly changes unless, for example, at least 50 % of the basalt has been altered for the case simulated in Fig. 4.18a. This drastically different sensitivity to alteration of fluid compared to rock is related to

the about 100 times larger concentration of Li in the basalt compared to seawater, the moderate water to rock ratio, and the small contribution of the altered part of the rock, f^t_{alt}, to the bulk rock composition for low extents of alteration. For higher water to rock ratios and large partition coefficients, a smaller degree of alteration is required to affect δ^7Li in the rock, as can be also seen from Fig. 4.17. The values for δ^7Li deviate from the simple mixing line depending on K_p, α, and reaction progress characterized here by the, f^t_{alt}, the fraction of rock altered. Interestingly, for $K_p = 1$ and $\alpha = 0.99$, δ^7Li of the altered basalt can become lower as a consequence of high/low water to rock ratio and the preference of clay minerals to incorporate light Li (Fig. 4.18a). For higher partition coefficients the altered rock typically becomes heavier. Thus, the effect of temperature according to the experimental partitioning data is two-fold: equilibrium isotopic fractionation tends to increase with decreasing temperature, whereas the behavior of K_p is the opposite. In summary, this results in very different possible scenarios for δ^7Li of the altered rock dependent on temperature and the water to rock ratio.

Data for fluid compositions from the alteration experiments of Millot et al. (2010) are broadly consistent with the above modeling results and plot close to the simple mixing line. However, the data measured at 75 °C seem to be more consistent with the predictions for 250 °C and vice versa. These slight discrepancies could be explained by the uncertainty of the experimental data, but kinetic effects potentially may also play a role here, because these may produce an effective partition coefficient and isotopic fractionation factor different from those applicable at thermodynamic equilibrium. For example, as discussed above, at low temperatures diffusion in the fluid may not be efficient enough to homogenize during secondary mineral precipitation and apparently higher or smaller partition coefficients are obtained. At higher temperatures the mineral–fluid partitioning may be closer to equilibrium but Li diffusion out of the glass becomes more efficient and enhances the levels of ^{6}Li compared to ^{7}Li in the fluid, compensating slightly for the equilibrium fractionation effect. Apparent smectite–fluid partition coefficients for Li calculated from Li contents in fluid and smectite found in the alteration experiments of Berger et al. (1987) are on the order of 10 and 800 at 320 and 200 °C, respectively, which is, at least for 320 °C, similar to the equilibrium partition coefficients measured by Decarreau et al. (2012) for Mg-rich smectite. However, the significantly larger apparent partition coefficient observed at 200 °C further points to disequilibrium partitioning with decreasing temperature.

Another observation of Millot et al. (2010) was that δ^7Li in the fluid ultimately increases with decreasing temperature (compare also with Fig. 4 in Millot et al. 2010). These authors argued that a steady state is reached where dissolution processes (or leaching) and re-precipitation of smectite are balanced. They obtained an apparent trend of Δ^7Li with smectite–fluid pair as a function of T, which was used as a thermometer for hydrothermal alteration of basalt. However, based on the above model the variation of this "steady state" δ^7Li with temperature could be simply explained by a smaller amount of basalt transformed into clay minerals due to more sluggish kinetics of the transformation process. Based on our calculations we would argue that this trend is specific for the experimental conditions (grain size and water to rock ratio) given in Millot et al. (2010) and cannot be applied in general. We further conclude that the "steady state" isotopic composition of the fluid in Millot et al. (2010) does not reflect equilibrium fractionation between solids and fluid and δ^7Li of the fluid would likely evolve further towards equilibrium if the experiments would be extended for sufficiently long times. Interestingly, the T dependence of the apparent $\Delta^7Li_{smectite–fluid}$ of Millot et al. (2010) is similar to the equilibrium fractionation measured by Vigier et al. (2008) for $T > 90$ °C, but the total extent of Li isotopic fractionation is stronger in the former case, which is probably related to the dominant contribution of the unaltered basalt to δ^7Li in the bulk sample (Fig. 4.19).

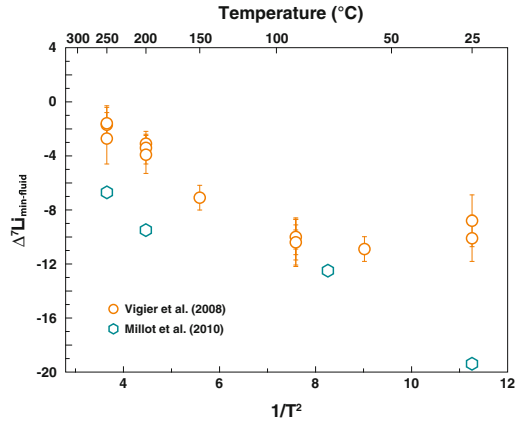

Fig. 4.19 Comparison of equilibrium fractionation of Li isotopes between smectite and fluid of Vigier et al. (2008) with apparent Δ^7Li between bulk rock and fluid from alteration experiments by Millot et al. (2010)

As mentioned above, kinetic fractionation effects, related to diffusion in the fluid, gel, glass, plagioclase, etc., or due to surface exchange reactions, may have an additional impact on δ^7Li in the produced phases. Two experimental studies were dedicated to potential effects of Li diffusion in solid materials (Verney-Carron et al. 2011; Brant et al. 2012). Brant et al. (2012) performed experiments at 125 °C with water to rock ratios of about 9 using crystalline and amorphous material and found surprisingly that Li is extracted more efficiently from the crystalline material. This observation seems to be in contradiction with that of Seyfried et al. (1984), who found that diabase is less reactive compared to basaltic glass at 375 °C and slightly lower water to rock ratios. The efficient leaching of Li out of partly crystallized basalt in Brant et al. (2012) was explained by diffusion of Li out of plagioclase although approximate calculations of the diffusive fluxes show that two orders of magnitude higher diffusion rates than those experimentally observed by Giletti and Shanahan (1997) would be required. Importantly, Li diffusion is supposed to be significantly faster in silicate glasses than in plagioclase at 125 °C (Fig. 4.8) and, as a consequence, leaching of Li out of basaltic glass should be more efficient than leaching out of plagioclase. This problem cannot be resolved without determining the Li concentration profiles in the altered glass and adjacent plagioclase (as in Berger et al. 1987, 1988).

The major element composition of differentiated glasses may also affect the kinetics of the leaching process. If chemical diffusion is responsible for the enhanced reaction rate it should also produce associated isotopic fractionation effects. Since ^{6}Li diffuses slightly faster (see Sect. 4.3) than ^{7}Li out of plagioclase, the plagioclase and, by inference, the bulk rock should become isotopically heavier. This effect was modeled by Brant et al. (2012) assuming a plane-sheet geometry. They concluded that in the temperature range between 350 and 450 °C δ^7Li of basalt could increase by up to 8.7 ‰ within a few hundred years, but for significantly longer times the Li content in plagioclase becomes very small and homogenous. Therefore, this fractionation effect would eventually be erased and δ^7Li of the basalt would become dominated by clinoproxene (see also Fig. 11c in Brant et al. 2012).

In the experimental study of Verney-Carron et al. (2011), leaching of Li out of synthetic basaltic glass was experimentally investigated and discussed in terms of associated kinetic fractionation effects. In these experiments synthetic glass powder doped with 1 % Li_2O was mixed with Li-free pure water at very high water/rock ratios (about 1000) and annealed at 50 and 90 °C for 15 min to 63 days. The main observations of Verney-Carron et al. (2011) were twofold: (i) Li was dissolved at a higher rate compared to Si, and (ii) δ^7Li of the reacted water was lower by up to 5 ‰ compared to the synthetic basalt at the beginning of the experiment and with increasing time approached the value of the fresh basaltic glass. Both observations are consistent with observations made by Wimpenny et al. (2010) in their dissolution experiments and are indicative of diffusive loss of Li, whereby ^{6}Li was leached more efficiently than ^{7}Li. This process was modeled by Verney-Carron et al. (2011) as a combination of diffusion of Li in the glass and dissolution of the leached layer. The latter process imparts a counter effect to δ^7Li compared to the pure diffusion process, since the leached

layer is relatively enriched in ^{7}Li because of the former diffusion process scavenging ^{6}Li. With this combined diffusion–dissolution model Verney-Carron et al. (2011) were able to reproduce the measured evolution of δ^{7}Li and obtained from these fittings the relative diffusion coefficients for both Li isotopes in the basaltic glass, which apparently differed by only 0.02 to 0.1 % at the experimental conditions. They also concluded from these experiments that dissolution rates became more important than diffusion at higher temperatures and eventually diffusion in basaltic glass imparted a minor effect to δ^{7}Li of natural systems.

In the experimental study of James et al. (2003) mostly crystalline basaltic powder was altered at water/rock ratio of 4 stepwise from 51 to 350 °C. The starting solution was prepared such that it resembles fluids estimated to, "recharge sediment and basalt-dominated hydrothermal systems at mid-ocean ridges." This solution lacked Mg and sulfate and as a consequence the formation of smectite or chlorite were potentially inhibited unless Mg would be leached from the basalt as the first major cation. James et al. (2003) observed that after a moderate decrease of Li content in the fluid at T = 150 °C from a starting value of 381 µg/L, its concentration increased continuously up to 790 µg/L at 350 °C. During stepwise cooling the Li concentration of the fluid remained approximately constant. These observations are generally consistent with the experimental study of Seyfried et al. (1984). In parallel to Li abundance, δ^{7}Li first increased during heating from room temperature to 150°C by about 7 ‰ from a starting value of −5.5 ‰ (the starting basalt had δ^{7}Li = +4.6 ‰), and decreased from +1.4 to −0.6 ‰ until the peak temperature of 350 °C was reached. The initial loss of Li from the fluid indicated uptake of Li by secondary mineral formation. According to the mass balance model above, for the experimental conditions of James et al. (2003) an effective partition coefficient of greater than about 100 is required to create this loss assuming a very low degree of alteration (few %). The secondary minerals formed during the experiments of James et al. (2003) are unknown since the solid product was not analyzed after the experiment was terminated. Nevertheless, with increasing temperature it can be expected that alteration proceeds more efficiently and the effective partition coefficient between the fluid and the alteration phases must correspondingly decrease to support the enrichment of Li in the fluid. Such a behavior could be explained by metastable formation of secondary minerals at lower temperatures, as also indicated by the apparent partition coefficient found in Berger et al. (1987).

Since weathered basalt (at T < 150 °C) retains Li in smectite (and Cs preferentially over Rb) and the basaltic glass is already leached with respect to Li (and Cs, Rb), it was speculated by Seyfried et al. (1998), based on observed Cs/Rb, that continuing alteration of the basalt at higher temperatures neither released Li into the fluid nor affected its isotopic composition. Therefore, Seyfried et al. (1998) investigated the alteration of weathered basalt at hydrothermal conditions (350 °C, 500 bars, fluid/rock ratio = 2). The basalt was considered to be altered based on trace element contents (e.g., high Cs/Rb ratio) although X-ray diffraction analysis of the starting material did not identify alteration phases like smectite but only crystalline phases typical of unaltered basalt, mainly plagioclase and clinopyroxene. In analogy to fresh basalt, a significant amount of Li was leached from the weathered basalt and Li isotopes were affected in a complex manner, with increasing δ^{7}Li in the solution in the early stage and a subsequent decrease in a later stage of the experiment (about 1 week). This observation is consistent with that of James et al. (2003), where step-wise heating from 150 °C to higher temperatures also led to the enrichment of Li into the fluid.

Two studies were specifically designed to measure dissolution rates of Li from basaltic glass (Pistiner and Henderson 2003; Wimpenny et al. 2003). Pistiner and Henderson (2003) used two experimental approaches: (i) Powdered crystalline basalt or granite were altered at pH = 0.1 at 25 and 45 °C at water to rock ratios of 33 and 50 for 1 week. (ii) Surface exchange experiments at 22 °C where mineral separates of smectite, gibbsite and ferrihydrite were stirred in

either pure water (for 24 h) or a solution (NIST L-SVEC) with 0.5 mg/L Li and pH = 7 for various times. The general idea of these two setups was to separate the effect of the two competing mechanisms of rock alteration, dissolution and re-precipitation (note that transport through the reacted layer is an additional relevant mechanism, as indicated by Berger et al. 1987, 1988). The acidic composition in the alteration experiment was chosen to prevent the precipitation of new phases, although the water to rock ratio was similar to other alteration experiments (e.g., Berger et al. 1987). Neither the Li concentrations in the reaction products were reported nor secondary minerals identified, but δ^7Li in the product solutions was determined. The partial dissolution of basalt produced δ^7Li in the fluid similar to the starting basalt, but the fluid obtained from granite dissolution was lighter by about 8 ‰ compared to the starting composition of the solid reactant. The result for basalt is in apparent contradiction to Verney-Carron et al. (2011), where at relatively similar experimental conditions the fluid became typically lighter. In the latter study it has also been shown that with increasing time δ^7Li in the fluid approached that of the fresh basalt and this occurred faster for more acidic compositions. Thus, for the very acidic conditions in Pistiner and Henderson (2003) it is reasonable to expect that the basalt dissolves more congruently and kinetic fractionation effects are irrelevant in the leaching of Li from basalt. In addition, in the study of Pistiner and Henderson (2003) mostly crystalline basalt was dissolved and it is unclear if leaching of Li out of crystalline phases occurred as suggested for plagioclase in Brant et al. (2012).

To explain the heavier isotopic composition in the fluid from granite dissolution, Pistiner and Henderson (2003) suggested that pre-existing secondary minerals in the starting material (chlorite, epidote, and calcite) are preferentially dissolved from the granite. For example chlorite has a high Li concentration and, probably, carries a light Li isotopic signature, according to its equilibrium fractionation behavior (see Fig. 4.5). These early endeavors preceded a fuller realization of the potential complexities in interpreting Li isotopic data from these kinds of experiments. Clearly, more carefully designed experiments are needed to understand and quantify the effects of granite alteration on δ^7Li.

Variable fractionation effects for Li isotopes were found in the surface exchange experiments: strong for gibbsite (up to 12 ‰), weak for ferryhydrite (2 ‰), and absent for smectite. This fractionation during physisorption must be clearly distinguished from equilibrium fractionation between the bulk mineral and fluid as for example investigated by Vigier et al. (2008) for smectites. Thus, these experiments cannot reproduce the behavior of Li isotopes during precipitation of alteration phases.

Compared to the study of Pistiner and Henderson (2003), the experimental design of Wimpenny et al. (2010) allowed a clearer separation of the effects of dissolution from secondary mineral formation. In these experiments basaltic glass powder was placed in flow-through reactors with flow rates between 1 and 8 g/min at 25–55 °C and low pH (2–4). Dissolution was incongruent with higher loss of Li, Mg, and Al compared to elements like Na or Ca, which were almost unchanged. Dissolution rates of the basalt were calculated based on the dissolved Si concentration. The concentrations of Li varied depending on pH between 0.03 µg/L and 0.5 µg/L (higher concentrations for lower pH corresponding to higher dissolution rates). No change of δ^7Li (+4.7 ‰) was detected for pH of 4, but for lower pH a slight increase by up to 1.5 ‰ was observed. The δ^7Li in the fluid was slightly lower for all pH values and varied between +2 and +3 ‰. The enrichment of ^{6}Li in the fluid could be explained by its faster diffusion rate in the leached layer of the basaltic glass compared to ^{7}Li, as also demonstrated by Verney-Carron et al. (2011).

4.4.2 Weathering of Olivine (Serpentinization)

In addition to the dissolution of basalt, Wimpenny et al. (2010) investigated the weathering of San Carlos olivine by two different approaches in the flow-through reactor to separate the effects of

dissolution and precipitation. Olivine dissolution experiments used similar experimental conditions (low pH) as for the dissolution of basalt. To allow re-precipitation of secondary minerals, a set of experiments was performed at high pH values (10–11). After the dissolution experiment δ^7Li in the olivine was about +2 ‰, on average heavier compared to the starting value of +1.5 ‰ but similar within broader uncertainties.

During the precipitation experiments at high pH, chrysotile formed as indicated by XRD measurements of the solid products. Related to the successive formation of secondary minerals, δ^7Li in the fluid increased with time from about +2 ‰ up to +12 ‰. According to the experimental study of Wunder et al. (2010) the serpentine phases antigorite and lizardite preferentially incorporate ^{6}Li but chrysotile slightly prefers ^{7}Li because of the lower coordination of Li incorporated in nano pores (see discussion in Sect. 4.2 and Fig. 4.5). Apparently, in the open system and at the low temperature conditions (25 and 75 °C) of Wimpenny et al. (2010), chrysotile shows a different behavior compared to the closed system and 400 °C as used in Wunder et al. (2010).

Berger et al. (1988) altered polycrystalline synthetic Li–Sc-forsterite in seawater devoid of Mg^{2+} and SO_4^{2-} at relatively higher temperatures (150–260 °C). A strong incongruent dissolution was observed at these conditions where the cations Mg^{2+} and Li^+ were dissolved preferentially compared to silica. Based on equilibrium calculations Berger et al. (1988) argued that no secondary phases were formed and hence they concluded that Li and Mg were leached from forsterite by diffusive processes. This statement remains speculative in the absence of analysis of the reacted forsterite. Congruent dissolution of forsterite with re-precipitation of silica gel would be an alternative hypothesis.

4.4.3 Alteration of Sediments

Chan et al. (1994) studied the Li isotopic geochemistry of marine sediments through alteration experiments with hemipelagic mudstone composed of quartz, plagioclase, carbonate, and clay minerals (illite, smectite, kaolinite, and chlorite). The mudstone was reacted with a synthetic NaCl–$CaCl_2$ solution devoid of Mg and near seawater salinity at temperatures from 25 to 350 °C, P = 80 MPa, and a starting fluid/rock ratio of 3. Two sets of experiments were performed with stepwise heating and cooling stages aimed to separate the effect of heating and cooling on the Li exchange process. Similar to the weathering of basalt, Li was progressively lost to the fluid with increasing time and temperature. During cooling the concentration of Li remained stable, indicating irreversible exchange of Li between the sediment and the fluid. The final Li content of the solid was smaller in this type of experiment compared to the heating experiment, consistent with higher Li concentrations in the final fluid. The concentration of Li in the fluid was for both types of experiments significantly higher than in experiments of basalt alteration (on the order of 30,000 µg/L vs. typically 100–1,000 µg/L), which was partly related to the low water/rock ratio but also to the higher initial Li content of the sediment compared to fresh basalt (75 µg/g vs. typically 5–8 µg/g).

In the heating experiment the Li isotopic composition of the first analyzed fluid after ca. 14 days at 97 °C was heavier by 4 ‰ than that of the initial sediment and approached the sediment composition with increasing T and time, corresponding to enhanced reaction progress. Interestingly, in the cooling experiment the fluid started with slightly isotopically heavier Li, and became lighter at 350 °C, similar to the starting solid, while during the cooling it became heavier again by up to 5 ‰. These observations indicate that while the net transfer of Li into the fluid effectively ceased during the longer cooling stage, Li isotopes still exchanged between the fluid and the solids and ^{6}Li became enriched in the solid with decreasing T, consistent with equilibrium fractionation data for clay minerals (Fig. 4.5).

In similar types of experiments at low water/rock ratios, hemipelagic sediments (You et al. 1996), diatomaceous ooze (Thornton and Seyfried 1987), and unaltered marine sediment (Von Damm 1991) were altered and Li released

into the fluid at similar, but slightly lower concentrations than in experiments of Chan et al. (1994). These differences can be explained by the smaller initial Li contents of the solid material. In two experiments, You and Gieskes (2001) altered hemi-pelagic sediment with similar mineral assemblage as in Chan et al. (1994). The fluid composition was also similar to that used by Chan et al. (1994), but in one experiment the starting fluid was heavily enriched with ^{6}Li. As in Chan et al. (1994), the reaction system was heated stepwise to 350 °C and cooled back to room temperature. The observations on the behavior of Li in the undoped experiment were exactly the same as in Chan et al. (1994). In case of the Li-enriched fluid, during the heating stage up to 100 °C no change in the Li concentration was apparent, followed by a depletion of Li and apparent uptake of Li into secondary minerals up to 250 °C. During heating to the final temperature Li was released again to the fluid and the concentration remained stable during cooling. During heating the Li isotopic compositions approached those of the sediments and also remained constant during cooling.

A terrigenous sediment, a mixture of fine-grained turbidites and hemipelagic muds (29 % quartz, 24 % feldspars, 34 % lithic fragments), was reacted with synthetic fluid (devoid of sulfate ions) by James et al. (2003) at fluid/solid ratio of 4 and by applying stepwise heating up to 350 °C. Again, Li was progressively released to the fluid with increasing time and temperature. Consistent with other alteration experiments, δ^{7}Li of the fluid increased (from −5.5 to +6.6 ‰) in the early stages of the experiment at 50 °C and finally yielded a value 2 ‰ lower than that of the unaltered sediment (+1.3 ‰) at the final temperature. This result would be consistent with the observations that at lower temperature ^{6}Li was taken up preferentially by secondary minerals, but with increasing T this preference decreases, as documented above.

Although the general picture for the behavior of Li during the alteration of sediments of various types and mineralogical composition seems to be consistent, it is unclear by exactly which process Li exchange is controlled. In all of these experimental studies the solid reaction products were not investigated and secondary minerals not identified. Based on the evolution of the fluid chemistry You and Gieskes (2001) speculated about the reactions occurring with different components of sediments, decomposition of organic matter, formation of secondary minerals, recrystallization of plagioclase, dissolution of silica, and retrograde alteration. Based on the evidence from basalt alteration experiments, the most relevant process for Li should be represented by the formation of secondary minerals, in particular clay minerals. In addition, exchange with or recrystallization of the initially present clay minerals should be important since they should control the Li budget of the bulk rock. The isotopic exchange observed during the cooling experiment of Chan et al. (1994) indicates that Li exchange between clay minerals and fluid is a very efficient process even at moderate temperatures.

4.4.4 Synopsis

Major elements in bulk rocks and fluids control the type of secondary minerals formed during aqueous alteration. The behavior of Li is mainly controlled by the formation of secondary minerals. However, kinetic fractionation associated with leaching processes out of the rock through diffusion from “fast” diffusion media (e.g., glass or plagioclase) needs to be considered as well. The contribution of leaching appears to be only important in the early stages of the reaction and at lower temperatures. The dissolution process by itself (transition of Li from the surface into the solution) seems to produce no significant isotopic fractionation for Li. However, especially at lower temperatures, non-equilibrium partitioning between secondary minerals and fluid is relevant, which may lead to large apparent mineral–fluid partition coefficients and, from mass balance, significant effects on δ^{7}Li of the bulk rock. In any case, even for large water/rock ratios, a large fraction of the solid needs to be altered to change its δ^{7}Li, whereas the fluid is universally very sensitive to alteration. Depending on the different

contributions of leaching, bulk dissolution and precipitation to the overall alteration process and the types of secondary minerals formed, very different scenarios are possible for the evolution of δ^7Li in the fluid and the altered rock. At the moment no kinetic model exists that fully describes, for example, the alteration of basalt as a function of various relevant input parameters (fluid flux, grain size, input fluid chemistry). Such a model would be required in order to accurately predict the flux of Li and variation of δ^7Li during rock alteration.

References

Adam J, Green T (2006) Trace element partitioning between mica- and amphibole-bearing garnet lherzolite and hydrous basanitic melt: 1. Experimental results and the investigation of controls on partitioning behavior. Contrib Miner Petrol 152:1–17

Aigner-Torres M, Blundy J, Ulmer P, Pettke T (2007) Laser ablation ICPMS study of trace element partitioning between plagioclase and basaltic melts: an experimental approach. Contrib Miner Petrol 153:647–667

Armbruster T, Irouschek A (1983) Cordierites from the Lepontine Alps: Na + Be - > Al substitution, gas content, cell parameters, and optics. Contrib Mineral Petrol 82:389–396

Beattie P (1994) Systematics and energetics of trace-element partitioning between olivine and silicate melts:implications for the nature of mineral/melt partitioning. Chemical Geology 117(1–4):57–71

Beck P, Chaussidon M, Barrat JA, Gillet Ph, Bohn M (2006) Diffusion induced Li isotopic fractionation during the cooling of magmatic rocks: the case of pyroxene phenocrysts from nakhlite meteorites. Geochim Cosmochim Acta 70:4813–4825

Behrens H, Zhang Y (2001) Ar diffusion in hydrous silicic melts: implications for volatile diffusion mechanisms and fractionation. Earth Planet Sci Lett 192:363–376

Bennett S, Blundy J, Elliott J (2004) The effect of sodium and titanium on crystal-melt partitioning of trace elements. Geochim Cosmochim Acta 68:2335–2347

Berger G, Schott J, Loubet M (1987) Fundamental processes controlling the first stage of alteration of a basalt glass by seawater: an experimental study between 200 and 320 °C. Earth Planet Sci Lett 84:431–445

Berger G, Schott J, Guy C (1988) Behavior of Li, Rb, and Cs during basalt glass and olivine dissolution and chlorite, smectite and zeolite precipitation from sea water: experimental investigations and modelization between 50 °C and 300 °C. Chem. Geol. 71:297–312

Berger G, Claparols C, Guy C, Daux V (1994) Dissolution rate of a basalt glass in silica-rich solutions: implications for long-term alteration. Geochim Cosmochim Acta 58:4875–4886

Bindeman I, Davis A (2000) Trace element partitioning between plagioclase and melt: investigation of dopant influence on partition behaviour. Geochim Cosmochim Acta 64:2863–2878

Bindeman IN, Davis AM, Drake MJ (1998) Ion microprobe study of plagioclase-basalt partition experiments at natural concentration level of trace elements. Geochim Cosmochim Acta 62:1175–1193

Blundy J (1997) Experimental study of a Kiglapait marginal rock and implications for trace element partitioning in layered intrusions. Chem Geol 141: 73–92

Blundy J, Dalton J (2000) Experimental comparison of trace element partitioning between clinopyroxene and melt in carbonate and silicate systems, and implications for mantle metasomatism. Contrib Miner Petrol 139:356–371

Blundy JD, Wood BJ (1991) Crystal-chemical controls on the partitioning of Sr and Ba betweenplagioclase feldspar, silicate melts, and hydrothermal solutions. Geochimica et Cosmochimica Acta 55(1):193–209

Blundy J, Wood B (1994) Prediction of crystal–melt partition-coefficients from elastic moduli. Nature 372:452–454

Blundy JD, Falloon TJ, Wood BJ, Dalton JA (1995) Sodium partitioning between clinopyroxene and silicate melts.J Geophys Res 100:15501–15516

Blundy J, Wood B (2003a) Partitioning of trace elements between crystals and melts. Earth Planet Sci Lett 210:383–397

Blundy J, Wood B (2003b) Mineral-melt partitioning of uranium, thorium and their daughters. In: Bourdon B et al (eds) Uranium-series geochemistry. Rev Miner Geochem 52:39–123

Blundy J, Robinson J, Wood B (1998) Heavy REE are compatible in clinopyroxene on the spinel lherzolite solidus. Earth Planet Sci Lett 160:493–504

Bokshtein BS, Bokshtein SZ, Zhukhovitskii AA (1985) Thermodynamics and kinetics of diffusion in solids. Oxonian Press, New Delhi

Bottinga Y, Javoy M (1973) Comments on oxygen isotope geothermometry. Earth Planet Sci Lett 20:250–265

Brady JB (1983) Intergranular diffusion in metamorphic rocks. Am J Sci 283:181–200

Brady JB, Cherniak DJ (2010) Diffusion in minerals: an overview of published experimental diffusion data. In: Zhang Y, Cherniak DJ (eds) Diffusion in minerals and melts. Rev Mineral Geochem 72:899–920

Brant C, Coogan LA, Gillis KM, Seyfried WE, Pester NJ, Spence J (2012) Lithium and Li-isotopes in young altered upper oceanic crust from the East Pacific Rise. Geochim Cosmochim Acta 96:272–293

Brenan JM, Neroda E, Lundstrom CC, Shaw HF, Ryerson FJ, Phinney DL (1998a) Behaviour of boron, beryllium, and lithium during melting and crystallization: constraints from mineral-melt partitioning experiments. Geochim Cosmochim Acta 62:2129–2141

Brenan JM, Ryerson FJ, Shaw HF (1998b) The role of aqueous fluids in the slab-to-mantle transfer of boron, beryllium and lithium during subduction: experiments and models. Geochim Cosmochim Acta 62:3337–3347

Brice JC (1975) Some thermodynamic aspects of the growth of strained crystals. J Cryst Growth 28:249–253

Caciagli N, Brenan JM, McDonough WF, Phinney D (2011) Mineral–fluid partitioning of lithium and implications for slab–mantle interaction. Chem Geol 280:384–398

Cahalan RC, Kelly ED, Carlson WD (2014) Rates of Li diffusion in garnet: coupled transport of Li and Y plus REEs. Am Miner 99:1676–1682

Carslaw HS, Jaeger JC (1959) Conduction of heat in solids. Clarendon Press, Oxford

Chakraborty S (1995) Diffusion in silicate melts. Rev Mineral 32:411–503

Chakraborty S (2008) Diffusion in solid silicates: a tool to track timescales of processes comes of age. Annu Rev Earth Planet Sci 36:153–190

Chan LH, Gieskes JM, You CF, Edmond JM (1994) Lithium isotope geochemistry of sediments and hydrothermal fluids of the Guaymas Basin, Gulf of California. Geochim Cosmochim Acta 58:4443–4454

Charlier BLA, Morgan DJ, Wilson CJN, Wooden JL, Allan ASR, Baker JA (2012) Lithium concentration gradients in feldspar and quartz record the final minutes of magma ascent in an explosive supereruption. Earth Planet Sci Lett 319–320:218–227

Cherniak DJ (2010) Cation diffusion in feldspars. In: Zhang Y, Cherniak DJ (eds) Diffusion in minerals and melts. Rev Mineral Geochem 72:691–733

Cherniak DJ, Watson EB (2010) Li diffusion in zircon. Contrib Mineral Petrol 160:383–390

Chopra R, Richter FM, Watson EB, Scullard CR (2012) Magnesium isotope fractionation by chemical diffusion in natural settings and in laboratory analogues. Geochim Cosmochim Acta 88:1–18

Coogan LA (2011) Preliminary experimental determination of the partitioning of lithium between plagioclase crystals of different anorthite contents. Lithos 125:711–715

Coogan LA, Kasemann SA, Chakraborty S (2005) Rates of hydrothermal cooling of new oceanic upper crust derived from lithium-geospeedometry. Earth Planet Sci Lett 240:415–424

Corgne A, Wood B (2005) Trace element partitioning and substitution mechanisms in calcium perovskites. Contrib Miner Petrol 149:85–97

Corgne A, Liebske C, Wood BJ, Rubie DC, Frost DJ (2005) Silicate perovskite-melt partitioning of trace elements and geochemical signature of a deep perovskitic reservoir. Geochim Cosmochim Acta 69:485–496

Costa F, Chakraborty S (2004) Decadal time gaps between mafic intrusion and silicic eruption obtained from chemical zoning patterns in olivine. Earth Planet Sci Lett 227:517–530

Costa F, Dohmen R, Chakraborty S (2008) time scales of magmatic processes from modelling the zoning patterns of crystals. In: Putirka, KD, Tepley FJ III (eds) Minerals, inclusions and volcanic processes. Rev Mineral Geochem 69:545–594

Crank J (1975) The mathematics of diffusion, 2nd edn. Oxford University Press, Oxford. viii + 414 p

Cunningham GJ, Henderson P, Lowry RK, Nolan J, Reed SJB, Long JVP (1983) Lithium diffusion in silicate melts. Earth Planet Sci Lett 65:203–205

Decarreau A, Vigier N, Pálková H, Petit S, Vieillard P, Fontaine C (2012) Partitioning of lithium between smectite and solution: an experimental approach. Geochim Cosmochim Acta 85:314–325

Dodson MH (1973) Closure temperature in cooling geochronological and petrological systems. Contrib Mineral Petrol 40:259–274

Dohmen R, Blundy J (2014) A predictive thermodynamic model for element partitioning between plagioclase and melt as a function of pressure, temperature and composition. Am J Sci 314:1319–1372

Dohmen R, Chakraborty S (2007) Fe-Mg diffusion in olivine II: point defect chemistry, change of diffusion mechanisms and a model for calculation of diffusion coefficients in natural olivine. Phys Chem Miner 34:409–430

Dohmen R, Milke R (2010) Diffusion in polycrystalline materials: grain boundaries, mathematical models, and experimental data. In: Zhang Y, Cherniak DJ (eds) Diffusion in minerals and melts. Rev Mineral Geochem 72:921–970

Dohmen R, Kasemann SA, Coogan LA, Chakraborty S (2010) Diffusion of Li in olivine. Part 1: Experimental observations and a multiple species diffusion model. Geochim Cosmochim Acta 74:274–292

Einstein A (1905) Über die von der molekularkinetischen Theorie der Wärme geforderte Bewegung von in ruhenden Flüssigkeiten suspendierten Teilchen. Ann D Phys 17:549

Elkins L, Gaetani G, Sims K (2008) Partitioning of U and Th during garnet pyroxenite partial melting: constraints on the source of alkaline ocean island basalts. Earth Planet Sci Lett 265:270–286

Evensen J, London D (2003) Experimental partitioning of Be, Cs, and other trace elements between cordierite and felsic melt, and the chemical signature of S-type granite. Contrib Miner Petrol 144:739–757

Eyring H (1936) Viscosity, plasticity, and diffusion as examples of absolute reaction rates. J Chem Phys 4:283–291

Faak K, Chakraborty S, Coogan L (2013) Mg in plagioclase: experimental calibration of a new geothermometer and diffusion coefficients. Geochim Cosmochim Acta 123:195–217

Fabbrizio A, Stalder R, Hametner K, Günther D, Marquardt K (2013) Experimental partitioning of halogens and other trace elements between olivine,

pyroxenes, amphibole and aqueous fluid at 2 GPa and 900–1,300 °C. Contrib Mineral Petrol 166:639–653

Flynn CP (1972) Point defects and diffusion. Clarendon Press, Oxford

Frei D, Liebscher A, Franz G, Wunder B, Klemme S, Blundy J (2009) Trace element partitioning between orthopyroxene and anhydrous silicate melt on the lherzolite solidus from 1.1 to 3.2 GPa and 1,230 to 1,535 degrees C in the model system Na_2O-CaO-MgO-Al_2O_3-SiO_2. Contrib Miner Petrol 157:473–490

Gaetani G, Kent A, Grove T, Hutchenson I, Stolper E (2003) Mineral/melt partitioning of trace elements during hydrous peridotite partial melting. Contrib Miner Petrol 145:391–405

Gallagher K, Elliott T (2009) Fractionation of lithium isotopes in magmatic systems as a natural consequence of cooling. Earth Planet Sci Lett 278:286–296

Ganguly J (2002) Diffusion kinetics in minerals: Principles and applications to tectono-metamorphic processes. EMU notes in mineralogy, vol 4. Chapter 10:271–309

Ganguly J (2008) Thermodynamics in earth and planetary sciences. Springer-Verlag Berlin Heidelber, p 501

Giletti BJ, Shanahan TM (1997) Alkali diffusion in plagioclase feldspar. Chem Geol 139:3–20

Glicksman ME (2000) Diffusion in solids: field theory, solid state principles and applications. Wiley

Gordillo CE, Schreyer W, Werding G, Abraham K (1985) Lithium in NaBe-cordierites from El Peñón, Sierrra de Córdoba, Argentina. Contrib Mineral Petrol 90:93–101

Grant KJ, Wood BJ (2010) Experimental study of the incorporation of Li, Sc, Al and other trace elements into olivine. Geochim Cosmochim Acta 74:2412–2428

Hajash A (1975) Hydrothermal processes along mid-ocean ridges: an experimental investigation. Contrib Mineral Petrol 53:205–226

Halama R, Savov IP, Rudnick RL, McDonough WF (2009) Insights into Li and Li isotope cycling and sub-arcmetasomatism from veined mantle xenoliths, Kamchatka. Contrib Mineral Petrol 158:197–222

Hanrahan M, Brey G, Woodland A, Altherr R, Seitz H-M (2009) Towards a Li barometer for bimineralic eclogites: experiments in CMAS. Contrib Mineral Petrol 158:169–183

Hart SR, Dunn T (1993) Experimental Cpx–melt partitioning of 24 trace-elements. Contrib Miner Petrol 113:1–8

Hashin Z, Shtrikman S (1963) Conductivity of polycrystals. Phys Rev 130:129–133

Hawthorne FC, Oberti R, Ungaretti L, Grice JD (1992) Leakeite, $NaNa(MgFe^{3+}Li)SiO(OH)$, a new alkali amphibole from the Kajlidongri manganese mine, Jhabua district, Madhya Pradesh, India. Am Mineral 77:1112–1115

Hawthorne FC, Ungaretti L, Oberti R, Bottazzi P, Czamanske GK (1993) Li: an important component in igneous alkali amphiboles. Am Mineral 78:733–745

Hawthorne FC, Ungaretti L, Oberti R, Cannillo E (1994) The mechanism of $^{[6]}$Li incorporation in amphiboles. Am Mineral 79:443–451

Hawthorne FC, Oberti R, Ottolini L, Foord EE (1996a) Lithium-bearing fluor-arfvedsonite from Hurricane Mountain, New Hampshire: a crystal-chemical study. Can Mineral 34:1015–1019

Hawthorne FC, Oberti R, Ungaretti L, Ottolini L, Grice JD, Czamanske GK (1996b) Fluor-ferro-leakeite, $NaNa_2(Fe^{2+}Fe_2^{3+}Li)Si_8O_{22}F_2$, a new alkali amphibole from the Canada Pinabete Pluton, Questa, New Mexico, U.S.A. Am Mineral 81:226–228

Hill E, Wood B, Blundy J (2000) The effect of Ca-Tschermaks component on trace element partitioning between clinopyroxene and silicate melt. Lithos 53:203–215

Huang F, Lundstrom C, Mcdonough W (2006) Effect of melt structure on trace-element partitioning between clinopyroxene and silicic, alkaline, aluminous melts. Am Mineral 91:1385–1400

Icenhower J, London D (1995) An experimental study of element partitioning among biotite, muscovite andcoexisting peraluminous silicic melt at 200 MPa (H O). American Mineralogist 80:1229–1251

Ito J (1977) Crystal synthesis of a new olivine, $LiScSiO_4$. Am Mineral 62:356–361

Jahn S, Wunder B (2009) Lithium speciation in aqueous fluids at high P and T studied by ab initio molecular dynamics and consequences for Li-isotope fractionation between minerals and fluids. Geochim Cosmochim Acta 73:5428–5434

Jambon A, Semet MP (1978) Lithium diffusion in silicate glasses of albite orthoclase and obsidian compositions: an ion-microprobe determination. Earth Planet Sci Lett 37:445–450

James RH, Allen DE, Seyfried WE (2003) An experimental study of alteration of oceanic crust and terrigenous sediments at moderate temperatures (51 to 350 °C): insights as to chemical processes in near-shore ridge-flank hydrothermal systems. Geochim Cosmochim Acta 67:681–691

Jeffcoate AB, Elliott T, Kasemann SA, Ionov D, Cooper K, Brooker R (2007) Li isotope fractionation in peridotites and mafic melts. Geochim Cosmochim Acta 71:202–218

John T, Gussone N, Podladchikov YY, Bebout GE, Dohmen R, Halama R, Klemd R, Magna T, Seitz HM (2012) Volcanic arcs fed by rapid pulsed fluid flow through subducting slabs. Nature Geosci 5:489–492

Johnson OW (1964) One-dimensional diffusion of Li in rutile. Phys Rev 136:A284–A290

Johnson PMS (1967) Hydrogen isotope diffusion. Nature 213:689–690

Johnson OW, Krouse HR (1966) Isotopic mass dependence of Li diffusion in rutile. J Appl Phys 37:668–670

Kaur I, Mishin Y, Gust W (1995) Fundamentals of grain and interphase boundary diffusion. Wiley

Kessel R, Ulmer P, Pettke T, Schmidt MW, Thompson AB (2004) A novel approach to determine high-pressure high-temperature fluid and melt compositions using diamond-trap experiments. Am Mineral 89:1078–1086

Kessel R, Schmidt MW, Ulmer P, Pettke T (2005) Trace element signature of subduction-zone fluids, melts and supercritical liquids at 120-180 km depth. Nature 437:724–727

Kirchner D, Mirwald PW, Schreyer W (1984) Experimenteller Li-Einbau in Mg-Cordierit. Fortschritt Mineral Beih 62:119–120

Klemme S, Dalpe C (2003) Trace element partitioning between apatite and carbonatite melt. Am Mineral 88:639–646

Klemme S, Blundy JD, Wood BJ (2002) Experimental constraints on major and trace element partitioning during partial melting of eclogite. Geochim Cosmochim Acta 66:3109–3123

Kohlstedt DL, Mackwell SJ (1998) Diffusion of hydrogen and intrinsic point defects in olivine. Z Phys Chem 207:147–162

Kowalski PM, Jahn S (2011) Prediction of equilibrium Li isotope fractionation between minerals and aqueous solutions at high P and T: an efficient *ab initio* approach. Geochim Cosmochim Acta 75:6112–6123

Kuzyura AV, Wall F, Jeffries T, Litvin YuA (2010) Partitioning of trace elements between garnet, clinopyroxene and diamond-forming carbonate-silicate melt at 7 GPa. Mineral Mag 74:227–239

Lai Y-J, Pogge von Strandmann PAE, Dohmen R, Takazawa E, Elliott T (2015) The influence of melt infiltration onthe Li and Mg isotopic composition of the Horoman Peridotite Massif. Geochimica et Cosmochimica Acta 164:318–332

Lasaga AC (1979) Multicomponent exchange and diffusion in silicates. Geochim Cosmochim Acta 43:455–469

Latourrette T, Hervig RL, Holloway JR (1995) Trace-element partitioning between amphibole, phlogopite, and basanite melt. Earth Planet Science Lett 135:13–30

Lesher CE (2010) Self-diffusion in silicate melts: theory, observations and applications to magmatic systems. In: Zhang Y, Cherniak DJ (eds) Diffusion in minerals and melts. Rev Mineral Geochem 72:269–309

Liebske C, Corgne A, Frost DJ, Rubie DC, Wood BJ (2005) Compositional effects on element partitioning between Mg-perovskite and silicate melts. Contrib Miner Petrol 149:113–128

Lowry RK, Reed SJB, Nolan J, Henderson P, Long JVP (1981) Lithium tracer-diffusion in an alkali-basaltic melt—an Ion-microprobe determination. Earth Planet Sci Lett 53:36–40

Lundstrom CC (2003) An experimental investigation of the diffusive infiltration of alkalis into partially molten peridotite: Implications for mantle melting processes. Geochem Geophys Geosys 4. doi:10.1029/2001GC000224

Lundstrom CC, Shaw HF, Ryerson FJ, Williams Q, Gill J (1998) Crystal chemical control of clinopyroxene-melt partitioning in the Di-Ab-An system: implications for elemental fractionations in the depleted mantle. Geochim Cosmochim Acta 62:2849–2862

Lundstrom CC, Sutton AL, Chaussidon M, McDonough WF, Ash R (2006) Trace element partitioning between type B CAI melts and melilite and spinel: implications for trace element distribution during CAI formation. Geochim Cosmochim Acta 70:3421–3435

Lynton SJ, Walker RJ, Candela PA (2005) Lithium isotopes in the system Qz-Ms-fluid: an experimental study. Geochim Cosmochim Acta 69:3337–3347

Magenheim AJ, Spivack AJ, Alt JC, Bayhurst G, Chan L-H, Zuleger E, Gieskes JM (1995) Borehole fluid chemistry in Hole 504B, Leg 137: formation water or in-situ reaction? ProcODP Sci Res 137/140:141–152

Manning JR (1968) Diffusion kinetics for atoms in crystals. Princeton (NJ), D. Van Nostrand

Marriott CS, Henderson GM, Belshaw NS, Tudhope AW (2004a) Temperature dependence of delta Li-7, delta Ca-44 and Li/Ca during growth of calcium carbonate. Earth Planet Sci Lett 222:615–624

Marriott CS, Henderson GM, Crompton R, Staubwasser M, Shaw S (2004b) Effect of mineralogy, salinity, and temperature on Li/Ca and Li isotope composition of calcium carbonate. Chem Geol 212:5–15

Martin LA, Wood BJ, Turner S, Rushmer T (2011) Experimental measurements of trace element partitioning between lawsonite, zoisite and fluid and their implication for the composition of arc magmas. J Petrol 52:1049–1075

McDade P, Blundy JD, Wood BJ (2003) Trace element partitioning on the Tinaquillo Lherzolite solidus at 1.5 GPa. Phys Earth Planet Inter 139:129–147

Miller SA, Asimow PD, Burnett DS (2006) Determination of melt influence on divalent elementpartitioning between anorthite and CMAS melts. Geochimica et Cosmochimica Acta 70(16):4258–4274

Millot R, Scaillet B, Sanjuan B (2010) Lithium isotopes in island arc geothermal systems: Guadeloupe, Martinique (French West Indies) and experimental approach. Geochim Cosmochim Acta 74:1852–1871

Mortlock AJ (1960) The effect of segregation on the solute diffusion enhancement due to the presence of dislocations. Acta Metall 8:132–134

Mungall JE (2002) Empirical models relating viscosity and tracer diffusion in magmatic silicate melts. Geochim Cosmochim Acta 66:125–143

Nakamura A, Schmalzried H (1983) On the nonstoichiometry and point defects of olivine. Phys Chem Minerals 10:27–37

Nye JF (1957) Physical properties of crystals. Clarendon Press, Oxford

Oberti R, Cámara F, Ottolini L, Caballero JM (2003) Lithium in amphiboles: detection, quantification, and incorporation mechanisms in the compositional space bridging sodic and ^{B}Li-amphiboles. Eur J Mineral 15:309–319

Oeser M, Dohmen R, Horn I, Schuth S, Weyer S (2015) Processes and time scales of magmatic evolution asrevealed by Fe-Mg chemical and isotopic zoning

in natural olivines. Geochim Cosmochim Acta 154:130–150
Onuma N, Higuchi H, Wakita H, Nagasawa H (1968) Trace element partition between two pyroxenes and the host lava. Earth Planet Sci Lett 5:47–51
Ottolini L, Laporte D, Raffone N, Devidal JL, Le Fevre B (2009) New experimental determination of Li and B partition coefficients during upper mantle partial melting. Contrib Miner Petrol 157:313–325
Parkinson IJ, Hammond SJ, James RH, Rogers NW (2007) High-temperature lithium isotope fractionation: insights from lithium isotope diffusion in magmatic systems. Earth Planet Sci Lett 257:609–621
Pell EM (1960) Diffusion of Li in Si at high T and the isotope effect. Phys Rev 119:1014–1021
Petry C, Chakraborty S, Palme H (2004) Experimental determination of Ni diffusion coefficients in olivine and their dependence on temperature, composition, oxygen fugacity, and crystallographic orientation. Geochim Cosmochim Acta 68:4179–4188
Philibert J (1991) Atom movements: diffusion and mass transport in solids. Les editions de physique
Pistiner JS, Henderson GM (2003) Lithium-isotope fractionation during continental weathering processes. Earth Planet Sci Lett 214:327–339
Putnis A, John T (2010) Replacement processes in the earth's crust. Elements 6:159–164
Richter FM, Liang Y, Davis AM (1999) Isotope fractionation by diffusion in molten oxides. Geochim Cosmochim Acta 63:2853–2861
Richter FM, Davis AM, DePaolo DJ, Watson EB (2003) Isotope fractionation by chemical diffusion between molten basalt and rhyolite. Geochim Cosmochim Acta 67:3905–3923
Richter FM, Mendybaev RA, Christensen JN, Hutcheon ID, Williams RW, Sturchio NC, Beloso AD Jr (2006) Kinetic isotope fractionation during diffusion of ionic species in water. Geochim Cosmochim Acta 70:277–289
Richter FM, Watson EB, Mendybaev RA, Teng F-Z, Janney PE (2008) Magnesium isotope fractionation in silicate melts by chemical and thermal diffusion. Geochim Cosmochim Acta 72:206–220
Richter FM, Watson EB, Mendybaev R, Dauphas N, Georg B, Watkins J, Valley J (2009) Isotopic fractionation of the major elements of molten basalt by chemical and thermal diffusion. Geochim Cosmochim Acta 73:4250–4263
Richter F, Watson B, Chaussidon M, Mendybaev R, Ruscitto D (2014) Lithium isotope fractionation by diffusion in minerals. Part 1: Pyroxenes. Geochim Cosmochim Acta 126:352–370
Roselieb K, Chaussidon M, Mangin D, Jambon A (1998) Lithium diffusion in vitreous jadeite (NaAISi206): an ion microprobe investigation. N Jb Miner Abh 172:245–257
Rubie DC, Thompson AB (1985) Kinetics of metamorphic reactions at elevated temperatures and pressures: an appraisal of available experimental data. In: Thompson AB, Rubie DC (eds) Metamorphic reactions. Kinetics, textures, and deformation. Adv Phys Geochem 4:27–79
Ruiz-Agudo E, Putnis CV, Putnis A (2014) Coupled dissolution and precipitation at mineral–fluid interfaces. Chem Geol 383:132–146
Sartbaeva A, Wells SA, Redfern SAT, Hinton RW, Reed SJB (2005) Ionic diffusion in quartz studied by transport measurements, SIMS and atomistic simulations. J Phys Condens Matter 17:1099–1112
Sasaki J, Peterson NL, Hoshino K (1985) Tracer impurity diffusion in single-crystal rutile (TiO_{2-x}). J Phys Chem Solids 46:1267–1283
Schmidt MW, Connolly JAD, Günther D, Bogaerts M (2006) Element partitioning: the role of meltstructure and composition. Science 312(5780):1646–1650
Schmidt MW, Ulmer P (2004) A rocking multi-anvil: elimination of chemical segregation in fluid-saturated high-pressure experiments. Geochim Cosmochim Acta 68:1889–1899
Schmidt K, Bottazzi P, Vannucci R, Mengel K (1999) Trace element partitioning between phlogopite, clinopyroxene, and leucite lamproite melt. Earth Planet Sci Lett 168:287–299
Schoen AH (1958) Correlation and the isotope effect for diffusion in crystalline solids. Phys Rev Lett 1:138–140
Seitz H-M, Woodland AB (2000) The distribution of lithium in peridotitic and pyroxenitic mantle lithologies—anindicator of magmatic and metasomatic processes. Chemical Geology 166:47–64
Seyfried WE Jr (1987) Experimental and theoretical constraints on hydrothermal alteration processes at mid-ocean ridges. Ann Rev Earth Planet Sci 15: 317–335
Seyfried WE Jr, BischoffJ L (1979) Low temperature basalt alteration by sea water: an experimental study at 70 °C and 150 °C. Geochim Cosmochim Acta 43:1937–1947
Seyfried WE Jr, Mottl MJ (1982) Hydrothermal alteration of basalt by seawater under seawater dominated conditions. Geochim Cosmochim Acta 46:985–1002
Seyfried Jr WE, Gordon PC, Dickson FW (1979) A new reaction cell for hydrothermal solution equipment. Am Mineral 44:646–649
Seyfried WE, Janecky DR Jr, Mottl MJ (1984) Alteration of the oceanic crust: implications for the geochemical cycles of lithium and boron. Geochim Cosmochim Acta 48:557–569
Seyfried WE Jr, Janecky DR, Berndt ME (1987) Rocking autoclaves for hydrothermal experiments II. The flexible reaction cell system. In: Barnes HL, Ulmer GC (eds) Hydrothermal experimental techniques. Wiley Interscience, pp 216–240
Seyfried WEJ, Ding K, Berndt ME (1991) Phase equilibria constraints on the chemistry of hot spring fluids at mid-ocean ridges. Geochim Cosmochim Acta 55:3559–3580
Seyfried WE, Chen X, Chan LH (1998) Trace element mobility and Lithium isotope exchange during hydrothermal alteration of seafloor weathered basalt:

an experimental study at 350 °C, 500 bars. Geochim Cosmochim Acta 62:949–960

Shannon RD (1976) Revised effective ionic radii in oxides and fluorides. Acta Crystallogr A 32:751–767

Spandler C, O'Neill HS (2010) Diffusion and partition coefficients of minor and trace elements in San Carlos olivine at 1,300 °C with some geochemical implications. Contrib Miner Petrol 159:791–818

Taura H, Yurimoto H, Kurita K, Sueno S (1998) Pressure dependence on partition coefficients for trace elements between olivine and the coexisting melts. Phys Chem Miner 25:469–484

Taura H, Yurimoto H, Kato T, and Sueno S (2001) Trace element partitioning between silicate perovskites andultracalcic melt. Phys Earth Planet Inter 124, 25–32

Teng FZ, McDonough WF, Rudnick RL, Dalpé C, Tomascak PB, Chappell BW, Gao S (2004) Lithium isotopic composition and concentration of the upper continental crust. Geochim Cosmochim Acta 68:4167–4178

Teng FZ, McDonough WF, Rudnick RL, Walker RJ (2006) Diffusion-driven extreme lithium isotopic fractionation in country rocks of the Tin Mountain pegmatite. Earth Planet Sci Lett 243:701–710

Tepley FJ III, Lundstrom CC, McDonough WF, Thompson A (2010) Trace element partitioning between high-An plagioclase and basaltic to basaltic andesite melt at 1 atmosphere pressure. Lithos 118:82–94

Thornton EC, Seyfried WE Jr (1987) Reactivity of organic-rich sediment in seawater at 350 °C, 500 bars: experimental and theoretical constraints for the Guaymas Basin hydrothermal system. Geochim Cosmochim Acta 51:1997–2010

Urey HC (1947) The thermodynamics of isotopic substances. J Chem Soc (London) 562–581

van Kan Parker M, Liebscher A, Frei D, van Sijl J, van Westrenen W, Blundy J, Franz G (2010) Experimental and computational study of trace element distribution between orthopyroxene and anhydrous silicate melt: substitution mechanisms and the effect of iron. Contrib Miner Petrol 159:459–473

van Kan Parker M, Mason PRD, van Westrenen W (2011) Experimental study of trace element partitioning between lunar orthopyroxene and anhydrous silicate melt: effects of lithium and iron. Chem Geol 285:1–14

Van Orman JA, Crispin KL (2010) Diffusion in oxides. In: Zhang Y, Cherniak DJ (eds) Diffusion in minerals and melts. Rev Mineral Geochem 72:691–733

van Westrenen W, Blundy J, Wood B (1999) Crystal chemical controls on trace element partitioning between garnet and anhydrous silicate melt. Am Mineral 84:838–847

van Westrenen W, Blundy J, Wood B (2000) Effect of Fe^{2+} on garnet-melt trace element partitioning: experiments in FCMAS and quantification of crystal-chemical controls in natural systems. Lithos 53:189–201

Veksler IV, Petibon C, Jenner GA, Dorfman AM, Dingwell DB (1998) Trace element partitioning in immiscible silicate-carbonate liquid systems: an initial experimental study using a centrifuge autoclave. J Petrol 39:2095–2104

Verhoogen J (1952) Ionic diffusion and electrical conductivity in quartz. Am Mineral 37:637–655

Verney-Carron A, Vigier N, Millot R (2011) Experimental determination of the role of diffusion on Li isotope fractionation during basaltic glass weathering. Geochim Cosmochim Acta 75:3452–3468

Vigier N, Decarreau A, Millot R, Carignan J, Petit S, France-Lanord C (2008) Quantifying Li isotope fractionation during smectite formation and implications for the Li cycle. Geochim Cosmochim Acta 72:780–792

Von Damm KL (1991) A comparison of Guaymas Basin hydrothermal solutions with other sedimented systems and experimental results. In: Dauphin JP, Simoneit BRT (eds) The Garland Pesuar Provinces of the Californas. Am Assoc Petrol Geol Memoir 47:743–751

Wasserburg GJ (1988) Diffusion of water in silicate melts. J Geol 96:363–367

Watkins JM, Liang Y, Richter F, Ryerson FJ, DePaolo DJ (2014) Diffusion of multi-isotopic chemical species in molten silicates. Geochim Cosmochim Acta 139: 313–326

Watson EB, Baxter EF (2007) Diffusion in solid-Earth systems. Earth Planet Sci Lett 253:307–327

Watson EB, Dohmen R (2010) Non-traditional and emerging methods for characterizing diffusion in minerals and mineral aggregates. In: Zhang Y, Cherniak DJ (eds) Diffusion in minerals and melts. Rev Mineral Geochem 72:61–105

Welsch A-M, Behrens H, Horn I, Roß S, Heitjans P (2012) Self-diffusion of lithium in $LiAlSi_2O_6$ glasses studied using mass spectrometry. J Phys Chem A 116:309–318

Wenger M, Armbruster T (1991) Crystal chemistry of lithium: oxygen coordination and bonding. Eur J Mineral 3:387–399

Whitney DL, Evans BW (2010) Abbreviations for names of rock-forming minerals. Am Mineral 95:185–187

Williams LB, Hervig RL (2005) Lithium and boron isotopes in illite-smectite: the importance of crystal size. Geochim Cosmochim Acta 69:5705–5716

Wimpenny J, Gislason SR, James RH, Gannoun A, Pogge von Strandmann PAE, Burton K (2010) The behaviour of Li and Mg isotopes during primary phase dissolution and secondary mineral formation in basalt. Geochim Cosmochim Acta 74:5259–5279

Wood BJ, Blundy JD (1997) A predictive model for rare earth element partitioning between clinopyroxene and anhydrous silicate melt. Contrib Miner Petrol 129:166–181

Wood BJ, Blundy JD (2001) The effect of cation charge on crystal-melt partitioning of trace elements. Earth Planet Sci Lett 188:59–71

Wood B, Trigila R (2001) Experimental determination of aluminous clinopyroxene-melt partition coefficients for potassic liquids, with application to the evolution

of the Roman province potassic magmas. Chem Geol 172:213–223

Wunder B, Meixner A, Romer RL, Heinrich W (2006) Temperature-dependent isotopic fractionation of lithium between clinopyroxene and high-pressure hydrous fluids. Contrib Mineral Petrol 151:112–120

Wunder B, Meixner A, Romer RL, Feenstra A, Schettler G, Heinrich W (2007) Lithium isotope fractionation between Li- bearing staurolite, Li-mica and aqueous fluids: an experimental study. Chem Geol 238:277–290

Wunder B, Deschamps F, Watenphul A, Guillot S, Meixner A, Romer RL, Wirth R (2010) The effect of chrysotile nano-tubes on the serpentine-fluid Li-isotopic fractionation. Contrib Mineral Petrol 159:781–790

Wunder B, Romer RL, Meixner A, Jahn S (2011) Li-isotope silicate fluid fractionation: pressure dependence and influence of the bonding environment. Eur J Mineral 23:333–342

Yakob JL, Feineman MD, Deane JA Jr, Eggler DH, Penniston-Dorland SC (2012) Lithium partitioning between olivine and diopside at upper mantle conditions: an experimental study. Earth Planet Sci Lett 329–330:11–21

You C-F, Gieskes JM (2001) Hydrothermal alteration of hemi-pelagic sediments: experimental evaluation of geochemical processes in shallow subduction zones. Appl Geochem 16:1055–1066

You CF, Castillo PR, Gieskes JM, Chan LH (1996) Trace element behaviour in hydrothermal experiments: implications for fluid processes at shallow depths in subduction zones. Earth Planet Sci Lett 140:41–52

Yurimoto H, Ohtani E (1992) Element partitioning between majorite and liquid: a secondary ion mass spectrometric study. Geophys Res Lett 19. doi:10.1029/91GL02824. ISSN:0094–8276

Zanetti A, Tiepolo M, Obertia R, Vannuccia R (2004) Trace-element partitioning in olivine: modelling of a complete data set from a synthetic hydrous basanite melt. Lithos 75:39–54

Zhang Y, Cherniak DJ (eds) (2010) Diffusion in minerals and melts. Rev Mineral Geochem 72,1038 pp

Zhang Y, Ni H (2010) Diffusion of H, C, and O components in silicate melts. In: Zhang Y, Cherniak DJ (eds) Diffusion in minerals and melts. Rev Mineral Geochem 72:171–225

Zhang F, Wright K (2012) Lithium defects and diffusivity in forsterite. Geochim Cosmochim Acta 91:32–39

Zhang YX, Stolper EM, Wasserburg GJ (1991) Diffusion of water in rhyolitic glasses. Geochim Cosmochim Acta 55:441–445

Lithium in the Deep Earth: Mantle and Crustal Systems

5

5.1 Lithium in the Mantle

It has been clear for some time that Earth's upper mantle is Li-poor relative to the bulk continental crust (<2 ppm compared to ~18 ppm; Jagoutz et al. 1979; Ryan and Langmuir 1987; Teng et al. 2008). It has become similarly manifest that isotopic contrasts exist between surface and deep Earth reservoirs (e.g., altered ocean crust with heavy isotopic signatures compared to mid-ocean ridge basalts; Chan and Edmond 1988). One of the great hopes for Li isotope studies in the deep Earth has been that the system could unlock some of the questions related to mantle evolution and quantify aspects of crust-mantle cycling (e.g., Elliott et al. 2004). Although this hope may ultimately be realized, a number of roadblocks have slowed progress toward it considerably. There are two major ways that can be paved in constraining Li in the mantle. Either pristine peridotites can be used or melt derivatives of the mantle can used as proxies, considering the lack of significant Li isotopic fractionation during mantle differentiation (Tomascak et al. 1999; Chan and Frey 2003). Both approaches have positive and negative aspects, however.

5.1.1 Mantle Xenoliths and Related Samples

The review by Tomascak (2004) noted that the then-available data for Li abundance and isotopic composition in pristine, unmetasomatized peridotite xenoliths were fairly sparse and thus detailed estimates of Li systematics in Earth's mantle were quite uncertain. This data deficit was mainly due to analytical challenges presented by high-Mg, low-Li materials, although more questions have arisen since that barrier has been broken. Ryan and Langmuir (1987) provided preliminary data for Li contents in coexisting mineral phases of several mantle nodules that showed a dominant control of olivine on Li distribution in spinel peridotites, although it may differ for garnet-bearing peridotites. This was later validated by Seitz and Woodland (2000) and Eggins et al. (1998) for a larger suite of mantle xenoliths, but these authors also showed dominant control exerted by clinopyroxene in many lithologies, such as pyroxenites. This finding in itself may imply differences between pristine and modified lithologies governed by post-magmatic processes. At equilibrium, olivine appears to be the major host of Li (Ottolini et al. 2004) followed by near-equal distribution between clinopyroxene and orthopyroxene ($D^{olivine/melt} \sim 0.3–0.45 > D^{cpx/melt} \approx D^{opx/melt} \sim 0.15–0.3$; Brenan et al. 1998a, b; Ottolini et al. 2009; Chap. 4); both spinel and garnet appear to generally contribute little to the total Li budget of mantle xenoliths and hence to the mantle itself (Seitz and Woodland 2000; Woodland et al. 2002; Ottolini et al. 2004), although in opportune settings garnet may carry significant loads of Li (Barry et al. 2015). Experimentally determined partitioning of Li suggests some pressure-dependence, at least for clinopyroxene (McDade et al. 2003), but more

P.B. Tomascak et al., *Advances in Lithium Isotope Geochemistry*,
Advances in Isotope Geochemistry, DOI: 10.1007/978-3-319-01430-2_5

focused examination would certainly provide clearer constraints. The implications of these observations are twofold: (i) one can broadly estimate the Li abundance of the planet in bulk with a rough understanding of the modal proportions and Li contents of only a few minerals (Foley et al. 2013), although an incomplete understanding of lower mantle Li has an uncertain impact on such estimates; (ii) the absence of a unique mineral that would, at mantle conditions, represent the bulk of Li (such as garnet does for lanthanoids, for example) may sometimes hamper a more detailed assessment of a particular process such as fractional crystallization of a specific mineral phase or more general conditions leading to formation of such phases.

The Li elemental and isotopic variability in mantle assemblages was confirmed by pilot studies of mantle xenoliths (Bouman et al. 2000; Brooker et al. 2000) which clearly showed variations in δ^7Li of bulk peridotites beyond analytical uncertainties. The interpretations of Bouman et al. (2000) were tied to distinct ages of different peridotites and temporal evolution of the mantle with respect to Li isotopic compositions. One additional peridotite analysis published shortly afterwards (Chan et al. 2002b) was consistent with the δ^7Li $\sim$ +5 ‰ for the Earth's upper mantle. It soon was realized that secondary processes such as serpentinization of oceanic peridotites (Decitre et al. 2002) or metasomatism through melt extraction and overprinting by hydrous fluids (Brooker et al. 2004) may significantly alter intrinsic δ^7Li signatures. Moreover, kinetic processes through sub-solidus diffusive fractionation were soon revealed to be capable of introducing further complexities to the original Li isotopic signatures (Lundstrom et al. 2005).

Because Li substitutes for Mg in major mantle minerals such as olivine and pyroxene, it appears

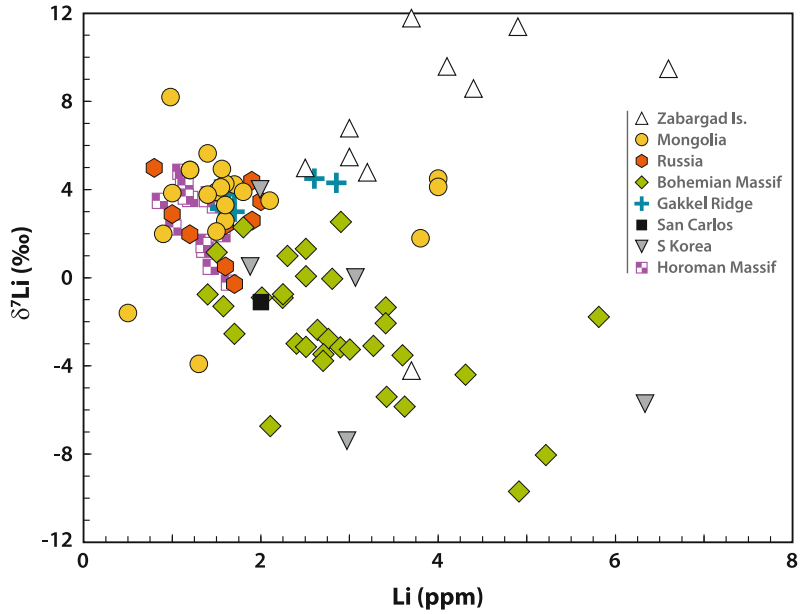

Fig. 5.1 Lithium concentration and δ^7Li of bulk mantle nodules, including peridotites (predominantly) with some pyroxenites. Compilation includes data from both pristine samples and those affected by secondary processes, as described in the text. Data sources: Bohemian Massif from Ackerman et al. (2013), Gakkel Ridge from Gao et al. (2011), Mongolia from Magna et al. (2006a, 2008) and Pogge von Strandmann et al. (2011), Zabargad from Brooker et al. (2004), S. Korea from Kil (2010), San Carlos (New Mexico) from Seitz et al. (2004), Russia (various localities) from Halama et al. (2009), Pogge von Strandmann et al. (2011), and Ionov and Seitz (2008) and Horoman from Lai et al. (2015)

that a non-negligible fraction of Li could be hosted in the lower mantle where high-pressure polymorphs of olivine and pyroxene, as well as garnet and other Mg-dominated silicates and oxides (silicate perovskite now known as bridgmanite, and magnesiowüstite), constitute the majority. To date only the studies of Kaminsky et al. (2001) and Seitz et al. (2003) have reported Li abundances in these uncommon minerals. It was clear, however, that there are significant differences among co-existing Ca-perovskite, Mg-perovskite and magnesiowüstite (a.k.a. ferropericlase), ranging from sub-ppm levels in the former species to ~50 ppm in the latter. Whether or not this enrichment relates to a particular Li-enriched source or hints at a yet unaccounted Li refertilization process remains to be answered by future Li isotopic analyses. A preliminary report on diamond-hosted ferropericlase inclusions by Seitz et al. (2006) gave highly variable δ^7Li (~−4 to ~+10 ‰). This may imply entrainment of sedimentary and eclogitic lithologies to the upper/lower mantle boundary through subduction. In any case, the Earth's lower mantle may appear distinctly enriched in Li which could reflect pressure- (but not temperature-) dependent behavior of Li coupled to complex substitutions involving Li, Si, Mg and Al (Seitz et al. 2003; Yang et al. 2009) and, presumably, Fe^{3+}. At least for lower region of the upper mantle and the transition zone, Li solubility increases in parallel with elevated majoritic garnet component (Seitz et al. 2003). But truly, our understanding of high-pressure processes that may affect Li solubility and/or mobility in lower mantle mineral phases requires dedicated studies. The extent of such explorations is at present hampered by the small-scale nature of available samples relative to capabilities of current analytical techniques.

5.1.1.1 Pristine Peridotites and the Primitive Upper Mantle Li Budget

The question as to the true Li isotopic signature of pristine unmodified mantle, considering the potential for secondary processes to modify Li isotopic systematics, has persisted. Although rather sparsely distributed across the globe, peridotite xenoliths are the best direct samples from the mantle, brought to the surface by erupted host lavas. Rapid transport from depths between ~30 and ~200 km often inhibits incipient low-degree partial melting which could modify incompatible element contents. Critically, large mantle xenoliths (commonly ≥0.5 m in diameter) may successfully preserve mantle signatures despite their fragility, whilst small peridotite xenoliths (<0.1 m in diameter) frequently are affected by secondary processes. Alternatively, massive alpine-type orogenic peridotites can be used because they, at least in part, may have escaped interactions with melts. Nonetheless, pristine examples of such peridotites are rare (e.g., Horoman peridotite, Japan; Lai et al. 2015).

Magna et al. (2006a) and Jeffcoate et al. (2007) have inferred that equilibrium fractionation translates into similar δ^7Li values in co-existing olivine and orthopyroxene whereas clinopyroxene commonly carries a heavier Li isotopic signature. A number of studies supplemented the early data set for pristine spinel lherzolites (Brooker et al. 2004; Seitz et al. 2004; Magna et al. 2006a, 2008; Jeffcoate et al. 2007; Pogge von Strandmann et al. 2011) and collectively have illustrated the Li elemental and isotopic homogeneity of fertile upper mantle with a narrow range of δ^7Li values between ~+2.5 and ~+4.9 ‰ (Fig. 5.1). More detailed investigations of bulk peridotite compositions (Magna et al. 2008; Pogge von Strandmann et al. 2011) constrained further the δ^7Li value of the Earth's pristine unmetasomatized upper mantle at ~+3.5 ‰ with limited variation of ~±1.0 ‰ at 2σ confidence. This is very similar to the range in δ^7Li values found by Gao et al. (2011) for abyssal mantle xenoliths dredged from the Gakkel Ridge. Combined with the earlier results for xenoliths collected in continental areas, these observations are important for further unraveling the secondary post-solidification effects in various tectonic settings in the mantle as well as for comparison with respect to Li isotopic systematics among the terrestrial planetary bodies.

The alternatives to xenoliths are orogenic peridotite massif exposures and oceanic abyssal peridotites. One apparent problem with these

exposures is the quick reaction of olivine with water at elevated temperatures which gives rise to serpentinites and similar lithologies, and which may partly or completely disguise the original Li isotopic signatures (e.g., Decitre et al. 2002; Benton et al. 2004). Abyssal peridotites may record ancient mantle melt depletion events (Stracke et al. 2011) that could influence the Li systematics. However, low-degree melting appears to impart limited variation to Li isotopes (Tomascak et al. 1999). Jeffcoate et al. (2007) estimated that equilibrium fractionation would generate magmas with <0.5 ‰ difference from their sources. Refractory harzburgitic residues and dominant silicate phases (olivine, orthopyroxene) analyzed by Ionov and Seitz (2008) had δ^7Li that were not drastically different from each other, providing evidence for insignificant modification to the original Li isotopic signature after melt depletion. Unmetasomatized samples of the Horoman peridotite massif also show a rather constrained variation of δ^7Li values at 3.8 ± 1.4 ‰ (2σ) (Lai et al. 2015), further attesting to a globally similar Li isotopic composition of the Earth's upper mantle irrespective of the nature of the peridotite samples (massive or xenolith). Hence it appears that some peridotite xenoliths faithfully record mantle Li, which is isotopically rather homogeneous.

5.1.1.2 Metasomatized Peridotites and Post-magmatic Modifications

Soon after introducing the δ^7Li of the Earth's mantle through analyses of pristine mantle peridotite xenoliths, it also became clear that much of the mantle may be isotopically modified as a consequence of secondary processes. Thus, isotopic variations may not uniquely reflect intrinsic heterogeneity. Brooker et al. (2004) attributed Li isotopic variations in modally metsomatized spinel peridotites to overprinting by fluids or melts enriched in isotopically heavy Li, prospectively ultimately derived from subducted crust. The comprehensive study of Seitz et al. (2004) documented post-magmatic shifts in δ^7Li of coexisting minerals which most notably affected clinopyroxene (Fig. 5.2). This finding was particularly

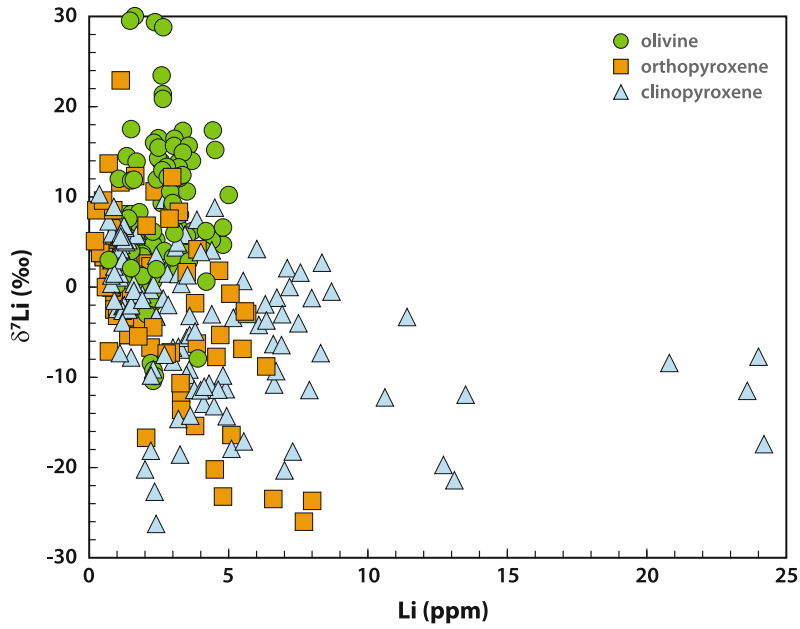

Fig. 5.2 Lithium concentration and δ^7Li of minerals from mantle nodules. Data sources: Magna et al. (2006a, 2008), Halama et al. (2009), Jeffcoate et al. (2007), Ionov and Seitz (2008), Seitz et al. (2004), Nishio et al. (2004), Rudnick and Ionov (2007), Tang et al. (2007, 2011), Aulbach et al. (2008), Aulbach and Rudnick (2009), Wagner and Deloule (2007) and Xiao et al. (2015)

significant in the face of apparently undisturbed bulk Li abundance systematics of the Mg-silicates. It was at this point that the hidden complexity within the world of mantle Li isotopes became apparent: samples which do not show obvious evidence of metasomatism or secondary processes are not necessarily safe targets for study. Indeed, the study of Nishio et al. (2004) revealed significant shifts in δ^7Li values in Li-enriched clinopyroxene from a variety of mantle xenoliths, initially ascribed to an exotic Li isotopic composition of the EM-1 mantle component with the anticipated δ^7Li < −17 ‰. Rudnick and Ionov (2007) found that these low values may instead result from kinetic effects caused by the diffusive ingress of isotopically light Li into clinopyroxene from recent (syn-eruptive) percolation of fluids. Nevertheless, the idea of an isotopically light component resident in the mantle over long time scales persists in some data compilations (Tang et al. 2010).

It has been verified that Li isotopes diffuse very rapidly compared to most species (with the exception of water and gases), paralleled by differential isotopic diffusion rates: ^{6}Li diffuses somewhat faster than ^{7}Li (see Chap. 4). Furthermore, and germane to studies such as Nishio et al. (2004), diffusion in clinopyroxene is faster than in olivine at mantle conditions (Jeffcoate et al. 2007; Parkinson et al. 2007; Rudnick and Ionov 2007), leading to sizeable isotopic differences in the final crystallization and/or post-solidification products from an originally homogeneous reservoir. In fact, geochemically-relevant Li isotopic diffusion was generated synthetically with the formation of smooth Li concentration and isotope profiles between molten basalt and rhyolite with vastly different starting compositions (Richter et al. 2003). Even an ephemeral thermal event ($\sim$6 min in the RB-5 experiment of Richter et al. 2003) led to a measurable re-distribution of Li, although other elements showed an abrupt concentration offset at basalt/rhyolite interface. This confirms high rates of Li diffusion in silicate melts compared with major cations such as Mg, Fe and alkali elements which had been noted earlier (Jambon and Semet 1978; Lowry et al. 1981; Cunningham et al. 1983). These observations must thus be taken into account when discussing large variations in δ^7Li observed in studies of peridotitic samples (as well as other rocks) and their individual minerals (see Chap. 4).

In one of the first detailed studies of diffusive re-mobilization of Li, Lundstrom et al. (2005) investigated a dunite–harzburgite–spinel lherzolite transect from an utramafic body of the Trinity peridotite in northern California. These authors found significant variations in δ^7Li of clinopyroxene along a profile and concluded that solely melt extraction cannot account for large Li isotopic troughs observed at dunite/harzburgite interface and that diffusion must be considered a potentially important driving force for Li isotopic variations. The numerical model of Lundstrom et al. (2005) showed that ^{6}Li would preferentially diffuse out of melt conduits into wall-rock peridotites.

Several later papers focused in greater detail on the topic of kinetic redistribution of Li isotopes in mantle lithologies. Jeffcoate et al. (2007) provided evidence for significant intra-mineral δ^7Li variations in coexisting olivine, orthopyroxene and clinopyroxene from a cryptically metasomatized xenoliths from San Carlos. The in situ data showed dramatic δ^7Li variations in pyroxenes (−43 to −5 ‰ in orthopyroxene, −37 to −3.5 ‰ in clinopyroxene) whilst δ^7Li varied between −6 and +8 ‰ in olivine. The Li abundances of pyroxenes varied in parallel with Li isotopic compositions, but for olivine this variation was inconsistent. It should be noted that MC-ICPMS measurements of Magna et al. (2006a) yielded δ^7Li of +3.6 and +3.3 ‰ in bulk aliquots of San Carlos olivine and orthopyroxene, respectively, leaving the variations to be only resolved at microscales and mostly preserved at the rims of crystals.

Significant Li enrichment associated with disequilibrium partitioning has also been observed for some spinel lherzolites from Boeun, South Korea (Kil 2010), and explained to be a consequence of diffusive fractionation rather than surface contamination or metasomatic process in the mantle. Gao et al. (2011) analyzed a suite of mantle xenoliths (spinel lherzolites, plagioclase lherzolites and a spinel harzburgite) from the Gakkel Ridge in the Arctic Ocean. Disequilibrium distribution of Li among clinopyroxene,

orthopyroxene and olivine (in order of decreasing Li abundances) was found, paralleled by decreasing δ^7Li from olivine to orthopyroxene to clinopyroxene. Interestingly, bulk rock δ^7Li values are still in the range of equilibrated mantle xenoliths which may be a consequence of limited modification of δ^7Li in orthopyroxene combined with the heavy Li signature (and low Li contents) in olivine counter-balanced by isotopically light Li in clinopyroxene with high Li contents (up to 5 ppm). The unmodified bulk values simply imply redistribution of Li in a closed system, which only affects Li and δ^7Li on the mineral scale but not hand specimen scale. Data of Gao et al. (2011) also imply temperature dependence of Li isotopic fractionation between olivine and clinopyroxene ($\Delta^7Li_{ol-cpx} = \delta^7Li_{ol} - \delta^7Li_{cpx}$) with significant increase in Δ^7Li_{ol-cpx} values with decreasing temperature (i.e., during cooling). Nonetheless these results may preferentially apply to closed-system evolution. According to Gao et al. (2011), this would translate to large δ^7Li difference between these co-existing minerals and possible preservation of negative δ^7Li values in mantle clinopyroxene for long enough time to be sampled after surface emplacement.

Ionov and Seitz (2008) emphasized the role of cooling rate of the final eruptive sequence carrying xenoliths as a key factor in the generation of kinetic Li isotopic effects. They analyzed olivine and orthopyroxene in a suite of harzburgitic xenoliths from the Avacha volcano, Kamchatka arc, and from the Vitim volcanic field, Siberia. They interpreted that xenoliths in pyroclastic eruptions, which experienced near-instantaneous cooling, had limited potential to develop Li isotopic disequilibria. On the contrary, xenoliths brought to surface in lava flows experienced protracted cooling times, which translated to significant δ^7Li variations at the mineral scale. The difference was particularly apparent for orthopyroxene with δ^7Li of +1.8 to +4.0 ‰ in xenoliths of pyroclastic lavas versus −16.7 ‰ in a single basaltic lava hosted harzburgite; these differences were paralleled by elevated Li content in the latter sample (Ionov and Seitz 2008).

Similar Li isotopic difference as that observed for olivine–orthopyroxene pairs in lava-hosted xenoliths (Ionov and Seitz 2008) has been found for olivine–clinopyroxene (and orthopyroxene in few cases) pairs in mantle xenoliths from far-east Russia (Rudnick and Ionov 2007). There, Li isotopic compositions varied greatly not only in pyroxenes (more vulnerable to post-magmatic effects) but also in the coexisting olivine (δ^7Li from −1.7 to +11.9 ‰), that in case of rapid cooling preserves the intrinsic isotopic signature. Thick bodies of alkali basalts appeared to prevent quick cooling, which translated to significant post-eruption kinetic redistribution of Li. Hence, cooling rate should figure prominently in the interpretation of Li isotopic data from mantle xenoliths, although other parameters may be taken into account such as fertility of the xenoliths and grain size (Rudnick and Ionov 2007). As explained in detail in Chap. 4, diffusion of Li in olivine and clinopyroxene is complex, which cannot be simply described by a single diffusion rate. So there might be conditions in which the fast diffusion mechanism of Li in olivine is activated, which would imply that δ^7Li in both olivine and clinopyroxene could be affected in similar timescales (e.g., Dohmen et al. 2010). However, that is still speculation.

These reports may lead to the question: are light Li isotopic signatures an indicator of diffusive redistribution, or can isotopically light mantle rocks be generated by primary processes? Of course, kinetic effects may ultimately generate the feedstock for light-Li melts through processes occurring in the sources of such rocks (e.g., subduction zone processes), but it is important to be able to distinguish isotopic signatures that derive from sources rather than processes occurring during transport and emplacement. Halama et al. (2009) analyzed refractory xenoliths from Avacha, far-east Russia, including veined pyroxenites representative of the modally metasomatized mantle. Perhaps contrary to expectations, they found mantle-like homogeneity of δ^7Li in both olivine and orthopyroxene (+3.0 to +5.6 ‰), paralleled by similar δ^7Li in veins and their mineral constituents (+3.0 to +5.1 ‰). To explain the lack of fractionated isotopic signatures in rocks that had undergone metasomatism by melts carrying a strong subduction signature in their trace

element geochemistry (e.g., Ba/Th, Pb/Ce), they invoked diffusive Li equilibration between cm-scale ascending melt channels and pervasive pristine mantle. This exchange was interpreted as happening on geologically short time scales (perhaps as rapidly as 100 years at subarc mantle temperatures), indicating that Li isotopic differences between slab-derived, isotopically distinct fluids or melts and ambient mantle are unlikely to survive if mass transfer takes place at this spatial scale (i.e., small veins with low melt/rock ratios). This point will be revisited in the following section on mantle-derived melts.

While diffusive effects certainly are important in considering δ^7Li variations in many mantle samples, Su et al. (2012) argued that extremely light Li in olivine from central China (down to −42 ‰, measured by SIMS) and can hardly be discussed in the framework of diffusive isotope fractionation. Beside the possible existence of low-δ^7Li lithologies in the mantle, Su et al. (2012) offer an alternative explanation, seeking metasomatism by natrocarbonatite melts as a culprit for the 'reversed' metasomatic δ^7Li systematics of co-existing olivine and clinopyroxene. They suggest that in the presence of high Na concentrations, ^{7}Li tends to enter pyroxenes more easily than ^{6}Li, which is left behind in the melts incorporated into olivine. However, before solid conclusions can be made a thorough experimental investigation must assess this intriguing possibility. Nevertheless, carbonatitic metasomatism is quite a common phenomenon which may place peculiar constraints on Li partitioning in mantle lithologies (Woodland et al. 2004). The very Li-rich, zoned olivine (tens of ppm) analyzed by Su et al. (2012) may, however, have been affected by diffusion. It was predicted by Dohmen et al. (2010) that the fast diffusion mechanism becomes activated if large Li contents are incorporated into olivine.

Carbonatitic metasomatism may be quite different from silicate metasomatic events. Wagner and Deloule (2007) have used in situ analyses (by SIMS) of Li isotopic compositions of co-existing minerals from hydrous as well as anhydrous peridotites from the Massif Central, France, in order to constrain the effects of variable extent of metasomatism and to compare unmetasomatized peridotites with those showing overprints by cryptic as well as modal metasomatism. Significant intra-grain variations in δ^7Li were observed for amphibole-bearing xenoliths whilst only modest variations were found for amphibole-poor xenoliths. By excluding late-stage post-eruption hydrous alteration, the variations in olivine, orthopyroxene, clinopyroxene and amphibole can be associated with diffusive fractionation during silicate melt percolation. The hydrous nature of such melt enables precipitation of amphibole which is otherwise unstable at mantle conditions. Wagner and Deloule (2007) further speculated that olivine and, to a lesser extent, orthopyroxene were less susceptible to metasomatic modifications as these minerals record Li isotopic equilibrium; on the contrary, clinopyroxene and amphibole mostly showed larger variations in δ^7Li.

Silicate melt has also been invoked as a metasomatic agent for a suite of spinel peridotites, spinel websterites and pyroxenites from Harrad Uwayrid, Saudi Arabia (Kaliwoda et al. 2008). Most of their in situ measured data across olivine, orthopyroxene, clinopyroxene and phlogopite grains showed convex Li elemental profiles, but often with homogeneous cores. In contrast, abundances of B and Be were very homogeneous across the whole grains analyzed. The Li isotopic profiles in most analyzed grains do not show a typical diffusive pattern, nor do the δ^7Li values depart significantly from mantle-like values (+1.1 to +9.7 ‰) with some uncertainty. For one particular sample Kaliwoda et al. (2008) revealed significant differences in abundances of Li, B and Be as well as δ^7Li for two adjacent clinopyroxenes, a phenocryst and a spongy specimen, with a clearly disturbed elemental and isotopic distribution in the latter. Whether a hydrous fluid or hydrous silicate melt could be responsible for the observed light element systematics remains to be validated.

Another source of metasomatic agents has been invoked for mantle xenoliths (garnet-bearing versus garnet-free peridotites, and spinel peridotites) from the Tanzanian part of the East African Rift system (Aulbach et al. 2008). Olivine samples in their study showed subtle lithologically correlated differences in Li contents and isotopic compositions. Although δ^7Li of

clinopyroxene samples varied, most were in isotopic equilibrium with coexisting olivine. One-dimensional numerical modeling led Aulbach et al. (2008) to infer that Li isotopic disequilibrium, recognized by isotopically light Li in pyroxene, may be attained en route to the surface through exchange with host melilitites. This process would only minimally affect Li contents in the same crystals, which were slightly higher than those typical of normal mantle. Based on major and trace element constraints coupled with radiogenic isotope considerations, Aulbach et al. (2008) invoked a plume-derived silicate melt that might have interacted with peridotites from Labait area. On the other hand, some other peridotites from Tanzania appear to have escaped significant metasomatic overprint despite interaction with silicate and/or carbonatite melts (Aulbach and Rudnick 2009). Modeling implies that low δ^7Li in clinopyroxene of some xenoliths coupled with apparent elemental equilibrium between olivine and clinopyroxene must be a pre-eruption feature taking place during transport to the surface in host magmas carrying high Li abundances with δ^7Li values more or less in the mantle range.

A number of additional studies have revealed Li systematics that do not conform to those predicted for equilibrium Li isotopic fractionation between major mantle minerals (Nishio et al. 2004; Tang et al. 2007, 2011, 2014a, b). Tang et al. (2007, 2011) measured Li abundances and isotopic compositions in a suite of spinel lherzolites from the North China Craton. In all cases, Li abundances were elevated in pyroxenes compared with olivine whereas δ^7Li of coexisting pyroxenes were shifted toward negative values, consistent with kinetic ingress of ^{6}Li from subduction-derived fluids. A later phase of interaction of these modified mantle xenoliths with melts derived from the asthenosphere was suggested from elevated δ^7Li values at rims of olivine and pyroxenes. This two-stage model was subsequently applied to other North China Craton mantle xenoliths (e.g., Tang et al. 2011, 2012). Tang et al. (2014a, b), using in situ SIMS determinations, argued that although the xenoliths did record effects of diffusion, this was not the major control on isotopic compositions, at least in case of mineral grain cores. If correct, a notable inference of these examinations is that the xenoliths record a low-δ^7Li source located in the mantle, plausibly formed by melting of subducted lithologies such as eclogites and perhaps lower crustal granulites (Su et al. 2012). Nevertheless, the observed zoning could be explained exclusively by diffusion; care must be exercised to avoid the potential masking effects introduced by grain sectioning.

Contrasting results for several distinct lithologies (normal lherzolites, clinopyroxene-rich lherzolites, wehrlites) were obtained by Xiao et al. (2015) using in situ SIMS technique. The data were screened for instrumental matrix-induced isotopic fractionation following the approach of Bell et al. (2009). Wehrlites showed mantle-like δ^7Li and slightly elevated Li contents at $\sim$3 ppm. Combined with previous petrological studies, Xiao et al. (2015) implied metasomatic overprint of peridotites by melts derived from the asthenosphere, although the Li isotopic signature of the asthenosphere remains largely unknown. Isotopically heavy clinopyroxene-rich lherzolites may be representative of precipitation of residual melts after previous loss of ^{6}Li due to diffusion.

Contrasting results in two geochemically diverse peridotite xenoliths from the North China Craton were obtained by Zhang et al. (2010) for Li elemental and isotopic profiles across co-existing mineral grains (olivine, orthopyroxene, clinopyroxene). Whereas the low-Mg# peridotite shows elemental and isotopic equilibrium with normal distribution of Li and Li isotopes, the high-Mg# harzburgites clearly carry signatures of post-magmatic modification, reflected in highly variable Li abundances and disequilibrium δ^7Li values among major minerals. This latter finding implicates sizeable modifications of refractory lithospheric mantle through interaction with fertile melts of subducted lower crust within the North China Craton. A combination of diffusive Li isotopic fractionation during melt/fluid–peridotite interaction and cooling-induced sub-solidus redistribution of Li in xenoliths entrapped in host magmas en route to the surface has been invoked for mantle xenoliths from the Hannuoba, Fanshi and Hebi areas in the North China Craton (Tang et al. 2011). Lithium

elemental and isotopic disequilibria found in most investigated samples are paralleled by Sr–Nd isotopic disequilibria between coexisting clinopyroxene and orthopyroxene as a consequence of recent interaction between peridotites and asthenosphere-derived melts.

Xu et al. (2013) applied an in situ approach using LA-MC-ICPMS to collect Li abundance and isotopic data in a suite of spinel peridotites from Kuandian Basin in the North China Craton. Despite large analytical errors compared with conventional MC-ICPMS (see Chap. 2), clearly resolved variations were found in δ^7Li for olivine, orthopyroxene, clinopyroxene and amphibole (where present). Coupled incompatible element indicators and Li systematics implied metasomatic overprint of the Kuandian xenoliths by silicate melts. In particular, the in situ character of the study allowed for detailed mapping of Li elemental profiles across different mineral grains. In almost all cases significant enrichment of Li in rims relative to cores, paralleled by highly negative δ^7Li in rims of both clinopyroxene and orthopyroxene (down to −56 ‰), hint to recent diffusive fractionation of Li induced by percolation of metasomatic liquids shortly before eruption and during cooling. In an attempt to unveil the source of these metasomatic agents, in situ determination of Sr isotopes was employed, combined with incompatible trace elements parameters (e.g., La/Nb, U/Nb). These appeared to exclude recycled continental crustal sources and instead invoked a possible relation to subducted Pacific oceanic crust (Xu et al. 2013), similar to findings of Tang et al. (2012) for another area in the North China Craton.

The study of Tang et al. (2012) showed 'reversed' sense of Li isotopic fractionation in metasomatized mantle xenoliths, with prevalently light signatures in olivine relative to co-existing clinopyroxene and orthopyroxene. The data were inconsistent with kinetic fractionation having produced the entire range in Li elemental and isotopic compositions, because of normal-mantle abundances in all minerals, as well as clinopyroxene being isotopically heavier than olivine despite faster Li diffusion in the former. They favored an evolutionary model requiring two temporally-distinct episodes of reaction between mantle and fluid/melts. The early metasomatic agent had low δ^7Li; more recent diffusive re-equilibration was in the presence of isotopically more "normal" melt. These authors suggested that the ultimate source of the isotopically light Li may be dehydrated residues of a subducted slab, although contradictory interpretations of the isotopic compositions of eclogites complicate this explanation.

Tang et al. (2014b) analyzed olivine cores and rims from a suite of high-Mg harzburgites from the Hebi area in the North China Craton. A remarkable aspect of their dataset was the rather normal Li content in most olivines, in the range of olivine from equilibrated peridotites; moreover, no significant difference in Li contents and δ^7Li was found by Tang et al. (2014b) for olivine cores (0.9–2.2 ppm Li; −27.2 to +2.4 ‰ (n = 11), two values at +1.2 and +21.5 ‰) and rims (0.9–3.6 ppm Li; −38.0 to −1.5 ‰ (n = 12), one value at +19.5 ‰ related to the isotopically heavy core). Thus, the observed δ^7Li range, paralleled by the lack of a developed diffusive isotopic profile, suggested participation of a component with unusually low δ^7Li, again pointing to subducted residues of oceanic crust. It thus appears that such processes may operate under appropriate conditions and that Li isotopic heterogeneities in the mantle may survive long and be more resistant to attenuation as a consequence of diffusion (cf. Halama et al. 2008).

These general inferences from the North China Craton may also apply to other areas. Ackerman et al. (2013) measured Li contents and isotopic compositions in a suite of basanite-hosted xenoliths from NE Bavaria, Germany, and revealed some of the lowest δ^7Li measured to date for bulk rocks (down to −9.7 ‰). With the exception of two samples with δ^7Li > +2.3 ‰, none of the peridotites showed mantle-like δ^7Li. These compositions were paralleled by extremely high Li/Yb ratios up to ~140, resulting from combined Li ingress and Yb depletion by melting. This was interpreted to reflect high degrees of melting and concomitant kinetic isotopic fractionation. However, the ingress of isotopically light Li

might have instead originated in subducted oceanic crust. No clear distinction could be made for Li systematics in terms of metasomatic agents (i.e., silicate or carbonate-rich), but not all xenoliths with low δ^7Li were associated with unusually high Li abundance in clinopyroxene, which often carries low δ^7Li values (as detailed above). A similar distribution of Li elemental and isotopic compositions has been observed for the vertically stratified mantle beneath the Kozákov volcano, Bohemian Massif, close to a major tectonic discontinuity. All investigated samples appear to carry a disturbed δ^7Li signature (−5.8 to −0.8 ‰). This was interpreted to reflect the combined effects of mantle metasomatism and melt depletion (Ackerman et al. 2013), similar to the interpretation of samples from the NE Bavaria suite (Medaris et al. 2015).

Taken as a whole, these observations provide evidence that significant volumes of the subcontinental lithospheric mantle beneath large continental areas may retain a record of Li isotopic modification, perhaps due to melt extraction associated with reactions between a melt-depleted mantle column and fertile melts en route to the surface. The evidence for processes other than solely kinetic fractionation, apparently strong in many cases, has generally not been backed up by diffusion modeling. It is our opinion that diffusive fractionation in igneous systems has not been given appropriate consideration in many cases. Detailed in situ Li and δ^7Li profile measurements (performed on multiple grains), accompanied by diffusion modeling, are required to clearly show that the observed δ^7Li signatures can **not** be produced by diffusion.

5.1.2 Mantle-Derived Magmas

Deviations from a global mean δ^7Li ($\sim$+3 to +5 ‰) in products of mantle melting could provide clues on processes of recycling of individual components of subduction-related materials. These include marine sediments, isotopically stratified oceanic lithosphere, fluid-modified mantle wedge and distinct continental components (terrigenous sediments and subcontinental lithospheric mantle). The idea behind a low-δ^7Li recycled component accommodated a previously introduced model by Zack et al. (2003) whose analyses of omphacite (clinopyroxene) as a prime constituent of eclogitic lithologies, together with low-Li garnet (e.g., Woodland et al. 2002), showed highly negative δ^7Li values as low as −11 ‰, that were thought to represent dehydrated subducted residue after aqueous solutions with isotopically heavy Li had been expelled off the slabs entering subduction zones. This model of introducing light Li into a deeper mantle was critically reviewed (Marschall et al. 2007b) by involving kinetic diffusive modifications and stating that dehydration alone would be capable of decreasing the resulting δ^7Li values in residual slab by no more than c. 3 ‰. However, the progressive Li isotope fractionation coupled with a large proportion of Li retained even after high-grade moderate-temperature metamorphism applicable to subduction zones (Marschall et al. 2006) may still remain an important alternative for explaining systematically decreasing δ^7Li away from the trench (e.g., Moriguti and Nakamura 1998; Magna et al. 2006b; Agostini et al. 2008). It is thus permissible that fractionated Li transferred further into the subduction factory may appear in distant time–space relations at the Earth's surface through MORB and/or OIB, but unraveling the ultimate sources and histories of reservoirs carrying this Li isotopic distinction still requires much work.

Rapidity of diffusive exchange in newly formed melts has been documented by Magna et al. (2008) who analyzed three melt pockets co-existing with either clinopyroxene or olivine. Notably, these newly formed melt pockets were isotopically lighter by 2–9 ‰ than the co-existing minerals. That the two olivine-associated melt pockets had heavier δ^7Li than that associated with clinopyroxene suggests that kinetic effects are faster into/out of clinopyroxene than olivine, consistent with more focused experimental studies (see Chap. 4). Jeffcoate et al. (2007) modeled peridotite mineral

data using observations of Lundstrom et al. (2005) to indicate that diffusive loss of Li to wall rocks of ascending melts is unlikely to have a >1 ‰ effect on systems where conduits transporting melts are spaced >50 m apart. Interestingly, a glassy sample of Hawaiian basalt analyzed by Jeffcoate et al. (2007) showed no Li isotopic zoning, which attests to the key role of cooling rate in developing diffusive Li profiles.

Generating isotopically heavy Li that could then be re-processed in and beyond the subduction zone appears to be a more complex issue. The isotopically heavy Li mainly enters the ocean floor rocks through exchange with isotopically heavy seawater so that Li becomes enriched and isotopically heavier in the ocean floor compared to deeper ocean crustal levels (Chan et al. 2002a). Decitre et al. (2002) and Benton et al. (2004) showed that serpentinites become isotopically quite heterogeneous with a slight bias towards elevated δ^7Li although modifications to Li budget of serpentinites only occur at high water/rock ratios (Vils et al. 2009) and serpentinization itself appears to provide subordinate contribution of Li to the global Li budget in oceanic lithosphere (Vils et al. 2008). Independently of each other, Chan et al. (2009) and Vlastélic et al. (2009) have inferred that elevated δ^7Li values (>+6 ‰) in some HIMU lavas are a result of incorporation of altered oceanic crust into the mantle source of HIMU basalts through recycling, an idea largely consistent with incompatible trace elements and radiogenic isotopic constraints (e.g., Hofmann 1997; Stracke et al. 2005), and that these heterogeneities can indeed survive in the mantle for a period of >1 Gyr without apparent attenuation (cf. Halama et al. 2008). Importantly, geographically distinct occurrences of mantle plume-related volcanic rocks with high δ^7Li values (up to +9 ‰ in rocks with the highest MgO contents) were reported from Iceland (Hansen et al. 2011; Magna et al. 2011) that cannot easily be assigned to a specific recycled material with HIMU affinity indicating that heavy Li isotopic signature may be more ubiquitous than it would appear from genetic connection to solely HIMU-type 'habitats'. It also cannot result from simple contamination by meteoric water because Iceland basaltic lavas are much younger than HIMU lavas (in fact, most of them are relatively recent at < ~10 ka) and a large part of these high-MgO (>7 wt% MgO) basaltic to picritic lavas erupted subaerially, thus escaping secondary contamination by melt water from ice sheets.

Finally, one potential shortcoming of using igneous derivatives to plumb Li isotopes in the mantle is the susceptibility of volcanic rocks to weathering. Although efforts are consistently made to avoid "visibly altered" samples and parts of sample, it seems likely that some of the volcanic rocks from which Li isotopic information has been extracted have been subject to subtle weathering, which could yield rocks with artificially lighter or heavier isotopic systematics. One early example of potentially unreliable isotopic measurements in what was described as unaltered MORB samples (Chan et al. 1992) had δ^7Li (+6.3 to +6.8 ‰) outside the subsequently verified global range, as well as anomalously high bulk K_2O content (0.16–0.22 wt%). Although foundational in our understanding of Li in the mantle, it is interesting to note that these two samples represented one third of the data set for the MORB samples in that study (Chan et al. 1992).

5.1.2.1 Mid-Ocean Ridge Rocks

Mid-ocean ridge basalts (MORB) are considered to reflect melt-derivation from depleted mantle. There appears to be a range in elemental and radiogenic isotopic systematics reflecting compositional heterogeneity of the depleted mantle that includes incompatible-element-depleted and variably enriched components (e.g., Salters and Stracke 2004). Thus the correlation between MORB and peridotitic mantle may be a somewhat complex one and not all MORB may reflect the isotopic composition of the majority of the mantle. Nevertheless, considering minimal fractionation of Li isotopes during low-degree melting (Tomascak et al. 1999), they may still possess important information about the mantle that lies beneath the ridges.

Despite widespread availability of MORB samples from many distinct locations in the Atlantic, Pacific and Indian Oceans, limited Li

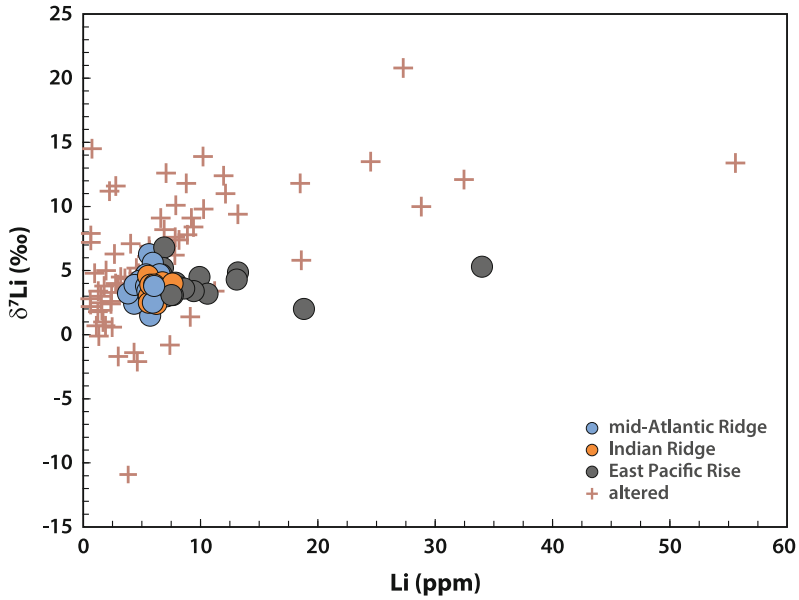

Fig. 5.3 Lithium concentration and δ^7Li of MORB and altered MORB. Data for altered MORB samples come from the Mid-Atlantic Ridge (Chan et al. 1992) and East Pacific Rise (Chan et al. 2002a, b; Brant et al. 2012). Sources of other data: Mid-Atlantic Ridge from Moriguti and Nakamura (1998), Nishio et al. (2007), Chan et al. (1992), Tomascak et al. (2008), East Pacific Rise from Chan et al. (1992), Elliott et al. (2006), Tomascak et al. (2008), Indian Ridge from Nishio et al. (2007) and Tomascak et al. (2008)

isotopic data were available until recently (Elliott et al. 2006; Nishio et al. 2007; Tomascak et al. 2008; Fig. 5.3). Although these studies served to strengthen the earlier data set, the more recent data ultimately did not change the fundamental characterization of Li in the MORB mantle relative to the preliminary study of Chan et al. (1992; δ^7Li = +3.4 to +4.7 ‰). This overlaps the range in δ^7Li estimated independently from peridotites.

The expanded MORB data set did provide some deeper insight, however. Tomascak et al. (2008) provided evidence for a lack of provinciality in distribution of Li isotopes in unaltered MORB from three distinct ridges. Additionally, no distinction could be made between normal-type MORB (more or less representative of depleted mantle) and enriched MORB varieties, irrespective of indices of incompatible element enrichment/depletion (for example, K_2O/TiO_2). In any case, ~3–10-fold enrichments in Li (~4 to ~13 ppm) relative to the precursor mantle could be observed (Elliott et al. 2006; Nishio et al. 2007; Tomascak et al. 2008) which may reflect moderately incompatible behavior of Li during melting of the mantle column, but consistent δ^7Li values reflect the inability of solely low-degree mantle melting to modify Li isotopes. Part of the δ^7Li variation seen in MORB may reflect incorporation of other lithologies and/or processes, most notably subduction-modified mantle enriched by fluids from the dehydrating slab (Elliott et al. 2006; Tomascak et al. 2008). However, the evidence that aberrations in δ^7Li of MORB stem exclusively from recycled components resident in the upper mantle falls far short of conclusive. For example, based on correlations between δ^7Li and halogen concentrations, Tomascak et al. (2008) favored a shallow magma chamber contamination model to explain some East Pacific Rise MORB data.

5.1.2.2 Intraplate Volcanic Rocks

The other possibility to constrain mantle composition of Li is linked to numerous occurrences

of hotspots. Although basalts from these locations derive from mantle melting, their characterization is complicated by chemical signatures which may carry evidence of recycling of distinct parts of the crust and/or marine sediments (Willbold and Stracke 2006). Thus, intraplate volcanic rocks may not be expected to yield constraints on Li in the average mantle, but they may instead be valuable tracers of the persistence of subducted components. For example, the interpretation of subduction zone rocks by Marschall et al. (2007b) is that isotopically heavy Li could later appear in OIB (ocean island basalts) through entrainment of ^{7}Li-enriched mantle wedge materials. This is consistent with the interpretation of Li isotopes from subduction zone magmatic rocks (e.g., Tomascak et al. 2000).

The first systematic Li abundance data available from various OIB such as Hawaii and Iceland pointed to limited Li enrichments and showed, with only few exceptions, concentrations <5 ppm (Ryan and Langmuir 1987). In particular locations, mostly confined to Polynesia, Li abundances up to ~10 ppm have been reported (Dostal et al. 1996). No studies of Li isotopes in OIB were published until 1999, despite the global importance of such large-scale mantle features. The results for a suite of Kilauea Iki lava lake samples, ranging from high MgO rocks to differentiated liquids with high SiO_2 and K_2O, showed δ^7Li values (+3.0 to +4.8 ‰) fully in the range of pristine MORB (Tomascak et al. 1999). Although no Li abundances were reported in that study, later results (Chan and Frey 2003) indicated that most Hawaiian basalts contained 3–5 ppm Li. These low values were supplemented by later studies of Li systematics in various OIB locations (Fig. 5.4; Pistiner and Henderson 2003; Ryan and Kyle 2004; Jeffcoate

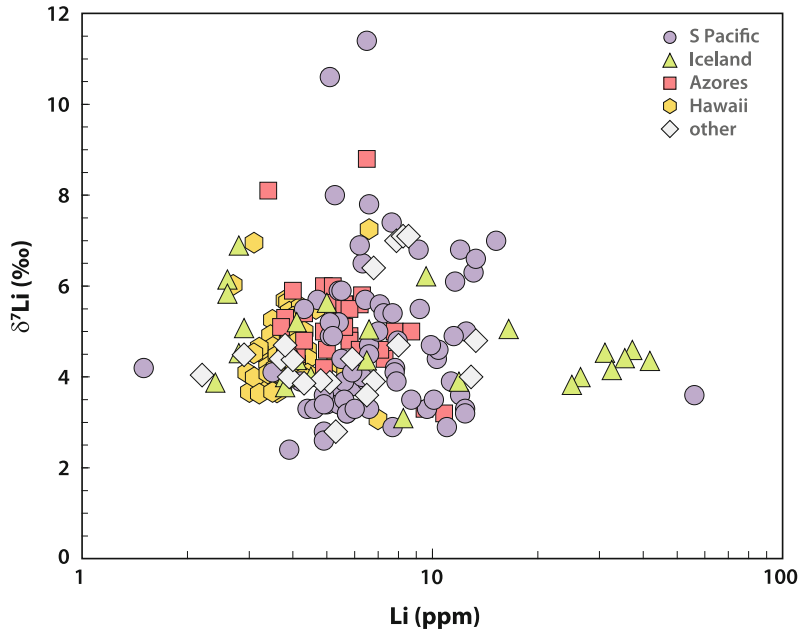

Fig. 5.4 Lithium concentration and δ^7Li in volcanic rocks from oceanic islands. These are primarily basaltic in composition, but not exclusively (e.g., some Iceland rocks with >50 wt% SiO_2). Hawaiian rocks with indication of surficial alteration have been excluded. Data sources: Hawaii from Chan and Frey (2003), Kobayashi et al. (2004), Nishio et al. (2007), Iceland from Ryan and Kyle (2004), Magna et al. (2011), Pogge von Strandmann et al. (2012), Schuessler et al. (2009), Azores from Krienitz et al. (2012), Genske et al. (2014), South Pacific (includes data of 14 different localities) from Vlastelic et al. (2009), Nishio et al. (2005), Chan et al. (2009), Krienitz et al. (2012), "other" (includes data from islands in the Atlantic and northern Pacific) from Ryan and Kyle (2004), Krienitz et al. (2012) and Magna et al. (2011)

et al. 2007; Schuessler et al. 2009; Magna et al. 2011). A bias towards higher Li contents, however, continued to be evident in classical HIMU (high μ; $\mu \equiv {}^{238}U/{}^{204}Pb$; Zindler and Hart 1986) occurrences in Polynesia (Nishio et al. 2005; Chan et al. 2009; Vlastélic et al. 2009; Krienitz et al. 2012).

Considering the lithological diversity among the inputs to subduction assemblages that contribute to the final chemical signature of subduction-modified mantle, and considering the large variability in both the Li contents and isotopic composition of these components (Bouman et al. 2004; Chan et al. 2006), it is intriguing that most OIB worldwide carry a homogeneous Li isotopic signature (Fig. 5.4). In particular, unaltered Hawaiian basalts have particularly well constrained δ^7Li values, roughly between +2.5 and +5.7 ‰ (Tomascak et al. 1999; Chan and Frey 2003; Kobayashi et al. 2004) with some subtle variations among individual volcanic systems (Mauna Kea, Mauna Loa, Koolau, Kilauea Iki). Interestingly, the Hawaiian certified reference basalt BHVO-2 has been shown to have δ^7Li in the range of the unmetasomatized peridotites (see Sect. 5.1.1.1). Most other OIB appear to mimic the mantle δ^7Li range, including lavas with (i) HIMU affinity (Cook–Austral Islands, St. Helena; Ryan and Kyle 2004; Nishio et al. 2005; Chan et al. 2009; Vlastélic et al. 2009; Krienitz et al. 2012), (ii) EM-1 affinity (Pitcairn; Krienitz et al. 2012), (iii) EM-2 affinity (Society Islands, Réunion; Ryan and Kyle 2004; Nishio et al. 2005; Vlastélic et al. 2009; Krienitz et al. 2012), and (iv) mixed affinities (Easter Island; Krienitz et al. 2012). Also, some hot spot localities associated with assumed, though not yet geophysically confirmed, mantle plume such as Jan Mayen (Debaille et al. 2009) appear to have Li systematics (Magna et al. 2011) indistinguishable from those reported for typical plume-related OIB occurrences.

Some OIB, though, carry distinctively heavy Li isotopic signature such as HIMU-type basalts with δ^7Li > +6 ‰ (Ryan and Kyle 2004; Nishio et al. 2005; Chan et al. 2009; Vlastélic et al. 2009). However, an isotopically heavy Li signature was also found in pristine non-HIMU lavas from Iceland (δ^7Li up to +9 ‰; Hansen et al. 2011; Magna et al. 2011). This signature could not be explained by contamination by meteoric water and wall rock, and may instead appeal to recycling of altered oceanic crust at large scales, or parts of previously metasomatized subarc mantle (Elliott et al. 2006; Marschall et al. 2007b). Genske et al. (2014) found that the majority of Azores lavas have MORB-like Li isotopes. Some samples in their study, however, range up to δ^7Li of +8.8 ‰; the majority of these isotopically heavy samples were attributed to shallow-level crustal contamination, although when combined with radiogenic isotope data a recycled source component in the mantle could not be ruled out. Kobayashi et al. (2004) implied a recycled component in the source of Hawaiian basaltic lavas from in situ (SIMS) Li isotopic analysis of glass inclusions enclosed in olivine phenocrysts. Their results showed a considerable spread in δ^7Li values from −10.2 to +8.4 ‰, but with low to negative δ^7Li prevailing among the data and broadly correlating with δ^{11}B values. These contrasting results indicate distinctly different compositions of recycled reservoirs that can only be more unambiguously distinguished with appropriate samples. Our understanding of behavior of Li is not yet sufficient to fully constrain the fate of subducted materials in the mantle.

Collectively, the available analyses suggest the worldwide Li isotopic homogeneity of OIB occurrences and indicate that the incorporation of materials with distinct chemistry, such as sediments (marine, terrigenous) and/or altered seafloor rocks, is not easily projected into the final δ^7Li signature. Unless these additives carry peculiar Li systematics that can be sustained through subduction processing and long-term residence in the Earth's mantle without much modification of their original Li inventory, the isotopic signal appears most commonly to be obliterated. This suggests that mixing in the mantle is largely an effective process with very few localities showing resolved departures towards non-mantle δ^7Li preserved through inefficient mixing of large-scale heterogeneities introduced into the deeper mantle. We cannot

exclude the impact of changes in physics of the mantle throughout Earth's history, considering, for example, that the HIMU signature is known to be of ancient origin (Hofmann and White 1982; Zindler and Hart 1986; Sobolev et al. 2007).

Compared with more or less localized OIB localities, continental basaltic volcanism includes large igneous provinces, some of the most voluminous effusive igneous products on Earth. These may exceed 1×10^6 km^3 total volume, cover areas often $>1 \times 10^6$ km^2, and vary in age from Mesoproterozoic to Neogene. Given such volumes present at the Earth's surface it is surprising the Li systematics of these occurrences are highly under-represented in the literature database. One of the commonly used basalt certified reference rocks, BCR, derives from the Columbia River large igneous province. Three different aliquots of the rock have been issued (BCR-1, BCR-2 and BCR-2G), all showing elevated Li contents (~9–12 ppm) relative to MORB and OIB, but with somewhat variable δ^7Li values between +2 and +5 ‰, mostly hinging on resolvedly higher δ^7Li of BCR-2G (+4 to +5 ‰). Liu et al. (2013) measured Li isotopes in Columbia River basalts at two sites, with average δ^7Li of +0.5 ± 1.0 ‰ and +1.7 ± 2.2 ‰. These values are in line with the low values measured in BCR-1 and BCR-2, and point to sources with a component isotopically lighter than N-MORB. One possibility would be represented by sources that assimilated continental crust, consistent with the interpretation of Carlson et al. (1981), based on radiogenic isotopic systematics.

The somewhat Li-enriched nature of alkali basalts in continental settings (Fig. 5.5) was already observed by Ryan and Langmuir (1987) for a few occurrences and later in more detail by Mengel and Hoefs (1990), who noted that

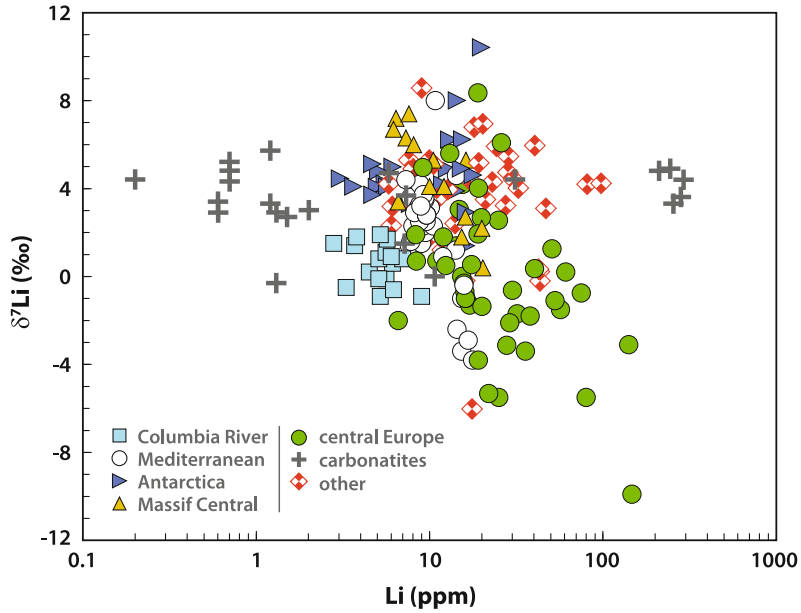

Fig. 5.5 Lithium concentration and δ^7Li in continental igneous rocks, primarily ultramafic to intermediate composition volcanic rocks, many associated with extensional tectonic settings, but also including carbonatites and selected mafic plutonic rocks. Data sources: Antarctica from Ryan and Kyle (2004), Columbia River flood basalts from Liu et al. (2013), Mediterranean (includes data from Sardinia and Stromboli) from Schiavi et al. (2010), Kim et al. (2011), Massif Central from Hamelin et al. (2009), central Europe from Abdelfadil et al. (2014), Ackerman et al. (2015), carbonatites from Halama et al. (2007, 2008), "other" (includes data from silicate rocks from eight globally dispersed regions) from Ackerman et al. (2013), Magna et al. (2008), Halama et al. (2008, 2009), Marks et al. (2007), Rudnick and Ionov (2007), Kil (2010) and Tomascak and Magna (2014)

contamination of alkaline magmas by continental crust may have operated for Cenozoic alkaline basalts from Germany based on Li–SiO_2–$\delta^{18}O$ variations. Contamination of this type would mask the indigenous Li inherited from alkali basalt sources due to the high Li content of the continental crust (Teng et al. 2004). However, the Li contents in such assemblages may be quite low. This is apparent from the study of Weyer and Seitz (2012) who analyzed matrix and olivine of several basaltic rocks from alkaline complexes in Germany (Vogelsberg, Hegau, Westerwald), related to pan-European Cenozoic volcanism (e.g., Wilson and Downes 1991). These data showed Li abundances to be at the lower end of alkaline volcanic rocks (6.2–7.9 ppm), paralleled by rather homogeneous δ^7Li values between +2.5 and +4.7 ‰. In all instances the olivine had lower Li concentration than matrix but highly variable δ^7Li (from −10.5 to +6.5 ‰), attesting to significant exchange between olivine and melt by diffusion, as predicted by Gallagher and Elliott (2009). In particular, the Li-rich olivine from Vogelsberg nephelinite carried the lightest Li isotopic signature but Weyer and Seitz (2012) estimated ∼50 % of this olivine to be xenocrystic in origin, supported by unusually high Ni contents and Mg# significantly above the mantle value. The ensemble data implied more pronounced effects of disequilibrium on lavas containing xenocrysts rather than phenocrysts.

The preliminary report of Magna and Rapprich (2012) for a suite of chemically pristine alkaline lavas (melteigites, ijolites, essexites) from the Bohemian Massif revealed low to moderate (∼4–16 ppm) Li abundances. Samples from the geochemically complex Doupovské hory Volcanic Complex, Czech Republic, yielded δ^7Li values that varied from mantle-like towards both ^7Li-depleted and ^7Li-enriched compositions (−1 to +11 ‰), whilst pristine high-MgO (>12 wt%) basanites from another suite showed little variation in δ^7Li, all within the mantle range. Similar Li elemental and isotopic homogeneity has been found for three host basanites from NE Bavaria, Germany, all with ∼6 ppm Li (Ackerman et al. 2013). On the other hand, a xenolith-bearing Cenozoic basalt from Mongolia had an isotopically heavy signature (δ^7Li = +8.6 ‰; Magna et al. 2008) but the nature of this distinctive value remains to be explored.

Several suites of Antarctic intraplate alkaline lavas were examined by Ryan and Kyle (2004), who noted moderately incompatible behavior of Li in magmatic processes and distinctive Li/Yb in intra-plate rocks versus MORB, tentatively ascribed to different mantle sources. Chemically less evolved Antarctic intraplate lavas (e.g., from the Crary Mountains with MgO > 6 wt%, but also other occurrences with MgO contents 3–5 wt%) confirm the largely homogeneous Li isotopic signature of source mantle of these alkaline rocks (δ^7Li = +3.3 to +5.0 ‰). Together, these samples were considered least affected by crustal contamination and open system processes. The homogeneity of Li isotopes in intraplate settings has further been validated by Halama et al. (2009) for several basaltic andesites from the Avachinsky volcano in Kamchatka that mimic Li elemental and isotopic systematics of the Antarctic rocks.

These suites that show only limited Li isotopic variability contrast to a certain extent with isotopically heavy Li found in alkaline basaltic lavas from the Massif Central in France (Hamelin et al. 2009). The δ^7Li values up to +7.4 ‰ were discussed in the context of a HIMU component in the source of Cenozoic basalts across Europe that has also emerged from the Sr–Nd–Pb isotopic perspective (e.g., Blusztajn and Hart 1989; Wilson and Downes 1991). On the other hand, a light Li isotopic signature (δ^7Li as low as +0.4 ‰) found in chemically more evolved lithologies of the Massif Central, such as benmoreites and trachytes, provides evidence for the assimilation of lower continental crust components, as gauged through metasedimentary xenoliths. These inferences are also in accord with variations in Li concentration from 6 to 20 ppm, increasing consistently with the degree of fractional crystallization (Hamelin et al. 2009). Contrary to findings of Hamelin et al. (2009), Ackerman et al. (2015) did not observe a similar unidirectional evolution of Li abundance and isotopic composition in a suite of trachytes, trachyandesites and phonolites from the Bohemian

Massif. This may, in part, be due to the fact that these samples were not co-genetic (cf. a closed-system suite analyzed by Hamelin et al. 2009), although modelling of fractional crystallization showed clear overall evolution trends. Large extents of fractional crystallization of olivine + clinopyroxene + amphibole + plagioclase appear to have been detected in elevated Li contents of some phonolites (up to 75 ppm) whereas open-system behavior is evidenced by (i) a peculiar dichotomy in Li–Cs elemental systematics, and (ii) a large variation of δ^7Li between −5.3 and +8.4 ‰ without any particular systematic behavior (Ackerman et al. 2015).

Interestingly, isotopically light mantle domains beneath some parts of Europe have also been invoked for tholeiites collected from the vicinity of Etna volcano on Sicily (Gurenko and Schmincke 2002), based on coupled Li–B isotopic compositions in glass inclusions and their host glasses (δ^7Li from −3.3 to +1.2 ‰). However, Gurenko and Schmincke (2002) implied former subduction as an ultimate source of light Li rather than assimilation of continental crustal rocks altered under hydrothermal conditions. Abdelfadil et al. (2014) reached the same conclusion from the isotopic compositions of Paleozoic calc-alkaline lamprophyres in the northern Bohemian Massif (δ^7Li from −5.5 to +1.9 ‰). In their study, correlations between Li concentration, δ^7Li, radiogenic isotopes and other trace elements were interpreted to rule out diffusional control and instead argued for a mantle component derived ultimately from subducted components, principally originating in sediments.

These findings perhaps explain predominantly light Li isotopic composition in basalts from Sardinia (δ^7Li from +1.5 to +3.6 ‰, with a single basalt with a distinct REE pattern at +8.0 ‰; Kim et al. 2011). These authors implied that the light Li and EM-1-like incompatible trace element signature could be reconciled with the absence of altered oceanic crust. They suggested that diffusion may have caused ^{7}Li depletion in the initial mantle source of the Sardinian basalts although at these scales complete diffusive modification may not be easily achieved. Predominantly light Li was also observed in olivine-hosted melt inclusions from the Stromboli volcano pumices (Schiavi et al. 2012) when compared with their host lithologies (Schiavi et al. 2010). Modeling suggested that this prevalently light Li (and B) isotopic signature may have originated through metasomatic overprinting by high-pressure fluids released from dehydrated metasediments and metabasites. This notion may be reasonable considering fractionated Li signature in fluids derived from a subducted slab (John et al. 2012).

The complex behavior of Li in alkaline complexes has been illustrated by Marks et al. (2007), who analyzed amphibole and clinopyroxene from feldspathoid-bearing rocks (agpaites: lujavrites, kakortokites, naujaites etc.) of the Ilímaussaq plutonic complex, South Greenland. The particularly Li-enriched character of sodic amphiboles (up to ~3100 ppm Li, broadly correlating with increasing degree of differentiation) contrasted strongly with low Li contents in Ca-amphibole (7–68 ppm) and consistently low Li contents in co-existing clinopyroxene (15–84 ppm). Moreover, Li correlated positively with $Fe^{3+}/\Sigma Fe$ in Na-amphibole, indicative of a possible proxy for redox conditions during magma crystallization (Marks et al. 2007). Homogeneity in δ^7Li values of amphiboles from the inner part of the Ilímaussaq complex (~+2 ± 2 ‰) were thought to reflect mantle-derived origin, a conclusion supported by coupled Nd–O isotopic systematics which largely precluded significant crustal contamination. Open system post-magmatic kinetic modifications resulting from the ingress/circulation of ^{7}Li-enriched fluids were advocated for outer lithologies of the complex (Marks et al. 2007).

Collectively, Li isotope systematics in intra-plate alkaline volcanic rocks may in favorable situations disclose important processes of tapping heterogeneous mantle components as well as assimilation of evolved lithologies associated with fractional crystallization although from a global perspective, the available Li abundances and isotopic compositions appear to be broadly consistent for distinct locations. Yet, the number of studies that consider tectonic settings with thick continental crust penetrated by

alkaline liquids derived from asthenospheric depths is so far very limited. Further studies of intra-plate plutonic and volcanic sequences carrying chemical signatures of distinctive secondary processes await more in-depth exploration.

Carbonatites have also been used to unravel the Li isotopic evolution of the Earth's upper mantle through time (Halama et al. 2007, 2008). Carbonatites have long been considered potential probes of the sub-continental mantle. Taking into account their rapid ascent and extremely low viscosities, carbonatite magmas are less susceptible to chemical modification during transport through the crust and can therefore preserve pristine mantle signatures better than other mantle-derived magmas (Bell 1989, 1998). Apart from massive enrichments in large ion lithophile elements (LILE; K, Rb, Cs, Sr, Ba), high-field-strength elements (HFSE; Zr, Hf, Nb, Ta, Th, U) and the light rare earth elements (LREE; La–Sm) (e.g., Bizimis et al. 2003; Chakhmouradian 2006), available Li data for carbonatites show variable depletions and enrichments from sub-ppm levels in calcic and silicic carbonatites to several hundred ppm Li in sodic carbonatites (up to ~300 ppm; Halama et al. 2007, 2008). It appears, too, that these values reflect the mantle source of carbonatites rather than kinetic processes and/or contamination (Cooper et al. 1995; Halama et al. 2008). The geochemical signatures of carbonatites have been explained by the involvement of enriched mantle, lithospheric mantle and/or HIMU mantle (e.g., Bell and Simonetti 1996; Bell 1998). Considering the Li isotopic disparity between some of these "global" mantle end members (Chan et al. 2009; Vlastélic et al. 2009; Krienitz et al. 2012), differences in δ^7Li could eventually distinguish between individual contributions from these geochemically distinctive reservoirs (Zindler and Hart 1986). Yet, carbonatites analyzed by Halama et al. (2007, 2008) fall into a narrow range of δ^7Li (+4.1, ± 2.6 ‰, 2σ); this isotopic homogeneity extends from recent back to ~2.7 Ga. This finding may suggest that either the mantle source of carbonatites is homogeneous across the time and space, or that any δ^7Li variation in the original carbonatite source has been homogenized with time as a consequence of the high mobility of Li.

A more detailed assessment of Li elemental and isotopic distribution in carbonatites from southwestern China and their relation to coexisting syenites was explored by Tian et al. (2015). Bulk carbonatites had between 1 and 120 ppm Li; arfvedsonite and biotite had >360 ppm Li, with apparent partition coefficient $K_d^{arfv-WR} \sim 8–12$. An even larger difference of ~22 was found for a single analyzed biotite–whole rock pair. The large range in Li contents of carbonatites contrasted with rather small abundance variation in associated syenites (4–39 ppm). Notable variation in δ^7Li for the whole suite (−4.5 to +10.8 ‰) was found, although the majority of data are between ~0 and ~+4 ‰. By excluding kinetic effects by diffusion, Tian et al. (2015) advocated for isotopically heterogeneous sub-continental lithospheric mantle modified by subduction-derived fluids that bore the imprint of marine sediments and subducted oceanic crust. Isotopically anomalous sub-continental lithosphere has been invoked also for other regions of China (see Sect. 5.1.1) based on detailed analyses of minerals from mantle xenoliths.

These findings may collectively suggest that Earth's upper mantle may, in places, be far from a homogeneous reservoir and that under particular conditions, regions in the mantle may exist that carry significantly different load of Li. Whether such 'oddities' are rather rare and related to specific petrogeny and what consequences for mantle dynamics these unusual magmas may have, remains to be investigated in the future.

5.1.2.3 Arc and Back-Arc Rocks

Volcanic arcs are among the dominant morphologic features shaping the Earth's surface and volcanism at convergent margins gives rise to large batches of magma with peculiar elemental budgets which contribute significantly to the construction of the continental crust (Gill 1981). Because these massive collisional arcs include an extraordinary lithological diversity from marine and continental sediments through magmatic

rocks to metamorphic sections, large variability in Li elemental distribution and isotopic composition of terminal products of arc magmatism may be expected. The variability of sedimentary input in Li contents from sub-ppm to a few hundred ppm, and in δ^7Li at the >20 ‰ scale (Chan et al. 1994; Chan and Kastner 2000; Bouman et al. 2004; Chan et al. 2006; Chan and Hein 2007) contrasts with largely homogeneous Li contents and isotopic compositions of non-sedimentary portion of the oceanic lithosphere, although important vertical Li variability of oceanic crust exists (Chan et al. 2002a; Gao et al. 2012).

The importance of sedimentary input to the Li budget of arc volcanic rocks when combined with other trace element indicators such as Li/Y has recently been evaluated by Plank (2014), noting that Li enrichment from the sedimentary column may become significant in some locations (e.g., Cascades, eastern Sunda, Aleutians) while it is less important for other arcs (e.g., Tonga, Mariana, Central America). Apart from sedimentary input (and altered oceanic crust in bulk), fluids operating in subduction zones may bear collateral information on their sources and processes that take place across the oceanic lithosphere as a consequence of progressive dehydration and preferential loss of isotopically heavy Li into the fluid (aqueous) phase for which ^{7}Li has greater affinity than ^{6}Li (Yamaji et al. 2001; Wunder et al. 2006). Ground truth for this relationship is inferred from the isotopically heavy muds exuded by serpentinite seamounts (Benton et al. 2004).

A prominent feature of Li is its dualistic behavior as (i) a moderately incompatible element in melting process (Brenan et al. 1998a) and (ii) a fluid-mobile element in aqueous transfer (Berger et al. 1988; Brenan et al. 1998b). Therefore, the changes in its distribution during dehydration can track the 'wet' history of the respective lithology and provide constraints on the nature of hydrously altered crust in early stages of subduction and beyond (Marschall et al. 2007a). An early experimental work of Seyfried et al. (1998) revealed large variations in δ^7Li for hydrothermal conditions related to the loss of fluid-mobile elements such as Li, K, Rb, Cs and B and implied significant Li isotopic fractionation during alteration of seafloor basalts (weathered basalt with starting δ^7Li = +7.4 ‰) as an important input to the subduction factory. The rapid development of fluid containing isotopically heavy Li (δ^7Li up to +14 ‰), paralleled by high Cs/Rb, suggested preferential decomposition of low-temperature alteration phases such as clay minerals. The role of these secondary phases in cycling of Li during seafloor weathering and hydrothermal circulation was further constrained by James et al. (2003) who implied that fluid/solid ratios may bear important control on Li isotopic fractionation as well as the partitioning of Li into fluid or solid phases at elevated temperatures.

The expulsion of fluids coupled with compaction of mainly the loose sedimentary cover in incipient stages of subduction is followed by prograde metamorphic dehydration reactions ultimately leading to 'dry' eclogites, representing dehydrated residues of subducted slabs. This paradigm originally led Zack et al. (2003) to propose a model of Li isotopic fractionation through loss of aqueous fluids during subduction. They found large Li isotopic variations in omphacite (a complex Ca–Na–Mg clinopyroxene) from eclogites (δ^7Li between −11 and +5.3 ‰, with negative δ^7Li measured in 9 out of 11 whole-rock samples) and interpreted these findings as a result of preferential loss of ^{7}Li into the aqueous phase, leaving the residual solid isotopically light Li. However, it is not yet clear whether Li should be fractionated during subduction at all. Employing more recent experimental constraints, Marschall et al. (2007b) examined a large set of worldwide orogenic ecogites and provided an alternative interpretation of their Li isotopic signatures. They estimated a maximum δ^7Li decrease of ∼3 ‰ in eclogites as a consequence of metamorphic dehydration reactions and stressed that much of the δ^7Li variation towards lower values observed in eclogites may be accommodated through kinetic re-distribution and addition of Li from ambient country rocks.

However, not all δ^7Li variations in subduction-related lithologies can be explained by the mobility of Li isotopes via diffusion (e.g., Agostini et al. 2008), and it is becoming increasingly clear that Li may be retained in subducted residues which resist attenuation of the original Li isotopic signature through diffusion over extended time scales (e.g., Marschall et al. 2006, 2007a; Chan et al. 2009; Vlastélic et al. 2009; Tang et al. 2012). Moreover, physical constraints such as the angle and rate of subduction, thickness of oceanic crust and sedimentary cover, temperature, heat flow, age, degree of alteration, etc. all play roles in determination of the fate of Li in the subduction factory.

The pilot studies of Li systematics at convergent margins were mixed on whether important across-arc variations occur in volcanic lavas. Moriguti and Nakamura (1998) noted strong correlation of δ^7Li and slab depth in the Izu–Bonin arc, concluding that the samples reflected mixtures of an isotopically light mantle component with an isotopically heavy slab fluid component. Their initial interpretation would require an uncontaminated mantle with δ^7Li $\sim$ 0 ‰, which is inconsistent with our understanding of the pristine mantle. Of note, the two isotopically lightest lavas were rhyolitic in composition. If, therefore, these samples reflect some degree of crustal contamination, the implied mantle end-member shifts to δ^7Li $\sim$ +2 ‰.

Tomascak et al. (2000) also examined lithologically heterogeneous arc volcanic rocks (all with SiO_2 > 50 wt%) and reached different conclusions on the nature of Li delivery to the sources of arc magmatism. The lack of correlation between δ^7Li and typical indicators such as B/Be among the Panama arc samples was interpreted to reflect in general a sequestration of slab-derived Li in the subarc mantle. That some samples showed elevated δ^7Li (up to +11.2 ‰) despite low B/Be was interpreted to reflect the influence of tectonics and the thermal state of the arc, with slab-derived ^{7}Li-enriched mantle being tapped after it had lost most of its slab B. Whereas Chan et al. (2002b) (a re-reporting of corrected data from Chan et al. 1999; see Sect. 5.2.2) incorporated high-MgO lavas, less prone to wall-rock contamination, in their Central American arc study, the samples had δ^7Li of roughly between +4 and +6 ‰. With a data set that included three intra-oceanic arcs and samples ranging from 43.9 to 64.7 wt% SiO_2, Tomascak et al. (2002) illustrated a general lack of correspondence between Li isotopes and indicators of slab fluid involvement (B/Be, Ba/La, Li/Y).

The results of these earlier investigations produced a pessimistic picture of the viability of arcs for elucidating the pathways of Li cycling. More recent studies, however, produce a more complex (and perhaps somewhat more optimistic) view (see Tomascak 2015). Primitive high-MgO tholeiites and basaltic andesites (>6 wt% MgO) from two different volcanic systems in the southern Cascades oriented perpendicular to the volcanic front were formed by near-anhydrous melting of spinel peridotite (Grove et al. 2002) and yet showed decreasing δ^7Li with increasing depth of the Wadati–Benioff zone (i.e., increasing distance from the arc trench; Magna et al. 2006b). By ruling out contamination by continental crustal materials, addition of slab-derived Li with apparently fractionated signature was suggested. A report by Leeman et al. (2004) for a suite of tholeiites, basaltic andesites and nephelinites from the northern section of the Cascades across southern Washington (some 500 km north of Mt. Shasta region studied by Magna et al. 2006b) revealed no apparent across-arc variations in δ^7Li. Indeed, the study of Leeman et al. (2004) traced the weakened signal of material from incoming slab to vanishing amounts in the back-arc region by using trace element parameters (e.g., Li/Y, B/Nb, Ba/Nb) combined with isotopic compositions of B and radiogenic lithophile elements (Sr–Nd–Pb).

It is interesting to note that similar discrepancy between Li isotopic systematics in two distinct sections of a single arc system (or spatially closely related arcs) was also found for the northeastern Japan arc which is nearly perpendicular to the Izu arc. Compared with well-defined negative correlation between δ^7Li and distance from the trench found for the Izu arc (Moriguti and Nakamura 1998). Moriguti et al.

(2004) found no across-arc variations in δ^7Li. Thus, more generally, it appears that there may be substantial differences in the products of arc volcanism in terms of their Li inventory. These differences may, in part, stem from distinctively different sedimentary inputs that could vary greatly not only among different arc systems but also along a single arc (Bouman et al. 2004; Chan et al. 2006). The Li budget of the complete sedimentary section entering individual arc segments should thus be ascertained in order to better understand (or indeed to more accurately quantify) the Li cycle in arcs. No better characterization of a sedimentary component in the source of arc magmas has been made than the study of Tang et al. (2014a). Their results show conclusively that isotopically light sea floor sediment transferred its Li payload to the subarc mantle, with approximately 4 % sediment component in the lightest lavas, as deduced from relationships between δ^7Li and Y/Li. Similar element-isotope coupling was demonstrated by the earlier findings of Clift et al. (2005) from Costa Rican tephra.

Agostini et al. (2008) analyzed Li–B isotopes in a suite of alkali-rich basaltic lavas through calc-alkaline to ultra-potassic lithologies from the convergent margin of western Anatolia (Turkey) that revealed a significant range in δ^7Li values (>15 ‰), paralleled by moderate to high Li abundances (7–53 ppm). The model developed to explain these results involved the interplay of tectonics on the variable role of slab-derived fluids. The authors ruled out kinetic modification of the Li isotopic signature in these rocks based on other geochemical parameters (δ^{11}B, B/Nb, B/Be, etc.), as well as a general skepticism of the scale of such effects. They also sidestepped the conclusion of Marschall et al. (2007b), that subducting slabs will not develop very isotopically light signatures by a distillation process, by implying that the cessation of subduction would more effectively dehydrate the slab. In this case, protracted dehydration would produce slab fluids with δ^7Li < MORB (Agostini et al. 2008).

Similar conclusions have been reached by analysis of melt inclusions in arc lavas, although two studies of the Lesser Antilles arc returned somewhat contrasting results. Gurenko et al. (2005) analyzed glass inclusions hosted from a rhyolite from the island of Dominica; they obtained generally lower δ^7Li values for inclusions entrapped in orthopyroxene (+4.2 to +11.6 ‰) relative to those in plagioclase (+7.4 to +14.7 ‰), paralleled by variable but overall high Li contents (20–60 ppm). Hydrothermally altered volcanic sequences of the subducted oceanic crust were advocated to contribute significantly to ^{7}Li-enriched character, also supported by high δ^{11}B values. The lower δ^7Li values in plagioclase-hosted inclusions were interpreted to reflect post-solidification kinetic effects that did not affect inclusions in orthopyroxene (Gurenko et al. 2005). Somewhat different results were presented for St. Vincent Island, c. 300 km south of Dominica (Bouvier et al. 2008). Olivine-hosted glass inclusions from St. Vincent had consistently lower Li abundances (2.6–9.2 ppm) compared to those examined by Gurenko et al. (2005), and δ^7Li appeared to vary greatly from MORB-like values (roughly between +2 and +6 ‰) towards significantly lighter ones (as low as −10 ‰; Bouvier et al. 2008). These latter authors advocated for fluids from dehydrated altered oceanic crust, without appeal to Li-rich sedimentary lithologies. To account for the abundances of Cl and S observed in some melt inclusions, seawater-like fluids were invoked in the mantle source of such melts. The lack of a distinguishable Li elemental and/or isotopic signature from such a source was considered a reasonable consequence of the low Li content of seawater; at very low mass fraction, such a component would be incapable of perturbing Li systematics. Collectively, it appears that understanding the exact process of transfer of fluids with peculiar Li systematics and transport efficiency from the subducted slab into and through the overlying mantle wedge still requires experimental work as well as field studies. A rapid rise of fluids produced in the dehydration of a subducting slab, during discrete events, has been invoked by John et al. (2012). An estimate of ~200 years for fluid transport through the system was derived from modeling diffusive Li elemental and isotopic data from veined

subduction zone rocks in China, taking into account changes in Li distribution and porosity. Dehydrated seawater-altered oceanic lithosphere was inferred as a source of these fluids although the exact origin (volcanic section of the oceanic crust or lithospheric mantle) could not be unequivocally distinguished (John et al. 2012).

A limited communication between the residual dehydrated slab and the sources of back-arc lavas appears to be a distinctive signature of Li isotopic system when compared to volcanic rocks from the arc front. Whilst Li systematics have been explored in a number of studies of convergent margins, little effort has been made in characterizing the fate of Li in back-arc regions where slab-derived liquids may already impart insignificant control on the bulk chemistry of back-arc magmas. The first reported data from back-arc region of the Lau basin (Chan et al. 2002b) centered at δ^7Li $\sim$ +4.5 ‰ and modest Li contents ($\sim$5 ppm) that are at the lower end of what has been reported for subduction-related magmas. Further analyses of back-arc lithologies (OIB-like basalts, basaltic andesites, high-K calc-alkaline basalts) were performed by Leeman et al. (2004) for the northern Cascades but neither Li contents (5.6–11.1 ppm) nor δ^7Li values (+2.9 to +4.9 ‰) implied distinctive variation in Li isotopes that could be caused by large-scale influx of subduction-related components. The MORB-like δ^7Li values were, in part, paralleled by δ^{11}B values (<−8 ‰) more typical of common OIB (Leeman et al. 2004). Rift-related Anatolian alkalic lavas (6–9 wt% MgO) (Agostini et al. 2008) showed moderate Li enrichment ($\sim$11 ppm) and broadly MORB-like δ^7Li ($\sim$+3 ‰ save for one sample at −0.4 ‰). The preliminary results of Brens et al. (2013) for an across-arc profile in the Tonga–Kermadec arc show large δ^7Li scatter in arc lavas as a consequence of possible fluid transfer from sediments (consistent with trace elements constraints) while the Fonualei back-arc lavas appear to have δ^7Li indistinguishable from the MORB range.

Two studies to date have focused exclusively on arc lavas related to processes behind the volcanic front. Back-arc Cenozoic alkaline lavas from the James Ross Island (Antarctic Peninsula) were analyzed for their Li contents and isotopic compositions by Košler et al. (2009). These authors did not find any significant variation beyond the values reported elsewhere (Li = 4.6–7.3 ppm; δ^7Li = +3.3 to +4.9 ‰). Two outliers with somewhat more variable δ^7Li (+1.5 and +6.8 ‰) were explained through the incorporation of either a sedimentary component or hydrothermally altered oceanic crust, as also inferred from trace element systematics, but it could also reflect local inhomogeneity at intra-sample scale. Janoušek et al. (2010) investigated the Li geochemistry and isotopic systematics of back-arc lavas from Nicaragua and adjacent Caribbean Sea occurrences. The homogeneous δ^7Li values of these samples (+3.8 to +5.2 ‰) underscore the lack of mass transfer from frontal arc systems into the source region of back-arc lavas. A localized sub-group of samples shows a slightly lighter average Li isotopic signature (δ^7Li $\sim$ +2 ‰), paralleled by resolved differences in Sr–Nd–Pb isotopic compositions compared with the rest of the suite. This may imply incorporation of a seafloor sediment component into the source of some Nicaraguan back-arc lavas. Walker et al. (2009) noted similarly light Li isotopic compositions (δ^7Li < +3 ‰) in a subset of behind-arc lavas from southeastern Guatemala and western Salvador whilst volcanic front lavas from the same area generally had MORB-like δ^7Li. Collectively, these studies have shown uniformly that mass transfer between the subduction region and the back-arc environment apparently is subordinate and does not result in volumetrically significant source components with isotopically distinguishable signature in back-arc lavas.

Whereas there is an increasing number of studies that show discernible Li isotopic variations in arcs, the number of locations with δ^7Li essentially equivalent to MORB is significant. This observation begs the question: why does such limited variation occurs so commonly? If slab Li is transferred into the sources of arc magmas, either its net isotopic signature is sufficiently similar to MORB that it leaves no isotopic trace or there is an isotopic fractionation in the subduction process for which we are inadequately accounting. The

following scenarios summarize the most probable resolutions to arcs where no Li isotopic "slab signature" is exhibited.

(1) *The Li isotopic signal of subducted material is attenuated before reaching the region of melting in the subarc mantle.* As proposed originally by Tomascak et al. (2000, 2002), this model calls for the fluid mobility of slab Li to be counteracted by its moderate compatibility in mantle silicate minerals. Evidence in favor of this may be manifest in certain xenoliths from the subcontinental lithosphere (e.g., Tang et al. 2007), whereas Plank (2014) argued against this mechanism on the basis of elevated Li/Y in all arc magmas.

(2) *Equilibrium slab inputs may not be isotopically distinct from MORB.* Based mainly on elemental systematics, Plank (2014) argued that a slab Li signature is reasonably well preserved in most arc settings. The original studies on the topic predicted isotopically heavy slab fluids, dominated by altered oceanic crust (Moriguti and Nakamura 1998; Tomascak et al. 2000; Chan et al. 2002b). Owing significantly to the paucity of early data on marine sediments, as well as the preliminary indications that such materials were isotopically heavy compared to MORB (Zhang et al. 1998), the Li perspective on the role of sediments in arc magma petrogenesis was initially hampered. With an improved estimate of Li in global marine sediments (mean δ^7Li $\sim$ +4: Chan et al. 2006; +2.4: Plank 2014), it is clear that, depending on the incoming lithologic assemblage, the incorporation of sedimentary source components in arcs may generate imperceptible isotopic effects (indeed it appears that a sediment signal traceable with Li isotopes may be rare; Tang et al. 2014a). Additionally, mixtures of isotopically heavy altered oceanic crust components with isotopically light sediment components are likely to yield fluids with broadly MORB-like Li isotopes.

(3) *Isotopic disequilibrium from kinetic processes during slab fluid release and/or transport.* The model proposed by Marschall et al. (2007b) suggests minimal isotopic fractionation into fluids from high pressure metamorphism of subducted sediments. This implies that fluids separated from metamorphosed MORB would lack a distinctive isotopic signature. Similarly, isotopically light fluids en route to the region of melt generation in the subarc mantle might preferentially lose an isotopically light component through diffusion, potentially wiping out or at least reducing the slab signature.

(4) *Contamination and isotopic re-equilibration during melt transport to and storage within the crust.* Walker et al. (2009) implied that much of the δ^7Li variation within part of the Central American arc system was likely related to kinetic overprinting of original Li isotopic systematics. Similarly, Cabato et al. (2013) indicated that variations in Li–Be–B concentrations, coupled with Li isotopes, in plagioclase phenocrysts from Santorini, are best explained by late-stage processes (e.g., magma chamber decompression). Detecting Li isotopic influences from this group of processes is facilitated by in situ analysis of crystals, where diffusion profiles can be assessed relative to the host magma.

5.2 Lithium in the Continental Crust

5.2.1 Products of Crustal Melting

Broadly speaking, melting of the continental crust produces silica-rich magmas, many of which form major granitic bodies. Attempts to use elemental and isotopic geochemistry to unravel the sources and petrogenetic histories of such bodies have met with mixed results (Taylor and McLennan 1985), although a paradigm that is widely used separates granitic rocks into generally distinct groups (e.g.,

Chappell and White 2001). The reader is directed to summaries such as that of Barbarin (1999) for more detail on granite typology. Despite the significance of granitic rocks to the architecture of the continental crust and their general enrichment in Li relative to the mantle, it has only been recently that Li isotopic research has turned to this subject in earnest. Some of these studies have focused on using granitic bodies as grand averagers of the bulk continental crust, whereas others have attempted to understand the extent to which Li isotopes may inform us about both source and magmatic processes.

Although before the era of well-quantified Li isotope measurements, Plyusnin et al. (1979) reported on Li isotopes in granitic rocks. Their results suggested that the more geochemically evolved samples of a suite of evolved granites had the lightest Li isotopic signatures. They suggested that a linear relationship between the Li isotopic composition and the content of F (and Li) in a suite of granitic rocks was best explained by closed system fractionation. This interpretation appears out of step, however, with more recent studies of high-F granitic suites (e.g., Romer et al. 2014) and of granites in general.

Nevertheless, the suggestion that Li isotopes could be used to distinguish rocks that had experienced metasomatic or other secondary phenomena from those which record purely magmatic histories (Plyusnin et al. 1979) remains viable. The calculations of Teng et al. (2006b) support this relationship: minerals that form from late-stage fluids or interact with sub-solidus fluids should be discernible through the development of heavier isotopic compositions. Data from the peralkaline Ilímaussaq complex in Greenland (Marks et al. 2007) support the action of late-stage, externally derived fluids to account for isotopically heavy pluton margin samples.

The first systematic study of granitic rocks in the more modern analytical era came from Bryant et al. (2004), with a data set from the New England Batholith of southeastern Australia. They examined both S-type (broadly sedimentary-derived) and I-type (broadly igneous-derived) sample suites. Their results provided further evidence that isotopic fractionation driven by fractional separation of mafic minerals like biotite and amphibole was inadequate to produce measurable (±1 ‰) isotopic variation. This conclusion has been echoed by other studies of granitic suites (Teng et al. 2004, 2009; Magna et al. 2010). This is good news, in that it verifies that granitic rocks should faithfully inherit the Li isotopic compositions of their sources.

Studies conducted in terranes with multiple granite types have yielded no consistent conclusion with regard to the interpretation of Li isotopic compositions. Lithium isotopes in Australian S-type samples were more homogeneous than those of I-type; δ^7Li in the I-type granites examined overlapped completely the S-type range, but extended to substantially higher values (up to c. +8 ‰; Bryant et al. 2004). A smaller data set of samples of southeastern Australian granites (Teng et al. 2004) reproduced the offset between isotopically lighter S-type and heavier I-type suites, although the mean values of δ^7Li for both were lower (Fig. 5.6a). This would be largely consistent with the Li isotopic systematics of the precursors of I and S-type granites: the former granites would reflect meta-igneous lithologies with a predominantly positive δ^7Li range whilst generally isotopically light meta-sedimentary parentage would be sought in the latter granites. However, granitic rocks from the Western Carpathians (Magna et al. 2010) showed a contrary Li isotopic relationship, with much more variable signatures of S-type granites than I-type. It should be noted that the majority of these studies concentrated on dispersed granitic bodies, typically using a single representative sample for an individual pluton. In cases where multiple samples were analyzed from one intrusion, internal δ^7Li variation of 3–4 ‰ was not uncommon (e.g., Qingshui, China: +0.05 to +4.6 ‰ for six samples; Teng et al. 2009). The extreme manifestation of this came from the detailed study of the layered Harney Peak Granite intrusion, where Teng et al. (2006b) found a total range in δ^7Li of 9.7 ‰ for 25 samples (Fig. 5.6b). Thus, the results of studies of granitic terranes which use individual samples to represent entire plutons may be misleading and should be interpreted with great caution.

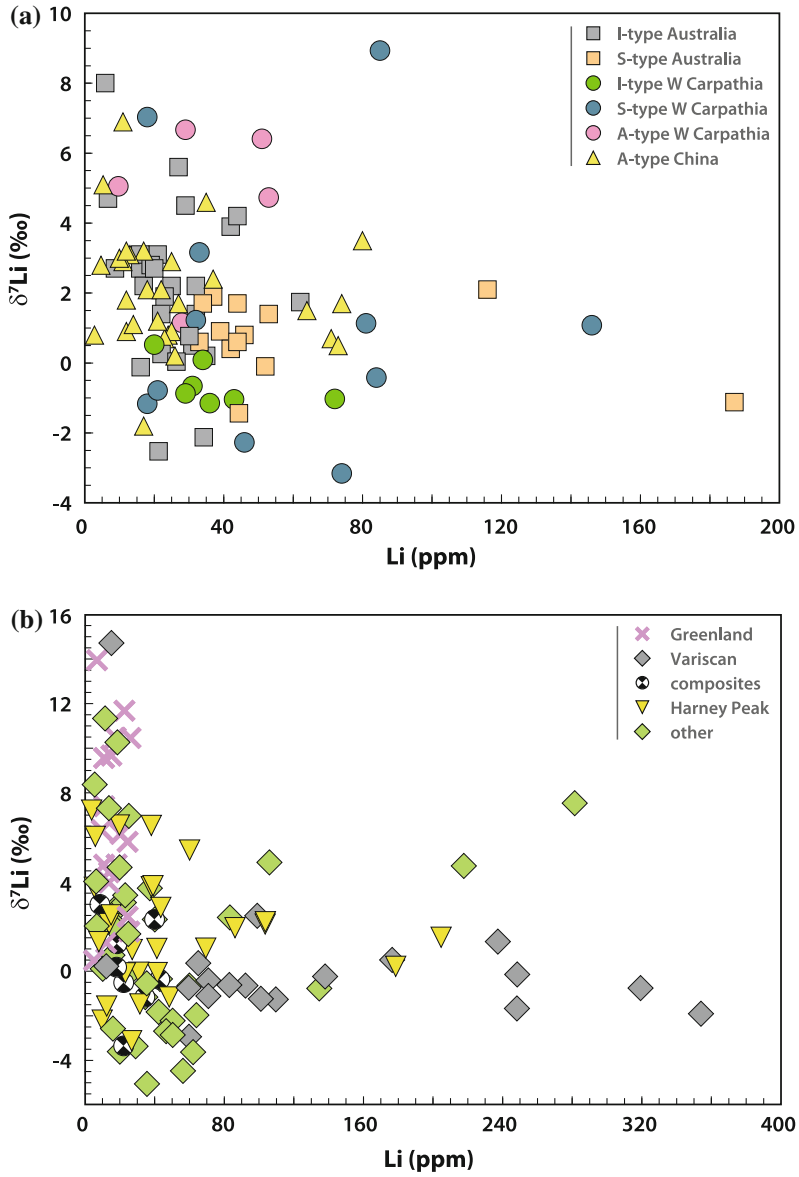

Fig. 5.6 Lithium concentration and δ^7Li in rocks of broadly granitic composition, ranging from true granites to more intermediate and more alkaline compositions, and their volcanic and metamorphic equivalents. **a** Granitic samples classified using the I, S, A nomenclature. Data sources: Australia from Bryant et al. (2004), Teng et al. (2004), Western Carpathia from Magna et al. (2010), China from Teng et al. (2009). **b** Other igneous rocks of broadly granitic composition. Data sources: Harney Peak granites from Teng et al. (2006), Variscan granites from Romer et al. (2014), Greenland, including syenitic compositions, from Marks et al. (2007), Wimpenny et al. (2010), composites are pooled samples from Teng et al. (2004), "other" (includes data from a number of globally dispersed locations) from: Bottomley et al. (2003), Sturchio and Chan (2003), Millot et al. (2007), Bryant et al. (2004), Teng et al. (2004), Magna et al. (2010), Kisakurek et al. (2004), Rudnick et al. (2004) and Godfrey et al. (2013)

Bryant et al. (2004) found their data consistent with the more isotopically homogenized sedimentary sources of the S-type granite suites compared to I-type plutons. The latter they took to represent what were originally mantle signatures variably contaminated by isotopically light

upper crust. Magna et al. (2010) underscored that granites with substantial source input from the lower crust (which, they point out based on the data of Teng et al. (2008), has been shown to exhibit, "rampant Li isotope variability") should be expected to possess a degree of isotopic heterogeneity. Indeed, that granitic suites show as *limited* isotopic variation as they do suggests an important disconnect from the lower crustal xenolith data set. Magna et al. (2010) ultimately concluded that there is no simple, universal interpretation of Li isotopes among S- and I-type granite suites.

Teng et al. (2009) indicated that Li isotopes appear unable to resolve the ongoing uncertainty over the derivation of I-type and A-type granites (classically considered "anorogenic" granites). In their study of A-type granitic rocks in northeastern China, Li isotopes were not useful in constraining petrogenesis or otherwise improving conclusions based on other geochemical data. Romer et al. (2014) reached similar conclusions based on the majority of central European granites in their study. Only Magna et al. (2010) were able to use Li isotopic data to significantly constrain interpretations of the petrogenesis of A-type granites from the Western Carpathians. The Li isotope–element relationships allowed Magna et al. (2010) to rule out several potential petrogenetic models, including some which involve "standard" A-type granite origins (e.g., reactivated lower crust and fractional crystallization of primary mantle melts). In their study, relatively high values of δ^7Li (+1.1 to +6.7 ‰) were essential to their deductions. In other areas A-type granites show generally lower δ^7Li, which, because of overlap with the isotopic composition of sedimentary and metasedimentary rocks, makes it effectively impossible to unequivocally rule out a variety of possible sources.

Are there conditions under which granitic rocks may not bear a true isotopic signal of their parentage? Bryant et al. (2004) posited that isotopic variability in a limited number of Australian leucogranite samples could have been introduced by isotopic fractionation driven by fluid separation. Although it has been argued that vapor separation introduces no significant Li isotope fractionation (e.g., Foustoukos et al. 2004), experimental data indicate measurable mineral–fluid isotopic partitioning under geologically relevant conditions (Lynton et al. 2005; Wunder et al. 2006, 2007). Nevertheless, leucogranitic rocks analyzed by Bryant et al. (2004) showed no marked Li isotopic offset from the ordinary granites they cross-cut. The absence of extreme fractionation among evolved and mineralized granites of central Europe (Magna et al. 2010; Romer et al. 2014) further tempers expectations that fluid–melt processes will invariably strongly affect Li isotope systematics. Teng et al. (2006b) suggested that the degree of fluid exsolution would need to be high in order to produce significant late-stage Li isotopic fractionation in granitic systems.

The exsolution of fluids or low-temperature melts from magma is inferred in many models attempting to explain the geochemistry of highly fractionated igneous systems, including granitic pegmatites (e.g., Sirbescu and Nabelek 2003), although this is only one potential mechanism for Li isotopic fractionation in such systems. As pegmatites are among the best examples of extreme enrichment of Li in the crust, it is somewhat paradoxical that they too have gone largely isotopically overlooked prior to very recently. Although there were early indications that pegmatites may record significant Li isotopic fractionation (Vocke et al. 1990; Tomascak et al. 1995), only more recent studies show this clearly and begin to offer explanations. Whereas the two pegmatitic rocks analyzed by Bottomley et al. (2003) and Magna et al. (2010) were notably isotopically heavy compared to ordinary granites (δ^7Li of +30.2 ‰ and +8.9 ‰, respectively), simple pegmatites in the Harney Peak Granite had a similar range in δ^7Li as the granites with which they coexist (Teng et al. 2006b). However, whole rocks and minerals from the Tin Mountain pegmatite are uniformly isotopically heavier than all samples from the parental Harney Peak Granite. On average higher δ^7Li in two pegmatites relative to those in neighboring country rocks were also revealed in study by Liu et al. (2010) and systematic decrease away from pegmatites was explained by diffusion.

Of the small number of Li isotopic studies on pegmatites to date, the majority deal not with issues of granite–pegmatite source relationships, but with internal processes. There is still considerable uncertainty on aspects of the internal evolution of large, zoned granitic pegmatites (London 2008, 2009); there has been some hope that Li isotopes could shed light on this. Lithium isotopic variations among pegmatite minerals hinges on a variety of factors, many of which are difficult to quantify with precision. The overriding control, however, appears to be the difference between the bonding of Li in the crystallizing medium (melt or fluid) compared to the that of the crystallographic site in a given mineral (Wenger and Armbruster 1991; Wunder et al. 2007, 2011); heavy Li appears to partition favorably into less coordinated sites with shorter Li–O bonds. If Li in silicate melts is predominantly in tetrahedrally coordinated groups (Soltay and Henderson 2005), then minerals that incorporate Li in sites of higher coordination should be isotopically lighter than the melt from which they crystallize (Teng et al. 2006b) because of the difference in bond lengths involved.

In addition to equilibrium effects, it has been suggested that kinetic effects may also be important in the Li isotopic geochemistry of granitic pegmatites. This follows from the likelihood that rapid crystal growth is a typical feature of pegmatites (London 2009). Such a driving force was suggested by Maloney et al. (2008) to explain the 3–10 ‰ difference between elongate tourmaline samples and those exhibiting radial growth. They interpreted the tourmaline data to have been produced in a system where Li diffusion was outpaced by crystal growth. Alternatively, it could point to crystallography-assisted fractionation along different axes, as has been reported for boron (Hinsberg and Marschall 2007).

Based on positive linear correlations between mineral δ^7Li and the K/Rb of coexisting minerals, Gordienko et al. (2007) inferred isotopic fractionation in response to progressive pegmatite crystallization. Although this conclusion may be valid, it was certainly for the wrong reasons. Gordienko et al. analyzed different minerals in the different zones (amphibole, pyroxene, mica). It is clear that, due to the crystallographic influence on isotopic fractionation, coexisting minerals in which Li inhabits differently coordinated sites will possess distinct δ^7Li despite crystallizing from the same medium (Teng et al. 2006b). The fact that δ^7Li in spodumene samples from the two localities examined by Gordienko et al. (2007) showed limited variation (0.2 ‰ difference for one pair, 2.4 ‰ for the other) appears to highlight their misconception. Nonetheless, Barnes et al. (2012) show that the positive correlation between bulk pegmatite F content and δ^7Li, although weak, is consistent with inferences from melt structure (Henderson 2005). The role of F-complexing in a silicate melt may have implications for the development of distinct isotopic signatures of highly evolved pegmatite populations. Reflecting back to earlier studies, although Plyusnin et al. (1979) suggested a link between Li isotopic fractionation and F content, their prediction was in the opposite sense (i.e., that higher δ^7Li would result in systems with lower bulk F).

Generally positive correlation between δ^7Li and concentration of Rb (as well as Li) in bulk pegmatitic rocks in and around the Tin Mountain pegmatite in South Dakota was interpreted by Teng et al. (2006b) to reflect the effects of large extents of equilibrium crystal fractionation in the formation of pegmatite magmas. The same extent of fractionation is not apparent within evolving pegmatites, however. For example, minerals crystallized in more elementally fractionated mineral assemblages of the Tin Mountain pegmatite had δ^7Li that overlapped values from the same minerals (quartz, plagioclase, muscovite) in less fractionated zones. The same lack of significant interzonal isotopic fractionation was seen among tourmaline samples from southern California pegmatites (Maloney et al. 2008). Thus, from the data accumulated to date, there is no evidence that Li isotopes can aid in better understanding the internal crystallization histories of granitic pegmatites.

Teng et al. (2006b) also measured Li isotopes in amalgamated fluid inclusions from quartz,

concluding that the offset between fluids (+8.1 to +13.4 ‰) and the pegmatite wall zone bulk rock with the lowest δ^7Li (+7.5 ‰) could reflect equilibrium fluid–mineral fractionation. The pooling of magmatic and possibly much later fluids in these analyses, however, creates significant uncertainty in their isotopic interpretation. Masukawa et al. (2013) analyzed Li and Sr isotopes in a set of ore-forming fluids from inclusions in vein quartz from the Takatori mine, Japan, in order to understand possible sources of tungsten ores. By selecting temporally disparate samples, Masukawa et al. (2013) associated low δ^7Li together with high contents of metals (W, Ni, Cu, etc.) in the earlier stages of hydrothermal mineralization as a result of sourcing an S-type granitic magma. Later phases of mineralization with progressively higher δ^7Li were probably more consistent with exchange of Li between metasediments with previous seafloor alteration and ore-bearing fluids, coupled with concomitant precipitation of Li-bearing phases.

Shabaga et al. (2010) used SIMS techniques to determine the Li isotopic composition in tourmaline from Brazil, Nigeria, and Mozambique in an attempt to establish Li as a provenance tool for precious gemstones. These authors implied significant differences in coupled δ^7Li–δ^{11}B relationships that might help unravel source regions for certain type of tourmaline. However, a later study of Ludwig et al. (2011), conducted on the same samples with the same analytical approach, revealed distinctly different Li and B isotopic compositions; the three locations could still be resolved with coupled Li–B isotopic systematics, however. It follows that such analytically-based differences (isobaric molecular interferences) have the potential to seriously affect geological explanations.

Magna et al. (2013) made a comprehensive study of minerals from a variety of granitic pegmatites representing varied crystallization ages from Archean to recent. Their preliminary results are three-fold. First, within individual pegmatite bodies, the Li isotopic composition of minerals is correlated strongly with Li-φ (O, OH, F) bond length. Although it was known that bond distance was a significant component of Li isotopic behavior in minerals (Wunder et al. 2011), the relationship had not previously been demonstrated empirically. Magna et al. (2013) showed that shorter bond lengths would favor heavy isotopes, regardless of the specific mineral or specific pegmatite, and consistent with experimental evidence (Wunder et al.2011). Second, δ^7Li in residual pegmatite liquids does not evolve in a particular direction. Instead, δ^7Li of co-crystallizing phases may differ substantially (cf. muscovite and beryl as the first phases to solidify consistently showing the lowest and highest δ^7Li, respectively). Third, significant variations in δ^7Li (up to 20 ‰) have been found for the same mineral species from different pegmatite bodies. Although the cause is unknown, it appears to be associated with sourcing distinctively different precursors. However, the exact link between individual pegmatites and their possible source regions cannot be easily proposed. Alternatively, it may hinge on the extent of melt/fluid–solid Li isotopic fractionation during the evolution of Earth's continental crust coupled to physical parameters (e.g., differences in heat production and transfer, paleogeography). The latter interpretation takes into account that large pegmatite bodies are predominantly Archean and Proterozoic phenomena; average post-Proterozoic pegmatite occurrences are significantly smaller (e.g., Tkachev 2011; Bradley and McCauley 2013; McCauley and Bradley 2014).

5.2.2 Crustal Metamorphism and Fluid Flow

Metamorphic effects are commonly so intimately related to the igneous process that discriminating the geochemical consequences of the two condition sets is problematical. Attempts to use Li isotopes to understand aspects of the metamorphic histories of crustal rocks have had to deal with distinct potential mechanisms of isotopic fractionation: those related to processes that can be quantified through equilibrium models, and kinetic models, including those that rely on the important difference in diffusion rates of ^{6}Li and

^{7}Li. In certain instances, the magnitude of the isotopic effects brought on by diffusional processes appears to create a diagnostic signature, although modeling the effect does not universally reach a satisfactory conclusion.

Contact zones around plutonic bodies have been popular targets for understanding metamorphic processes, particularly cases where the host rocks are lithologically homogeneous and well defined (Nabelek et al. 1984; Ferry 1994), and so it is logical that these geological scenarios have been employed in Li isotopic studies. Romer et al. (2005) discussed the geochemistry of an intrusion of alkali syenite (and pegmatite) magma into dominantly carbonate rocks in Mexico. The study encompassed a wide array of elemental and isotopic tools and showcased the meter- to millimeter-scale complexity that can be recorded in what might appear a geologically straightforward setting; complexity, in this case, interpreted to be caused by multiple chemically distinct fluids. The variations in Li isotopes in samples from this contact zone were attributed to inputs from decarbonation reactions as well as from isotopically distinct magmatic and metamorphic fluids.

In contrast to that study, the intrusion of the granodioritic Onawa pluton in Maine (Teng et al. 2007) introduced minimal Li isotopic variation despite causing kilometer-scale contact metamorphism up to the formation of migmatites. Teng et al. (2007) saw no correlated Li isotopic variation with the extent of contact metamorphism (i.e., distance from contact), although contact metapelites experienced apparent Li loss during dehydration. This was a somewhat ideal study area in that little retrogression took place, which permitted unaltered prograde isotopic signatures to be preserved. The metamorphic dehydration in rocks hosting the Onawa pluton caused only 1–2 ‰ decrease in δ^{7}Li of aureole rocks and was successfully modeled by Rayleigh fractionation. The model suggested that very high fluid/rock Li distribution coefficients coupled with modest isotopic fractionation factors would be required to produce more significant change in δ^{7}Li in the absence of, for example, input of isotopically distinct magmatic fluid. The mean δ^{7}Li of metasedimentary rocks from the Catalina Schist (Penniston-Dorland et al. 2012), California, is indistinguishable from that of clastic sedimentary rocks from Teng et al. (2004), this in spite of the Catalina rocks being metamorphosed up to ~750 °C. The relative homogeneity in Li isotopic composition across metamorphic grade for the Catalina Schist, coupled with only minor decrease in Li concentration, was interpreted to reflect predominance of relatively closed-system behavior (Penniston-Dorland et al. 2012). Lithium released with reactions consuming lower-grade chlorite was taken up, without isotopic effects, in the crystallization of higher-grade phengite. Xiao et al. (2011) found restricted Li isotopic variation between eclogites and coexisting high pressure veins, as well as between coexisting mantle peridotite and eclogite, although the data set was small. Thus, in abundant metamorphic settings, it appears that no significant geochemical driving forces exist to produce substantive variations in Li isotopes. Whether such isotopic effects are produced relates vitally to the nature of syn- and post-metamorphic fluid flow.

On the contrary, Romer and Meixner (2014) interpreted increasing metamorphic temperatures to have driven isotopic fractionation in Variscan metapelites from central Europe. They made clear that the bulk composition (and hence mineralogy) of the protoliths was crucial in determining the ultimate extent of isotopic change, owing to the differences in Li availability in the original sediment. Sedimentary rocks enriched in Li may manifest minimal isotopic fractionation during progressive metamorphism as long as Li in the detrital minerals was primarily structurally incorporated, as opposed to being present on surfaces or other readily-exchangeable positions. The data of Romer and Meixner (2014) demonstrate that the process of metamorphism through eclogite facies may introduce only a <2 ‰ decrease in δ^{7}Li, consistent with the model of Marschall et al. (2007b). A similar magnitude of fractionation was seen in the Onawa aureole, although in other protoliths the total fractionation introduced was perhaps as great as −20 ‰.

Because they contain high Li contents and commonly exsolve fluids which cause

exomorphic effects in their host rocks (e.g., Morgan and London 1987), many of the studies of metamorphic fluid–rock interaction involve granitic pegmatites. Host metamorphic rocks of the Tin Mountain pegmatite in South Dakota (Teng et al. 2006a) were invaded by Li-rich fluids following the intrusion of the spodumene-bearing pegmatite, resulting in perturbations of their elemental and isotopic systematics to a distance of at least 30 m. The possibility that these perturbations were the result of either mixing (between of fluid and rock Li) or Rayleigh-type fractionation could be ruled out, as both would require the host rocks to have geochemically unreasonable δ^7Li < −20 ‰. Teng et al. (2006a) instead argued that the data were more consistent with diffusion-driven isotopic fractionation. The horizontal magnitude of the resultant diffusional halo depended on the nature of the host rock, but both mica schist and amphibolite achieved similar "peak" δ^7Li (∼−20 ‰).

A similar conclusion was reached by Liu et al. (2010) in a study of the rocks hosting a series of much smaller Li-rich pegmatite bodies in Wisconsin (2–3 m wide dikes compared to the ∼30 m thick Tin Mountain pegmatite). In both the case of Teng et al. (2006a) and Liu et al. (2010), the interpreted process involved Li-rich fluids reacting with surrounding rocks, with the advance of the faster-diffusing ^{6}Li being recorded in metasomatized schists and amphibolites as the very light isotopic compositions. Liu et al. (2010) pointed out that the extent of Li transport into country rocks for the Wisconsin pegmatites was similar to that at Tin Mountain, despite the difference in scale of the pegmatites. Thus multiple factors must govern the magnitude of Li export from Li-rich magmas/fluids into host rocks. Nonetheless, the results of both Teng et al. (2006a) and Liu et al. (2010) were inconsistent with volume diffusion, further implicating a fluid-mediated process.

Maloney et al. (2008) entertained the possibility that high δ^7Li values in minerals from southern California pegmatites (and hence high δ^7Li in pegmatite magmas) may result from pre- or syn-emplacement open system behavior. They suggested that Li in pegmatite magmas may have been influenced to some extent by fluid-mediated exchange with wall rocks involving concomitant diffusion-driven isotopic fractionation. Assuming Li in the melt behaves like Li in an aqueous fluid, exchange would favor ^{6}Li partitioning into wall rocks. Such a process would be expected to drive melt δ^7Li to higher values, although no direct evidence (i.e., analysis of surrounding rocks) was given to support this speculation.

Light Li isotopic compositions are characteristic in eclogite facies rocks, largely regardless of protolith (Zack et al. 2003; Marschall et al. 2007b; Xiao et al. 2011; Romer and Meixner 2014), with a range from −21.5 to +8.2 ‰ (the majority falling between −9.7 and +6.9 ‰; Fig. 5.7). Zack et al. (2003) explained the isotopic variations in eclogite facies rocks from the Alps as reflecting a Rayleigh process that took place during progressive slab dehydration; a similar conclusion was reached by Bouman et al. (2004) with their modeling of subduction zone processes. This interpretation, however, was questioned by Marschall et al. (2007b). Marschall et al. (2007b) modeled Li fractionation during eclogite facies metamorphism using experimental data published after the work of Zack et al. (2003). Their results indicated that at relevant temperatures and pressure, slab dehydration was unlikely to involve Li isotopic fractionation of more than ∼3 ‰. Hence the explanation of very isotopically light data from most eclogites required other mechanisms.

Marschall et al. (2007b) proposed two factors to influence Li contents and Li isotopes in subduction zone metamorphic complexes. First, they called for significant flux of Li derived from subducted sediments or sedimentary rocks. These materials both carry on average higher Li concentrations than coexisting mafic rocks and have lower δ^7Li (see Sect. 6.3). A prominent source of enriched, isotopically light sedimentary-source Li was called for by both Penniston-Dorland et al. (2010, 2012) and Simons et al. (2010) in their studies of high pressure rocks from other subduction zones.

A simple fluid exchange model is inadequate to account for the nearly 20 % of eclogite facies data with very low δ^7Li (< c. −5 ‰). Neither do

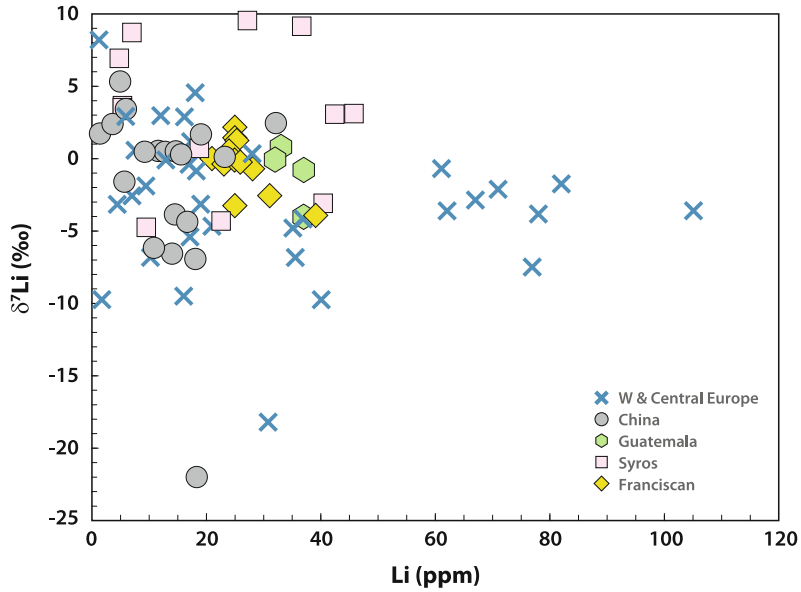

Fig. 5.7 Lithium concentration and δ^7Li in high pressure metamorphic rocks (primarily eclogite facies metamorphosed sedimentary and mafic igneous rocks, with some blueschists). Data sources: Syros from Marschall et al. (2007b), China (multiple localities) from Marschall et al. (2007b), Xiao et al. (2011), Western Europe (multiple localities) from Romer and Meixner (2014), Marschall et al. (2007b), Zack et al. (2003), Franciscan from Penniston-Dorland et al. (2010), Simons et al. (2010) and Guatemala from Simons et al. (2010)

geochemically reasonable sources exist to generate fluids sufficiently isotopically light, nor do known Li isotopic fractionation factors permit isotopically heavier fluids developing such characteristics. Although Marschall et al. (2007b) did not quantitatively demonstrate the feasibility of diffusive fractionation of Li isotopes in the eclogitic rocks, it seems inescapable that kinetic fractionation driven by diffusive influx of Li is required to explain such extremely light isotopic compositions in rocks with elevated Li contents. Such driving forces had not been brought into the mainstream when the study of Zack et al. (2003) was published. Similarly, Penniston-Dorland et al. (2012) resorted to diffusive fractionation to explain the low δ^7Li (< c. −4 ‰) of a minority of Catalina Schist samples. In conclusion, it is clear that diffusion-driven isotopic fractionation is an important consideration in understanding Li dynamics in many metamorphic terranes, although the quantification of this process has not yet been rigorously evaluated in most settings.

References

Abdelfadil KM, Romer RL, Glodny J (2014) Mantle wedge metasomatism revealed by Li isotopes in orogenic lamprophyres. Lithos 196–197:14–26

Ackerman L, Špaček P, Magna T, Ulrych J, Svojtka M, Hegner E, Balogh K (2013) Alkaline and carbonate-rich melt metasomatism and melting of subcontinental Lithospheric mantle: evidence from mantle Xenoliths, NE Bavaria, Bohemian Massif. J Petrol 54:2597–2633

Ackerman L, Ulrych J, Řanda Z, Erban V, Hegner E, Magna T, Balogh K, Frána J, Lang M, Novák JK (2015) Geochemical characteristics and petrogenesis of phonolites and trachytic rocks from the České Středohoří Volcanic Complex, the Ohře Rift, Bohemian Massif. Lithos 224–225:256–271

Agostini S, Ryan JG, Tonarini S, Innocenti F (2008) Drying and dying of a subducted slab: coupled Li and B isotope variations in Western Anatolia Cenozoic Volcanism. Earth Planet Sci Lett 272:139–147

Aulbach S, Rudnick RL, McDonough WF, (2008) Li–Sr–Nd Isotope Signatures of the Plume and Cratonic Lithospheric Mantle Beneath the Margin of the Rifted Tanzanian Craton (Labait). Contrib. Mineral. Petrol. 155:79–92

Aulbach S, Rudnick RL, (2009) Origins of non-equilibrium lithium isotopic fractionation in xenolithic peridotite minerals: examples from Tanzania. Chem. Geol. 258:17–27

Barbarin B (1999) A review of the relationship between granitoid types, their origins and their geodynamic environments. Lithos 46:605–626

Barnes EM, Weis D, and Groat LA (2012) Significant Li isotope fractionation in geochemically evolved rare element-bearing pegmatites from the Little Nahanni Pegmatite Group, NWT, Canada. Lithos 132/133:21–36

Barry PH, Hilton DR, Day JMD, Pernet-Fisher JF, Howarth GH, Magna T, Agashev AM, Pokhilenko NP, Pokhilenko LN, Taylor LA (2015) Helium isotopic evidence for modification of the cratonic lithosphere during the Permo-Triassic Siberian flood basalt event. Lithos 216–217:73–80

Bell DR, Hervig RL, Buseck PR & Aulbach S (2009) Lithium isotope analysis of olivine by SIMS: Calibration of a matrix effect and application to magmatic phenocrysts. Chem. Geol. 258:5–16

Bell K (1989) Carbonatites: genesis and evolution. Unwin Hyman, London, p 618

Bell K (1998) Radiogenic isotope constraints on relationships between carbonatites and associated silicate rocks. J Petrol 39:1987–1996

Bell K, Simonetti A (1996) Carbonatite magmatism and plume activity: implications from the Nd, Pb and Sr isotope systematics of Oldoinyo Lengai. J Petrol 37:1321–1339

Benton LD, Ryan JG, Savov IP (2004) Lithium abundance and isotope systematics of forearc serpentinites, Conical Seamount, Mariana forearc: insights into the mechanics of slab-mantle exchange during subduction. Geochem Geophys Geosys 5, paper number Q08J12. doi:10.1029/2004GC000708

Berger G, Schott J, Guy C (1988) Behavior of Li, Rb and Cs during basalt glass and olivine dissolution and chlorite, smectite and zeolite precipitation from seawater: experimental investigations and modelization between 50 and 300 °C. Chem Geol 71:297–312

Bizimis M, Salters VJM, Dawson JB (2003) The brevity of carbonatite sources in the mantle: evidence from Hf isotopes. Contrib Mineral Petrol 145:281–300

Blusztajn J, Hart SR, (1989) Sr, Nd and Pb isotopic character of Tertiary basalts from southwest Poland. Geochim Cosmochim Acta 53:2689–2696

Bottomley DJ, Chan LH, Katz A, Starinsky A and Clark ID (2003) Lithium Isotope Geochemistry and Origin of Canadian Shield Brines. Groundwater, 41:847–856

Bouman C, Elliott T, Vroon PZ (2004) Lithium inputs to subduction zones. Chem Geol 212:59–79

Bouman C, Elliott TR, Vroon PZ, Pearson DG (2000) Li isotope evolution of the mantle from analyses of mantle xenoliths. J Conf Abstr 5:239

Bouvier A-S, Métrich N, Deloule E (2008) Slab-derived fluids in magma sources of St. Vincent (Lesser Antilles Arc): volatile and light element imprints. J Petrol 49:1427–1448

Bradley D, McCauley A (2013) A preliminary deposit model for lithium-cesium-tantalum (LCT) pegmatites. U.S. Geology Survey Open-File Report 2013-1008, p 7

Brant C, Coogan LA, Gillis KM, Seyfried WE, Pester NJ, Spence J (2012) Lithium and Li-isotopes in young altered upper oceanic crust from the East Pacific Rise. Geochim Cosmochim Acta 96:272–293

Brenan JM, Neroda E, Lundstrom CC, Shaw HF, Ryerson FJ, Phinney DL (1998a) Behaviour of boron, beryllium and lithium during melting and crystallization: constraints from mineral-melt partitioning experiments. Geochim Cosmochim Acta 62:2129–2141

Brenan JM, Ryerson FJ, Shaw HF (1998b) The role of aqueous fluids in the slab-to-mantle transfer of boron, beryllium and lithium during subduction: experiments and models. Geochim Cosmochim Acta 62:3337–3347

Brens P Jr, Liu X-M, Rudnick R, Turner S, Rushmer T (2013) Lithium isotopic composition of the Tonga-Kermadec arc and its constraints on subduction recycling. Mineral Mag 77:A770

Brooker R, Blundy J, James RH (2000) Subduction-related mantle pyroxenites from Zabargad Island, Red Sea. J Conf Abstr 5:249

Brooker RA, James RH, Blundy JD (2004) Trace elements and Li isotope systematics in Zabargad peridotites: evidence of ancient subduction processes in the Red Sea mantle. Chem Geol 212:179–204

Bryant CJ, Chappell BW, Bennett VC and McCulloch MT (2004) Lithium isotopic composition of the New England Batholith: correlations with inferred source rock compositions. Trans. R. Soc. Edinb. Earth Sci. 95:199–214

Cabato J, Altherr R, Ludwig T, Meyer H-P (2013) Li, Be, B concentrations and δ^7Li values in plagioclase phenocrysts of dacites from Nea Kameni (Santorini, Greece). Contrib Miner Petrol 165:1135–1154

Carlson RW, Lugmair GW, Macdougall JD (1981) Crustal influence in the generation of continental flood basalts. Nature 289:160–162

Chakhmouradian A (2006) High-field-strength elements in carbonatitic rocks: geochemistry, crystal chemistry and significance for constraining the sources of carbonatites. Chem Geol 235:138–160

Chan L-H, Edmond JM (1988) Variation of lithium isotope composition in the marine environment: a preliminary report. Geochim Cosmochim Acta 52:1711–1717

Chan L-H, Frey FA (2003) Lithium isotope geochemistry of the Hawaiian plume: results from the Hawaii Scientific Drilling Project and Koolau volcano. Geochem Geophys Geosys 4, paper number 8707. doi:10.1029/2002GC000365

Chan L-H, Hein JR (2007) Lithium contents and isotopic compositions of ferromanganese deposits from the global ocean. Deep-Sea Res II 54:1147–1162

Chan L-H, Kastner M (2000) Lithium isotopic composition of pore fluids and sediments in the Costa Rica subduction zone: implications for fluid processes and sediment contribution to the arc volcanoes. Earth Planet Sci Lett 183:275–290

Chan L-H, Leeman WP, You C-F (1999) Lithium isotopic composition of Central American Volcanic Arc lavas: implications for modification of subarc mantle by slab-derived fluids. Chem Geol 160:255–280

Chan L-H, Alt JC, Teagle DAH (2002a) Lithium and lithium isotope profiles through the upper oceanic crust: a study of seawater-basalt exchange at ODP sites 504B and 896A. Earth Planet Sci Lett 201:187–201

Chan L-H, Leeman WP, You C-F (2002b) Lithium isotopic composition of Central American Volcanic Arc lavas: implications for modification of subarc mantle by slab-derived fluids: correction. Chem Geol 182:293–300

Chan L-H, Leeman WP, Plank T (2006) Lithium isotopic composition of marine sediments. Geochem Geophys Geosys 7, paper number Q06005. doi: 10.1029/2005GC001202

Chan L-H, Edmond JM, Thompson G, Gillis K (1992) Lithium isotopic composition of submarine basalts: implication for the lithium cycle in the oceans. Earth Planet Sci Lett 108:151–160

Chan L-H, Gieskes JM, You C-F, Edmond JM (1994) Lithium isotope geochemistry of sediments and hydrothermal fluids of the Guaymas Basin, Gulf of California. Geochim Cosmochim Acta 58:4443–4454

Chan L-H, Lassiter JC, Hauri EH, Hart SR, Blusztajn J (2009) Lithium isotope systematics of lavas from the Cook-Austral Islands: constraints on the origin of HIMU mantle. Earth Planet Sci Lett 277:433–442

Chappell BW, White AJR (2001) Two contrasting granite types: 25 years later. Australian J Earth Sci 48:489–499

Clift PD, Chan L-H, Blusztajn J, Layne GD, Kastner M, Kelly RK (2005) Pulsed subduction accretion and tectonic erosion reconstructed since 2.5 Ma from the tephra record offshore Costa Rica. Geochem Geophys Geosyst 6, paper number Q09016. doi:10.1029/2005GC000963

Cooper AF, Paterson LA, Reid DL (1995) Lithium in carbonatites: consequence of an enriched mantle source? Mineral Mag 59:401–408

Cunningham GJ, Henderson P, Lowry RK, Nolan J, Reed SJB, Long JVP (1983) Lithium diffusion in silicate melts. Earth Planet Sci Lett 65:203–205

Debaille V, Trønnes RG, Brandon AD, Waight TE, Graham DW, Lee C-TA (2009) Primitive off-rift basalts from Iceland and Jan Mayen: Os-isotopic evidence for a mantle source containing enriched subcontinental lithosphere. Geochim Cosmochim Acta 73:3423–3449

Decitre S, Deloule E, Reisberg L, James RH, Agrinier P, Mével C (2002) Behavior of Li and its isotopes during serpentinization of oceanic peridotites. Geochem Geophys Geosys 3. doi:10.1029/2001GC000178

Dohmen R, Kasemann SA, Coogan LA, Chakraborty S (2010) Diffusion of Li in olivine. Part 1: experimental observations and a multiple species diffusion model. Geochim Cosmochim Acta 74:274–292

Dostal J, Dupuy C, Dudoignon P (1996) Distribution of boron, lithium and beryllium in ocean island basalts from French Polynesia: implications for B/Be and Li/Be ratios as tracers of subducted components. Mineral Mag 60:563–580

Eggins SM, Rudnick RL, McDonough WF (1998) The composition of peridotites and their minerals: a laser-ablation ICP-MS study. Earth Planet Sci Lett 154:53–71

Elliott T, Jeffcoate A, Bouman C (2004) The terrestrial Li isotope cycle: light-weight constraints on mantle convection. Earth Planet Sci Lett 220:231–245

Elliott T, Thomas A, Jeffcoate A, Niu Y (2006) Lithium isotope evidence for subduction-enriched mantle in the source of mid-ocean-ridge basalts. Nature 443:565–568

Ferry JM (1994) Role of fluid flow in the contact metamorphism of siliceous dolomitic limestones. Am Mineral 79:719–736

Foley SF, Prelevic D, Rehfeldt T, Jacob DE (2013) Minor and trace elements in olivines as probes into early igneous and mantle melting processes. Earth Planet Sci Lett 363:181–191

Foustoukos DI, James RH, Berndt ME and Seyfried WEJ (2004) Lithium isotopic systematics of hydrothermal vent fluids at the Main Endeavour Field, Northern Juan de Fuca Ridge. Chem. Geol. 212:17–26

Gallagher K, Elliott T (2009) Fractionation of lithium isotopes in magmatic systems as a natural consequence of cooling. Earth Planet Sci Lett 278:286–296

Gao Y, Snow JE, Casey JF, Yu J (2011) Cooling-induced fractionation of mantle Li isotopes from the ultraslow-spreading Gakkel Ridge. Earth Planet Sci Lett 301:231–240

Gao Y, Vils F, Cooper KM, Banerjee N, Harris M, Hoefs J, Teagle DAH, Casey JF, Elliott T, Laverne C, Alt JC, Muehlenbachs K (2012) Downhole variation of lithium and oxygen isotopic compositions of oceanic crust at East Pacific Rise, ODP Site 1256. Geochem Geophys Geosys 13, paper number Q10001. doi: 10.1029/2012GC004207

Genske FS, Turner SP, Beier C, Chu MF, Tonarini S, Pearson NJ, Haase KM (2014) Lithium and boron isotope systematics in lavas from the Azores islands reveal crustal assimilation. Chem Geol 373:27–36

Gill JB (1981) Orogenic andesites and plate tectonics. Springer, Berlin. p 391

Godfrey LV, Chan LH, Alonso RN, Lowenstein TK, McDonough WF, Houston J, Li J, Bobst A, Jordan TE (2013) The role of climate in the accumulation of lithium-rich brine in the Central Andes. Appl Geochem 38:92–102

Gordienko VV, Gordienko VlVl, Sergeev AS, Levskii LK, Lokhov KI, Kapitonov IN, Sergeev SA (2007) Doklady Akad Nauk 413:676–678

Grove TL, Parman SW, Bowring SA, Price RC, Baker MB (2002) The role of an H_2O-rich fluid component in the generation of primitive basaltic andesites and andesites from the Mt. Shasta region, N California. Contrib Mineral Petrol 142:375–396

Gurenko AA, Trumbull RB, Thomas R, Lindsay JM (2005) A melt inclusion record of volatiles, trace elements and Li–B isotope variations in a single

magma system from the Plat Pays Volcanic Complex, Dominica, Lesser Antilles. J Petrol 46:2495–2526
Gurenko AA, Schmincke H-U (2002) Orthopyroxene-bearing tholeiites of the Iblean Plateau (Sicily): constraints on magma origin and evolution from glass inclusions in olivine and orthopyroxene. Chem Geol 183:305–331
Halama R, McDonough WF, Rudnick RL, Keller J, Klaudius J (2007) The Li isotopic composition of Oldoinyo Lengai: nature of the mantle sources and lack of isotopic fractionation during carbonatite petrogenesis. Earth Planet Sci Lett 254:77–89
Halama R, McDonough WF, Rudnick RL, Bell K (2008) Tracking the lithium isotopic evolution of the mantle using carbonatites. Earth Planet Sci Lett 265:726–742
Halama R, Savov IP, Rudnick RL, McDonough WF (2009) Insights into Li and Li isotope cycling and sub-arc metasomatism from veined mantle xenoliths, Kamchatka. Contrib Mineral Petrol 158:197–222
Hamelin C, Seitz HM, Barrat JA, Dosso L, Maury R, Chaussidon M (2009) A low δ^7Li lower crustal component: evidence from an alkalic intraplate volcanic series (Chaîne des Puys, French Massif Central). Chem Geol 266:205–217
Hansen H-E, Magna T, Košler J, Pedersen R-B (2011) Lithium isotope perspective on the Iceland mantle plume. Mineral Mag 75:A977
Henderson GS (2005) The structure of silicate melts: a glass perspective. Can Mineral 43:1921–1958
Hofmann AW (1997) Mantle geochemistry: the message from oceanic volcanism. Nature 385:218–229
Hofmann AW, White WM (1982) Mantle plumes from ancient oceanic crust. Earth Planet Sci Lett 57:421–436
Ionov DA, Seitz H-M (2008) Lithium abundances and isotopic compositions in mantle xenoliths from subduction and intra-plate settings: mantle sources vs. eruption histories. Earth Planet Sci Lett 266:316–331
Jagoutz E, Palme H, Baddenhausen H, Blum K, Cendales M, Dreibus G, Spettel B, Lorenz V, Wänke H (1979) The abundances of major, minor and trace elements in the earth's mantle as derived from primitive ultramafic nodules. Lunar Planet Sci Conf 10th:2031–2050
Jambon A, Semet MP (1978) Lithium diffusion in silicate glasses of albite, orthoclase, and obsidian composition: an ion-microprobe determination. Earth Planet Sci Lett 37:445–450
James RH, Allen DE, Seyfried WE Jr (2003) An experimental study of alteration of oceanic crust and terrigenous sediments at moderate temperatures (51 to 350 °C): insights as to chemical processes in near-shore ridge-flank hydrothermal systems. Geochim Cosmochim Acta 67:681–691
Janoušek V, Erban V, Holub FV, Magna T, Bellon H, Mlčoch B, Wiechert U, Rapprich V (2010) Geochemistry and genesis of behind-arc basaltic lavas from eastern Nicaragua. J Volcanol Geotherm Res 192:232–256
Jeffcoate AB, Elliott T, Kasemann SA, Ionov D, Cooper KM (2007) Li isotope fractionation in peridotites and mafic melts. Geochim Cosmochim Acta 71:202–218
John T, Gussone N, Podladchikov YY, Bebout GE, Dohmen R, Halama R, Klemd R, Magna T, Seitz H-M (2012) Volcanic arcs fed by rapid pulsed fluid flow through subducting slabs. Nature Geosci 5:489–492
Kaliwoda M, Ludwig T, Altherr R (2008) A new SIMS study of Li, Be, B and δ^7Li in mantle xenoliths from Harrat Uwayrid (Saudi Arabia). Lithos 106:261–279
Kaminsky FV, Zakharchenko OD, Davies R, Griffin WL, Khachatryan-Blinova GK, Shiryaev AA (2001) Superdeep diamonds from the Juina area, Matto Grosso State, Brazil. Contrib Mineral Petrol 140:734–753
Kil Y (2010) Lithium isotopic disequilibrium of minerals in the spinel lherzolite xenoliths from Boeun, Korea. J Geochem Explor 107:56–62
Kim T, Nakai S, Gasperini D (2011) Lithium abundance and isotope composition of Logudoro basalts, Sardinia: origin of light Li signature. Geochem J 45:323–340
Kisakürek B, Widdowson M, James RH (2004) Behaviour of Li isotopes during continental weathering: the Bidar laterite profile, India. Chem. Geol. 212:27–44
Kobayashi K, Tanaka R, Moriguti T, Shimizu K, Nakamura E (2004) Lithium, boron and lead isotope systematics of glass inclusions in olivines from Hawaiian lavas: evidence for recycled components in the Hawaiian plume. Chem Geol 212:143–161
Košler J, Magna T, Mlčoch B, Mixa P, Nývlt D, Holub FV (2009) Combined Sr, Nd, Pb and Li isotope geochemistry of alkaline lavas from northern James Ross Island (Antarctic Peninsula) and implications for back-arc magma formation. Chem Geol 258:207–218
Krienitz M-S, Garbe-Schönberg C-D, Romer RL, Meixner A, Haase KM, Stroncik NA (2012) Lithium isotope variations in ocean island basalts: implications for the development of mantle heterogeneity. J Petrol 53:2333–2347
Lai Y-J, Pogge von Strandmann PAE, Dohmen R, Takazawa E, Elliott T (2015) The influence of melt infiltration on the Li and Mg isotopic composition of the Horoman Peridotite Massif. Geochim Cosmochim Acta 164:318–332
Leeman WP, Tonarini S, Chan L-H, Borg LE (2004) Boron and lithium isotopic variations in a hot subduction zone: the southern Washington Cascades. Chem Geol 212:101–124
Liu X-M, Rudnick RL, Hier-Majumder S, Sirbescu MLC (2010) Processes controlling lithium isotopic distribution in contact aureoles: a case study of the Florence County pegmatites, Wisconsin. Geochem Geophys Geosys 11, paper number Q08014. doi:10.1029/2010GC003063
Liu X-M, Rudnick RL, McDonough WM, Cummings ML (2013) Influence of chemical weathering on the composition of the continental crust: Insights from Li and Nd isotopes in bauxite profiles developed on Columbia River Basalts. Geochim Cosmochim Acta 115:73–91
London D (2008) Pegmatites. Can Mineral Spec Publ 10, pp 368

London D (2009) The origin of primary textures in granitic pegmatites. Can Mineral 47:697–724

Lowry RK, Reed SJB, Nolan J, Henderson P, Long JVP (1981) Lithium tracer diffusion in an alkali-basaltic melt: an ion-microprobe determination. Earth Planet Sci Lett 53:36–40

Ludwig T, Marschall HR, Pogge von Strandmann PAE, Shabaga BM, Fayek M, Hawthorne FC (2011) A secondary ion mass spectrometry (SIMS) re-evaluation of B and Li isotopic compositions of Cu-bearing elbaite from three global localities. Mineral Mag 75:2485–2494

Lundstrom CC, Chaussidon M, Hsui AT, Kelemen P, Zimmerman M (2005) Observations of Li isotopic variations in the Trinity Ophiolite: evidence for isotopic fractionation by diffusion during mantle melting. Geochim Cosmochim Acta 69:735–751

Lynton SJ, Walker RJ, Candela PA (2005) Lithium isotopes in the system Qz-Ms-fluid: an experimental study. Geochim Cosmochim Acta 69:3337–3347

Magna T, Rapprich V (2012) The lithium isotope composition of volcanic sequences of the Český ráj region and Doupovské hory Mts. (in Czech). In: 3rd volcanology group meeting of the Czech geological society, Křivoklát, Czech Republic. Sborník Západočeského Muzea Plzeň, Příroda, 116, 11–12

Magna T, Wiechert U, Halliday AN (2006a) New constraints on the lithium isotope compositions of the moon and terrestrial planets. Earth Planet Sci Lett 243:336–353

Magna T, Wiechert U, Grove TL, Halliday AN (2006b) Lithium isotope fractionation in the Southern Cascadia subduction zone. Earth Planet Sci Lett 250:428–443

Magna T, Ionov DA, Oberli F, Wiechert U (2008) Links between mantle metasomatism and lithium isotopes: evidence from glass-bearing and cryptically metasomatized xenoliths from Mongolia. Earth Planet Sci Lett 276:214–222

Magna T, Janousek V, Kohút M, Oberli F and Wiechert U (2010) Fingerprinting sources of orogenic plutonic rocks from Variscan belt with lithium isotopes and possible link to subduction-related origin of some A-type granites. Chem. Geol. 274:94–107

Magna T, Wiechert U, Stuart FM, Halliday AN, Harrison D (2011) Combined Li–He isotopes in Iceland and Jan Mayen basalts and constraints on the nature of the North Atlantic mantle. Geochim Cosmochim Acta 75:922–936

Maloney JS, Nabelek PI, Sirbescu M-LC, Halama R (2008) Lithium and its isotopes in tourmaline as indicators of the crystallization process in the San Diego County pegmatites, California, USA. Eur J Mineral 20:905–916

Marks MAW, Rudnick RL, McCammon C, Vennemann T, Markl G, (2007) Arrested kinetic Li isotope fractionation at the margin of the Ilímaussaq complex, South Greenland: Evidence for open-system processes during final cooling of peralkaline igneous rocks. Chem Geol 246:207–230

Marschall H, Altherr R, Lüpke L (2007a) Squeezing out the slab: modelling the release of Li, Be, and B during progressive high-pressure metamorphism. Chem Geol 239:323–335

Marschall HR, Altherr R, Ludwig T, Kalt A, Gméling K, Kasztovszky Z (2006) Partitioning and budget of Li, Be and B in high-pressure metamorphic rocks. Geochim Cosmochim Acta 70:4750–4769

Marschall HR, Pogge von Strandmann PAE, Seitz H-M, Elliott T, Niu Y (2007b) The lithium isotopic composition of orogenic eclogites and deep subducted slabs. Earth Planet Sci Lett 262:563–580

McCauley A, Bradley DC (2014) The global age distribution of granitic pegmatites. Can Mineral 52:183–190

McDade P, Blundy JD, Wood BJ (2003) Trace element partitioning on the Tinaquillo Lherzolite solidus at 1.5 GPa. Phys Earth Planet Int 139:129–147

Medaris GL Jr, Ackerman L, Jelínek E, Magna T (2015) Depletion, cryptic metasomatism, and modal metasomatism of central European lithospheric mantle: evidence from elemental and Li isotope compositions of spinel peridotite xenoliths, Kozákov volcano, Czech Republic. Int J Earth Sci 104:1925–1956

Mengel K; Hoefs, Jochen (1990) Li-δ^{18}O-SiO_2 systematics in volcanic rocks and mafic lower crustal granulite xenoliths. Earth Planet Sci Lett, 101:42–53

Millot R, Négrel Ph, Petelet-Giraud E (2007) Multi-isotopic (Li, B, Sr, Nd) approach for geothermal reservoir characterization in the Limagne Basin (Massif Central, France). Appl. Geochem. 22:2307–2325

Morgan VI GB, London D (1987) Alteration of amphibolitic wallrocks around the Tanco rare-element pegmatite, Bernic Lake, Manitoba. Am Mineral 72:1097–1121

Moriguti T, Nakamura E (1998) Across-arc variation of Li isotopes in lavas and implication for crust/mantle recycling at subduction zones. Earth Planet Sci Lett 163:167–174

Moriguti T, Shibata T, Nakamura E (2004) Lithium, boron and lead isotope and trace element systematics of Quaternary basaltic volcanic rocks in northeastern Japan: mineralogical controls on slab-derived fluid composition. Chem Geol 212:81–100

Masukawa K, Nishio Y, Hayashi KI (2013) Lithium–strontium isotope and heavy metal content of fluid inclusions and origin of ore-forming fluid responsible for tungsten mineralization at Takatori mine, Japan. Geochem J 47:309–319

Nabelek PI, Labotka TC, O'Neil JR, Papike JJ (1984) Contrasting fluid/rock interaction between the Notch Peak granitic intrusion and argillites and limestones in western Utah: evidence from stable isotopes and phase assemblages. Contrib Mineral Petrol 86:25–34

Nishio Y, Nakai S, Kogiso T, Barsczus HG (2005) Lithium, strontium, and neodymium isotopic compositions of oceanic island basalts in the Polynesian region: constraints on a Polynesian HIMU origin. Geochem J 39:91–103

Nishio Y, Nakai S, Ishii T, Sano Y (2007) Isotope systematics of Li, Sr, Nd, and volatiles in Indian Ocean MORBs of the Rodriguez Triple Junction: constraints on the origin of the DUPAL anomaly. Geochim Cosmochim Acta 71:745–759

Nishio Y, Nakai S, Yamamoto J, Sumino H, Matsumoto T, Prikhod'ko VS, Arai S (2004) Lithium isotopic systematics of the mantle-derived ultramafic xenoliths: implications for EM1 origin. Earth Planet. Sci. Lett. 217:245–261

Ottolini L, Le Fèvre B, Vannucci R (2004) Direct assessment of mantle boron and lithium contents and distribution by SIMS analyses of peridotite minerals. Earth Planet Sci Lett 228:19–36

Ottolini L, Laporte D, Raffone N, Devidal J-L, Le Fèvre B (2009) New experimental determination of Li and B partition coefficients during upper mantle partial melting. Contrib Mineral Petrol 157:313–325

Parkinson IJ, Hammond SJ, James RH, Rogers NW, (2007) High-temperature lithium isotope fractionation: Insights from lithium isotope diffusion in magmatic systems. Earth Planet. Sci. Lett. 257:609–621

Penniston-Dorland SC, Bebout GE, Pogge von Strandmann PA, Elliott T and Sorensen SS (2012) Lithium and its isotopes as tracers of subduction zone fluids and metasomatic processes: evidence from the Catalina Schist, California, USA. Geochim. Cosmochim. Acta 77:530–545

Penniston-Dorland SC, Sorensen SS, Ash RD and Khadke SV (2010) Lithium isotopes as a tracer of fluids in a subduction zone melange: Franciscan complex, CA. Earth Planet. Sci. Lett. 292:181–190.

Pistiner JS, Henderson GM (2003) Lithium-isotope fractionation during continental weathering processes. Earth Planet Sci Lett 214:327–339

Plank T (2014) The chemical composition of subducting sediments. In: Rudnick RL (ed) Treatise on geochemistry, vol 4, 2nd edn. Elsevier Ltd., Oxford, pp 607–629

Plyusnin GS, Posokhov VF, Sandimirova GP (1979) Magmatic differentiation and reliationship of Li/ Li ratio to fluorine content. Doklady Acad. Sci. USSR, Earth Sci 248:187–189

Pogge von Strandmann PAE, Elliott T, Marschall HR, Coath C, Lai Y-J, Jeffcoate AB, Ionov DA (2011) Variations of Li and Mg isotope ratios in bulk chondrites and mantle xenoliths. Geochim Cosmochim Acta 75:5247–5268

Pogge von Strandmann PAE, Opfergelt S, Lai YJ, Sigfússon B, Gislason SR, Burton KW (2012) Lithium, magnesium and silicon isotope behaviour accompanying weathering in a basaltic soil and pore water profile in Iceland. Earth Planet Sci Lett 339/340:11–23

Richter FM, Davis AM, DePaolo DJ, Watson EB (2003) Isotope fractionation by chemical diffusion between molten basalt and rhyolite. Geochim. Cosmochim. Acta 67:3905–3923

Romer RL, Meixner A (2014) Lithium and boron isotopic fractionation in sedimentary rocks during metamorphism: the role of rock composition and protolith mineralogy. Geochim Cosmochim Acta 128:158–177

Romer RL, Heinrich W, Schröder-Smeibidl B, Meixner A, Fischer K-O, Schulz C (2005) Elemental dispersion and stable isotope fractionation during reactive fluid-flow and fluid immiscibility in the Bufa del Diente aureole, NE-Mexico: evidence from radiographies and Li, B, Sr, Nd, and Pb isotope systematics. Contrib Mineral Petrol 149:400–429

Romer RL, Meixner A, Förster H-J (2014) Lithium and boron in late-orogenic granites: isotopic fingerprints for the source of crustal melts? Geochim Cosmochim Acta 131:98–114

Rudnick RL, Ionov DA (2007) Lithium elemental and isotopic disequilibrium in minerals from peridotite xenoliths from far-east Russia: Product of recent melt/fluid–rock reaction. Earth Planet. Sci. Lett. 256:278-293

Rudnick RL, Tomascak PB, Njo HB, Gardner LR (2004) Extreme lithium isotopic fractionation during continental weathering revealed in saprolites from South Carolina. Chem. Geol. 212:45–57

Ryan JG, Langmuir CH (1987) The systematics of lithium abundances in young volcanic rocks. Geochim Cosmochim Acta 51:1727–1741

Ryan JG, Kyle PR (2004) Lithium abundance and lithium isotope variations in the mantle sources: insights from intraplate volcanic rocks from Ross Island and Marie Byrd Land (Antarctica) and other oceanic islands. Chem Geol 212:125–142

Salters VJM, Stracke A (2004) Composition of the depleted mantle. Geochem Geophys Geosys 5, paper number Q05004. doi: 10.1029/2003GC000597

Schiavi F, Kobayashi K, Nakamura E, Tiepolo M, Vannucci R (2012) Trace element and Pb-B-Li isotope systematics of olivine-hosted melt inclusions: insights into source metasomatism beneath Stromboli (southern Italy). Contrib Mineral Petrol 163:1011–1031

Schiavi F, Kobayashi K, Moriguti T, Nakamura E, Pompilio M, Tiepolo M, Vannucci R (2010) Degassing, crystallization and eruption dynamics at Stromboli: trace element and lithium isotopic evidence from 2003 ashes. Contrib Mineral Petrol 159:541–561

Schuessler JA, Schoenberg R, Sigmarsson O (2009) Iron and lithium isotope systematics of the Hekla volcano, Iceland: evidence for Fe isotope fractionation during magma differentiation. Chem Geol 258:78–91

Seitz H-M, Woodland AB (2000) The distribution of lithium in peridotitic and pyroxenitic mantle lithologies: an indicator of magmatic and metasomatic processes. Chem Geol 166:47–64

Seitz H-M, Brey GP, Stachel T, Harris JW (2003) Li abundances in inclusions in diamonds from the upper and lower mantle. Chem Geol 201:307–318

Seitz H-M, Brey GP, Harris JW, Ludwig T (2006) Lithium isotope composition of lower mantle ferropericlase inclusions in diamanods from Sao Luiz, Brazil. Geochim Cosmochim Acta 70:A569

Seitz H-M, Brey GP, Lahaye Y, Durali S, Weyer S (2004) Lithium isotopic signatures of peridotite xenoliths and isotopic fractionation at high temperature between olivine and pyroxenes. Chem Geol 212:163–177

Seyfried WEJ, Chen X, Chan L-H (1998) Trace element mobility and lithium isotope exchange during hydrothermal alteration of seafloor weathered basalt: An experimental study at 350 °C, 500 bars. Geochim Cosmochim Acta 62:949–960

Shabaga BM, Fayek M, Hawthorne FC (2010) Boron and lithium isotopic compositions as provenance indicators of Cu-bearing tourmalines. Mineral Mag 74:241–255

Simons KK, Harlow GE, Brueckner HK, Goldstein SL, Sorensen SS, Hemming NG and Langmuir CH (2010) Lithium isotopes in Guatemalan and Franciscan HP–LT rocks: insights into the role of sediment-derived fluids during subduction. Geochim. Cosmochim. Acta 74:3621–3641

Sirbescu M-LC and Nabelek PI (2003) Crustal melts below 400°C. Geology 31:685–688

Sobolev AV, Hofmann AW, Kuzmin DV, Yaxley GA, Arndt NT, Chung S-L, Danyushevsky LV, Elliott T, Frey FA, Garcia MO, Gurenko AA, Kamenetsky VS, Kerr AC, Krivolutskaya NA, Matvienkov VV, Nikogosian IK, Rocholl A, Sigurdsson IA, Sushchevskaya NM, Teklay M (2007) The amount of recycled crust in sources of mantle-derived melts. Science 316:412–417

Soltay LG, Henderson GS (2005) Structural differences between lithium silicate and lithium germanate glasses by Raman spectroscopy. Phys Chem Glasses, 46 (4):381–384

Sturchio NC and Chan L-H (2003) Lithium isotope geochemistry of the Yellowstone hydrothermal system. Soc. Econ. Geol. Spec. Publ. 10:171–180

Stracke A, Hofmann AW, Hart SR (2005) FOZO, HIMU, and the rest of the mantle zoo. Geochem Geophys Geosys 6, paper number Q05007. doi: 10.1029/2004GC000824

Stracke A, Snow JE, Hellebrand E, von der Handt A, Bourdon B, Birbaum K, Günther D (2011) Abyssal peridotite Hf isotopes identify extreme mantle depletion. Earth Planet Sci Lett 308:359–368

Su B-X, Zhang H-F, Deloule E, Asamoah Sakyi P, Xiao Y, Tang Y-J, Hu Y, Ying J-F, Liu P-P (2012) Extremely high and low δ^7Li signatures in the lithospheric mantle. Chem Geol 292–293:149–157

Tang M, Rudnick RL, Chauvel C (2014a) Sedimentary input to the source of Lesser Antilles lavas: a Li perspective. Geochim Cosmochim Acta 144:43–58

Tang Y-J, Zhang H-F, Ying J-F (2010) A brief review of isotopically light Li: a feature of the enriched mantle? Int Geol. Rev 52:964–976

Tang Y-J, Zhang H-F, Nakamura E, Ying J-F (2011) Multistage melt/fluid-peridotite interactions in the refertilized lithospheric mantle beneath the North China Craton: constraints from the Li–Sr–Nd isotopic disequilibrium between minerals of peridotite xenoliths. Contrib Mineral Petrol 161:845–861

Tang Y-J, Zhang H-F, Nakamura E, Moriguti T, Kobayashi K, Ying J-F (2007) Lithium isotopic systematics of peridotite xenoliths from Hannuoba, North China Craton: implications for melt-rock interaction in the considerably thinned lithospheric mantle. Geochim Cosmochim Acta 71:4327–4341

Tang Y-J, Zhang H-F, Deloule E, Su B-X, Ying J-F, Xiao Y, Hu Y (2012) Slab-derived lithium isotopic signatures in mantle xenoliths from northeastern North China Craton. Lithos 149:79–90

Tang Y-J, Zhang H-F, Deloule E, Su B-X, Ying J-F, Santosh M, Xiao Y (2014b) Abnormal lithium isotope composition from the ancient lithospheric mantle beneath the North China Craton. Sci Rep 4:4274. doi:10.1038/srep04274

Taylor SR & McLennan SM (1985) The continental crust: Its composition and evolution. Oxford, London, xvi + pp 312

Teng F-Z, Rudnick RL, McDonough WF, Gao S, Tomascak PB, Liu Y (2008) Lithium isotopic composition and concentration of the deep continental crust. Chem Geol 255:47–59

Teng F-Z, Rudnick RL, McDonough WF and Wu F-Y (2009) Lithium isotopic systematics of A-type granites and their mafic enclaves: further constraints on the Li isotopic composition of the continental crust. Chem. Geol. 262:370–379

Teng F-Z, McDonough WF, Rudnick RL, Dalpé C, Tomascak PB, Chappell BW, Gao S (2004) Lithium isotopic composition and concentration of the upper continental crust. Geochim Cosmochim Acta 68:4167–4178

Teng F-Z, McDonough, WF, Rudnick RL, Walker RJ, Sirbescu M-L, (2006)a. Lithium isotopic systematics of granites and pegmatites from the Black Hills, South Dakota. Am. Mineral. 91:1488–1498

Teng, F-Z, McDonough, WF, Rudnick, RL, Walker, RJ, (2006)b. Diffusion-driven extreme lithium isotopic fractionation in country rocks of the Tin Mountain pegmatite. Earth Planet Sci Lett 243:701–710

Tian S, Hou Z, Su A, Qui L, Xuanuue M, Hou K, Zhao Y, Hu W, Yang Y (2015) The anomalous lithium isotopic signature of Himalayan collisional zone carbonatites in western Sichuan, SW China: enriched mantle source and petrogenesis. Geochim Cosmochim Acta 159:42–60

Tkachev AV (2011) Evolution of metallogeny of granitic pegmatites associated with orogens throughout geologic time. In: Sial AN, Bettencourt JS, De Campos CP (eds) Granite-related ore deposits. Geol Soc Lond Spec Publ 350:7–23

Tomascak PB (2004) Developments in the understanding and application of lithium isotopes in the Earth and planetary sciences. In: Johnson CM, Beard BL, Albarède F (eds) Geochemistry of non-traditional stable isotopes. Rev Mineral Geochem 55:153–195

Tomascak PB (2015) Lithium and sediment: the Martinique connection. Sci Bull 60:1136–1137

Tomascak PB and Magna T (2014) Lithium isotopes in magmatic rocks from the Crazy Mountains, Montana. 4 Meeting of the Expert Volcanology Group of the Czech Geological Society. pp 27/28

Tomascak PB, Ryan JG, Defant MJ (2000) Lithium isotope evidence for light element decoupling in the Panama subarc mantle. Geology 28:507–510

Tomascak PB, Lynton SJ, Walker RJ, Krogstad EJ (1995) Li isotope geochemistry of the Tin Mountain pegmatite,

Black Hills, South Dakota. In: Brown M, Piccoli PM (eds) The origin of granites and related rocks. U.S. Geological Survey Circular, vol 1129, pp 151–152

Tomascak PB, Tera F, Helz RT, Walker RJ (1999) The absence of lithium isotope fractionation during basalt differentiation: new measurements by multicollector sector ICP-MS. Geochim Cosmochim Acta 63:907–910

Tomascak PB, Langmuir CH, le Roux PJ, Shirey SB (2008) Lithium isotopes in global mid-ocean ridge basalts. Geochim Cosmochim Acta 72:1626–1637

Tomascak PB, Widom E, Benton LD, Goldstein SL, Ryan JG (2002) The control of lithium budgets in island arcs. Earth Planet Sci Lett 196:227–238

van Hinsberg, Marschall VJ, HR (2007) Boron isotope and light element sector zoning in tourmaline: Implications for the formation of B-isotopic signatures. Chem Geol 238:141–148

Vils F, Pelletier L, Kalt A, Müntener O, Ludwig T (2008) The lithium, boron and beryllium content of serpentinized peridotites from ODP leg 209 (sites 1272A and 1274A): implications for lithium and boron budgets of oceanic lithosphere. Geochim Cosmochim Acta 72:5475–5504

Vils F, Tonarini S, Kalt A, Seitz H-M (2009) Boron, lithium and strontium isotopes as tracers of seawater–serpentinite interaction at Mid-Atlantic ridge, ODP Leg 209. Earth Planet Sci Lett 286:414–425

Vlastélic I, Koga K, Chauvel C, Jacques G, Télouk P (2009) Survival of lithium isotopic heterogeneities in the mantle supported by HIMU-lavas from Rurutu Island, Austral Chain. Earth Planet Sci Lett 286:456–466

Vocke RD, Beary ES, Walker RJ (1990) High precision lithium isotope ratio measurement of samples from a variety of natural sources. In: Abstract inVM Goldschmidt conference program, 89

Wagner C, Deloule E, (2007) Behaviour of Li and its isotopes during metasomatism of French Massif Central lherzolites. Geochim. Cosmochim. Acta 71:4279–4296

Walker JA, Teipel AP, Ryan JG, Syracuse E (2009) Light elements and Li isotopes across the northern portion of the Central American subduction zone. Geochem Geophys Geosys 10, paper number Q06S16. doi:10.1029/2009GC002414

Weyer S, Seitz H-M (2012) Coupled lithium- and iron isotope fractionation during magmatic differentiation, Chem Geol 294/295, 42–50

Willbold M, Stracke A (2006) Trace element composition of mantle end-members: implications for recycling of oceanic and upper and lower continental crust. Geochem Geophys Geosys 7, paper number Q04004. doi: 10.1029/2005GC001005

Wilson M, Downes H (1991) Tertiary-Quaternary extension related alkaline magmatism in western and central Europe. J Petrol 32:811–849

Wimpenny J, Gíslason SR, James RH, Gannoun A, Pogge von Strandmann PAE and Burton KW (2010) The behaviour of Li and Mg isotopes during primary phase dissolution and secondary mineral formation in basalt. Geochim. Cosmochim. Acta 74:5259–5279

Woodland AB, Seitz H-M, Altherr R, Marschall H, Olker B, Ludwig T (2002) Li abundances in eclogite minerals: a clue to a crustal or mantle origin? Contrib Mineral Petrol 143:587–601

Woodland AB, Seitz H-M, Yaxley GM, (2004) Varying behaviour of Li in metasomatised spinel peridotite xenoliths from Western Victoria, Australia. Lithos 75:55–66.

Wunder B, Meixner A, Romer RL, Feenstra A, Schettler G, Heinrich W (2007) Lithium isotope fractionation between Li-bearing staurolite, Li-mica and aqueous fluids: an experimental study. Chem Geol 238:277–290

Wunder B, Meixner A, Romer RL, Heinrich W (2006) Temperature-dependent isotopic fractionation of lithium between clinopyroxene and high-pressure hydrous fluids. Contrib Mineral Petrol 151:112–120

Wunder B, Meixner A, Romer RL, Jahn S (2011) Li-isotope fractionation between silicates and fluids: Pressure dependence and influence of the bonding environment. Eur J Min 23:333–342

Xiao Y, Hoefs J, Hou Z, Simon K, Zhang Z (2011) Fluid/rock interaction and mass transfer in continental subduction zones: constraints from trace elements and isotopes (Li, B, O, Sr, Nd, Pb) in UHP rocks from the Chinese Continental Scientific Drilling Program, Sulu, East China. Contrib Mineral petrol 162:797–819

Xiao Y, Zhang H-F, Deloule E, Su B-X, Tang Y-J, Sakyi P, Hu Y, Ying J-F (2015) Large lithium isotopic variations in minerals from peridotite xenoliths from the Eastern North China Craton. J Geol 123:79–94

Xu R, Liu Y, Tong X, Hu Z, Zong K, Gao S (2013) In-situ trace elements and Li and Sr isotopes in peridotite xenoliths from Kuandian, North China Craton: insights into Pacific slab subduction-related mantle modification. Chem Geol 354:107–123

Yamaji K, Makita Y, Watanabe H, Sonoda A, Kanoh H, Hirotsu T, Ooi K (2001) Theoretical estimation of lithium isotopic reduced partition function ratio for lithium ions in aqueous solution. J Phys Chem A 105:602–613

Yang H, Konzett J, Downs RT, Frost DL (2009) Crystal structure and Raman spectrum of a high-pressure Li-rich majoritic garnet, $(Li_2Mg)Si_2(SiO_4)_3$. Am Mineral 94:630–633

Zack T, Tomascak PB, Rudnick RL, Dalpé C, McDonough WF (2003) Extremely light Li in orogenic eclogites: the role of isotope fractionation during dehydration in subducted oceanic crust. Earth Planet Sci Lett 208:279–290

Zhang L, Chan L-H, Gieskes JM (1998) Lithium isotope geochemistry of pore waters from Ocean Drilling Program Sites 918 and 919, Irminger Basin. Geochim Cosmochim Acta 62:2437–2450

Zhang H-F, Deloule E, Tang Y-J, Ying J-F (2010) Melt/rock interaction in the remains of refertilized Archean lithospheric mantle in Jiaodong Peninsula, North China Craton: Li isotopic evidence. Contrib Mineral Petrol 160:261–277

Zindler A, Hart SR (1986) Chemical geodynamics. Annu Rev Earth Planet Sci 14:493–571

The Surficial Realm: Low Temperature Geochemistry of Lithium

6

In this section we consider the variations shown by Li isotopes in materials related to near-surface (classically referred to as "low temperature") systems, ranging from sediments and sedimentary rocks to natural waters and possible anthropogenic impacts. The combination of modest abundance in many minerals and fluid solubility make Li an element of interest in many surficial environments. The strong fractionation of Li isotopes has been exploited substantially in the examination of a variety of near-Earth-surface processes. In addition to their intrinsic value, many of these studies are critical toward the understanding of the cycling of Li between shallow and deep Earth reservoirs, as, relative to the latter, the bulk of the mass fractionation goes on in the former. Many studies aim also to develop Li isotopic tools for better quantifying processes in the shallow Earth, such as geothermometry of hydrothermal systems.

The division of major classes of processes affecting isotopic distributions inevitably becomes somewhat arbitrary, given that the Earth system presents few situations in which a sole process can be identified. Thus, although we acquiesce that elemental and isotopic fractionation at hydrothermal temperatures is distinct from that occurring at conditions of shallow burial, diagenesis or surficial weathering, many (most?) geological settings contain superimposed aspects of some or all of these pathways. For the purpose of this summary, we have chosen to divide conditions into two compartments: hydrothermal (by which we intend to describe shallow crustal systems of temperature $\geq \sim 200$ °C) and, essentially, everything sub-hydrothermal. We begin with the latter, moving from the ultimate feedstock for surficial waters and then move on to other reservoirs.

6.1 Meteoric Water

The Li isotopic composition of atmospheric precipitation has been only rarely reported. To some extent this may reflect the low Li concentration in average rainfall (generally <3 ppb; Millot et al. 2010a), which made analysis more challenging prior to the development of modern analytical methods. Single samples of rainfall from Hawaii (Pistiner and Henderson 2003; δ^7Li = +14.3 ‰ in filtered aliquot) and Sao Miguel (Pogge von Strandmann et al. 2010; δ^7Li = +32.8 ‰) were analyzed, the latter noting the congruence with seawater. Although Pistiner and Henderson (2003) did not interpret the absolute isotopic composition of the sample they reported, they made the observation that filtration of the original sample removed an isotopically light atmospheric dust component (δ^7Li = +10.2 ‰ in unfiltered aliquot). As will be seen below, the same relationship is manifest in river water dissolved/suspended load comparisons.

To date only one systematic study has considered Li isotopes in rainfall (Millot et al. 2010a), which produced several interesting and

P.B. Tomascak et al., *Advances in Lithium Isotope Geochemistry*,
Advances in Isotope Geochemistry, DOI: 10.1007/978-3-319-01430-2_6

unexpected outcomes. Analyzing filtered samples from different physiographic regions in France, Millot et al. (2010a) found that even in sea-coast sampling locations marine sources did not dominate the Li budget. The largest contribution of seawater aerosol Li to samples only approached 50 %, and in one of two sites within 100 km of the Atlantic Ocean the proportion was at most ~20 %. Lithium in rainfall from sites >300 km distant from the ocean contained at most 10 % sea-salt-derived Li. In samples from Clermont-Ferrand in particular it was clear that anthropogenically-influenced sources were significant, with δ^7Li as high as +95 ‰ (see Sect. 6.5.2 for more detail on this process).

Witherow et al. (2010) reported δ^7Li of surface snow from three Antarctic glaciers (δ^7Li = +0.8 to +2.9 ‰), and Pogge von Strandmann et al. (2006) analyzed Li in one water sample directly derived from melting of glacial ice in Iceland (δ^7Li = +33.3 ‰). All of these waters have very low Li concentrations (<1 ppb). Whereas the Iceland sample might have seawater aerosols as a major source of Li, clearly the Antarctic samples do not. The low Li abundance in modern rain water corresponds well with generally low Li contents in airborne particles, although speciation of Li in atmospheric deposits may, to a certain extent, depend on climatic conditions (Siggaard-Andersen et al. 2007). These cumulative findings imply a rather high reactivity of Li particles in the air and their effective removal from the atmosphere.

6.2 Groundwater and Pore Waters

6.2.1 Shallow Groundwaters

Most groundwaters within the upper ~100 m of the Earth's surface are characterized by low to modest dissolved solid contents (generally <1000 ppm) in all but very arid regions (Fig. 6.1). Relatively short storage times limit the role of mineral–fluid reactions in shaping the geochemistry of these waters compared to their deep brethren.

In arid areas the lack of abundant recharge coupled with evaporation may produce groundwaters that are, in some cases, as saline as formation waters. For example, none of the Great Artesian Basin groundwaters sampled by

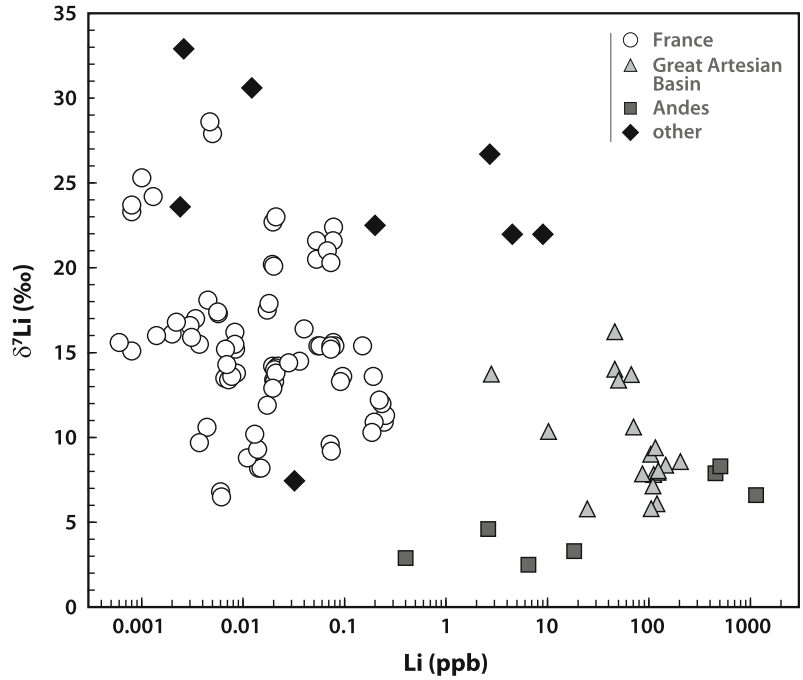

Fig. 6.1 Lithium concentration and δ^7Li of shallow groundwaters. Data sources: France from Negrel et al. (2012), Andes from Godfrey et al. (2013), Great Artesian Basin (GAB) from Meredith et al. (2013), "other" (includes data from four separate localities) from Hogan and Blum (2003), Kloppmann et al. (2009), Rad et al. (2013), Tomascak et al. (2003)

Meredith et al. (2013) was ancient (all <10 ka), but the total dissolved solid content of most samples was >30,000 ppm. The deepest of these waters was withdrawn from only 126 m.

Water-sediment or water-rock interactions have the capacity to complicate interpretation of Li isotope data from shallow groundwaters. In a feasibility study for the use of intrinsic stable isotopic tracers in groundwaters, Kloppmann et al. (2009) interpreted that Li isotopic signatures showed cryptic effects of interaction between injection water and sediments. With prolongation of water-sediment interaction, Li was removed from groundwaters, and isotopic signatures shifted to lighter values by c. 15 ‰. Similar cryptic isotopic effects were seen by Meredith et al. (2013). The waters in the latter study appeared, based solely on elemental data, to conform to two-component mixing between relatively fresh (shallow) and saline (deep) reservoirs. Lithium isotopes invalidated such a simple interpretation, suggesting the retention of isotopically distinct signatures by components of the hydrologic system separated both by depth and horizontal distance. This could be at least partially accounted for by variable mineralogy of aquifer sediments, but mapping this out would require a more involved campaign of sampling of both waters and solids. The results of Meredith et al. (2013) were broadly confirmed by a study of deeply issued waters (>427 m) from the Great Artesian Basin (Pogge von Strandmann et al. 2014). The δ^7Li of these samples ranged between +9 and +16 ‰ with the highest Li contents in low-δ^7Li waters. The ratio of weathering/dissolution of primary minerals and precipitation of secondary minerals controlled Li abundance whereas δ^7Li was largely controlled by the extent to which secondary minerals (e.g., kaolinite, gibbsite, smectite, illite, chlorite, etc.) fractionate Li isotopes. An important consideration in the study of Pogge von Strandmann et al. (2014) was that these large aquifer systems may be an important input of isotopically light Li to seawater.

Ambient temperature groundwaters in the western U.S. Great Basin analyzed by Tomascak et al. (2003) were not uniform in Li isotopic composition, but tended to be characterized by $\delta^7\text{Li} \geq +30$ ‰. In the absence of marine sources, such heavy Li signatures may derive from sorption reactions or through the formation of low temperature minerals in the shallow subsurface; without more detail on the mineralogy of aquifers, neither interpretation can be invalidated.

Whereas most of the focus on Li isotopic fractionation during mineral crystallization at low temperatures centers on silicates, Huh et al. (1998) suggested that the crystallization of carbonates or halides could drive Li isotopic fractionation. The laboratory results of Marriott et al. (2004a) appear to support this in terms of aragonite, and to a lesser extent calcite. One attempt to quantify fractionation effects during halite crystallization from brine showed only minimal isotopic effect (Godfrey et al. 2013). It is, however, correct to say that carbonates themselves are in most cases depleted in Li relative to silicates (e.g., Hoefs and Sywall 1997; Chan et al. 2006) and thus, their contribution to the total mass balance of Li at low temperatures appears to be minor in the majority of geological environments.

In an area where rigorous monitoring of groundwater quality is in place, Négrel et al. (2012) were able to promulgate a much more complete assessment of Li isotopic variations in a large aquifer system. The groundwaters of southwestern France showed the effects of mixing between rainwaters of variable δ^7Li and waters that carry an imprint of interaction with sediments and/or bedrock (all isotopically lighter than rainwaters) at elevated temperature.

6.2.2 Deep Groundwaters

Many groundwater systems are completely transitional with hydrothermal systems, which were documented in Sect. 6.1. We include in this section settings that range down-temperature from "passive" geothermal waters (generally ≤100 °C). Formation waters, basinal brines and oilfield brines differ from ordinary groundwaters in that their histories of water-rock interaction are more extensive. They show a range in Li isotopic

character, reflecting, in general, variability in starting water isotopic composition, lithology, and the extent of water-mineral interaction.

Inasmuch as the Li isotopic composition of modern seawater is distinctively heavy, the system has a significant role in assessing the contribution of marine sources to basinal waters (Fig. 6.2). In many cases it is clear that seawater was the primary source of formation waters (Chan et al. 2002b), although whether waters reached concentrations 24× that of seawater through evaporation or freezing could not be resolved (Bottomley et al. 1999).

It should be noted that although seawater Li has been isotopically consistent over the last c. 6 Myr (Misra and Froelich 2012), shifts to compositions as light as δ^7Li = +5 ‰ appear to have occurred during the last 100 Myr (Pogge von Strandman et al. 2013). This tempers the utility of Li as a direct seawater fingerprint. These short-term variations may be compromised by conservative behavior of Li in seawater, with the mean residence time of c. 1–1.5 Myr (Stoffyn-Egli and Mackenzie 1984; Huh et al. 1998), allowing for long-term processes to be accounted for whilst temporally restricted events may remain unresolved. For example, Devonian seawater Li remains isotopically uncharacterized; thus we cannot unambiguously determine a seawater Li isotopic signature in formation waters that derive Li from rocks deposited during that era. This has a direct impact on the interpretation of sources of groundwaters such as those of the Canadian Shield (Bottomley et al. 1999, 2003). In this study, data from deep waters were interpreted to possess significant Devonian seawater components.

Using Li isotopes to constrain the temperatures of deep basin fluids has received substantial attention. Considering the frequent lack of convergence among geothermal temperatures acquired through other geochemical techniques (e.g., Helgeson et al. 1978; Fournier and Potter 1979), if successful this would indeed be a major advancement.

Millot and Négrel (2007) took a novel approach with French geothermal waters of well-understood temperature to suggest that Li isotopes could be used as a geothermometer. By their results, for waters in reservoirs with T < c. 250 °C which were least affected by secondary processes, the system appeared to yield viable results, with a precision of ±50 °C. Although this precision is poorer than many of the conventional methods (e.g., silica solubility; Fournier and Rowe 1966), Li isotopic thermometry may apply to a wide array of thermal waters where the applicability of some other methods is limited by

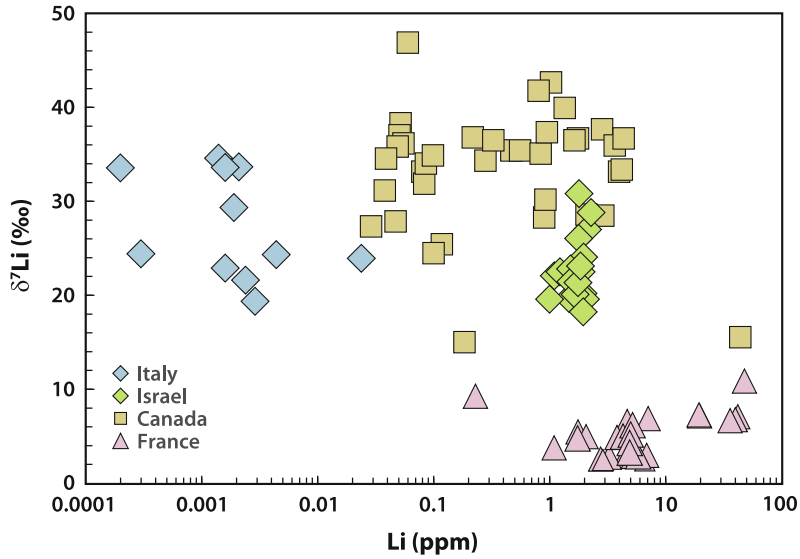

Fig. 6.2 Lithium concentration and δ^7Li of deep groundwaters and basinal brines. Data sources: France from Millot et al. (2007, 2011), Millot and Négrel (2007), Italy (serpentine springs) from Boschetti et al. (2013), Israel from Chan et al. (2002b), Canada from Bottomley et al. (1999, 2003)

major ion composition. The same approach had been outlined previously for sea floor systems (e.g., Chan et al. 1994), but in these cases there appear more prominent pathways to obliterate meaningful thermometric potential of many thermal waters (e.g., Decitre et al. 2004). Millot et al. (2011) achieved very geologically reasonable temperature estimates from Paris basin waters from two localities, in the range 45–95 °C, with precisions of ±10–20 °C. Using this approach to thermometry, however, does not always yield conclusive results, as demonstrated by data from saline waters from the Appalachian Plateau and Gulf Coast of the U.S. (Macpherson et al. 2015). Their samples did not fall on model curves predicted from Li isotopic equilibrium between water and average shales.

To the extent they have been studied, springs issuing from terrestrial (that is, continental) serpentinites have a peculiar geochemical signature, being highly alkaline with generally strongly elevated trace elements (B, Li) yet low dissolved solid contents. Apennine serpentinites do not show strong Li concentration variation, but do have a wide range in Li isotopes (Boschetti et al. 2013). The Li isotopes strongly suggested that serpentinite springs represent variable degrees of fractionation during crystallization of secondary minerals. Initial waters would thereby have had δ^7Li < +20 ‰.

6.2.3 Pore Waters

Pore waters have been sampled predominantly in the sediment piles of convergent margins, but also as subaerial and submarine seeps and mud volcanoes. The compositions of these waters reflect a continuum of processes. With seawater as the principle starting fluid, these waters may evolve along distinct paths depending on the influences of mineral alteration and ion exchange; their geochemistry may also be influenced by influx of deeper, hydrothermal waters. Even the deepest of these accumulations do not reach hydrothermal temperatures (e.g., even with a thick accumulation and steep geotherm, the basal sediments in the Gulf of Cadiz reached only slightly over 200 °C; Scholz et al. 2009).

Lithium isotopes have contributed to better understanding the geochemical evolution of these waters owing to the divergent isotopic fingerprints of the processes involved. Chan and Kastner (2000), expanding on earlier work by Zhang et al. (1998), proposed two isotopically distinct drivers for Li isotopes in pore water. Low temperature alteration of volcanic material in sea floor sediments will generate clay minerals that favor incorporation of light Li, driving pore water compositions to δ^7Li > seawater (Fig. 6.3). Contrarily, reactions wherein clay minerals exchange Li from crystallographic sites in favor of NH_4^+ will liberate light Li and drive pore water to isotopically lighter compositions (see also Vigier et al. 2008). The same conclusion was reached for pore waters in the Escanaba trough (James and Palmer 2000). This process is especially important in sediments where bacterial processes yield high contents of dissolved ammonium. You et al. (1995) called on influx of dilute, isotopically light fluid from deep within the Nankai accretionary prism to explain variation of pore fluids compositions in the vicinity of the decollement.

Scholz et al. (2010) discovered, from comparison of compositions from a global pore water data, a relationship between Li in pore waters and the nature of tectonics in the margin delivering sediment. Their analysis showed that passive margin pore waters were enriched in Li relative to those at convergent margins. The alteration of volcanogenic material, inherently poorer in Li than sediment derived from continental weathering, was shown to produce low temperature minerals that strongly retain Li without imparting isotopic fractionation. Diagenetic alteration of carbonate-rich sediments was implicated by You et al. (2003) to explain down-core variations in Li concentration and isotopic composition of pore waters from the eastern Pacific.

Mud volcano fluids from the Nankai accretionary prism (Nishio et al. 2015) had low δ^7Li (seawater-corrected values < +8 ‰), equivalent to those from hydrothermal samples from the

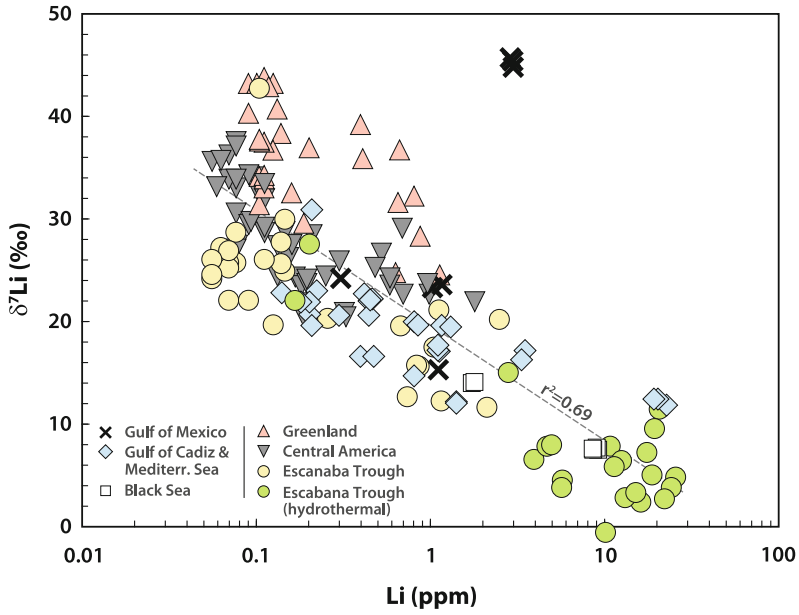

Fig. 6.3 Lithium concentration and δ^7Li of marine sediment pore waters. Data sources: Greenland (Irminger Basin) from Zhang et al. (1998), Central America from Chan and Kastner (2000), Scholz et al. (2010), Pacific (Escanaba Trough with and without hydrothermal influence) from James et al. (1999), James and Palmer (2000), Gulf of Cadiz and Mediterranean Sea from Scholz et al. (2009, 2010), Gulf of Mexico, Black Sea from Scholz et al. (2010)

Escanaba trough (James and Palmer 2000) and some fluids in the Black Sea (Scholz et al. 2010). Nishio et al. (2015) suggested that their results reflect the identifiable influx of geochemically distinct fluids during times of seismic slip. One value reported from the subaerial mud volcanoes of Taiwan was slightly isotopically heavier than these (c. +13 ‰; You et al. 2004).

Although a significant proportion of the earlier pore water data show dilute compositions and heavy Li isotope signatures (i.e., δ^7Li ≥ that of seawater), more recent data show that waters with Li concentrations greater than modern seawater make up less than half of the ensemble. There is a reasonable inverse correlation between pore water δ^7Li and concentration (R^2 = 0.69; Fig. 6.3). Scholz et al. (2010) applied a reactive transport model to quantitatively explain this, as did James et al. (1999), using a smaller data set. The latter study concluded that pore waters from part of the Escanaba trough system derived their high Li contents (some >100× seawater) through upward advection of waters carrying Li liberated from hydrothermal alteration of sediments. Although low-temperature fractionation may drive processes within individual sediment piles, when viewed collectively, the global pore water data set shows that an isotopically light, Li-enriched advected component is present in most systems (Fig. 6.3). The consensus of these studies is that pore water processes have only small influence on the marine budget of Li.

6.3 Continental Weathering

The quantitative understanding of continental weathering processes has become a major focus of geochemical studies, spurred by the potential for connecting weathering on the continents to marine geochemical records. Extraterrestrial application of the system has recently been discussed (Fairén et al. 2015). The interest in these records is clear given the feedback processes between chemical weathering reactions and atmospheric greenhouse gas contents. Lithium

and its isotopic composition have begun to be integrated into studies of this kind through both major world watersheds and smaller catchments with greater controls on geological variables, as well as intact soil sections.

6.3.1 Soils and Sediments

A limited number of studies have considered Li isotopes in the realm of soils (Fig. 6.4). Pistiner and Henderson (2003) measured Li in weathered volcanic materials from Iceland and Hawaii, but did not find compelling isotopic fractionation. Since that study it has become apparent that the secondary mineralogy is a master variable in the quantification of isotopic fractionation during weathering (Wimpenny et al. 2010a). Given the many factors that influence secondary mineral formation (source mineralogy, solution chemistry, etc.), variability in the products of chemical weathering is to be expected.

The first systematic study (Rudnick et al. 2004) was an attempt to understand isotopic fractionation during weathering in a simple natural setting. Exposed transects from unweathered to completely saprolitized rocks (granite and meta-diabase) permitted examination of Li through the progressive alteration of the original rocks. In both saprolites there was a general correlation between the degree of weathering (lower bulk rock density and higher chemical index of alteration) and the decrease in δ^7Li, with overall δ^7Li from −9 to −16 ‰. Secondary mineral formation in the granite could plausibly be described by a Rayleigh-type process, in which Li is lost during progressive fractionation. The diabase transect only partially followed this scheme; post-saprolitization overprinting from interaction with groundwater appears to have complicated the Li elemental and isotopic systematics of many of those samples.

Considering the importance of weathering basaltic rocks on global CO_2 dynamics, exposed basalt terranes have been popular targets for Li isotopic studies. Huh et al. (2004) performed a targeted study of Hawaiian soils in an attempt to understand Li mass balance during weathering.

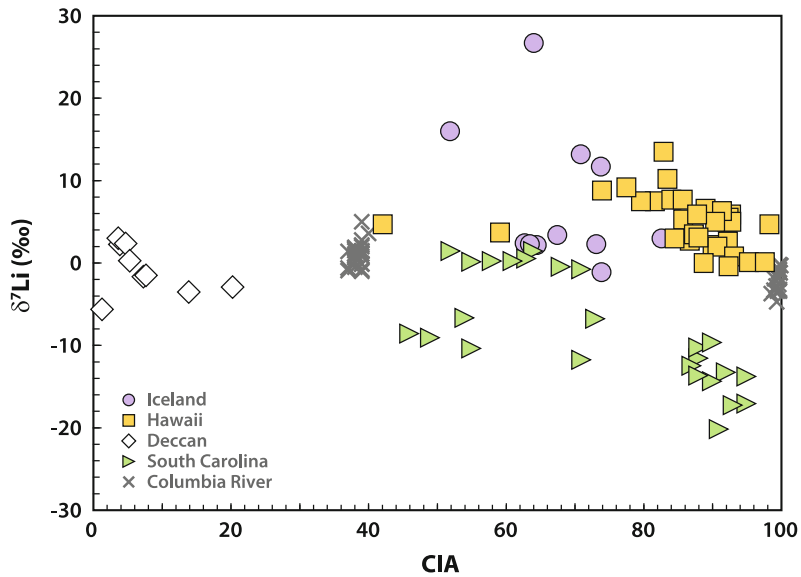

Fig. 6.4 Lithium isotopes relative to CIA (chemical index of alteration) in soil samples. Data sources: Iceland from Pogge von Strandmann et al. (2012), Columbia River (CR) from Liu et al. (2013), Deccan traps from Kısakürek et al. (2004), Hawaii from Huh et al. (2004), South Carolina (SC) from Rudnick et al. (2004), Also included are loess paleosol samples (non-carbonate fraction) from Tsai et al. (2014)

They found that, like the saprolites studied by Rudnick et al. (2004), under wet conditions (e.g., mean annual precipitation >200 cm) weathered materials generally lose Li, and secondary minerals prefer the light isotope. Nonetheless, loss of Li is not always synonymous with shift in isotopic composition. Ryu et al. (2014) also studied tropical soils from Hawaii Islands and found that, in young sequences (c. 3 ka), shallow soil samples that experienced as much as 30 % loss of Li showed no isotopic deviation from pristine source basalt.

Isotopically heavier soil samples from Huh et al. (2004), particularly those from more arid sampling sites, were thought to reflect input of seawater-derived aerosol Li, with its characteristically high δ^7Li (c. +31 ‰). The same conclusion was reached by Pogge von Strandmann et al. (2012) in their analysis of a basaltic soil section in Iceland. Soils least affected by aerosols, comprising mainly glass and mixed Al-silicate clays and oxyhydroxides, maintained δ^7Li up to 5 ‰ lighter than pristine tephra. These results, however, are somewhat opposite to those of Millot et al. (2010a; Sect. 6.1) who implied a minor fraction of seawater-borne aerosols in rain waters in France. This suggests that the size of the land mass (continent versus localized island) may impart a critical control on δ^7Li of the atmospheric deposition through differences in climatic cycles.

In a similar study of a soil section developed from intensive weathering of flood basalt in India, Kısakürek et al. (2004) saw somewhat different Li isotopic behavior. In the Deccan Traps they noted an overall decrease in Li concentration with progress of weathering, coupled with an influx of isotopically heavy Li in samples representing the paleo-water table. Lithium redistribution interpreted in the meta-diabase samples of Rudnick et al. (2004) yielded higher Li concentrations and δ^7Li values. Kısakürek et al. (2004) used mass balance principles to implicate an isotopically light atmospheric input (δ^7Li ~ +1 ‰) as a major Li source in these soils. In addition to bulk samples, Kısakürek et al. (2004) leached samples with dilute acetic acid; in general the leachates were Li depleted and slightly isotopically heavier than the residues. The implication of isotopically distinct Li imported from aerosol or dust sources in these studies (Huh et al. 2004; Kısakürek et al. 2004; Pogge von Strandmann et al. 2012) was not shared by Ryu et al. (2014), whose mass balance

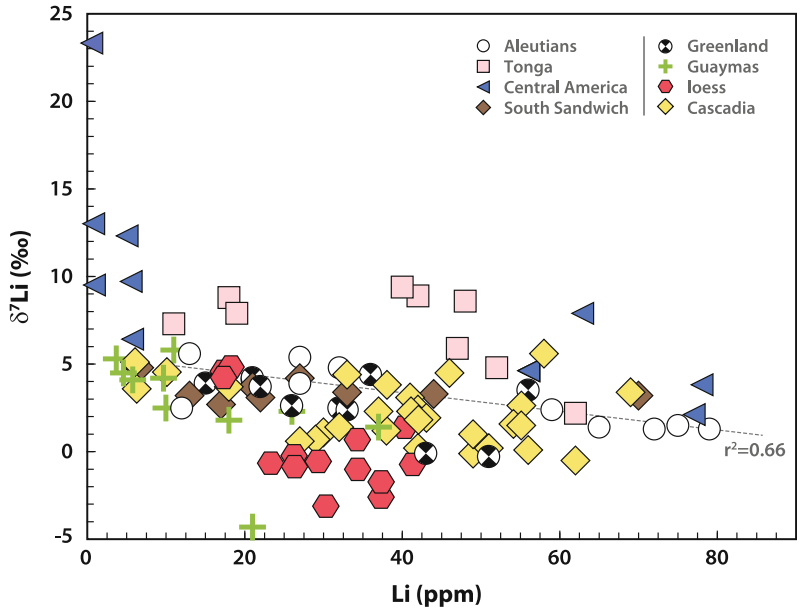

Fig. 6.5 Lithium concentration and δ^7Li of marine sediments. Data sources: Aleutians, Tonga, Central America, South Sandwich, Guaymas and Greenland all from Chan et al. (2006), Cascadia (includes Escanaba Trough) from Chan et al. (2006), James et al. (1999), Also included are loess samples from Teng et al. (2004) and Aeolian dust from Liu et al. (2013)

model allowed <20 % total contribution from atmospheric deposition, with a majority of the six Hawaiian sites yielding <10 %.

Bedload and suspended loads in rivers help to understand aspects of the soil data. Of the four published studies that include pairs of suspended and bedload sediment from the same rivers (Kısakűrek et al. 2005; Pogge von Strandmann et al. 2006; Wimpenny et al. 2010b; Millot et al. 2010c), there is a reasonable positive correlation between Li isotopes in the two ($R^2 = 0.81$; n = 61 pairs; Fig. 6.6). This relationship indicates that the average bedload is ~2 ‰ heavier than the coexisting suspended sediment. Dellinger et al. (2014) used a combination of new and existing data to demonstrate that the sediments carried by three major world rivers showed strong correlation of δ^7Li and Al/Si, a proxy for grain size. The sediment with lowest Al/Si corresponded to the highest δ^7Li in bedload sands (up to +5.3 ‰) and the corresponding suspended material had high Al/Si and δ^7Li as low as −3.6 ‰. This study emphasized the potential sampling bias that can affect interpretations derived from studies of river sediment.

The study of Dellinger et al. (2014) brought to light several interesting details in the consideration of Li isotopes in river sediments, and, hence, in the study of continental weathering. They were able to use isotope–element relations to define contributions of different major rock types in the catchments of tributaries, showing the variability of Li isotopic yield from different fundamental rock types (primarily igneous versus sedimentary, with some contribution from metasedimentary rocks). Additionally, their data suggested that the extent of recent chemical weathering was not a primary driving force modifying the δ^7Li of suspended loads. This is particularly so for particles derived from sedimentary lithologies, where, logically, minerals had been through the sedimentary process before, achieving a degree of stability, and hence limiting their capacity for Li isotopic fractionation.

The majority of river sediment studies were conducted in areas where bedrock geology was

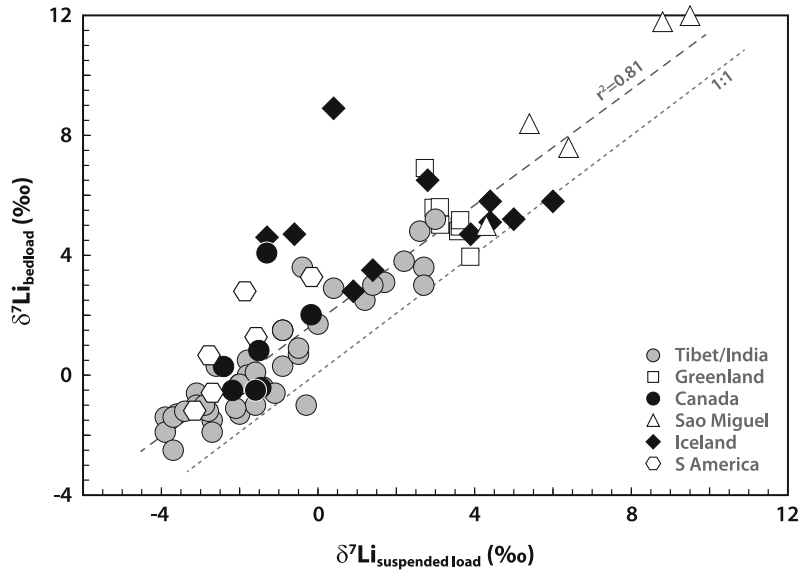

Fig. 6.6 Lithium isotopes in river suspended loads relative to bedloads. *Dashed line* is the regression of all data ($R^2 = 0.81$), which essentially has a slope of 1. Data sources: Tibet/India from Kısakürek et al. (2005), Dellinger et al. (2014), Greenland from Wimpenny et al. (2010a, b); Iceland from Pogge von Strandmann et al. (2006), Canada from Millot et al. (2010c), Sao Miguel from Pogge von Strandmann et al. (2010), South America from Dellinger et al. (2014)

largely invariant, and isotopic fractionation effects could be explicitly dissected. The production of secondary minerals in both suspended particles and bedload mineral grains involves fractionation of variable extents. Wimpenny et al. (2010b) measured offsets of 2 to 6 ‰ between source basalts and river sediments, with the latter uniformly isotopically lighter than gneissic bedrock of western Greenland. Vigier et al. (2009) found negligible source rock/sediment fractionation in Iceland. In the tropical (i.e., non-glaciated) island of Sao Miguel, Pogge von Strandmann et al. (2010) observed river sediments to be up to 9 ‰ *heavier* than the volcanic source bedrock. Whereas the specific secondary mineralogy plays a role in the fractionation that takes place during weathering, the difference observed between these studies illustrates the significance of the intensity of chemical weathering on Li isotopic behavior. This will be examined further in sections to follow.

In the headwaters of the Ganges River in Tibet, Li isotopes of sediments corresponded to the general variability in bedrock (Kısakűrek et al. 2005). Suspended loads and bedload in tributaries draining dolomitic substrates had higher δ^7Li than those draining silicate-dominant rocks. However, the absence of data for rocks inhibits deeper interpretation of the sediment data.

A distinct approach to the use of terrigenous sediments to evaluate paleoclimate was that of Dosseto et al. (2015), in which material from terraces of rivers draining a modern mountain range (the Himalayas) was examined. Given the problem of time lag between weathering and deposition, Dosseto et al. (2015) used deposits in the river headwaters. The variation of Li isotopes in bulk sediments (δ^7Li = −1.5 to +2.0 ‰) was consistent with but more restricted than in clay-size separates of the same samples (δ^7Li = −4.3 to +2.7 ‰). The covariation of sediment δ^7Li with Tibetan ice core δ^{18}O over the last c. 40 ka was interpreted to support the predominance of runoff and physical erosion (and hence tectonics) as drivers of chemical weathering, more so than changing temperature. Thus accelerated tectonic uplift will promote decreased chemical weathering and hence decreased removal of atmospheric CO_2.

Chan et al. (2006) compiled the most authoritative data set on Li in marine sediments, with 69 samples from seven globally-dispersed sites. The samples represent the primary marine lithologies, with an emphasis on clays and muds and comparatively few purely carbonates (four samples). The overall data set has a mean δ^7Li = +4.4 ± 3.6 ‰; without the strictly carbonate samples the mean is +4.0 ± 2.6 ‰ (Fig. 6.5). Variations in the Li isotopic signatures of samples from individual collection sites from this study are apparent. For example, nine samples from off the Tonga arc record a mean δ^7Li = +7.1 ± 2.4 ‰, whereas the same number of samples collected from the Pacific seafloor off of the Cascadia arc had a mean δ^7Li = +2.6 ± 1.1 ‰. All of the sample suites show a consistent, if slight, decline in δ^7Li with increasing Li concentration. Similar Li elemental and isotopic systematics were observed by Bouman et al. (2004) for marine sediments from East Sunda and the Lesser Antilles. Terrigenous sediments with distinctly high Th/Sc and La/Sm ratios also carry high loads of Li with isotopically light signature (Bouman et al. 2004), consistent with derivation from mature continent by weathering.

Complimentary to the data from marine and fluvial sediments, Teng et al. (2004) analyzed bulk samples of loess from various localities. The mean δ^7Li for loess (+0.3 ‰), analytically indistinguishable from aeolian dust from Washington (Liu et al. 2013), is isotopically lighter than both the suspended load (+1.3 ‰) and bedload (+2.9 ‰) averages. Teng et al. argued that loess ought to be a reliable estimator for the bulk Li isotopic composition of the upper crust. Rather than integrating global sources, Tsai et al. (2014) suggested that loess samples from China track regional sources in proximal Chinese deserts. In their study, Tsai et al. (2014) analyzed both detrital (δ^7Li from −3.5 to +5.6 ‰) and carbonate components (δ^7Li from −4.1 to +14.2 ‰), unlike the other studies that used only bulk samples.

In the most unique use of Li and Li isotopes to date in relation to weathering proxies, Ushikubo et al. (2008) used detrital zircon grains in ancient quartzites to investigate the early history of the Earth's continental crust. Although the main argument from Ushikubo et al. (2008) for an evolved continental crust on Earth at c. 4.3 Ga was the high Li contents in the zircon, the Li isotopes from these grains were far more variable than would be expected if derived from primitive sources. The large number of grains and spots analyzed turned up a significant range in δ^7Li, from −20 to +15 ‰. This study contained comparative data from younger zircons from igneous and high grade metamorphic rocks, testifying to the resiliency of Li to diffusion in zircon and opening the pathway to future studies using Li in zircon as a monitor of magmatic and metamorphic processes in crustal terranes.

6.3.2 Sedimentary Rocks

Although sediments themselves have, in various forms, been extensively analyzed for Li isotopes, the product of lithification of these materials has garnered comparatively little study (Fig. 6.7). Sedimentary rocks carry with them added layers of potential stable isotope complexity owing not only to the processes inherent in diagenesis and lithification, but in all of the subsequent fluid–mineral interactions that may occur, both in deep burial and after exhumation.

The data of Qiu et al. (2009) were interpreted to reflect a rather simple relationship between Li isotopes and the magnitude of weathering of the source lithologies. Importantly, their results suggested, at least for the case of the Paleozoic of southern England, that low grade metamorphism does not affect Li isotopic systematics of sediments (see Sect. 5.2.2 for more on metamorphism). The results from Teng et al. (2004), in their examination of globally distributed examples of sedimentary rocks, were slightly isotopically heavier (average δ^7Li = −0.2 ‰ compared to −1.0 ‰ from Qui et al. 2009). More variable still are the isotopic compositions recorded in sedimentary rocks from the Massif Central (Millot et al. 2007) and northern Canada (Millot et al. 2010c), with a total range of δ^7Li from −7.0 to +9.8 ‰. These rocks had an average δ^7Li of +1.8 ‰, although 1/3 of the rocks in these two studies were carbonates.

Given the variability in degree of weathering of source rocks, coupled with the likelihood of variable post-lithification processes, the observed range in Li isotopic composition is surely to be expected. Similar isotopic diversity superimposed

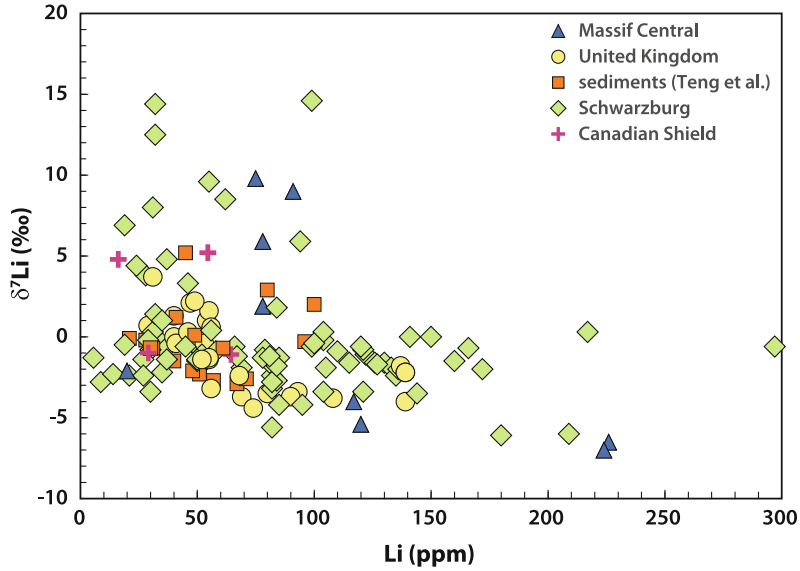

Fig. 6.7 Lithium concentration and δ^7Li of (largely) unmetamorphosed sedimentary rocks. Data sources: Canadian Shield from Millot et al. (2010c), UK from Qiu et al. (2009), Massif Central from Millot et al. (2007), Schwarzburg from Romer et al. (2014b), "other" are data from globally dispersed shales and Chinese sedimentary rock composites from Teng et al. (2004)

on overall homogeneity was clear from the data of Romer et al. (2014b) from Paleozoic shales from central Europe (δ^7Li ranged from −6.1 to +14.6 ‰, with an average of −0.1 ‰). Although the literature on sedimentary basins focuses significantly on temperature, Romer et al. (2014b) made the important observation that an equally if not more important parameter in the generation of Li isotopic signatures of clastic sedimentary rocks is the timing of dehydration in the sequence of diagenetic events. The loss of Li from exchangeable sites as opposed to structural positions in the crystal lattice is a major factor in determining the ultimate δ^7Li of the sedimentary rock, and hence the evolution of Li in subaerial versus subaqueous environments will be significant.

Using laboratory experiments, Williams and Hervig (2005) evaluated exchange and dissolution/precipitation of smectite/illite relative to Li and B isotopes at conditions relevant to the lithification of sedimentary materials (300 °C, 100 MPa). The transition to illite was accomplished by smectite dissolution and illite neocrystallization, and was accompanied by Li isotopic fractionation. They observed effects introduced by size distributions, with very fine grain size resulting in slower approach to apparent equilibrium. Their results suggested a fractionation factor at 300 °C that is ∼6 ‰ larger (i.e., illite is 6 ‰ lighter) than predicted from the empirical data (Chan et al. 1992, 1994), but consistent with theoretical estimates (Yamaji et al. 2001).

6.3.3 Lakes and Rivers: Dissolved Loads

The first publication containing Li isotopic data for river waters (Falkner et al. 1997) gave a hint at the potential for Li as a tool for understanding weathering processes. Subsequently, many studies have geochemically taken apart catchments on various scales toward this ultimate goal. One unavoidable finding from any of these studies is that the Li released during weathering is isotopically heavier than that present in the minerals of the unweathered rocks (estimated global flow-weighted average δ^7Li = +23.5 ‰; Huh et al. 1998; Fig. 6.8). It is clear that for most major rivers the bulk of the transported Li (typically >80 %) is in suspended phases rather than the dissolved load (e.g., Dellinger et al. 2015). The factors that influence how this fractionation develops are varied, and understanding how river fluxes affect marine Li hinges, in part, on more clear resolution of these factors.

In examining rivers of the world, Huh et al. (1998) found rather poor correlation between dissolved riverine Li and the major catchment lithology. It was not until the more detailed study of Huh et al. (2001) on the Orinoco River system that it became apparent that weathering outweighs lithology when assessing the isotopic composition of dissolved Li. This is good news for global paleoclimate research, in that it suggests that the sensitivity of Li isotopes to weathering intensity can be a useful proxy: rivers that drain stable, intensely weathered terranes (transport-limited) will contribute lighter Li than those that drain actively eroding terranes (reaction- or weathering-limited). This assessment was further strengthened by results from Kısakűrek et al. (2005) on a detailed study of the Ganges River system (Fig. 6.8a).

Nevertheless, with more detailed study has come evidence for greater complexity. The study of Pogge von Strandmann et al. (2010) drew no single connection between dissolved Li in rivers draining young basaltic terranes and Li isotopes (Fig. 6.8b). They indicated that the balancing role of pH, as a determinative factor in the formation of secondary minerals, dominates in some settings. In something of an all's-well-that-ends-well conclusion, Pogge von Strandmann et al. (2010) added that due to the low Li content of glacial rivers that tend not to follow the Huh et al. (2001) paradigm, these rivers are not apt to contribute significantly to the global marine Li pool, and thus the potential paleoclimate proxy probably remains viable. The restricted area of catchments such as those in Iceland also limit their global impact compared to, for instance, the Ganges, Amazon and Mackenzie.

An extensive study of Li in the Amazon system by Dellinger et al. (2015) yielded several

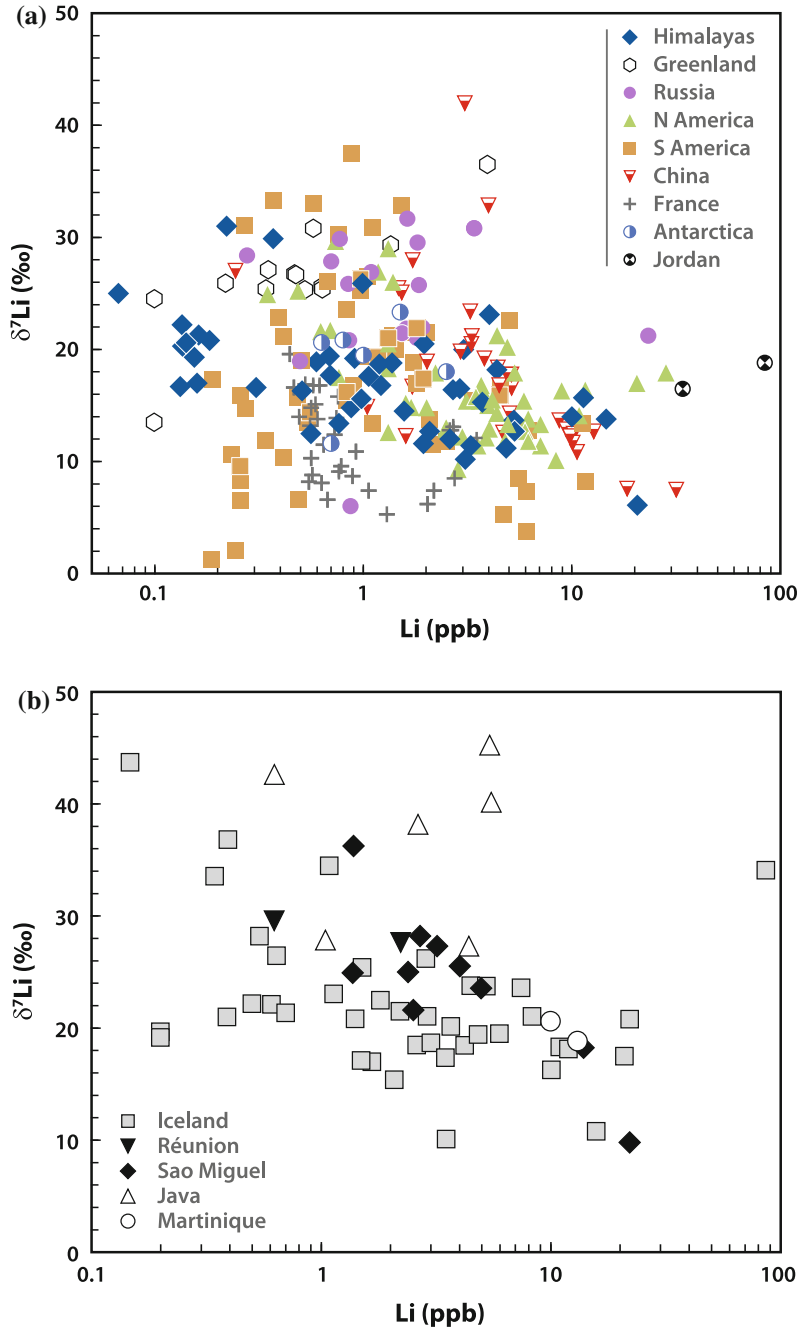

Fig. 6.8 Lithium concentration and δ^7Li of dissolved loads from rivers. **a** Rivers in continental basins. Data sources: Himalayas (including high Himalayan and Ganges-Brahmaputra) from Huh et al. (1998), Kısakürek et al. (2005), China from Huh et al. (1998), Wang et al. (2015), South America from Huh et al. (1998, 2001), Dellinger et al. (2015), North America, Russia from Huh et al. (1998), Millot et al. (2010c), Greenland from Wimpenny et al. (Wimpenny et al. 2010a, b), Antarctica from Witherow et al. (2010), France from Lemarchand et al. (2010), Négrel et al. (2010), Jordan from Chan et al. (1992). **b** Rivers in volcanic (mainly basaltic) terranes (without hydrothermal impact). Data sources: Iceland from Pogge von Strandmann et al. (2006), Vigier et al. (2009), Sao Miguel from Pogge von Strandmann et al. (2010), Java, Reunion form Henchiri et al. (2014), Martinique from Rad et al. (2013)

important conclusions concerning the control of Li in the dissolved load ultimately delivered to the oceans. They found no single relation between the δ^7Li of dissolved Li and factors such as Li flux or weathering rate, as the behavior of high relief tributaries were moderated by lower altitude floodplain processes. The relationship they instead identified indicated that the lowest δ^7Li waters were from both tributaries that record low and high weathering intensities, and hence δ^7Li could not be used independently to characterize weathering regime. Thus low δ^7Li in

paleocean sediment records interpreted to reflect periods of enhanced continental erosion becomes a non-unique solution.

Lithium isotopic variability in dissolved loads of other river systems (Vigier et al. 2009; Millot et al. 2010c; Liu et al. 2011; Wimpenny et al. 2010b; Witherow et al. 2010) have largely upheld the lack of correlation with catchment lithology first described by Huh et al. (1998). Fractionation has been primarily linked to particles: the nature and extent of precipitation of secondary minerals and/or water/particle interaction history. However, when examined closely, the Li isotopic systematics of river systems commonly show intricacy that transcends single-step interpretations. For example, Pogge von Strandmann et al. (2006) noted that the aggregate Li isotopic composition of a river (at its mouth) could not be reconstructed by a simple source dilution model, and that fractionation processes going on in the channel were essential components of the Li isotopic evolution of the water. Also, Yoon (2010) and Wang et al. (2015) showed that some mineralogical control appears to be present in catchments with significant exposed evaporite (halite, gypsum).

The average sedimentary rock δ^7Li of −0.1 ‰ is lower than the mean values for marine clastic sediments (+4.1 ‰), river bedloads (+2.9 ‰) and river suspended loads (+1.3 ‰). As pointed out previously, the Li isotopic compositions of sedimentary rocks incorporate both the variability in source material, with its particular weathering history, and the many processes that affect the sediment following deposition. As most of these processes tend to favor extraction of an isotopically heavy component, it is no surprise that these rocks have a lower mean δ^7Li.

Studies that couple Li and other stable isotopic systems have shown the capacity to clarify some of the questions generated among the purely Li isotopic studies. For example, Tipper et al. (2012) measured Mg isotopes in their re-examination of waters from the MacKenzie River system whose Li isotope systematics were originally investigated by Millot et al. (2010c). The Mg data produced the opposite trend to what was expected from theory, leading to separate, equally plausible interpretations of the geochemistry of the waters (through ternary mixing or through a Rayleigh-type fractionation process). These complications do not, however, appear to derail the potential usefulness of Li as a weathering proxy.

Pogge von Strandmann and Henderson (2015) used combined Li isotopic and U activity ratios of river waters from New Zealand to demonstrate a potential of this geochemical tandem in addressing key questions in continental erosion. Rivers in areas with rapid uplift have low δ^7Li whereas the opposite is observed for regions with slow uplift rates. Pogge von Strandmann and Henderson (2015) implied that more fresh material with primary mineralogy is exposed at high uplift rates to silicate weathering, limiting the formation of secondary mineral phases. Thus, tectonically stabilized regions would allow for saturated waters and a greater opportunity for the precipitation of isotopically light minerals. Lithium isotopes may thus provide a novel proxy for estimating the efficiency of continental weathering in CO_2 removal. Note, however, that the findings of Pogge von Strandmann and Henderson (2015) are contrary to what Huh et al. (2001) determined for rivers in the Orinoco drainage.

In a unique approach to the assessment of paleoclimate, Godfrey et al. (2013) used data from bulk fluid inclusions in lacustrine halite from an intensely arid salar in northwestern Argentina. Based on laboratory experiments Godfrey et al. determined that Li isotopic fractionation during halite crystallization was minimal. The data from two Pleistocene halite samples were up to ~10 ‰ heavier than modern waters in the salar. This difference was interpreted to be the record of wetter conditions in the region 60–90 ka. A different approach to understanding the sources of Li in evaporites from the western U.S. Great Basin (Araoka et al. 2014) involved the comparison of Li from pure water and nitric acid leaches of playa sediments. The small data set from this study did not provide a conclusive view of Li in this environment, although the authors suggested that generally light Li isotopic compositions (δ^7Li of leaches between −1.0 and +9.3 ‰) were more consistent

with hydrothermal sources rather than with Li derived from chemical weathering.

Tomascak et al. (2003) had suggested the use of sedimentary carbonate in a similar capacity for paleoclimatology. The equilibrium fractionation associated with carbonate crystallization has only been broadly studied at this point (Marriott et al. 2004a). The one aragonitic carbonate analyzed by Godfrey et al. (2013) had δ^7Li which corrected to a value similar to that predicted for the Pleistocene lake, but also consistent with those of modern regional spring waters.

6.4 Hydrothermal Systems

Geothermal systems have been targeted in several Li isotopic studies, on the continents and in the oceans. In hydrothermal systems the temperature of exchange is significant toward the specific Li concentration and isotopic outcome, as is the ratio of solid to fluid. Details have been established by many empirical and laboratory studies. The majority of these have considered the most globally relevant case of interaction between seawater and basalt, although some studies have introduced other geological complications to try to better understand Li in the shallow Earth.

6.4.1 Rocks in Sea Floor Hydrothermal Systems

If the discussion is limited to high temperature alteration (>300 °C), resultant altered sea floor rocks are typically leached of Li (Seyfried et al. 1984; Berger et al. 1988). Lithium does not show a strong tendency for incorporation in secondary minerals at these temperatures. In the absence of the crystallization of secondary minerals, the altered rocks will not be isotopically fractionated, similar to what is observed during laboratory experiments of congruent dissolution at low temperatures (Pistiner and Henderson 2003). This observation appears to be borne out in MOR basalts at Hess Deep (East Pacific Rise) which show minimal petrographic evidence for recrystallization, but which have been leached of Li; yet, they are isotopically essentially unperturbed (Brant et al. 2012). Among the natural systems that have been investigated, though, this result is rare.

One of the original foci of Li isotopic research was on the nature of Li in seafloor basalts (Chan and Edmond 1988; Chan et al. 1992). Despite this extensive history of study, it is an area that has proved slippery in arriving at a consensus (not only for Li!). Until recently, the prevailing model invoked uptake of seawater Li into neocrystallized hydrothermal minerals to explain a correlation between Li concentration and isotopic composition (Chan et al. 1992, 2002a; Fig. 5.3). The same trend is seen when sample age is compared to the Li concentration and isotopic ratio (Chan et al. 1993). This model implies equilibrium Li isotopic fractionation during sea floor recrystallization with $\alpha \sim 0.981$ at 2 °C, and $\alpha \sim 0.984$ at 80 °C. Low temperature (~80 °C) alteration of sea floor basalt has been shown to result in Li uptake by solids (Seyfried et al. 1984; Chan et al. 1994).

It is uniformly seen that the recrystallization-induced fractionation of basalt protoliths at low greenschist facies produces rocks that are isotopically lighter than the unaltered basalt. Rocks such as these, with Li concentrations and δ^7Li < MORB, are uncommon among the current catalog of seafloor drilled and dredged samples (Chan et al. 1992, 1994, 2002a), probably because subsequent, lower temperature reactions overprint the higher temperature mineralogical and chemical composition. Nevertheless, the specific fractionation that takes place is highly dependent on local conditions. For example, neocrystallized smectites at T > 200 °C were shown to not fractionate Li isotopes to a measurable degree, regardless of fluid composition (Vigier et al. 2008).

Isotopically heavy Li, derived from seawater, is incorporated in low temperature minerals, such that altered sea floor basalts have δ^7Li as high as +21 ‰ (Chan et al. 2002a). Smectite separates from altered basalts are similarly isotopically heavy (δ^7Li = +15 to +19 ‰; Chan et al. 2002a). These were bulk mineral samples, so the content of structurally-incorporated Li relative to a

sorbed fraction is unknown. Pistiner and Henderson (2003) gave a glimpse at the significance of sorption relative to crystallographic incorporation in fractionation of Li isotopes. The analysis of purified individual alteration minerals has lagged behind the analysis of bulk rock samples, suggesting that there may be more to learn here, especially as the precision of spatially-resolved analytical methods improves.

The model of Brant et al. (2012) was needed to explain data from Hess Deep basalts that did not agree with the trend established by previous investigators (Fig. 5.3). It is interesting to note that several of the ODP Hole 504B and 896A rocks fall similarly off the trend. Additionally, sheeted dike basalts at Hess Deep had δ^7Li generally higher than unaltered MORB, as opposed to previous studies where deep MOR dike rocks were mostly isotopically lighter than MORB (e.g., Chan et al. 2002a).

If their model is accurate, submarine lava flows had Li extracted by moderate-temperature fluids (50–100 °C), but the lack of recrystallization resulted in minimal Li isotopic fractionation. This is consistent with the results of Verney-Carron et al. (2015). By extrapolation to other MOR systems, Li is generally lost to discharging fluids in the hot, axial portion of the ridge and the gain of Li in MORB is almost entirely an off-axis phenomenon. This contrasts with the interpretation of Chan et al. (2002a), which viewed the axial region as a net sink for marine Li, rather than a source. Isotopic fractionation of Li seen in sheeted dike samples at Hess Deep was interpreted to reflect combinations of crystallization of low temperature alteration minerals as well as, importantly, diffusion from plagioclase.

Hydrothermal alteration of the upper mantle to produce serpentinites has been studied with Li isotopes. Decitre et al. (2002) observed widely variable Li isotopic compositions in serpentinites from dredges of the southwest Indian ridge (δ^7Li from +2.9 to +14.2 ‰ in bulk samples). In situ analyses of serpentinized minerals in the same samples yielded δ^7Li as low as −19 ‰. Serpentine muds and clasts from the Mariana forearc show bulk compositions that overlap this range (Benton et al. 2004).

The isotopically light values are consistent with bulk rock serpentinite data from Vils et al. (2009), in samples drilled from the mid-Atlantic ridge. They found samples with δ^7Li as low as −28.5 ‰. The data suggested, contrary to expectations, that Li in the serpentine was derived from oceanic basalts rather than primarily from seawater. Furthermore, the crystallography of the serpentine may exert a control on the fluid/serpentinite Li isotopic behavior of the system. In a study of laboratory synthesis products, Wunder et al. (2010) suggested that the serpentine polymorph chrysotile, with its tubular growth, does not fractionate Li isotopes as do its siblings antigorite and lizardite. Experimental fluid-mineral reactions with the latter two polymorphs show strong preference for ^{6}Li in solids, with ^{7}Li concentrated in coexisting aqueous fluids in the range 200–500 °C and crustal to shallow mantle pressures. The lack of strong fluid/serpentine isotopic fractionation when chrysotile was involved implicated Li-water complexes in nanotubes.

Contrarily, in laboratory experiments in which basalt glass and olivine crystals were weathered at nominally Earth surface conditions and with controlled fluid composition, Wimpenny et al. (2010a) generated secondary chrysotile which fractionated Li isotopes. The sense and magnitude of the fractionation was consistent with empirical results from natural serpentinites, with fluids reaching compositions ~10 ‰ heavier than coexisting chrysotile. Collectively, the results on serpentinites have implications for the marine Li cycle (Sect. 6.4) as well as for Li in subduction systems (Chap. 5).

Marine ferromanganese encrustations may be used to assess hydrothermal processes, although Li isotopic systematics in these materials appear complicated. You and Chan (1996) published the first data from ferromanganese crusts in a paper devoted to analytical technique development. A more comprehensive analysis of marine ferromanganese crusts (Chan and Hein 2007) found that, although primary Mn-oxides appear to

initially record an isotopic record of the seawater from which the minerals form, this signature is almost certain to be overprinted during subsequent re-equilibration.

Although not a robust tracer of paleoseawater Li, the data of Chan and Hein (2007) indicate that the concentration of leachable Li in Fe–Mn crusts is a strong indicator of process, with purely hydrothermally-generated precipitates yielding nearly two orders of magnitude more Li than comparable hydrogenetic/diagenetic and weakly hydrothermal encrustations. Leaching of these samples by hydrochloric acid yields isotopically lighter Li (δ^7Li as low as +8.9 ‰) than that removed by acetic acid (which has seawater-like δ^7Li ~ +31 ‰). Presumably, Li sorbed to Mn-oxides records seawater conditions, whereas isotopic fractionation takes place when incorporation into structural sites in Mn- and Fe-oxides and oxyhydroxides occurs, consistent with laboratory studies (e.g., Pistiner and Henderson 2003).

6.4.2 Fluids in Sea Floor Hydrothermal Systems

After relatively small reaction times, hydrothermal alteration releases fluids that are isotopically analogous to the rocks from which they derive much of their dissolved Li (Seyfried et al. 1998; James et al. 2003). However, the light isotope may be appreciably enriched in minerals generated at these conditions (Chan et al. 1994; Scholz et al. 2009). At lower temperature hydrothermal conditions, release and uptake of Li from/into basalts may operate concurrently.

Pristine marine vent fluids (those for which seawater incorporation is corrected) typically show restricted Li isotopic variation, δ^7Li in the range +3 to +11 ‰ (Chan et al. 1993, 1994; Foustoukos et al. 2004) and have Li concentrations >10× that of seawater (c. 180 ppb; Morozov 1968). Lithium in these fluids thus cannot have been derived entirely from either seawater (δ^7Li = + 31 ‰) or from unaltered MORB (δ^7Li = +4 ‰), implicating seafloor alteration of basalt (±sediments) as significant sources of Li in these fluids. The overall interpretations of Brant et al. (2012) are consistent with the isotopic composition of hydrothermal vent fluids as well as the products of laboratory experiments. The reactive transport model of Verney-Carron et al. (2015) appears to reproduce the relative isotopic consistency of MOR hydrothermal fluids from systems with diverse Li contents.

Significantly in the interpretation of data from such systems, the separation of vapor and brine has been examined. Several studies have indicated that vapor separation does not introduce Li isotopic fractionation (James et al. 1999; Foustoukos et al. 2004; Millot et al. 2010b), although it can introduce elemental variations that are being used in monitoring the evolution of volcanic systems (e.g., Berlo et al. 2004). Schiavi et al. (2010), however, interpreted data from Stromboli samples to require melt–fluid (vapor) isotopic fractionation. Similarly, Vlastélic et al. (2011) concluded that Li isotopic variation in Piton de la Fournaise eruptive samples stems from vapor separation. Nevertheless, it is apparent that in eruptive settings such as MOR, Li is not appreciably lost in a vapor phase, and hence not isotopically fractionated (as compiled by Brant et al. 2012).

Vent fluids in the Lau back-arc basin spreading show similar δ^7Li to MOR vent fluids (+2.9 to +7.0 ‰; Mottl et al. 2011), although with a lower mean δ^7Li value (Fig. 6.9a). Temperatures of the Lau Basin fluids are generally in the range 200–350 °C (after correction for bottom water mixing). It is possible that earlier data for MOR vent fluids (e.g., Chan et al. 1994) are on average 1–2 ‰ too high as a consequence of the lack of minor bottom water correction. Mottl et al. (2011) interpreted Li isotopic variations along strike in the Lau vent fluids to reflect increased input of sediment-derived fluid, largely on the basis of geochemical variations of other elements. This appears plausible, given the slightly higher average δ^7Li of sediment from the Tonga trench compared to marine sediments elsewhere (Bouman et al. 2004; Chan et al. 2006).

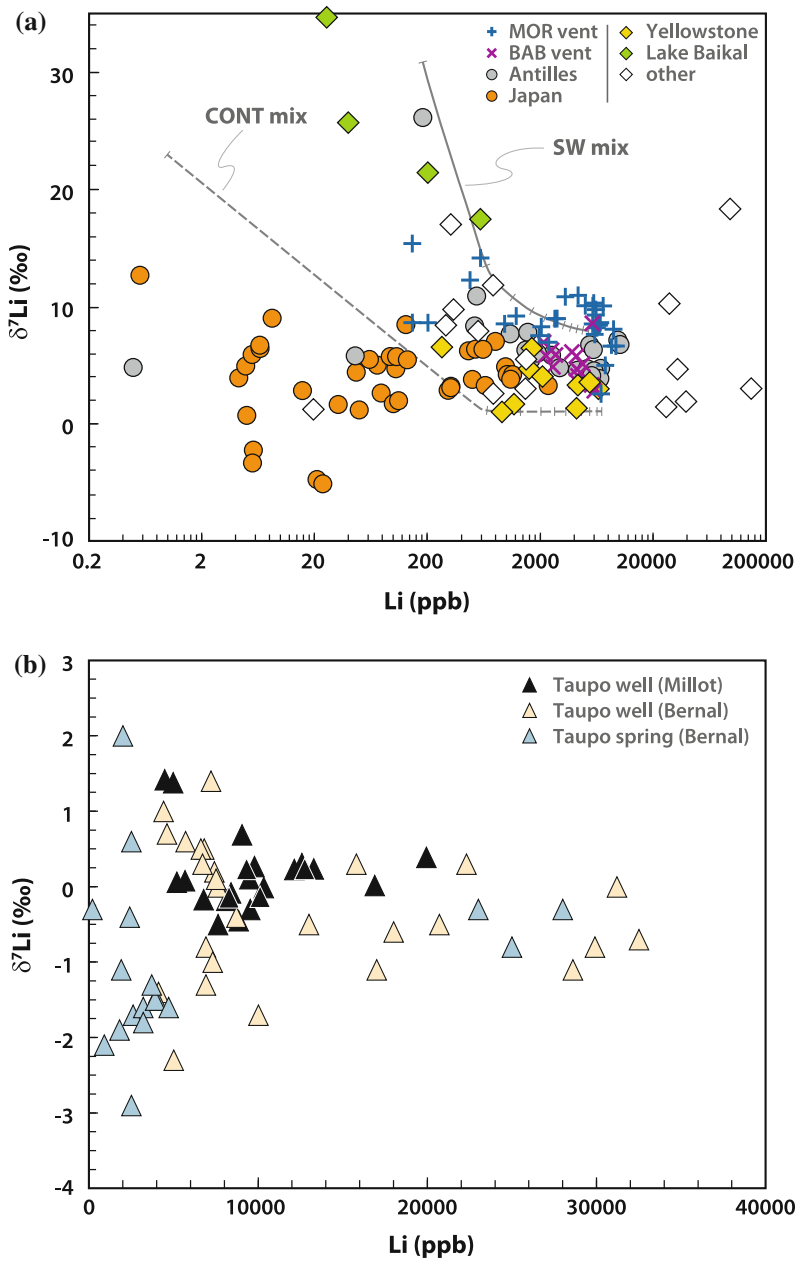

Fig. 6.9 Lithium concentration and δ^7Li of hydrothermal fluids. Model binary mixtures are between seawater (SW) and a sea floor vent source and between average river water and a source like average continental crust (CONT). **a** Data sources: MOR (Mid-ocean ridge) vents from Chan et al. (1993, 1994), Foustoukos et al. (2004), BAB (back-arc basin) vents from Millot et al. (2011), Lake Baikal from Falkner et al. (1997), Yellowstone from Sturchio and Chan (2003), Japan (Ontake volcano) from Nishio et al. (2010), Lesser Antilles from Millot et al. (2010b), Rad et al. (2013), "other" (includes data from multiple continental and ocean island localities) from Godfrey et al. (2013), Henchiri et al. (2014), Kısakűrek et al. (2005), Tomascak et al. (2003). **b** Hydrothermal fluids from springs and well at Taupo, New Zealand. Data sources: Bernal et al. (2014), Millot et al. (2012)

6.4.3 Continental Geothermal Systems

Continental geothermal systems have received comparatively less attention than their marine analogs, but generally mimic the findings from the sea floor. On the continents, however, both the composition of initial waters and the rocks through which they flow may vary far from the comparatively limited starting compositions present on the ocean floor. Hence continental hydrothermal waters show a range in chemical and isotopic compositions.

Individually, though, continental and continental margin geothermal systems show a tendency toward equilibration with respect to Li

isotopes (Fig. 6.9a). That is, Li in thermal waters from individual localities or regions shows restricted isotopic heterogeneity.

A definitive study to use Li in exploring high temperature terrestrial water-rock interaction is that of Sturchio and Chan (2003). They analyzed 11 Yellowstone geothermal springs, finding average δ^7Li of +3.7 ± 2 ‰. Altered rhyolites through which these waters flowed had generally slightly lower δ^7Li (average −0.4 ‰), which correlated strongly with Li concentration (R^2 = 0.88). They concluded that the Li isotopic budget could be explained primarily through progressive addition of Li to altered rocks with concomitant isotopic fractionation, producing isotopically heavier waters at higher water/rock ratios. One point not clear from this study was the Li isotopic signature of regional meteoric water; their calculations used a starting δ^7Li of +1 ‰ for waters, which is not constrained by measurements from the area, and perhaps not consistent with other studies.

Bullen and Kharaka (1992) presented preliminary data from several of the same Yellowstone localities, with all values some ~12 ‰ lower than those of Sturchio and Chan (2003). Given the relatively consistent offset between the two data sets, combined with the fact that the Bullen and Kharaka (1992) data are so different from any published since, it seems likely that the Sturchio and Chan (2003) data are correct and that an analytical or other laboratory issue resulted in the apparent very isotopically light water values from Bullen and Kharaka.

Two hydrothermal springs from an exclusively volcanic setting in the Azores (Pogge von Strandmann et al. 2010) were isotopically inconsistent, but the heavier value was from a cool spring (33 °C) that likely reflects greater down-temperature fractionation (δ^7Li = + 6.9 ‰, compared to +1.0 ‰ for T > 100 °C). Thermal springs from multiple sites hosted by volcanic rocks in the western U.S. (Tomascak et al. 2003) had δ^7Li ranging from +3 to +17.1 ‰. The heavier compositions measured in this study appear to reflect samples containing variable contamination of isotopically heavier lake water (δ^7Li ~ +20 ‰).

Among 23 New Zealand geothermal well waters of variable temperature (205–320 °C) reported by Millot et al. (2012), there was virtually no Li isotopic variation (δ^7Li = 0.2 ± 0.5 ‰; Fig. 6.9b). Bernal et al. (2014) also reported data from the Taupo Volcanic Zone, both thermal springs and geothermal wells, whose δ^7Li were ostensibly identical to those of Millot et al. (2012), with average δ^7Li = − 0.6 ± 1.0 ‰ (Fig. 6.9b). The minimal isotopic variation was consistent with the source waters having equilibrated with regional volcanic and/or metasedimentary rocks (global average δ^7Li = −0.1 ‰) with no significant seawater components.

A diverse group of waters in an island arc setting was investigated by Millot et al. (2010b). These included hydrothermal waters from continental wells as well as shallow sea floor vent fluids, distributed between two islands of the Antilles arc. Waters ranged from high (up to 260 °C) to moderate (as low as 90 °C) estimated reservoir temperatures. Despite substantial homogeneity of the Li isotopic compositions of waters from some of the sites (overall δ^7Li average = +6.5 ‰), the concentration data for the Bouillante springs fell along a mixing curve with seawater.

This study was particularly noteworthy in that the authors used data from laboratory seawater–basalt interaction experiments to develop a predictive model for the Li source rock isotopic composition. This required accurate estimation of the reservoir temperature and isotopic composition. The results indicated source rocks with light Li isotopic signatures (δ^7Li from about −2 to −7 ‰). Few rocks have been analyzed that extend to such low values, among them sedimentary rocks from Millot et al. (2007); their marls averaged δ^7Li = −6.3 ‰. It is also possible that the fractionation model, based on data from basalts, is not suitable for systems with sedimentary host rocks.

Interplay between hydrothermal activity on active volcanic islands and the composition of associated river waters has been documented (Rad et al. 2013; Henchiri et al. 2014). The study of three distinct volcanic islands indicated covariation between δ^7Li and Li/Na, with isotopically heavy river water generally having the

lowest elemental ratio. The river waters analyzed by Henchiri et al. (2014) that were most affected by hydrothermal sources had δ^7Li c. 10 ‰ lower than waters that had negligible hydrothermal influence. Although the Rayleigh fractionation model used by Henchiri et al. (2014) adequately explained Li isotopic–elemental relations in most data sets, it failed in the case of Iceland (Pogge von Strandmann et al. 2006; Vigier et al. 2009), which shows broadly overlapping Li isotopic compositions for rivers with both strong and weak hydrothermal impacts.

Nishio et al. (2010) have attempted to use Li in fluids from volcanic areas in Japan as a tool for understanding the connection between convergent margin fluid flow and seismicity. In a young volcano on the mainland Nishio et al. identified an isotopically light fluid component that was present in samples collected from the primary earthquake epicenters. They explained the light isotopic composition of these samples (δ^7Li as low as −5.2 ‰) as reflecting Li derived from the lower crust. Alternately, applying the reasoning of Verney-Carron et al. (2011), these low δ^7Li values might reflect diffusive exchange at moderate temperature. However, further studies by Nishio et al. (2015), applied to fluids from offshore mud volcanoes in the Nankai accretionary complex, appear to substantiate the connection between fluid flow regimes (deep versus shallow) and seismic activity.

Laboratory experiments on basalt leaching at near-surface conditions (temperature, pH) from Verney-Carron et al. (2011) may be important in future interpretation of hydrothermal fluids in some systems. Unlike experiments in which secondary minerals crystallize, saturation was not allowed to take place in the Verney-Carron et al. experiments, and isotopic fractionation between starting basalt glass and fluid enriched the latter in light and not heavy Li. The results were consistent with the greater diffusivity of ^{6}Li, and although isotopically unimportant at low temperatures, the authors suggested that in natural hydrothermal systems the diffusive fractionation needs to be considered. Indeed they re-interpreted data from Wimpenny et al. (2010a) to implicate diffusion in controlling the isotopic composition of some experimental fluids.

When marine and continental hydrothermal fluids are compared (Fig. 6.9), similar systematics, as would be expected, are clear. The major difference is likely due to isotopically lighter host rocks in the continental crust. Mixing arrays given dilution of rock-derived Li by marine or meteoric Li yield plausible fits to the observed data (Fig. 6.9a).

6.5 Marine Geochemistry of Li

The first goal of Li isotopic study in the "modern analytical era" was to use the system to better understand marine geochemistry (Chan and Edmond 1988). At that time this goal was motivated somewhat by improvements in understanding of the dynamics of Li the element in the oceans (e.g., Edmond et al. 1979; Delaney and Boyle 1986; Stoffyn-Egli and Mackenzie 1984). It is instructive to look back at what Chan and Edmond called a preliminary report of Li in the oceans and see, on the strength of a small number of what are, by modern standards, rather imprecise data, how lasting their interpretations were. Although we have advanced far in terms of application of proxies in the oceans, their 1988 study mapped out in a very compelling fashion the framework of much that would follow.

6.5.1 The Marine Li Cycle

The Li dissolved in modern seawater is isotopically heavier than the primary inputs (rivers and hydrothermal systems), which requires that sink (s) exist that preferentially remove light Li on short time scales. The seawater Li budget is controlled largely by a small number of major factors. The combination of hydrothermal systems and processes that act at lower temperatures generally exert major controls on this budget.

Based on modeling of ocean crust samples from ODP Hole 504B, Chan et al. (2002a) suggested that the upper 1.8 km of the basaltic crust

is, in bulk, a sink for marine Li, albeit a minor one. This is consistent with the experimental results of James et al. (2003). In contrast, marine sediments have been shown to be a viable Li source, liberating Li even at sub-hydrothermal temperatures (James et al. 2003).

Calculations appear to restrict the role of water–sediment interaction on the sea floor (diffusion and adsorption, collectively) to only a minor sink of marine Li (Zhang et al. 1998). It is interesting to note the correlation between the seawater Li isotopic record of Misra and Froelich (2012) with the pore water data of Zhang et al. (1998). Despite the presumably significant controls on pore water chemistry by water–sediment interaction processes, the data from ODP Site 918 reproduce the notable c. 15 Ma δ^7Li low.

The thorough treatment of river sediments by Wimpenny et al. (2010b) placed two major constraints on marine Li. Although they noted that the majority of Li export in western Greenland is in suspended and not dissolved form, the extant data indicate that only a fraction of this Li will reach the open ocean. Furthermore, their data indicate that glacial sources are minor globally (<6 % of the flux from rivers during the last glacial maximum).

Pogge von Strandmann et al. (2008) verified, in looking at estuaries, that although dissolved Li behaves conservatively in these environments (Stoffyn-Egli 1982), suspended particles may be subject to continued chemical weathering in the water column. They estimated that a significant proportion of riverine Li may fail to reach the oceans because of estuarine processes. This amount (15–25 % of the global flux) would measurably affect the river/hydrothermal budget of marine Li. The rapid decrease in Li abundance in coastal seawater from riverine input has been further demonstrated by Brunskill et al. (2003). From sampling in the Gulf of Papua over 6 years, they showed that (i) Li abundance increases with increasing salinity in dissolved loads but not in particulate matter, and (ii) as much as ~90 % of riverine Li input is deposited in shallow shelf region and on shelf slope whereas only ~10 % of Li is transported further to deep sea. Behavior of Li in low-salinity estuarine environment has been investigated by Murphy et al. (2014) for Kalix and Råne rivers in northern Sweden. The water of Bothnian Bay is isotopically akin to seawater but has much lower salinity (~3 vs. ~35 psu for seawater) and has been proposed as isotopically heavy end member to river waters with δ^7Li as low as +21.7 ‰ for low-salinity samples. A non-conservative behavior of Li in estuarine systems, involving chromatographic effects from suspended river particles may have large consequences for global Li input to oceans. Pogge von Strandmann et al. (2008) suggested that such behavior over time would result in a secular effect of the magnitude that has been measured in Cenozoic foraminifera (e.g., Hathorne and James 2006).

6.5.2 Secular Variation of Li in Seawater

6.5.2.1 Experiments and Observations

If Li isotopes can be useful proxies of, for example, continental weathering intensity, it is critical to find ways of unlocking temporal records. Early measurement of Li in three marine ferromanganese crusts gave seawater-like values (δ^7Li ~ +33.2 ‰; You and Chan 1996) for two of the samples, giving some encouragement of Li as a paleocean chemistry tool. However, rapid Li diffusion was subsequently determined to essentially nullify this use (Henderson and Burton 1999). This finding was upheld by a later investigation of globally-dispersed ferromanganese deposits (Chan and Hein 2007).

Marriott et al. (2004b) demonstrated that calcite and aragonite fractionate Li differently, both elementally and isotopically. Inorganically crystallized aragonite showed a δ^7Li offset of −12 to −11 ‰ from coexisting seawater-like fluid, whereas calcite grown the same way was offset only by −3 to −2 ‰. The Ca site in aragonite is ninefold coordinated, as opposed to a sixfold site in calcite (Reeder 1983), although Okumura and Kitano (1986) suggested that the difference between these sites is unlikely to drive this isotopic difference. They instead suggested that the interstitial incorporation of Li in calcite yields

less isotopic preference in calcite than in aragonite under equilibrium conditions.

In some cases, the applicability of these experiments to nature seems clear. For example, Sturchio and Chan (2003) analyzed travertine with δ^7Li value 11 ‰ lighter than coexisting spring water and Tomascak et al. (2003) found that spring-precipitated "carbonate" (presumably calcite) had δ^7Li approximately 2 ‰ lighter than contemporaneous lake water. Foraminifera reported by Marriott et al. (2004b) carried with them the expected ~ −3 ‰ offset relative to modern seawater; similarly, foraminifera reported by Košler et al. (2001) ranged in offset from −5 to −1 ‰. However, not all studies of foraminiferal δ^7Li report an offset from modern seawater in core-top samples. Hathorne and James (2006), Hall et al. (2005) and Misra and Froelich (2012) all report modern foraminifera with broadly seawater Li. For calcite, the offset is minor relative to the scale of marine Li isotopic variation (see below). Although kinetic effects may be responsible for the lack of consistency in the modern foraminiferal data set (i.e., crystallization rate: Marriott et al. 2004a; Gabitov et al. 2011), the effect has yet to be specifically addressed.

Vigier and Goddéris (2015) suggest that vital effects in foraminifera may play a role in generating some of the short time-span isotopic variations in the Cenozoic record of Misra and Froelich (2012). However, this has yet to be rigorously tested. Broadly speaking, Li isotopes in the carbonate skeletons of marine organisms do not appear to be dominated by the vital effects which are manifest in stable isotopic systems of biologically mediated elements, such as C and O (i.e., Duplessy et al. 1970; McConnaughey 1989), making Li a potentially sensitive tracer in foraminifera. That is not to say that Li plays no role biologically (see Sect. 6.6), but, at least in higher animals, this role is complex (Schrauzer 2002) and requires specific study.

Until recently, analytical limitations made the study of small, monospecific foraminiferal samples impossible. Advances in analytical techniques have opened up new possibilities in Li isotopic studies of foraminifera. Hoefs and Sywall (1997) used 20–100 mg of carbonate for a single analysis. Marriott et al. (2004b) needed 20 mg of foraminifera for a single sample and Košler et al. (2001) used an average of 6.8 mg per sample. The methods of You and Chan (1996), Hall et al. (2005), and Hathorne and James (2006) all used approximately 2.5 mg of foraminifera per sample. The most recent bulk foraminifera study using bulk methods was that of Misra and Froelich (2012), in which 1–2 mg of foraminifera was used per sample.

The data of Košler et al. (2001) showed no dependency on Li isotopes from variable size of foraminifera. Hathorne and James (2006) provided further support for that relationship, as well as a hint that individual foraminiferal species do not differently fractionate Li isotopes. They also demonstrated that fractionation is not influenced by seawater temperature, consistent with laboratory experiments (Marriott et al. 2004b).

Hoefs and Sywall (1997) were the first to present a large marine carbonate data set, including a total of 75 analyses of foraminifera, bivalves, carbonate oozes, and limestones. The data set, however, faces several problems that may relate to the analytical technique, the large sample size, or a combination of these. The cardinal trouble is the lack of modern seawater values for any of the modern samples that were analyzed: their modern foraminifera, for example, ranged in δ^7Li from +7 to +20 ‰, very far below the modern value. The down-core variations they saw in foraminifera and oozes were inconsistent and difficult to reconcile with the known behavior of Li in the oceans. It is possible that diagenesis could have played a role with some samples. Ullmann et al. (2013) provide evidence for effects of diagenesis on fossil belemnites (calcite), and suggest that in the case of their sample set diffusion is not an important cause of isotopic alteration. Instead the primary means of corrupting original isotopic signatures is from fractionation during recrystallization.

Although some of the foraminiferal data of Košler et al. (2001) from seafloor (core top) samples were equivalent to modern seawater, about 30 % were significantly isotopically offset (up to 20 ‰ heavier). None of the four bulk foraminiferal samples from You and Chan (1996), all from the Pleistocene, had modern

seawater Li isotopes; δ^7Li ranged from as low as +19 ‰ (c. 12 ‰ lighter than modern seawater) to as high as +42 ‰ (c. 11 ‰ heavier than modern seawater). As the Li concentration of the final, cleaned carbonate samples were within the ordinary range for marine carbonates (~1 ppm), it is clear that the results of these studies cannot be ascribed to silicate or ferromanganese contamination. However, neither of these studies focused on the interpretation of these samples, so the data are difficult to more deeply interpret.

All of the foraminifera analyzed by Hall et al. (2005), ranging from 0.4 to 44 ka, turned up modern seawater values within uncertainty, indicating a lack of glacial/interglacial Li isotopic offset. The lack of significant Li isotopic variation during the Pleistocene is consistent with the results from foraminifera samples of both Hathorne and James (2006) and Misra and Froelich (2012). The consensus is thus that, in the absence of complicating effects unrelated to the isotopic composition of the water from which the minerals grew, marine carbonates faithfully record seawater δ^7Li (Fig. 6.10).

This conclusion has been used in three studies to date to examine secular variation in marine Li isotopes. Hathorne and James (2006) analyzed foraminifera from sediments in Atlantic and Pacific cores dating back 18 Ma. The data show an increase in marine δ^7Li from a minimum around +26 ‰ at 16 Ma to the modern value by around 6 Ma. Misra and Froelich (2012) expanded the marine record back beyond the K–Pg boundary (c. 66 Ma; Kuiper et al. 2008) with foraminifera taken from seven different sites and 10 specific locations. This large data set produced an amazingly concise record which showed both correlations with and distinctions from the marine records of O, Sr, and Os isotopes. From their data it appears that during the bulk of the Cenozoic the marine δ^7Li was lower than today, reaching a nadir in the Paleocene. Significantly, there is excellent agreement between the data sets of Hathorne and James (2006) and Misra and Froelich (2012). Aside from the upturn in δ^7Li in the mid-Miocene, the major change in marine Li captured in the data of Misra and Froelich (2012) is at the K–Pg boundary, where late Cretaceous Li appears close to modern (δ^7Li ~ +31 ‰), and within ~1 Myr it drops to ~ +23 ‰. They also contend that their record documents "pulsed" change in seawater δ^7Li through the Cenozoic, although to unambiguously understand the absolute nature of the secular variation will require a more continuous data set.

Instead of foraminifera, Pogge von Strandmann et al. (2013) examined bulk shallow marine carbonate, targeting specific time–stratigraphic

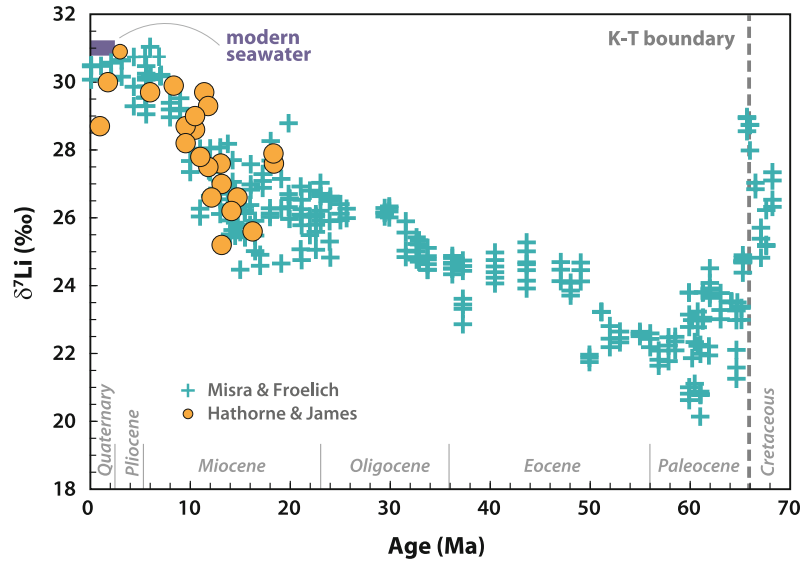

Fig. 6.10 Cenozoic marine δ^7Li records from foraminifera. Data from Misra and Froelich (2012) and Hathorne and James (2006)

horizons represented in three locations in Europe. The c. 1.2 Myr interval examined was around the Cenomanian–Turonian boundary (c. 93.5 Ma) and recorded δ^7Li variation from c. +7 to c. +30 ‰. In all of these sections the onset of oceanic anoxia ("Ocean Anoxic Event 2") appears to be marked by a rapid and enormous decrease in marine δ^7Li (by 10–20 ‰). Coupled with other data, Pogge von Strandmann et al. (2013) interpreted this drop in δ^7Li to reflect the weathering of subaerially exposed basaltic terranes that were generated globally just prior to the onset of anoxia. Presuming these sediments retained their original Li isotopic signatures, the large Li isotopic variations over a geologically short period of time requires that the marine residence time has changed over time from its current value of c. 1 Myr (Stoffyn-Egli and Mackenzie 1984), owing to reorganization of the hydrologic cycle.

Laboratory studies of Li incorporation in inorganic carbonate precipitates have been conducted. Some caution was indicated by the results of Gabitov et al. (2011). Although their laboratory-grown marine aragonite showed bulk solid–fluid offsets similar to those measured by Marriott et al. (−7.7 to −10.5 ‰), they found substantial variation in δ^7Li within individual parts of the texturally-heterogeneous aragonite matrix. However, these all overlapped within 2σ uncertainty.

It is unclear why some studies of modern marine carbonates report values inconsistent with contemporaneous seawater. The effects of diagenesis and diffusion of Li in a sediment pore network are concerns in dealing with sub-sea floor materials. Misra and Froelich (2012) provided a convincing argument that their samples were not influenced in such ways. Same-age samples taken from cores from different regions of the oceans and those representing a range in water depth returned identical data within uncertainty, effectively ruling out diagenetic control of Li signatures. Also, analysis of coexisting pore waters showed no co-variation of δ^7Li values with the foraminifera, as would be the case if Li diffusion through the sediment column was significant. In general, the consistency in Li isotopes in sediments from different same-age sites (that have certainly experienced distinct post-depositional histories) provides confidence that the role of diagenesis is minimized (Hathorne and James 2006; Pogge von Strandmann et al. 2013).

Even in the methods that permit analysis of relatively small bulk samples, there are concerns about micro-scale complications that may go unseen by these techniques. As a result, in situ analytical methods present many benefits. Although the generally low Li concentration in marine carbonate presents challenges to high precision measurement of these materials, as we have seen, the scale of natural variability may be so great as to tolerate even rather low precision.

The first study to use such techniques on foraminifera was that by Vigier et al. (2007). Their study showed the importance of the rigorous cleaning of foraminiferal tests to eliminate materials included during shell growth with spurious Li isotopic characteristics. The authors suggested that such contamination was not present in the coral samples they evaluated. To that end, Rollion-Bard et al. (2009) measured Li isotopes in various corals (natural and laboratory-cultured) to better understand the intricacies of Li in the skeletal components of these animals. From their results combined with earlier coral analyses (Marriott et al. 2004b) a few conclusions could be made. First, it appears that, unlike B isotopes, there is no significant internal difference in Li isotopes relative to the morphology of the skeletal element (dense zones versus fibrous). Second, among the small number of species examined, there was an apparent offset in δ^7Li between those inhabiting deep water and those living in shallow water, in this case approximately 3 ‰. Marriott et al. (2004a) noted a c. 2 ‰ difference in the two species of shallow water coral analyzed.

Vigier et al. (2015) applied the in situ analytical approach to a series of cultured foraminiferal tests (genus *Amphistegina*). Their experiments looked to deconvolve effects of variable seawater temperature, pH, and dissolved inorganic carbon (DIC) on both Li isotopes and Li/Ca. The major finding that samples cultured in

high DIC water carry elevated δ^7Li permits determination of secular variation of DIC. When applied to late Quaternary bulk core-top samples from Hall et al. (2005) the initial set of experimental results, conducted over five different DIC concentrations, when coupled with ice core pCO_2 data, produced pH variations that were within uncertainty of those calculated over the same time period from other geochemical proxies.

6.5.2.2 Interpretation and Modeling

Substantial sets of secular marine Li data (e.g., Misra and Froelich 2012; Hathorne and James 2006) have provided the basis for a new surge in interpretive studies, as the community grapples with the meaning of seawater Li isotopic change over time. Lithium isotopes have the major advantage over the radiogenic Sr isotope system in that silicates dominate the budget for Li, whereas both silicates and carbonate contribute importantly to the Sr that is liberated during continental weathering. Since continental weathering is tied to atmospheric CO_2, understanding marine Li should, in principle, strengthen the understanding of the carbon cycle. The extent to which this can be applied quantitatively has been the subject of significant ongoing scrutiny, as models are constructed with varying intrinsic assumptions.

The model of Li and West (2014) explained marine Li variation like Misra and Froelich (2012) by balancing changes in the deep sea sinks and their inherent fractionation signatures with changes in river water Li isotopes. They suggested the mean global δ^7Li of rivers at c. 60 Ma may have been as low as +13 ‰, consistent with the modeling of Wanner et al. (2014). Misra and Froelich (2012) and Froelich and Misra (2014) suggested that this value could have been as low as +3 ‰ heading into the Paleocene–Eocene thermal maximum, arguing for a predominance of congruent weathering.

Vigier and Goddéris (2015) argued that the secular variation in marine Li isotopes does not require the δ^7Li of rivers to change. Although secondary minerals fractionate Li isotopes during weathering reactions, Vigier and Goddéris preferred the Li isotopic composition of seawater to rely more on the change in the Li flux from continental weathering, ultimately dictated by the variable rate of soil formation (i.e., their model matched the Misra and Froelich marine Li curve with a decrease of river δ^7Li through the Cenozoic). Their calculations presumed the modern dominance of Li in suspended particles over dissolved load in rivers to have persisted through time.

The Vigier and Goddéris (2015) model is unlike that of Wanner et al. (2014) in that it took a broader view of weathering as a continent-scale process. Vigier and Goddéris (2015) substantiated the interpretation that globally thick soil accumulations around 60 Ma argue against low seawater δ^7Li at that time, as suggested by Misra and Froelich (2012). The Vigier and Goddéris (2015) model was the first to explicitly link marine Li isotopic variations to carbon cycle change, which appears to afford it an advantage in terms of constraining variables in the series of calculations involved.

None of the modeling studies independently shed light on the question of causation: models attempt to calculate fluxes that satisfy measured isotopic proxy results, but do not specify the driver (atmospheric temperature, tectonics, hydrology, etc.). Clearly this is an area of rapid evolution which will benefit significantly from future empirical studies which add to the set of high quality and high resolution Li isotopic data from the oceans over time. Although the utility of Li isotopic data in examining paleoclimate questions appears strong, the exact shape of its application continues to be sketched out.

6.6 Biological and Anthropogenic Li Isotopic Fractionation

6.6.1 Lithium in Plants and Animals

Kabata-Pendias (2011) lists the ranges in Li abundances for many plant families worldwide in order to link them with specific lithological substrate and to assess more useful information on individual families. These ranges are, in many cases, quite large (from tens of ppb to tens ppm

dry weight). It is clear, however, that some plants may accumulate Li when grown in arid areas. Although there is some information available on Li abundances in specific materials (e.g., leaves, needles, etc.; Wu et al. 1997; Sucharová and Suchara 2006), there are few studies of the toxicity of Li to plants when supplied in overabundance (e.g., Naranjo et al. 2003; Kalinowska et al. 2013).

Lithium isotopic studies of vegetation materials are, expectedly, even more limited in number and the extent. It may come to pass that Li isotopes could enable a better understanding of the transfer of water from the soil environment to plant tissues, as Li is mobile in aqueous solutions and its isotopes may respond differentially to changing chemical–physical conditions, but this has yet to be realized empirically. Lemarchand et al. (2010) found rather limited variations in both Li contents (7.3–154 μmol/kg) and isotopic compositions (< –4.3 ‰) for spruce needles, branches, and roots. The Li abundance in plant tissues was about three orders of magnitude lower than soils the spruce grows on. The individual δ^7Li values did not vary greatly between above ground (needles, branches) and below ground (roots) biomass, and were in the range of soil solutions. Thus, biological uptake from soil solutions may have little effect on the isotopic balance of Li. Nevertheless, Schmitt et al. (2012) pointed out the potential utility of combined studies of Li isotopes with other biologically-sensitive stable isotopic systems (Mg, Ca) in studies of the dynamics of dissolved components in soils.

The findings of Lemarchand et al. (2010) were confirmed by the pilot study of Myška et al. (2011), who analyzed Li contents and isotopic compositions in spruce (roots, stem wood, young needles, old needles) and beech (roots, stem wood), as well as in the underlying soils (>5 ppm; δ^7Li < −2 ‰). Sub-ppm Li abundances (0.07–0.44 ppm) were found for all tree components but large δ^7Li variations were discovered (−5 to +13 ‰), in particular for spruce. However, further work is required to constrain the key variables that produce this range: taxonomy, properties of the wood, source lithology, climate conditions, or other parameters.

It has long been known that Li is a non-essential element for the human body. In fact, it may be quite toxic when administered in larger doses (Aral and Vecchio-Sadus 2008). Alexander et al. (1982) supplied artificially ^{6}Li- and ^{7}Li-enriched lithium to mice and noted substantially deteriorated behavior as well as increased lethality for ^{6}Li-enriched dosing. These results were also stressed by tests applying acute overdosing with ^{6}Li- or ^{7}Li-enriched substances that, again, resulted in dramatically different biological response for the two respective isotopes. Conversely, unchanged motor properties and recovery to full health were superior for ^{7}Li-doped mice. These effects may perhaps result from different ionic radii and masses of the respective isotopes during transfer through the living body, and perhaps higher efficacy of ^{6}Li uptake by erythrocytes via membrane transport (Hughes and Birch 1992). Stoll et al. (2001) also found that for longer treatment periods, more serious malfunctions of the kidney system follow dosing with ^{6}Li-rich substances, and that ^{7}Li is more benign in this respect. However, the enhanced toxicity of ^{6}Li compared to ^{7}Li is accompanied by somewhat better therapeutic effects. Clearly, carefully controlled medical experiments could provide important information on the mobility and isotopic fractionation of Li in the human body. Such experiments may serve to improve our knowledge of the effects of dosing Li to patients suffering from manic-depressive illness (also known as bipolar disorder) as well as the consequences of long-term treatment and its withdrawal.

The indications that Li is not a biologically mediated element do not necessarily spell an end to the chapter of Li and biology. Vigier et al. (2015) suggest, based on data from foraminifera, that biological calcification is accompanied by a fractionation distinct from purely inorganic crystallization. This fractionation, which favors ^{7}Li incorporation in shell calcite, may relate to the kinetics of the biochemical reaction. In a somewhat less direct approach, Pogge von

Strandmann et al. (2010) made the astute observation that dissolved Li in river water relates (in principle, at least) to weathering intensity. Since biomass has a potentially significant role in mineral breakdown in soils, biological activity may indeed help establish the link to Li isotopes in studies of weathering.

6.6.2 Tracer Applications in Water Treatment and Agriculture

The use of Li isotopes as tracers in both surface and groundwater studies has only begun to show promise, which seems counterintuitive, given the significant potential for the development of isotopically distinct, traceable reservoirs in these settings. The study of Qi et al. (1997) showed massive (c. 400 ‰) isotopic shifts present in certain anthropogenically-manufactured materials. That materials can become highly isotopically enriched has been demonstrated by the generation of percent-level fractionation by ion exchange chromatography (Taylor and Urey 1938; Oi et al. 1991). Indeed, one of the banes of Li isotopic analysis is the very fact that ~100 % yield must be assured in the ion exchange process in order for isotopic measurements to be meaningful (see Chap. 2). Tiny fractions of such isotopically anomalous Li would be easily traceable signals of specific pollutants surface and ground waters.

Some studies have begun to use Li as an environmental tracer, though, and to useful effect. The best example to date comes from a study of waters from a peat bog from southern France, where Négrel et al. (2010) found anomalous δ^7Li in groundwater samples that were best explained by mixing between normal aquifer Li and isotopically heavy-enriched Li deriving from fertilizer. The analyses of soil amendments in this study showed substances with δ^7Li as high as +215 ‰, whereas the predicted end member composition generating the isotopically anomalous water had δ^7Li of at least +1250 ‰ (i.e., with absolute ^{7}Li/^{6}Li ratio more than twice that of the L-SVEC standard!). Waste water analyzed by Wang et al. (2015) was not extraordinarily isotopically heavy (δ^7Li = +40.8 ‰), but permitted the determination that some parts of the Changjiang River system had significant (c. 15 %) anthropogenic contributions. The results of Kısakűrek et al. (2005) also hinted at an anthropogenic component in some Tibetan river waters that bore anomalously, if not definitively, heavy isotope signatures, but this hypothesis was not carried further in their study.

Another tactic for the use of Li isotopes in environmental studies draws its basis in the work of Fritz and Whitworth (1994), who suggested that membrane filtration would yield significant isotopic effects. These effects would certainly apply to anthropogenic filtration, but perhaps also to fluid movement through impermeable sediments in nature. Kloppmann et al. (2008a) found that during the desalination process of seawater and brackish water, (i) Li abundance decreased by up to four orders of magnitude from ~180 ppb down to 0.01 ppb, and (ii) measurable Li isotopic effects were imparted due to lower retardation of ^{6}Li in the reverse osmosis membranes, with δ^7Li values lower by 12 ‰ in stages of desalination associated with decreased pH. It was also stressed that the extent and direction of Li isotopic fractionation may hinge on membrane type and operating conditions (Kloppmann et al. 2008a).

The impact on water quality of wastewater injection has been evaluated by Kloppmann et al. (2008b), who tested blending of wastewater recharge into natural aquifers under controlled conditions. Whilst there was no significant effect on both Li concentration and Li isotopic composition in the injection–recharge zone, apart from minor fractionation associated with clay mineral precipitation, significant mixing takes place with brackish aquifer water loads from a wider area of the test site. Further experimental work by Kloppmann et al. (2009) revealed a steady-state decrease in Li contents, likely due to sorption paralleled by decrease in δ^7Li. Thus, a sink for heavy Li must exist within the aquifer. Kloppmann et al. (2009) suggest that Li becomes a non-conservative monitor in these dynamic regimes. Water management becomes an

increasingly important topic with time considering decreased availability of drinking water in many populated areas, and hence Li isotopic applications in this field may play a more significant role in the future.

6.6.3 Nuclear Forensics

One goal of nuclear forensics is to identify nuclear material through isotopic and elemental properties in parallel with chemical and physical characteristics. In the past, Li was used extensively in certain nuclear facilities owing to the fact that ^{6}Li has a very high cross section for thermal neutrons ($\sim$940 barn; the barn is generally considered as the probability of a neutron collision with the target nucleus, and is defined as 10^{-28} m^2, roughly corresponding to cross-section area of a uranium nucleus). Contrary to this, ^{7}Li has very small thermal neutron cross section ($\sim$0.045 barn) and hence is of little use in the nuclear industry. These bifurcated properties combined with the predominance of ^{7}Li in nature resulted in vast amounts of ^{7}Li-enriched residues after the isolation of the sought-after ^{6}Li. Such volumes of non-natural Li materials were then commercially distributed for laboratory and industrial use. No records of which we are aware exist to estimate how much of these materials was distributed or to where these volumes ultimately went. That such materials were distributed, however, is not in doubt (e.g., Qi et al. 1997).

The light isotope ^{6}Li was also used as a fusion fuel in the form of lithium deuteride in order to boost thermonuclear reaction yields because ^{6}Li can produce tritium. Although ^{7}Li has somewhat different physical properties, it may breed ^{6}Li through an (n,2n) reaction which is quite effective. Such secondary ^{6}Li then produces further tritium and thus, the yields of tritium, fusion and fission efficiency increase significantly.

To our knowledge, no tests of the effect of nuclear blasts on the Li isotopic compositions have been made so far. Preliminary data from Alamogordo (Magna and Simonetti, unpublished data 2013) show no distinctive ^{7}Li/^{6}Li ratios between near-ground zero samples and those collected radially away from ground zero (from 48 to >74 m), whereas distance and ^{152}Eu activities were effectively anti-correlated (Bellucci et al. 2013). It may well be that the time for implementing the Li isotopic anomalies was too short, or that neutron consumption by the reactions was too large to induce measurable variations, or that the samples did not contain a large enough fraction of materials from the detonating device. Further analyses of trinitite glass, considered as remnants of the blast tower and the bomb itself, are warranted.

References

Alexander GJ, Lieberman KW, Okamoto M, Stokes PE, Triana E (1982) Lithium toxicology: effect of isotopic composition on lethality and behavior. Pharmacol Biochem Behavior 16:801–804

Aral H, Vecchio-Sadus A (2008) Toxicity of lithium to humans and the environment–a literature review. Ecotoxicol Environ Safety 70:349–356

Araoka D, Kawahata H, Takagi T, Watanabe Y, Nishimura K, Nishio Y (2014) Lithium and strontium isotopic systematics in playas in Nevada, USA: constraints on the origin of lithium. Miner Deposita 49:371–379

Bellucci JJ, Simonetti A, Wallace C, Koeman EC, Burns PC (2013) Isotopic fingerprinting of the World's first nuclear device using post-detonation materials. Anal Chem 85:4195–4198

Benton LD, Ryan JG, Savov IP (2004) Lithium abundance and isotope systematics of forearc serpentinites, Conical Seamount, Mariana forearc: insights into the mechanics of slab-mantle exchange during subduction. Geochem Geophys Geosys 5, paper number Q08J12. doi:10.1029/2004GC000708

Berger G, Schott J, Guy C (1988) Behavior of lithium, rubidium, and cesium during basalt glass and olivine dissolution and chlorite, smectite and zeolite precipitation from seawater: experimental investigations and modeling between 50 and 300 °C. Chem Geol 71:297–312

Berlo K, Blundy J, Turner S, Cashman K, Hawkesworth C, Black S (2004) Geochemical precursors to volcanic activity at Mount St. Helens, USA. Science 306:1167–1169

Bernal NF, Gleeson SA, Dean AS, Liu XM, Hoskin P (2014) The source of halogens in geothermal fluids from the Taupo Volcanic Zone, North Island, New Zealand. Geochim Cosmochim Acta 126:265–283

Boschetti T, Etiope G, Pennisi M, Millot R, Toscani L (2013) Boron, lithium and methane isotope composition of hyperalkaline waters (Northern Apennines, Italy): terrestrial serpentinization or mixing with brine? Appl Geochem 32:17–25

Bottomley DJ, Katz A, Chan LH, Starinsky A, Douglas M, Clark ID, Raven KG (1999) The origin and evolution of Canadian Shield brines: evaporation or freezing of seawater? New lithium isotope and geochemical evidence from the Slave craton. Chem Geol 155:295–320

Bottomley DJ, Chan LH, Katz A, Starinsky A, Clark ID (2003) Lithium isotope geochemistry and origin of Canadian Shield brines. Groundwater 41:847–856

Bouman C, Elliott T, Vroon PZ (2004) Lithium inputs to subduction zones. Chem Geol 212:59–79

Brant C, Coogan LA, Gillis KM, Seyfried WE, Pester NJ, Spence J (2012) Lithium and Li-isotopes in young altered upper oceanic crust from the East Pacific Rise. Geochim Cosmochim Acta 96:272–293

Brunskill GJ, Zagorskis I, Pfitzner J (2003) Geochemical mass balance for lithium, boron, and strontium in the Gulf of Papua New Guinea (Project TROPICS). Geochim Cosmochim Acta 67:3365–3383

Bullen TD, Kharaka YK (1992) Isotopic composition of Sr, Nd, and Li in thermal waters from the Norris-Mammoth corridor, Yellowstone National Park and surrounding region. In: Kharaka YK, Maest AS (eds) Water-Rock interaction, proceedings of the seventh international symposium on water-rock interaction. Balkema Publishers, Rotterdam, pp 897–901

Chan LH, Edmond JM (1988) Variation of lithium isotope composition in the marine environment: a preliminary report. Geochim Cosmochim Acta 52:1711–1717

Chan LH, Hein JR (2007) Lithium contents and isotopic compositions of ferromanganese deposits from the global ocean. Deep-Sea Res II, Top Stud Oceanogr 54:1147–1162

Chan LH, Kastner M (2000) Lithium isotopic compositions of pore fluids and sediments in the Costa Rica subduction zone: implications for fluid processes and sediment contribution to the arc volcanoes. Earth Planet Sci Lett 183:275–290

Chan LH, Alt JC, Teagle DAH (2002a) Lithium and lithium isotope profiles through the upper oceanic crust: as study of seawater-basalt exchange at ODP Sites 504B and 896A. Earth Planet Sci Lett 201:187–201

Chan LH, Edmond JM, Thompson G (1993) A lithium isotope study of hot springs and metabasalts from mid-ocean ridge hydrothermal systems. J Geophys Res 98:9653–9659

Chan LH, Leeman WP, Plank T (2006) Lithium isotopic composition of marine sediments. Geochem Geophys Geosys 7, paper number Q06005. doi:10.1029/2005GC001202

Chan LH, Starinsky A, Katz A (2002b) The behavior of lithium and its isotopes in oilfield brines: evidence from the Heletz-Kokhav field, Israel. Geochim Cosmochim Acta 66:615–623

Chan LH, Edmond JM, Thompson G, Gillis K (1992) Lithium isotopic composition of submarine basalts: implications for the lithium cycle in the oceans. Earth Planet Sci Lett 108:151–160

Chan LH, Gieskes JM, You CF, Edmond JM (1994) Lithium isotope geochemistry of sediments and hydrothermal fluids of the Guaymas Basin, Gulf of California. Geochim Cosmochim Acta 58:4443–4454

Decitre S, Buatier M, James R (2004) Li and Li isotopic composition of hydrothermally altered sediments at Middle Valley, Juan De Fuca. Chem Geol 211:363–373

Decitre S, Deloule E, Reisberg L, James R, Agrinier P, Mével C (2002) Behavior of lithium and its isotopes during serpentinization of oceanic peridotites. Geochem Geophys Geosys 3. doi:10.1029/2001GC000178

Delaney ML, Boyle EA (1986) Lithium in foraminiferal shells: implications for high-temperature hydrothermal circulation fluxes and oceanic crustal generation rates. Earth Planet Sci Lett 80:91–105

Dellinger M, Gaillardet J, Bouchez J, Calmels D, Galy V, Hilton RG, Louvat P, France-Lanord C (2014) Lithium isotopes in large rivers reveal the cannibalistic nature of modern continental weathering and erosion. Earth Planet Sci Lett 401:359–372

Dellinger M, Gaillardet J, Bouchez J, Calmels D, Louvat P, Dosseto A, Gorge C, Alanoca L, Maurice L (2015) Riverine Li isotope fractionation in the Amazon River basin controlled by the weathering regimes. Geochim Cosmochim Acta 164:71–93

Dosseto A, Vigier N, Joannes-Boyau R, Moffat I, Singh T, Srivastava P (2015) Rapid response of silicate weathering rates to climate change in the Himalaya. Geochem Persp Lett 1:10–19

Duplessy JC, Lalou C, Vinot AC (1970) Differential isotopic fractionation in benthic foraminifera and paleotemperatures re-assessed. Science 168:250–251

Edmond JM, Measures C, McDuff RE, Chan LH, Collier R, Grant B, Gordon LI, Corliss JB (1979) Ridge crest hydrothermal activity and the balances of the major and minor elements in the ocean: the Galapagos data. Earth Planet Sci Lett 46:1–18

Falkner KK, Church M, Measures CI, LeBaron G, Thouron D, Jeandel C, Stordal MC, Gill GA, Mortlock R, Froelich P, Chan LH (1997) Minor and trace element chemistry of Lake Baikal, its tributaries, and surrounding hot springs. Limnol Oceanogr 42:329–345

Fairén AG, Losa-Adams E, Gil-Lozano C, Gago-Duport L, Uceda ER, Squyres SW, Rodríguez JAP, Davila AF, McKay CP (2015) Tracking the weathering of basalts on Mars using lithium isotope fractionation models. Geochem Geophys Geosys 16. doi:10.1002/2015GC005748

Fournier RO, Rowe JJ (1966) Estimation of underground temperatures from the silica content of water from hot springs and wet-steam wells. Am J Sci 264:685–697

Fournier RO, Potter RW (1979) Magnesium correction to the Na–K–Ca chemical geothermometer. Geochim Cosmochim Acta 43:1543–1550

Foustoukos DI, James RH, Berndt ME, Seyfried WE Jr (2004) Lithium isotopic systematics of hydrothermal vent fluids at the Main Endeavour Field. Northern Juan de Fuca Ridge. Chem Geol 212:17–26

Fritz SJ, Whitworth TM (1994) Hyperfiltration-induced fractionation of lithium isotopes: ramifications relating to the representativeness of aquifer sampling. Water Resour Res 30:225–235

Froelich PN, Misra S (2014) Was the late Paleocene-early Eocene hot because Earth was flat? An ocean lithium isotope view of mountain building, continental weathering, carbon dioxide, and Earth's Cenozoic climate. Oceanog 27:36–49

Gabitov RI, Schmitt AK, Rosner M, McKeegan KD, Gaetani GA, Cohen AL, Watson EB, Harrison TM (2011) In situ δ^7Li, Li/Ca, and Mg/Ca analyses of synthetic aragonites. Geochem Geophys Geosyst 12, paper number Q03001. doi:10.1029/2010GC003322

Godfrey LV, Chan LH, Alonso RN, Lowenstein TK, McDonough WF, Houston J, Li J, Bobst A, Jordan TE (2013) The role of climate in the accumulation of lithium-rich brine in the Central Andes. Appl Geochem 38:92–102

Hall JM, Chan LH, McDonough WF, Turekian KK (2005) Determination of the lithium isotopic composition of planktonic foraminifera and its application as a paleo-seawater proxy. Marine Geol 217:255–265

Hathorne EC, James RH (2006) Temporal record of lithium in seawater: a tracer for silicate weathering? Earth Planet Sci Lett 246:393–406

Helgeson HC, Delany JM, Nesbitt HW, Bird DK (1978) Summary and critique of the thermodynamic properties of rock-forming minerals. Am J Sci 278A:1–220

Henchiri S, Clergue C, Dellinger M, Gaillardet J, Louvat P, Bouchez J (2014) The influence of hydrothermal activity on the Li isotopic signature of rivers draining volcanic areas. Procedia Earth Planet Sci 10:223–230

Henderson GM, Burton KW (1999) Using (^{234}U/^{238}U) to assess diffusion rates of isotopic tracers in Mn crusts. Earth Planet Sci Lett 170:169–179

Hoefs J, Sywall M (1997) Lithium isotope compositions of quaternary and tertiary biogene carbonates and a global lithium isotope balance. Geochim Cosmochim Acta 61:2679–2690

Hogan JF, Blum JD (2003) Boron and lithium isotopes as groundwater tracers: a study at the Fresh Kills Landfill, Staten Island, New York, USA. Appl Geochem 18:615–627

Hughes MS, Birch NJ (1992) Isotopic differences in the lithium transport rate in human erythrocytes during simultaneous incubations with the stable isotopes Li-6 and Li-7. Comptes Rendus de l'Académie des Sciences III - Life Sci 314:153–158

Huh Y, Chan LH and Chadwick OA (2004) Behavior of lithium and its isotopes during weathering of Hawaiian basalt. Geochem Geophys Geosyst 5. paper number Q09002. doi:10.1029/2004GC000729

Huh Y, Chan LH, Edmond JM (2001) Lithium isotopes as a probe of weathering processes: Orinoco River. Earth Planet Sci Lett 194:189–199

Huh Y, Chan LH, Zhang L, Edmond JM (1998) Lithium and its isotopes in major world rivers: implications for weathering and the oceanic budget. Geochim Cosmochim Acta 62:2039–2051

James RH, Palmer MR (2000) Marine geochemical cycles of the alkali elements and boron: the role of sediments. Geochim Cosmochim Acta 64:3111–3122

James RH, Rudnicki MD, Palmer MR (1999) The alkali element and boron geochemistry of the Escanaba Trough sediment-hosted hydrothermal system: the role of sediments. Earth Planet Sci Lett 171:157–169

James RH, Allen DE, Seyfried WE Jr (2003) An experimental study of alteration of oceanic crust and terrigenous sediments at moderate temperatures (51 to 350 °C): Insights as to chemical processes in near-shore ridge-flank hydrothermal systems. Geochim Cosmochim Acta 67:681–691

Kabata-Pendias A (2011) Trace elements in solis and plants, 4th edn. CRC Press, Boca Raton. 520 p

Kalinowska M, Hawrylak-Nowak B, Szymanska M (2013) The influence of two lithium forms on the growth, l-Ascorbic acid content and lithium accumulation in lettuce plants. Biol Trace Element Res 152:251–257

Kısakürek B, Widdowson M, James RH (2004) Behaviour of Li isotopes during continental weathering: the Bidar laterite profile, India. Chem Geol 212:27–44

Kısakűrek B, James RH, Harris NBW (2005) Li and δ^7Li in Himalayan rivers: proxies for silicate weathering? Earth Planet Sci Lett 237:387–401

Kloppmann W, Van Houtte E, Picot G, Vandenbohede A, Lebbe L, Guerrot C, Millot R, Gaus I, Wintgens T (2008a) Monitoring reverse osmosis treated wastewater recharge into a coastal aquifer by environmental isotopes (B, Li, O, H). Env Sci Tech 42:8759–8765

Kloppmann W, Vengosh A, Guerrot C, Millot R, Pankratov I (2008b) Isotope and ion selectivity in reverse osmosis desalination: geochemical tracers for man-made freshwater. Env Sci Tech 42:4723–4731

Kloppmann W, Chikurel H, Picot G, Guttman J, Pettani M, Aharoni A, Guerrot C, Millot R, Gaus I, Wintgens T (2009) B and Li isotopes as intrinsic tracers for injection tests in aquifer storage and recovery systems. App Geochem 24:1214–1223

Košler J, Kučera M, Sylvester P (2001) Precise measurement of Li isotopes in planktonic foraminiferal tests by quadrupole ICPMS. Chem Geol 181:169–179

Kuiper KF, Deino A, Hilgen FJ, Krijgsman W, Renne PR, Wijbrans JR (2008) Synchronizing rock clocks of Earth history. Science 320:500–504

Lemarchand E, Chabaux F, Vigier N, Millot R, Pierret M-C (2010) Lithium isotope systematics in a forested granitic catchment (Strengbach, Vosges Mountains, France). Geochim Cosmochim Acta 74:4612–4628

Li G, West AJ (2014) Evolution of Cenozoic seawater lithium isotopes: Coupling of global denudation regime and shifting seawater sinks. Earth Planet Sci Lett 401:284–293

Liu XM, Rudnick RL (2011) Constraints on continental crustal mass loss via chemical weathering using lithium and its isotopes. Proc Nat Acad Sci U.S.A. 108:20873–20880.

Liu XM, Rudnick RL, McDonough WF, Cummings, ML (2013) Influence of chemical weathering on the composition of the continental crust: Insights from Li and Nd isotopes in bauxite profiles developed on Columbia River Basalts. Geochimica et Cosmochimica Acta 115:73–90

Macpherson GL, Capo RC, Stewart BW, Phan TT, Schroeder K, Hammack RW (2015) Temperature-dependent Li isotope ratios in Appalachian Plateau and Gulf Coast Sedimentary Basin saline water. Geofluids 14:419-429

Marriott CS, Henderson GM, Crompton R, Staubwasser M, Shaw S (2004a) Effect of mineralogy, temperature, and salinity on Li/Ca and Li isotopic composition of calcium carbonate. Chem Geol 212:5–15

Marriott CS, Henderson GM, Belshaw NS, Tudhope AW (2004b) Temperature dependence of δ^7Li, δ^{44}Ca and Li/Ca incorporation into calcium carbonate. Earth Planet Sci Lett 222:615–624

McConnaughey T (1989) ^{13}C and ^{18}O isotopic disequilibrium in biological carbonates: I. Patterns. Geochim Cosmochim Acta 53:151–162

Meredith K, Moriguti T, Tomascak P, Hollins S, Nakamura E (2013) The lithium, boron and strontium isotopic systematics of groundwaters from an arid aquifer system: implications for recharge and weathering processes. Geochim Cosmochim Acta 112:20–31

Millot R, Négrel P (2007) Multi-isotopic tracing (δ^7Li, δ^{11}B, ^{87}Sr/^{86}Sr) and chemical geothermometry: evidence from hydro- geothermal systems in France. Chem Geol 244:664–678

Millot R, Négrel Ph, Petelet-Giraud E (2007). Multi-isotopic (Li, B, Sr, Nd) approach for geothermal reservoir characterization in the Limagne Basin (Massif Central, France). Appl Geochem 22:2307–2325

Millot R, Petelet-Giraud E, Guerrot C, Négrel P (2010a) Multi-isotopic composition (δ^7Li–δ^{11}B–δD–δ^{18}O) of rainwaters in France: origin and spatio-temporal characterization. Appl Geochem 25:1510–1524

Millot R, Scaillet B, Sanjuan B (2010b) Lithium isotopes in island arc geothermal systems: Guadeloupe, Martinique (French West Indies) and experimental approach. Geochim Cosmochim Acta 74:1852–1871

Millot R, Vigier N, Gaillardet J (2010c) Behaviour of lithium and its isotopes during weathering in the Mackenzie Basin, Canada. Geochim Cosmochim Acta 74:3897–3912

Millot R, Guerrot C, Innocent C, Négrel P, Sanjuan B (2011) Chemical, multi-isotopic (Li–B–Sr–U–H–O) and thermal characterization of Triassic formation waters from the Paris Basin. Chem Geol 283:226–241

Millot R, Hegan A, Négrel P (2012) Geothermal waters from the Taupo Volcanic Zone, New Zealand: Li, B and Sr isotopes characterization. Appl Geochem 27:677–688

Misra S, Froelich PN (2012) Lithium isotope history of Cenozoic seawater: changes in silicate weathering and reverse weathering. Science 335:818–823

Morozov NP (1968) Geochemistry of rare alkaline elements in the oceans and seas. Oceanology 8:169–178

Mottl MJ, Seewald JS, Wheat CG, Tivey MK, Michael PJ, Proskurowski G, McCollom TM, Reeves E, Sharkey J, You CF, Chan LH, Pichler T (2011) Chemistry of hot springs along the Eastern Lau Spreading Center. Geochim Cosmochim Acta 75:1013–1038

Murphy MJ, Pogge von Strandmann PAE, Porcelli D, Ingri J (2014) Li isotope behaviour in the low salinity zone during estuarine mixing. Procedia Earth Planet Sci 10:204–207

Myška O, Magna T, Novák M, Šikl J, Zoulková V, Oulehle F (2011) Lithium isotope fractionation at the soil–plant interface. Mineral Mag 75:A1520

Naranjo MA, Romero C, Belles JM, Montesinos C, Vicente O, Serrano R (2003) Lithium treatment induces a hypersensitive-like response in tobacco. Planta 217:417–424

Négrel P, Millot R, Brenot A, Bertin C (2010) Lithium isotopes as tracers of groundwater circulation in a peat land. Chem Geol 276:119–127

Négrel P, Millot R, Guerrot C, Petelet-Giraud E, Brenot A, Malcuit E (2012) Heterogeneities and interconnections in groundwaters: Coupled B, Li and stable-isotope variations in a large aquifer system (Eocene Sand aquifer, Southwestern France). Chem Geol 296–297:83–95

Nishio Y, Okamura K, Tanimizu M, Ishikawa T, Sano Y (2010) Lithium and strontium isotopic systematics of waters around Ontake volcano, Japan: implications for deep-seated fluids and earthquake swarms. Earth Planet Sci Lett 297:567–576

Nishio Y, Ijiria A, Toki T, Morono Y, Tanimizu M, Nagaishi K, Inagaki F (2015) Origins of lithium in submarine mud volcano fluid in the Nankai accretionary wedge. Earth Planet Sci Lett 414:144–155

Oi T, Kawada K, Hosoe M, Kakihana H (1991) Fractionation of lithium isotopes in cation-exchange chromatography. Sep Sci Tech 26:1353–1375

Okumura M, Kitano Y (1986) Coprecipitation of alkali metal ions with calcium carbonate. Geochim Cosmochim Acta 50:49–58

Pistiner J, Henderson GM (2003) Lithium isotope fractionation during continental weathering processes. Earth Planet Sci Lett 214:327–339

Pogge von Strandmann PAE, James RH, van Calsteren P, Gislason SR, Burton KW (2008). Lithium, magnesium and uranium isotope behaviour in the estuarine environment of basaltic islands. Earth and Planetary Science Letters 274:3–4

Pogge von Strandmann PAE, Porcelli D, James RH, van Calsteren P, Schaefer B, Cartwright I, Reynolds BC, Burton KW (2014) Chemical weathering processes in the Great Artesian Basin: Evidence from lithium and silicon isotopes. Earth and Planetary Science Letters 406:24–36

Pogge von Strandmann PAE, Henderson GM (2015) The lithium isotope response to mountain uplift. Geology 43:67–70

Pogge von Strandmann PAE, Jenkyns HC, Woodfine RG (2013) Lithium isotope evidence for enhanced weathering during Oceanic Anoxic Event 2. Nature Geosci 6:668-672

Pogge von Strandmann PAE, Burton KW, James RH, van Calsteren P, Gislason SR (2010) Assessing the role of climate on uranium and lithium isotope behaviour in rivers draining a basaltic terrain. Chem Geol 270:227–239

Pogge von Strandmann PAE, Burton KW, James RH, van Calsteren P, Gislason SR, Mokadem F (2006) Riverine behaviour of uranium and lithium isotopes in an actively glaciated basaltic terrain. Earth Planet Sci Lett 251:134–147

Pogge von Strandmann PAE, Opfergelt S, Lai YJ, Sigfússon B, Gislason SR, Burton KW (2012) Lithium, magnesium and silicon isotope behaviour accompanying weathering in a basaltic soil and pore water profile in Iceland. Earth Planet Sci Lett 339–340:11–23

Qi HP, Coplen TB, Wang QZ, Wang YH (1997) Unnatural isotopic composition of lithium reagents. Anal Chem 69:4076–4078

Qiu L, Rudnick RL, McDonough WF, Merriman RJ (2009) Li and δ^7Li in mudrocks from the British Caledonides: metamorphism and source influences. Geochim Cosmochim Acta 73:7325–7340

Rad S, Rivé K, Vittecoq B, Cerdan O, Allègre CJ (2013) Chemical weathering and erosion rates in the Lesser Antilles: an overview in Guadeloupe, Martinique and Dominica. J S Am Earth Sci 45:331–344

Reeder RJ (1983) Crystal chemistry of the rhombohedral carbonates. In: Reeder RJ (ed) Carbonates: Mineralogy and Chemistry. Mineralogical Society of America. Rev Mineral Geochem 11:1–48

Rollion-Bard C, Vigier N, Meibom A, Blamart D, Reynaud S, Rodolfo-Metalpa R, Martin S, Gattuso J-P (2009) Effect of environmental conditions and skeletal ultrastructure on the Li isotopic composition of scleractinian corals. Earth Planet Sci Lett 286:63–70

Romer RL, Meixner A, Hahne K (2014) Lithium and boron isotopic composition of sedimentary rocks—The role of source history and depositional environment: A 250 Ma record from the Cadomian orogeny to the Variscan orogeny. Gondwana Res 26:1093–1110

Rudnick, RL, Tomascak PB, Njo HB, Gardner LR (2004). Extreme lithium isotopic fractionation during continental weathering revealed in saprolites from South Carolina. Chem Geol 212:45–57

Ryu JS, Vigier N, Lee SW, Lee KS, Chadwick OA (2014) Variation of lithium isotope geochemistry during basalt weathering and secondary mineral transformations in Hawaii. Geochim Cosmochim Acta 145:103–115

Schiavi F, Kobayashi K, Moriguti T, Nakamura N, Pompilio M, Tiepolo M, Vannucci R (2010) Degassing, crystallization and eruption dynamics at Stromboli: trace element and lithium isotopic evidence from 2003 ashes. Contrib Mineral Petrol 159:541–561

Scholz F, Hensen C, Reitz A, Romer RL, Liebetrau V, Meixner A, Weise SM, Haeckel M (2009) Isotopic evidence (^{87}Sr/^{86}Sr, δ^7Li) for alteration of the oceanic crust at deep-rooted mud volcanoes in the Gulf of Cadiz, NE Atlantic Ocean. Geochim Cosmochim Acta 73:5444–5459

Scholz F, Hensen C, De Lange GJ, Haeckel M, Liebetrau V, Meixner A, Reitz A, Romer RL (2010) Lithium isotope geochemistry of marine pore waters—Insights from cold seep fluids. Geochim Cosmochim Acta 74:3459–3475

Schrauzer GN (2002) Lithium: Occurrence, dietary intakes, nutritional essentiality. J Am Coll Nutr 21:14–21

Seyfried WE Jr, Janecky DR, Mottl M (1984) Alteration of the oceanic crust by seawater: implications for the geochemical cycles of boron and lithium. Geochim Cosmochim Acta 48:557–569

Seyfried WE Jr, Chen X, Chan LH (1998) Trace element mobility and lithium isotope exchange during hydrothermal alteration of seafloor weathered basalt: an experimental study at 350 °C, 500 bars. Geochim Cosmochim Acta 62:949–960

Schmitt AD, Vigier N, Lemarchand D, Millot R, Stille P, Chabaux F (2012) Processes controlling the stable isotope compositions of Li, B, Mg and Ca in plants, soils and waters: a review. Comptes Rendus Geosci 344:704–722

Siggaard-Andersen ML, Gabrielli P, Steffensen JP, Strømfeldt T, Barbante C, Boutron C, Fischer H, Miller H (2007) Soluble and insoluble lithium dust in the EPICA Dome C ice core—implications for changes of the East Antarctic dust provenance during the recent glacial–interglacial transition. Earth Planet Sci Lett 258:32–43

Stoffyn-Egli P (1982) Conservative behavior of dissolved lithium in estuarine waters. Estuarine Coast Shelf Sci 14:577–587

Stoffyn-Egli P, Mackenzie FT (1984) Mass balance of dissolved lithium in the oceans. Geochim Cosmochim Acta 48:859–872

Stoll PM, Stokes PE, Okamoto M (2001) Lithium isotopes: differential effects on renal function and histology. Bipolar Disorders: 3:174–180

Sturchio NC, Chan LH (2003) Lithium isotope geochemistry of the Yellowstone hydrothermal system. Soc Econ Geol Spec Pub 10:171–180

Sucharová J, Suchara I (2006) Determination of 36 elements in plant reference materials with different Si contents by inductively coupled plasma mass spectrometry: comparison of microwave digestions assisted by three types of digestion mixtures. Anal Chim Acta 576:163–176

Taylor TI, Urey HC (1938) Fractionation of the lithium and potassium isotopes by chemical exchange with zeolites. J Chem Phys 6:429–438

Teng FZ, McDonough WF, Rudnick RL, Dalpé C, Tomascak PB, Chappell BW, Gao S (2004) Lithium isotopic composition and concentration of the upper continental crust. Geochim Cosmochim Acta 68:4167–4178

Tipper E. T, Calmels D, Gaillardet J, Louvat P, Capmas F, Dubacq B (2012) Positive correlation between Li and

Mg isotope ratios in the river waters of the Mackenzie Basin challenges the interpretation of apparent isotopic fractionation during weathering. Earth Planet Sci Lett 333:35–45

Tomascak PB, Hemming NG, Hemming SR (2003) The lithium isotopic composition of waters from the Mono Basin, California. Geochim Cosmochim Acta 67:601–611

Tsai PH, You CF, Huang KF, Chung CH, Sun YB (2014) Lithium distribution and isotopic fractionation during chemical weathering and soil formation in a loess profile. J Asian Earth Sci 87:1–10

Ullman CV, Campbell HJ, Frei R, Hesselbo SP, Pogge von Strandmann PAE, Korte C (2013) Partial diagenetic overprint of Late Jurassic belemnites from New Zealand: implications for the preservation potential of δ^7Li values in calcite fossils. Geochim Cosmochim Acta 120:80–96

Ushikubo T, Kita N, Cavosie AJ, Wilde SA, Rudnick RL, Valley JW (2008) Lithium in Jack Hills zircons: evidence for extensive weathering of Earth's earliest crust. Earth Planet Sci Lett 272:666–676

Verney-Carron A, Vigier N, Millot R (2011) Experimental determination of the role of diffusion on Li isotope fractionation during basaltic glass weathering. Geochim Cosmochim Acta 75:3452–3468

Verney-Carron A, Vigier N, Millot R, Hardarson BS (2015) Lithium isotopes in hydrothermally altered basalts from Hengill (SW Iceland). Earth Planet Sci Lett 411:62–71

Vigier N, Goddéris Y (2015) A new approach for modeling the Cenozoic oceanic lithium isotope paleo-variations: the key role of climate. Clim Past 11:635–645

Vigier N, Decarreau A, Millot R, Carignan J, Petit S, France-Lanord C (2008) Quantifying Li isotope fractionation during smectite formation and implications for the Li cycle. Geochim Cosmochim Acta 72:780–792

Vigier N, Rollion-Bard C, Levenson Y, Erez J (2015) Lithium isotopes in foraminifera shells as a novel proxy for the ocean dissolved inorganic carbon (DIC). Comptes Rendus Geosci 347:43–51

Vigier N, Rollion-Bard C, Spezzaferri S, Brunet F (2007) In situ measurements of Li isotopes in foraminifera. Geochem Geophys Geosyst 8:Q01003

Vigier N, Gislason SR, Burton KW, Millot R, Mokadem F (2009) The relationship between riverine lithium isotope composition and silicate weathering rates in Iceland. Earth Planet Sci Lett 287:434–441

Vils F, Tonarini S, Kalt A, Seitz HM (2009) Boron, lithium and strontium isotopes as tracers of seawater–serpentinite interaction at Mid-Atlantic ridge, ODP Leg 209. Earth Planet Sci Lett 286:414–425

Vlastélic I, Staudacher T, Bachèlery P, Télouk P, Neuville D, Benbakkar M (2011) Lithium isotope fractionation during magma degassing: constraints from silicic differentiates and natural gas condensates from Piton de la Fournaise volcano (Réunion Island). Chem Geol 284:26–34

Wanner C, Sonnenthal EL, Liu X-M (2014) Seawater δ^7Li: a direct proxy for global CO_2 consumption by continental silicate weathering? Chem Geol 381:154–167

Wang Q-L, Chetelat B, Zhao Z-Q, Ding H, Li S-L, Wang B-L, Li J, Liu X-L (2015) Behavior of lithium isotopes in the Changjiang River system: sources effects and response to weathering and erosion. Geochim Cosmochim Acta 151:117–132

Williams LB, Hervig RL (2005) Lithium and boron isotopes in illite-smectite: the importance of crystal size. Geochim Cosmochim Acta 69:5705–5716

Wimpenny J, Gıslason S, James RH, Gannoun A, Pogge von Strandmann PAE, Burton K (2010a) The behaviour of Li and Mg isotopes during primary phase dissolution and secondary mineral formation in basalt. Geochim Cosmochim Acta 74:5259–5279

Wimpenny J, James R, Burton K, Gannoun A, Mokadem F, Gıslason S (2010b) Glacial effects on weathering processes: new insights from the elemental and lithium isotopic composition of West Greenland rivers. Earth Planet Sci Lett 290:427–437

Witherow RA, Lyons WB, Henderson GM (2010) Lithium isotopic composition of the McMurdo Dry Valleys aquatic systems. Chem Geol 275:139–147

Wu S, Feng X, Wittmeier A (1997) Microwave digestion of plant and grain Reference Materials in nitric acid or a mixture of nitric acid and hydrogen peroxide for the determination of multi-elements by Inductively Coupled Plasma Mass Spectrometry. J Anal Atom Spectrom 12:797–806

Wunder B, Deschamps F, Watenphul A, Guillot S, Meixner A, Romer RL, Wirth R (2010) The effect of chrysotile nanotubes on the serpentine-fluid Li-isotope fractionation. Contrib Miner Petrol 159:781–790

Yamaji K, Makita Y, Watanabe H, Sonoda A, Kanoh H, Hirotsu T, Ooi K (2001) Theoretical estimation of lithium isotopic reduced partition function ratio for lithium ions in aqueous solution. J Phys Chem A 105:602–613

Yoon J (2010) Lithium as a silicate weathering proxy: problems and perspectives. Aquat Geochem 16:189–206

You CF, Chan LH (1996) Precise determination of lithium isotopic composition in low concentration natural samples. Geochim Cosmochim Acta 60:909–915

You CF, Chan LH, Spivack AJ, Gieskes JM (1995) Lithium, boron, and their isotopes in sediments and pore waters of Ocean Drilling Program Site 808, Nankai Trough: implications for fluid expulsion in accretionary prisms. Geology 23:37–40

You CF, Chan LH, Gieskes JM, Klinkhammer GP (2003) Seawater intrusion through the oceanic crust and carbonate sediment in the Equatorial Pacific: lithium abundance and isotopic evidence. Geophys Res Lett 30, paper number 2120. doi:10.1029/2003GL018412

You CF, Gieskes JM, Lee T, Yui TF, Chen HW (2004) Geochemistry of mud volcano fluids in the Taiwan accretionary prism. Appl Geochem 19:695–707

Zhang L, Chan LH, Gieskes JM (1998) Lithium isotope geochemistry of pore waters from Ocean Drilling Program Sites 918 and 919, Irminger Basin. Geochim Cosmochim Acta 62:2437–2450

Summation: What Have We Learned and Where Can We Go?

7

7.1 Retrospective

In the 2004 review of the state of Li isotope research by Tomascak, a series of conclusions were put forth. Some of these were actually suggestions of where Li isotopes had either not been effectively applied or where the existing data failed to completely assess a topic. In light of the studies that have followed, many areas of progress are apparent, and the 2004 list can be re-evaluated. Below we recount the concluding points from Tomascak (2004) and indicate where progress has been made (i.e., where understanding now prevails over uncertainty) as well as where new questions have emerged and where some of the larger gaps remain in the field.

- "There is no consensus on the specific mantle Li isotopic composition. Currently reported values for normal MORB suggest a range (δ^7Li = +1.5 to +5.6), but no single study has shed light on whether this range is an intrinsic feature of the upper mantle, to what extent cryptic contamination plays a role, or if bulk samples can only define an average for a reservoir with broad heterogeneity."

Between a richer set of data for MORB and more thorough study of direct mantle samples, there is now clear consensus on the Li isotopic composition of the upper mantle. Sampling MORB at different spatial scales has yielded suggestions of heterogeneity that may be long-lived (recycled components) or may be shallow level in origin (magma chamber contamination). There is still a level of uncertainty in the interpretation of Li isotope variability in MORB samples. However, the global average appears robust and, ironically, recapitulates the estimates from the very first MORB study (Chan and Edmond 1988).

The potential influence of diffusion on the isotopic compositions of high temperature materials has become apparent in the intervening years (see Chap. 4). The results of laboratory experiments and computational studies serve to temper (and in some cases invalidate) many of the original interpretations from igneous and metamorphic rocks. Future natural studies need to take the constraints imposed by diffusional processes into consideration to avoid erroneous conclusions. On the other hand, substantial improvement of in situ analytical capacity has opened the door to use diffusion-induced fractionation in productive ways, for example in quantifying rates of geological processes. Although the specter of diffusion may hang heavily over many studies of the mantle and crust, there are still fundamental lessons to be learned in translating laboratory observations into natural settings.

- "Given the fractionation of Li isotopes by processes near the Earth's surface, fractionated materials should be returned to the mantle throughout geologic time. There is

P.B. Tomascak et al., *Advances in Lithium Isotope Geochemistry*, Advances in Isotope Geochemistry, DOI: 10.1007/978-3-319-01430-2_7

apparent correlation between mantle heterogeneity in radiogenic isotopes and Li. Thus far the incorporation of material with δ^7Li < MORB, as predicted based on studies of subduction zone lavas and eclogites, is not evident in oceanic lavas. An initial attempt to track this recycling process over Earth history with peridotite xenoliths suggested an increase in δ^7Li by ~4 ‰ since the mid-Archean."

As indicated in Chaps. 4 and 5, the impact of diffusion on understanding the isotopic evolution of metamorphic rocks has advanced in fundamental ways since the 2004 summary of the field. Earlier inferences of extreme Li isotopic depletion during prograde metamorphism have been significantly curtailed. Even so, traceable Li isotopic signatures are clearly developed in the crust which should be applicable to the study of mantle heterogeneity.

For example, the "HIMU" signature of many OIB groups appears to carry an imprint of heavy Li (Nishio et al. 2005), indicating the survival of crustally-fractionated material in at least one part of the upper mantle smorgasbord of recycled components enumerated primarily through radiogenic isotopes. The capacity to measure isotopic variations to higher and higher precision during the last decade has made constraining the nature of less isotopically distinct deeply-recycled components feasible. Nevertheless, the isotopically heavy HIMU component is currently the only convincing Li isotopic fingerprint of broad-scale mantle heterogeneity so far revealed.

Formation of crustal silicate reservoirs with predominantly light Li isotopic composition, coupled with quantification of Li in the modern mantle, implies secular Li isotopic fractionation of the mantle. This was envisaged by Bouman et al. (2000) and Elliott et al. (2004), although the results of Halama et al. (2007, 2008) do not indicate a fundamental change in mantle Li since the late Archean. The potential impact of diffusional fractionation on the interpretation of mantle rocks as recorders of mantle Li isotopes over time present challenges to the realization of a mantle evolution diagram like those used with radiogenic isotopes. Whether carefully selected samples can defeat such problems remains to be demonstrated.

- "The extent to which isotopic fractionation occurs at sub-1000 °C temperatures in magmatic and regional metamorphic systems is unstudied in detail, but limited natural and experimental data in granitic systems suggest that measurable fractionation may occur under these conditions. This fractionation might be applied in studies of magmatic and ore evolution, either for thermometry or mineral deposit exploration."

Laboratory experiments in the appropriate temperature range for the rigorous study of crustal metamorphism are challenging, but Chap. 4 maps out the current state of understanding. Existing studies have not yielded a clear vision of the utility of Li isotopes in studying metamorphic terranes, although some have begun to clarify the conditions in nature in which they can help us understand such processes (e.g., Romer and Meixner 2014). Although potentially quite complex in terms of the interplay between diffusion and heterogeneous fluid flow, the capacity to approach Li isotope analysis on varying spatial scales may yet allow valuable constraints on the histories of rocks in these settings.

- "Clastic sediments are reservoirs of information about weathering processes, but are sufficiently complex that no study has yet to realize their potential. Despite a number of initial reports of relatively isotopically heavy samples, the majority of data for clastic sedimentary rocks have an average δ^7Li ~ 0 ‰, equivalent to the estimated average isotopic composition of the continental crust.

Abundant data now exist for both terrigenous and marine sediment, as well as for sedimentary rocks. The processes by which sedimentary rocks develop their Li isotopic signatures are now relatively well documented, as is the average isotopic composition of the crust itself. The capacity

of Li isotopes to constrain the incorporation of subducted sediment in the sources of arc magmas (e.g., Tang et al. 2014) is among the most compelling recent findings.

- "Although ocean water is well mixed with respect to Li, and many laboratories measure Li isotopes in seawater, the range in values reported in the literature (δ^7Li = +29.3 to +33 ‰) cast some uncertainty on this reservoir. As precision of analytical methods improves, a check of the viability of the "seawater standard" should be carried out."

The isotopic composition of Li in the modern ocean is now well-characterized, through several excellent studies. The existence of a widely available certified seawater standard for Li isotopes (IRMM BCR-403; Millot et al. 2004) is a reality.

- "Initial experiments on the viability of marine (as well as lacustrine) carbonates as geochemical proxies have produced encouraging results toward the goal of tracing temporal changes in the Li isotopic composition of the Earth's surface. Inorganic and biogenic carbonate precipitation appears to favorably incorporate light Li, but this fractionation is not temperature sensitive. A better understanding of metabolic effects of invertebrate species will be necessary. More laboratory experiments and controlled natural studies should address the prospective of Li isotopes in assessing compositional changes in waters over time. Modern analytical techniques, permitting precise analysis of small (≤1 ng Li) samples, will permit the examination of detailed populations of these low concentration materials."
  "Weathering releases isotopically heavy Li to the near-surface environment, regardless of the intensity of chemical weathering. Much of this Li goes to stream flow, contributing to the riverine average δ^7Li ~ +24 ‰. The detailed histories of weathering products on the continents—sediments and soils—can be complex, but studies of simple systems suggest retention of isotopically light material, and hence an evolution of the continents toward lower δ^7Li over Earth history."

Some of the greatest advances in the use of Li isotopes to better understand the Earth system have been in paleoceanography. Some rather thrilling results (e.g., Misra and Froelich 2012) expand on interpretations derived from established oceanic geochemical tracers (e.g., ^{87}Sr/^{86}Sr) and pave the way for future studies of Li as a proxy for global change. Exactly how Li will be best used, though, is controversial. Studies have approached the problem from the oceans (in marine sediments or foraminifera) and from the continents (dissolved and particulate constituents of river systems and fluvial sediments).

There remains, however, considerable uncertainty on the interpretation of driving forces for these isotopic records. The extent to which Li isotopes can be tied to continental weathering, atmospheric temperature, and/or greenhouse gas fluctuation is hotly debated (no pun intended). Needless to say there is abundant room for important contributions in this area of research, from natural studies (including studies extending records further back in time), laboratory experiments, and computational models.

- "Consensus should be reached on the interpretation of Li isotope data for chondritic meteorites. Can bulk planetary Li isotopic compositions be accurately estimated from meteorites, or do these objects preserve only parent body near-surface or metamorphic histories? Are either of these possibilities viable? Detailed, high precision studies should permit this assessment."

Despite exciting new data from meteorites, major questions persist in cosmochemical applications of Li isotopes. The study of Li isotopes in components of individual meteorites appears to be an essential step toward better defining both the nature and evolution of these materials. Whether the complex thermal and/or aqueous histories of certain meteorites do not allow for Li isotopes to fully record the entire lifetime of

these materials remains to be seen, but it appears that coupling Li with other novel stable isotope systems (Mg, Si, Fe, Cd) offers potential for reaching heretofore unattainable understanding of the evolution of the early Solar System.

Although a more comprehensive set of analyses now exists for lunar materials, we are only beginning to understand the Li isotopic systematics of our nearest celestial neighbor. Like with asteroidal meteorites, dissected planetary materials need to be examined in order to fully appreciate what Li isotopes have to tell about the histories of these rocks and their source planets. Speculations into the capacity of Li isotopes to address questions of water in planetary mantles require further detailed investigation.

7.2 Analytical Prospects

Progress since 2004 on the precise and accurate analysis of Li isotopes makes the measurement a much more routine effort in a much greater diversity of laboratories around the globe today. The development of very high precision analytical techniques (e.g., external precision better than ±0.4 ‰) has opened up whole new areas of study. Recent advances using less costly instrumentation have paved the way for measurements at intermediate precision (±c. 1 ‰), particularly applicable for studies requiring large data throughput, and making a substantial array of scientifically important work feasible for many more laboratories world-wide. In bulk analysis it is still clear that emphasis must be maintained on demonstrating the efficacy of chemical separation, but this stricture appears to be well known now, and experimenters are watchful.

The analysis of tiny bulk samples (e.g., individual foraminifera tests, sub-millimeter inclusions in diamonds or meteorites, minute experimental run products) can be realistically conceived. At the same time, the threshold of in situ analysis, especially with newer generation SIMS instrumentation, has been greatly refined and geochemical problems whose solutions rely on high spatial resolution (e.g., to examine evidence of diffusional processes) can be carried out. Spatially-resolved analytical techniques finally are producing accurate and in many cases very precise Li isotopic data.

7.3 Final Words

Chapter 4 lays out in great detail the theoretical and laboratory basis for understanding Li elemental and isotopic variations in natural materials. Because of the fast diffusion of Li compared to other elements, and because of the difference in rates of diffusion of the Li isotopes, several cautions resonate from this chapter. Experiments and computations give very clear boundary conditions on time- and length-scales of diffusion and must be taken into consideration in the interpretation of data from natural materials. Even when in situ analysis permits the evaluation of zoning within crystals, elemental and isotopic zonation have been misinterpreted. In light of the complex effects of diffusion on Li and its isotopes the admonitions of Sect. 4.3.4 need to be kept in mind, especially, but not exclusively, for the study of high temperature materials. Although the prospects for exciting discoveries in the field of Li isotopes appear certain, future work must attentively abide by the constraints imparted by theory and laboratory studies in order for authentic progress to be made.

References

Bouman C, Elliott TR, Vroon PZ, Pearson DG (2000) Li isotope evolution of the mantle from analyses of mantle xenoliths. J Conf Abstr 5:239

Chan L-H, Edmond JM (1988) Variation of lithium isotope composition in the marine environment: a preliminary report. Geochim Cosmochim Acta 52:1711–1717

Elliott T, Jeffcoate A, Bouman C (2004) The terrestrial Li isotope cycle: light-weight constraints on mantle convection. Earth Planet Sci Lett 220:231–245

Halama R, McDonough WF, Rudnick RL, Keller J, Klaudius J (2007) The Li isotopic composition of Oldoinyo Lengai: nature of the mantle sources and lack of isotopic fractionation during carbonatite petrogenesis. Earth Planet Sci Lett 254:77–89

Halama R, McDonough WF, Rudnick RL, Bell K (2008) Tracking the lithium isotopic evolution of the mantle using carbonatites. Earth Planet Sci Lett 265:726–742

Millot R, Guerrot C, Vigier N (2004) Accurate and high-precision measurement of lithium isotopes in two reference materials by MC-ICP-MS. Geostand Geoanal Res 28:153–159

Misra S, Froelich PN (2012) Lithium isotope history of Cenozoic seawater: changes in silicate weathering and reverse weathering. Science 335:818–823

Nishio Y, Nakai S, Kogiso T, Barsczus HG (2005) Lithium, strontium, and neodymium isotopic compositions of oceanic island basalts in the Polynesian region: constraints on a Polynesian HIMU origin. Geochem J 39:91–103

Romer RL, Meixner A (2014) Lithium and boron isotopic fractionation in sedimentary rocks during metamorphism—the role of rock composition and protolith mineralogy. Geochim Cosmochim Acta 128:158–177

Tang M, Rudnick RL, Chauvel C (2014) Sedimentary input to the source of Lesser Antilles lavas: a Li perspective. Geochim Cosmochim Acta 144:43–58

Tomascak PB (2004) Developments in the understanding and application of lithium isotopes in the Earth and planetary sciences. In: Johnson CM, Beard BL, Albarède F (eds) Geochemistry of non-traditional stable isotopes. Rev Mineral Geochem 55:153–195